Max-Planck-Institut für Molekulare Pflanzenphysiologie

Prof. Dr. Lothar Willmitzer

Characterization of metabolomic dynamics in synchronized *Chlamydomonas reinhardtii* cell cultures and the impact of TOR inhibition on cell cycle, proliferation and growth

Dissertation

zur Erlangung des akademischen Grades "doctor rerum naturalium" (Dr. rer. nat.)
in der Wissenschaftsdisziplin „Molekulare Pflanzenphysiologie"
eingereicht an der Mathematisch-Naturwissenschaftlichen Fakultät der
Universität Potsdam

von

Jessica Jüppner

Potsdam, August 2014

Published online at the
Institutional Repository of the University of Potsdam:
URN urn:nbn:de:kobv:517-opus4-76923
http://nbn-resolving.de/urn:nbn:de:kobv:517-opus4-76923

Table of Content

List of figures

List of tables

List of abbreviations

3PGA	Glycerate-3-phosphate
ADP	Adenosine diphosphate
AMP	Adenosine monophosphate
ATP	Adenosine triphosphate
CDK	Cyclin dependent kinase
CP	Commitment point
DAG	Diacylglycerol
db	Double bound
DC	Daughter cell
DGDG	Digalactosyldiacylglycerol
DGTS	Diacylglycerol-N,N,N-trimethylhomoserine
DHAP	Dihydroxyacetonphosphate
DNA	Desoxyribonucleic acid
F6P	Fructose-6-phosphate
FFA	Free fatty acid
FT-ICR	Fourier transform-ion cyclotron resonance
G6P	Glucose-6-phosphate
GC	Gas chromatography
GMP	Guanosine monophosphate
HCA	Hierarchical cluster analysis
HSM	High salt medium
IMP	Inosine monophosphate
LC	Liquid chromatography
MC	Mother cell
MCV	Mean cell volume
MGDG	Monogalactosyldiacylglycerol
MS	Mass spectrometry
MTBE	Methanol:methyl-tert-butyl-ether
NADP	Nicotinamide adenine dinucleotide phosphate
PCA	Principal component analysis
PE	Phosphatidylethanolamine
PEP	Phosphoenolpyruvate
PG	Phosphatidylglycerol
RNA	Ribonucleic acid
ROS	Reactive oxygen species
RT	Room temperature
SD	Standard deviation
SQDG	Sulfoquinovosylglycerol

TAG	Triacylglycerol
TAP	TRIS-acetate-phosphate
TCA cycle	Tricarbonic acid cycle
TIC	Total ion count
Tof	Time of flight
TOR	Target of rapamycin
TP	Time point
UPLC	Ultra performance liquid chromatography
WT	Wild type

List of sematics

°C	degrees Celsius
g	gram
mg	milligram
µg	microgram
pg	picogram
ml	milliliter
µl	microliter
µM	micromolar
nM	nanomolar
pM	picomolar
nmol	nanomole
h	hour
min	minute
sec	second
µm	micrometer
nm	nanometer
m/z	mass to charge ratio
ppm	parts per million
rpm	revolutions per minute
kV	kilovolt
V	volt

Summary

The adaptation of cell growth and proliferation to environmental changes is essential for the surviving of biological systems. The evolutionary conserved Ser/Thr protein kinase "Target of Rapamycin" (TOR) has emerged as a major signaling node that integrates the sensing of numerous growth signals to the coordinated regulation of cellular metabolism and growth. Although the TOR signaling pathway has been widely studied in heterotrophic organisms, the research on TOR in photosynthetic eukaryotes has been hampered by the reported land plant resistance to rapamycin. Thus, the finding that *Chlamydomonas reinhardtii* is sensitive to rapamycin, establish this unicellular green alga as a useful model system to investigate TOR signaling in photosynthetic eukaryotes.

The observation that rapamycin does not fully arrest *Chlamydomonas* growth, which is different from observations made in other organisms, prompted us to investigate the regulatory function of TOR in *Chlamydomonas* in context of the cell cycle. Therefore, a growth system that allowed synchronously growth under widely unperturbed cultivation in a fermenter system was set up and the synchronized cells were characterized in detail. In a highly resolved kinetic study, the synchronized cells were analyzed for their changes in cytological parameters as cell number and size distribution and their starch content. Furthermore, we applied mass spectrometric analysis for profiling of primary and lipid metabolism. This system was then used to analyze the response dynamics of the *Chlamydomonas* metabolome and lipidome to TOR-inhibition by rapamycin

The results show that TOR inhibition reduces cell growth, delays cell division and daughter cell release and results in a 50% reduced cell number at the end of the cell cycle. Consistent with the growth phenotype we observed strong changes in carbon and nitrogen partitioning in the direction of rapid conversion into carbon and nitrogen storage through an accumulation of starch, triacylglycerol and arginine. Interestingly, it seems that the conversion of carbon into triacylglycerol occurred faster than into starch after TOR inhibition, which may indicate a more dominant role of TOR in the regulation of TAG biosynthesis than in the regulation of starch.

This study clearly shows, for the first time, a complex picture of metabolic and lipidomic dynamically changes during the cell cycle of *Chlamydomonas reinhardtii* and furthermore reveals a complex regulation and adjustment of metabolite pools and lipid composition in response to TOR inhibition.

Allgemeinverständliche Zusammenfassung

Die Anpassung der Wachstumsrate an Umweltveränderungen ist essentiell für das Überleben biologischer Systeme. Mit der Identifikation der evolutionär konservierten Serin/Threonin Kinase "Target of Rapamycin" (TOR) war ein zentraler Regulator gefunden, der in Abhängigkeit einer Vielzahl von Wachstumsfaktoren den zellulären Metabolismus und das Wachstum reguliert. Während zum heutigen Zeitpunkt schon relativ gute Kenntnisse über die Funktionen und Signalwege dieser Kinase in heterotrophen Organismen gewonnen werden konnten, wurden die Untersuchungen des TOR-Signalweges in photoautotrophen Organismen durch deren Resistenz gegenüber dem TOR-spezifischen Inhibitor Rapamycin für lange Zeit erschwert. Daher bietet die Entdeckung, dass die einzelligen Grünalge *Chlamydomonas reinhardtii* eine natürliche Sensitivität gegenüber Rapamycin aufweist, eine gute Grundlage zur Erforschung des TOR-Signalweges in photosynthetisch aktiven Eukaryoten.

Aufgrund der Beobachtung, dass das Wachstum von *Chlamydomonas* nicht vollständig durch Rapamycin inhibiert werden konnte, was im Gegensatz zu Beobachtungen in anderen Organismen steht, entschieden wir uns für eine detailliertere Analyse des Einflusses von TOR auf den Zellzyklus. Dazu wurde ein System etabliert das eine Synchronisation der Zellen unter weitestgehend ungestörten Bedingungen in einem Fermenter-system erlaubte. Dieses System wurde dann für eine detaillierte Charakterisierung der synchronisierten Zellen genutzt. Mittels einer hochaufgelösten Zeitreihe wurden Veränderungen zytologischer Parameter (Zellzahl und Zellgrößenverteilung) und des Stärkegehalts analysiert. Zusätzlich wurden massenspektrometrische Verfahren zur Analyse des Primär- und Lipidmetabolismus verwendet. Dieses System wurde des Weiteren dazu genutzt dynamische Veränderungen im Metabolom und Lipidom von *Chlamydomonas* nach Inhibition der TOR Kinase durch Rapamycin zu untersuchen

Die Ergebnisse der TOR-Inhibition zeigen ein vermindertes Wachstum, eine Verzögerung in der Zellteilung und der Entlassung der Tochterzellen und resultieren in einer um 50% verringerten Zellzahl am Ende des Zellzyklus. Des Weiteren konnte eine Akkumulation von Kohlenstoff– und Stickstoff-Reserven in Form von Stärke und Triacylglyceriden, sowie Arginin beobachtet werden. Dabei ist vor allem interessant, dass die der Einbau von Kohlenstoff in Triacylglyceride offenbar schneller erfolgt als der in Stärke, was auf eine dominantere Rolle von TOR in der Regulation der Triacylglycerid-Biosynthese gegenüber der Stärkesynthese hindeutet.

Diese Studie zeigt zum ersten Mal eine komplexe Analyse der dynamischen Veränderungen im Primär- und Lipidmetabolismus im Verlauf des Zellzyklus von Chlamydomonas und zeigt weiterhin die komplexe Regulation und Adjustierung des Metabolit-Pools und der Lipidzusammensetzung als Antwort auf die Inhibition von TOR.

1 Introduction

1.1 Cell growth – a central and fundamental aspect in biology

Beside the fundamental issue that there would be no life on earth without growth, the understanding of the mechanisms underlying growth regulation becomes nowadays more and more important in the fields of medicine (e.g. clinical diseases such as cancer) , agriculture (e.g. climate changes, feeding of the rapidly growing global population) and biotic natural resources (e.g. biofuels).

When we talk about cell growth in biology, we talk about two distinct but tightly connected processes. One is the increase in mass which is actually the meaning of growth, and the other one is the increase in cell number also termed cell proliferation which requires cell division. Although cell growth and proliferation are often used as synonyms, it is evident to distinguish between them as they are not necessarily relying on each other. For example, a mutation that blocks the cell cycle could prevent cell division, but does not inevitably blocks cell growth [3]. Thus, although cell growth and cell division are often coordinated processes, they are also separate processes that can be uncoupled [4].

The cell cycle is the ordered sequence of events that occur in cells involving cell growth, replication and cell division. The classical cell cycle can be separated into four phases in which cells increase in size (G1 phase), replicate their genetic material (DNA synthesis, S phase), prepare for division (G2 phase) and finally divide (mitosis, M phase). The phases G1, S and G2 make up the interphase which is distinguished from the mitotic phase. During the interphase cells have to double their whole molecular inventory (organelles, proteins and metabolites) next to their genetic material. To ensure that the cell cycle progresses properly, cells use special checkpoint signaling systems. Although our knowledge about the regulation of the cell cycle machinery is in state flux [5-9] there are quite a number of gaps, especially in the field of the mechanism that couple cell growth and cell cycle progression and their coordination within a changing environment.

During cell growth cells have to tightly coordinate the synthesis of cellular components in a precise temporal and quantitative way. The elucidation of those processes requires a controlled experimental system and the comprehensive analysis on the multiple layers of regulation such as transcripts, proteins, lipids and metabolites. So far those comprehensive studies have lagged behind those of cell cycle progression, cell proliferation and coupling between cell growth and cell division. First comprehensive studies at the transcritomic, proteomic and metabolomic levels of growth in response to external nutrient supply were performed by the group of Stephen G. Oliver at the university of Cambridge [10-12]. For these studies chemostat cultures of the well-established eukaryotic model organism, *Saccharomyces cerevisiae* were used. Using chemostat cultures has the

advantage of keeping cells in a steady state growth by controlling the volumetric feeding rate and therefore studying physiologically patterns under very controlled conditions [13-15]. Although their studies allowed combination of changes in growth rates with changes in the transcript or protein level they could not include cell cycle dependent dynamically changes, as their cell culture was a mix of cells in different cell cycle phases. Accordingly, taking cell cycle dependent regulations into account would require a proper synchronization of the analyzed cell cultures. Synchronization of a cell culture under widely undisturbed physiological conditions is of course desired to prevent side effects, which often occur by using chemical or physical methods for synchronization [16].

1.2 *Chlamydomonas reinhardtii* as a model system for studying growth and cell cycle

Many characteristics of living organisms, including homeostasis, spatial and temporal organization, reproduction and adaptation to environmental cues, are also exhibited by individual cells [17]. Unicellular organisms provide therefore a useful tool to study fundamental issues of cell growth and proliferation as they offer a simple handling in laboratory, a short life cycle and a variety of techniques for genetic manipulation. While yeast is the simpler unicellular version of heterotrophic eukaryotes, the unicellular green alga *Chlamydomonas reinhardtii* (hereinafter referred to as *Chlamydomonas*) could be regarded as the unicellular model organism of photosynthetic eukaryotes. Like yeast, *Chlamydomonas* offers a simple life cycle, a well annotated genome [18] and powerful molecular genetic tools [19]. Since the early 1990s *Chlamydomonas* has emerged as a model for plant cell biology and physiology [20-22]. But still, *Chlamydomonas* has lagged behind yeast in the field of studying cell growth regulation. Nevertheless, the unicellular, biflagellate green alga *Chlamydomonas reinhardtii* has a great potential as a system for studying the control of cell growth and cell division as it can be synchronized under widely undisturbed physiological conditions by alternating light-dark cycles. Beside its specialized cell cycle (which will be explained in more detail below), *Chlamydomonas* encodes orthologs of the major plant cell cycle regulators (CDK and cyclin families) [1]. Moreover, most of the *Chlamydomonas* cell cycle regulatory genes exist in a single copy, while those of higher plants and vertebrates undergone multiple duplications [23-25]. In combination with its extensive genetic toolkit [19] this makes *Chlamydomonas* a very attractive model for eukaryotic cell cycle analyses.

1.2.1 The cell cycle of *Chlamydomonas reinhardtii*

The vegetative cells of the unicellular green alga *Chlamydomonas* can divide by a noncanonical mechanism, termed multiple fission (Figure 1) [26]. In contrast to the classical cell cycle model (Figure 1 B), this cell cycle is characterized by a prolonged G1 phase during which cells can double several fold in size (Figure 1 A). The growth phase is followed by the division phase in which cells undergo multiple division rounds, each round consists of DNA synthesis (S phase), mitosis (M phase) and cytokinesis [27], whereas a G2 phase is essentially undetectable [28].

A B

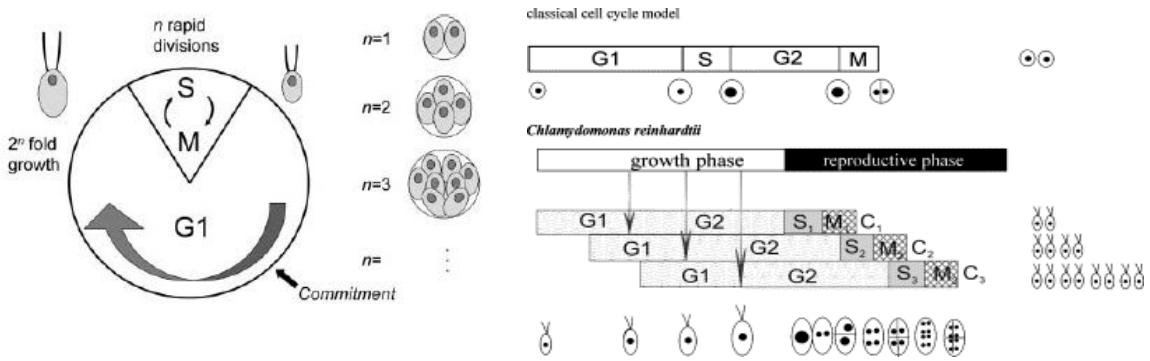

Figure 1. Multiple fission cell cycle of *Chlamydomonas* reinhardtii
Clock-type diagram showing the phases of the *Chlamydomonas* cell cycle (A). Postmitotic mother cells with different values of n are presented [1]. The scheme on the right side (B) compares the classical type of cell cycle in eukaryotic cells and that, found in *Chlamydomonas*. Arrows present the time when commitment points are reached [2].

Thus, within one cell cycle *Chlamydomonas* can produce 2^n daughter cells (DC) of uniform size. Craigie and Cavalier-Smith could show that there is a correlation between the size the mother cell (MC) attained in a given cell cycle and the number of divisions that will occur [29]. After each cytokinesis all DCs remain surrounded by the MC wall (sporangia) until the entire division period is completed (Figure 1 A). The release of DCs occurs by enzymatic digestion of the sporangial cell wall [30]. Matsuda and coworkers found that expression of the vegetative lytic enzyme, which they named sporangin, is also under cell cycle control. The sporangin gene is specifically expressed during S/M phase and the enzyme is translated after mitotic cell division and localized along the entire length of the flagella of the DCs [31]. The authors suggest that excreting the sporangin through the flagella is more efficient at transporting the sporangin to the surface of the sporangial cell wall.

Chlamydomonas contains a size checkpoint, termed "Commitment point" (CP), which separates the growth phase to pre-commitment and post-commitment periods. Cells that passed the CP will divide at least one time during the S/M phase, even if subsequent growth is halted by the withdrawal of light or nutrients [29, 32]. After passing the first CP, cells of *Chlamydomonas* remain in G1 phase for additional 5 - 8 h (post-commitment period). Under favorable conditions the cells continue to increase in size during post-commitment period and therefore attain one or more additional CPs consecutively. A cell cycle in which multiple cell divisions occur is not fundamentally different from others, but in this case cells can pass more than one CP before the DCs are released from the sporangia (Figure 1 B) [33]. Each commitment is the major rate-limiting control point for the subsequent DNA doubling, mitosis and cytokinesis. In addition, Donnan and John reported that cell cycle phases are under control of timer mechanisms as they could show that temperature shifts in the range of 20 - 30 °C have no effect on the duration of the pre-commitment period and the post-commitment period regained its duration after one cell cycle [34]. Nevertheless, the underlying mechanisms for the timing of division and number of division rounds within one cell cycle remain to be elucidated.

1.2.2 Synchronization of *Chlamydomonas reinhardtii cell cultures*

Synchronous cell division of *Chlamydomonas* is usually achieved by alternating light and dark periods under photoautotrophic conditions [35]. To obtain synchronous growth of this unicellular green alga a variation of culture conditions have been used in different publications. Lien and Knutsen provide an overview of different methods used for synchronization [36]. Important parameters for synchronization are the length of light and dark phase, the light intensity, the temperature and the CO_2 concentration. Depending on the used strain and culture conditions the growth rate, the progression and the timing of cell cycle and the degree of synchrony vary. Therefore it is indispensable to establish the kinetics of the cell cycle under the selected growth parameters. The most commonly used alternation of light and dark is a 12:12 h light-dark cycle, but also other cycles (14:10 h, 12:4 h) have given suitable results. A light intensity of 200 - 400 $\mu mol/m^2s$ is recommended for the growth of phototrophic liquid cultures [37]. Furthermore, a CO_2 concentration of 2 - 3 % is widely used. The temperature used in synchronization experiments ranges from 20 - 35 °C. It has been shown that the length of cell cycle is mostly dependent on the temperature, irrespective of the light intensity. On the other hand, the time point at which cells attain the CP for the first division was dependent on the growth rate, which is mainly determined by light intensity and nutrient availability [38].

1.3 The target of rapamycin (TOR) – a central growth regulator

The adaptation of cells to diverse environmental cues requires a regulated reprogramming of the metabolism. To ensure this, there must be molecular links that integrate environmental or growth stimuli to regulate key metabolic pathways that ultimately drive cell growth. The evolutionary conserved Ser/Thr protein kinase "Target of Rapamycin" (TOR) has emerged as a major signaling node that integrates the sensing of numerous growth signals to the coordinated regulation of cellular metabolism and growth. This makes TOR an important key to understand cell growth.

As the name implies, TOR is the target of a molecule named rapamycin or sirolimus, which is an antifungal agent first isolated in the 1970s from the soil bacterium *Strepomyces hygroscopius* [39, 40]. Due to the broad range of antiproliferative activity rapamycin became an important tool for studying cell growth regulation [41, 42]. For further investigation it was therefore evident to identify its target and the underlying mechanistic of growth repression. Only about 16 years after the discovery of rapamycin Heitman et al. succeeded to identify two target genes, namely *TOR1* and *TOR2* by employing a genetic mutant screening in the budding yeast *S. cerevisiae* [43]. Whereas rapamycin treatment leads to a growth arrest at G1 state in growing yeast, the two mutants affected in either *TOR1* or *TOR2* did not show any growth phenotype. This result therefore provided the starting point for the investigation and elucidation of the function and regulation of TOR and leads to the identification of TOR homologues in all eukaryotic organisms, including fungi, mammals, worms, flies, plants and algae (reviewed in [44, 45].

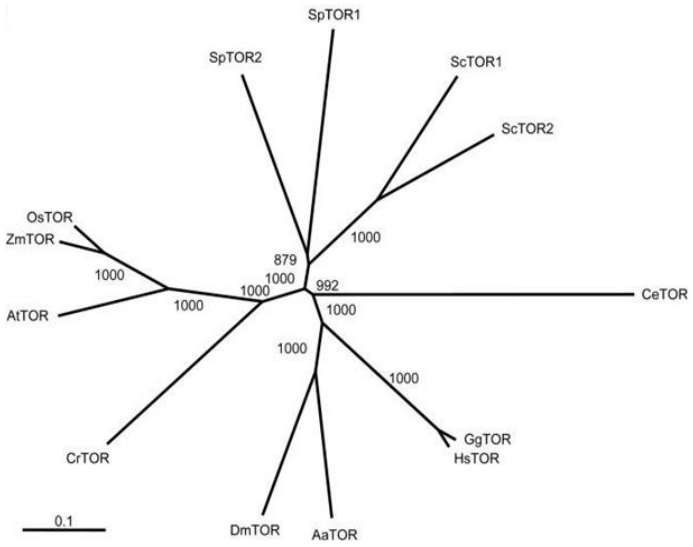

Figure 2. Phylogenetic relationship of TOR proteins from eukaryotes
The phylogenetic tree was constructed with full-length TOR amino acid sequences and aligned using the ClustalW program. Sc, *S. cerevisiae;* Sp, *S pombe;* Os, *O. sativa*; Zm, *Zea mays*; At, *A. thaliana*; Cr, *C. reinhardtii*; Dm, *D. melanogaster*; Aa, *A. aedes*; Hs, *H. spiens*; Gg, *G. gallus*; Ce, *C. elegans*. The bootstrap values represent 1000 replications and the scale bar corresponds to 0.1 estimated amino acid substitutions per site.[46]

The high degree of sequence homology of TOR within those different species is clearly visible in phylogenetic tree in Figure 2 [46] and therefore underlines the conserved and essential function of TOR within the eukaryotic organisms. The sequence comparison of the different TOR proteins revealed the existence of three main clusters, namely one yeast (*Saccharomyces cerevisiae*, *Saccharomyces pombe*), one of higher plants and green alga (*Oryza sativa, Zea mays*, *Arabidopsis thaliana, Chlamydomonas reinhardtii*) and one of higher vertebrates, insects and nematodes (*Gallus gallus*, *Homo sapiens sapiens*, *Drosophila melanogaster, Anopheles aedes, Caenorhabditis elegans*).

1.3.1 Structure of TOR

The current knowledge of the structure and function of TOR will be summarized in the following chapters. Therefore, it should be noted that even though TOR has been identified in several organisms the best described TOR signaling pathway is probably that of yeast and the mammalian system. The main driving force behind this is the potential use of TOR in clinical research [47].

1.3.1.1 TOR - a multi-domain protein

The initial discovery in yeast identified two TOR genes of which the predicted TOR1 and TOR2 proteins show a homology of 67% [48]. Interestingly, unlike yeast almost all other eukaryotes seem to contain only a single *TOR* gene [44]. The large (~290 kDa) multi-domain TOR protein belongs to the family of kinases termed phosphatidylinositol kinase-related kinases (PIKK). Although all PIKK members contain a domain that highly resembles the catalytic domain of a lipid kinase, none of them thus far has been shown to contain lipid kinase activity. Instead, all of them are all atypical Ser/Thr specific protein kinases [49]. The second one of the highly conserved TOR domains is a tandem HEAT (Huntingtin, elongation factor 3, protein phosphatase 2A and TOR1) domain, which is located at the N-terminal site (Figure 3).

The HEAT domain consists of 20 HEAT-repeat motifs, which form antiparallel α-helices with large interfaces for protein-protein interaction [50]. The next two domains are the FAT domain (FRAP, ATM and TTRAP) and the C-terminal FATC domain, which are always appearing paired within the PIKK family and flank the FRB (FKBP12-rapamycin binding) and the above mentioned kinase domain [51-53]. The FRB domain is the region where rapamycin can bind, but only in a ternary complex with an essential FK506-binding protein 12 (FKBP12). The identification that rapamycin can only bind TOR in the presence of FKBP12 was accomplished by Heitman et al. (1991) as they could show that disruption of *FPR1* gene encoding FKBP12 confers rapamycin resistance.

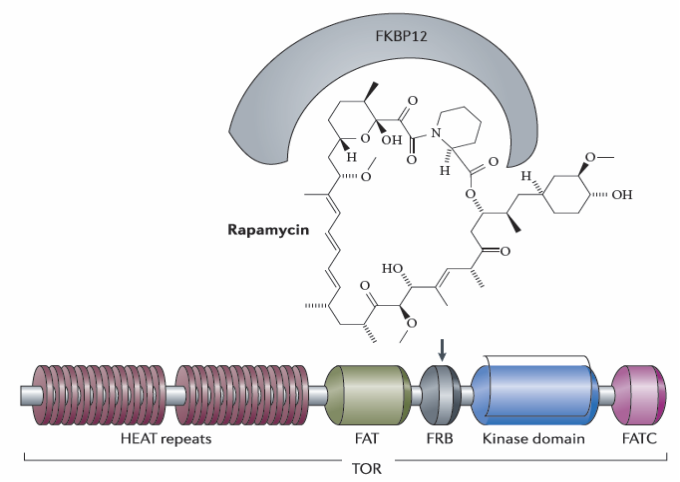

Figure 3. TOR structure and rapamycin interaction
The N-terminus of target of rapamycin (TOR) contains tandem HEAT repeats that are important for protein–protein interactions. The FAT and FATC domains can interact and modulate the activity of the kinase domain; The FRB (FKBP12–rapamycin binding) domain is the docking site of the FKBP12–rapamycin complex. [54]

1.3.1.2 The TOR protein is part of two distinct protein complexes

The coincidence that TOR was initially cloned in yeast, where two genes code for the growth regulator, was fortunate since it presumed that there might be diverse functions of these two distinct TORs. Accordingly, yeast research resulted in another breakthrough in the TOR field in 2002, namely the identification of two distinct multiprotein complexes termed TOR complex 1 (TORC1) and 2 (TORC2) [55-57]. The subsequent identification of both TORCs in other eukaryotes (plants, forms, flies and mammals) revealed that next to the TOR-protein itself the two complexes are also highly conserved, even though they do not require two distinct *TOR* genes (Table 1) (reviewed in [44, 49]).

In the mammalian system, TORC1 and TORC2 are large protein complexes consisting of six or seven known protein components, respectively (Table 1). Next to the mammalian (or mechanistic) TOR (mTOR), they share three additional core proteins (indicated in violet; Table 1), namely mammalian lethal with sec-13 protein 8 (mLST8) [58, 59], DEP domain containing mTOR-interacting protein (DEPTOR) [60] and the Ttil/Tel2 complex [61]. Accordingly, there are also proteins which are only part of either mTORC1 or mTORC2. Thus, these components indicate different physiological functions. The two proteins specific for TORC1 are regulatory-associated protein of mammalian target of rapamycin (raptor) [62, 63] and proline-rich Akt-substrate 40kDa (PRAS40) [64-67], whereas rapamycin-insensitive companion of mTOR (rictor) [59, 68], mammalian stress-activated map kinase interacting protein 1 (mSin1) [69, 70] and protein observed with rictor 1 and 2 (protor1/2) [66, 71, 72] are specific for TORC2. Known molecular functions of the mTOR complex components are described in Figure 4.

Table 1. Othologs of TORC1 and TORC2 in various eukaryotes

Saccharomyces cerevisisae	*Homo sapiens*	*Caenothabditis elegans*	*Drosophila melanogaster*	*Arabidopsis thaliana*	*Oryza sativa*	*Zea mays*	*Chlamydomonas reinhardtii*
TORC1							
TOR1 or TOR2	mTOR	CeTOR	dTOR	AtTOR	OsTOR	ZmTOR	CrTOR
Kog1/Las24	raptor	daf-15	dRaptor	AtRaptor1 AtRaptor2	OsRaptor	-	CrRaptor
Lst8	mLST8	lst-8?	CG3004	AtLST8-1 AtLST8-2	OsLst8	-	CrLST8
Tco89	-	-	-	-	-	-	-
-	PRAS40	-	-	-	-	-	-
-	DEPTOR	-	-	-	-	-	-
-	Tti1/Tel2	-	-	-	-	-	-
TORC2							
TOR2	mTOR	CeTOR	dTOR	AtTOR	OsTOR	ZmTOR	CrTOR
Avo1	mSin1	sinh-1	Sin1	-	-	-	-
Avo2	-	-	-	-	-	-	-
Avo3/Tsc11	rictor	rict-1	dRictor	-	-	-	-
Lst8	mLST8	lst-8	CG3004	AtLST8-1 AtLST8-2	OsLst8	-	CrLST8
Bit61	protor1/2	-	-	-	-	-	-
-	DEPTOR	-	-	-	-	-	-
-	Tti1/Tel2	-	-	-	-	-	-

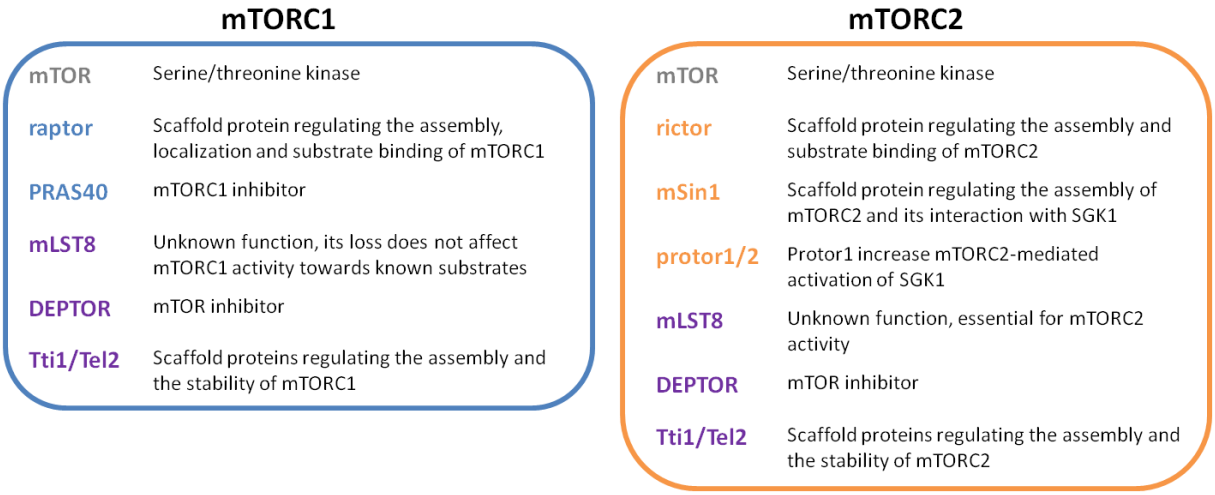

Figure 4. Functions of the mTORC1 and mTORC2 components
Composition of mTORC1 (blue) and mTORC2 (orange). Proteins which were identified in both complexes are indicated in violet or grey. Proteins that are only part of TORC1 or TORC2 are indicated in blue or orange, respectively (modified from [47]).

1.3.2 Function of TOR

In accordance to their composition, the two TORCs share specific upstream inputs and downstream outputs, but in general they are functionally distinct complexes [73, 74]. In a very simplified way it can be concluded that TORC1 mediates the temporal control of cell growth, while TORC2 mediates the spatial control of cell growth (Figure 5) [44, 57]. A further difference between both complexes is their sensitivity to rapamycin. As mentioned above it is known that rapamycin forms a complex with FKBP12 [75, 76]. Rapamycin can only bind and inhibit TOR if it is present in TORC1 [43, 57]. TOR in TORC2 is therefore insensitive to rapamycin, indicating that the FRB binding site is blocked by another protein-protein interaction, most likely by rictor [59, 68]. Due to its insensitivity to rapamycin, a major analytical tool was missing for the analysis of TORC2, which resulted in a huge gap in the mechanistic and functional understanding of the two complexes (Figure 5). However, the exact mechanism by which the FKBP12-rapamycin complex inhibits the activity of TOR is still not fully understood.

As rapamycin treatment or loss of *TOR* function causes yeast cells to arrest in G1 (G0), it was initially thought that TOR regulates cell division [77]. Nowadays, we know that TOR controls many major cellular processes, including ribosome biogenesis, protein and lipid synthesis and autophagy [47]. These processes collectively determine cell growth (increase in cell size and/or mass). Thus, it is assumed that the defect in cell cycle progression upon TOR inhibition is an indirect effect of growth inhibition [49].

1.3.2.1 Targets of TOR – Regulation of cellular growth

Cell growth and proliferation require robust protein synthesis. Protein synthesis, in turn, can be upregulated by increasing translation initiation and/or translation efficiency of existing ribosomes, but also by increasing the total capacity of translation through the production of new ribosomes (ribosome biogenesis). Both of these processes are regulated by TORC1 [78]. Two well-known substrates that mediate part of this translational regulation are the S6 kinase 1 (S6K1; Sch9 the functional homolog in yeast) and the eukaryotic translation initiation factor 4E (eIF4E)-binding protein 1 (4E-BP1) [79]. mTORC1 promotes protein synthesis by activation of S6K1 and inhibition of 4E-BP1 in response to growth factor stimulations as well as nutrient availability. Further known substrates upregulating protein synthesis through mTORC1 are tripartite motif-containing protein-24 (TIF-1A) [80] and Maf1 [81]. In addition to protein synthesis, mTORC1 modulates lipid synthesis [82], at least in some cell types, through S6K1, which, in turn, regulates the sterol regulatory element-binding protein 1/2 (SREBP1/2). A recent study identified lipin-1, a phosphatidic acid phosphatase, as a novel mTORC1 substrate. mTORC1 regulates SREBP1/2 by controlling the nuclear entry of lipin-1 [83]. Inhibition of mTORC1 reduces SREBP1/2 expression,

which leads to a lower expression of genes involved in fatty acid and cholesterol synthesis [84, 85]. mTORC1 signaling can also promote nucleic acid synthesis by stimulating the flux through *de novo* pyrimidine synthesis. This process is also mediated through S6K1, which phosphorylates the enzyme CAD (carbamoyl phosphate synthetase 2, aspartate transcarbamoylase, dihydroorotase) and thereby leads to an increase of the pool of nucleotides available for RNA and DNA synthesis [86, 87].

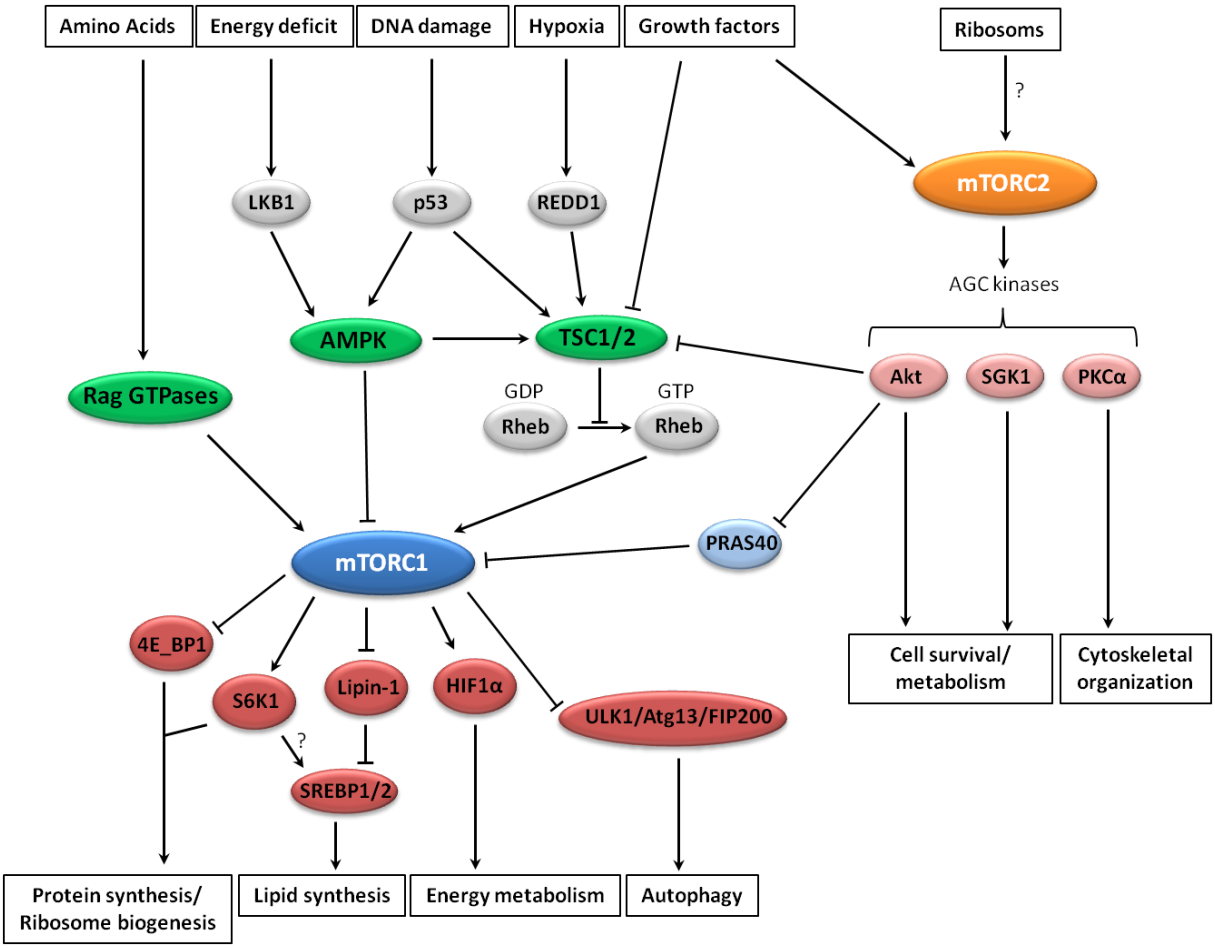

Figure 5. Schematic overview of mTOR signaling pathway
The key signaling nodes that regulate mTORC1 and mTORC2. Modified from [47].

In addition, mTORC1 is a key regulator in energy homeostasis. By increasing the transcription and the translation of hypoxia inducible factor 1α (HIF1α) mTORC1 promotes the expression of glucose transporters and glycolytic enzymes, which in consequence leads to a switch from

mitochondrial oxidative metabolism to glycolysis [85, 88-90]. Beside the role of mTORC1 in promoting anabolic processes, mTORC1 potently inhibits autophagy, a cellular recycling process important for the removal of cytotoxic material and to maintain levels of essential biomolecules under starvation [91]. mTORC1 inhibits autophagy through several mechanisms. The most well-characterized target of TORC1 is ULK1/Atg13/FIP200 kinase complex (unc-51-like kinase/mammalian autophagy-related gene 13/focal adhesions kinase family-interacting protein of 200kDa), which have an essential role in the initiation of autophagy [92, 93]. In mammals, TORC1 phosphorylates both, Atg13 and ULK1 (the ortholog of yeast ATG1) subunits to repress ULK1 kinase activity, and thereby inhibit autophagy [94].

1.3.2.2 Upstream of TOR

Transcriptome profiling of yeast cells revealed that inhibition of TORC1 was showing highly similar responses as seen in nutrient starvation and noxious stresses [77, 95, 96].The observation that TOR integrates environmental cues were later on proven by identification and monitoring of Sch9 (S6K1) phosphorylation [97, 98]. To date, it is known that TORC1 activity is regulated in response to at least five major intra- and extracellular cues, namely growth factors, stress, energy status, oxygen and nutrient availability (Figure 5). Many of the upstream signals act, at least in part, through the heterodimer consisting of tuberous sclerosis 1 (TSC1) and TSC2. TSC1/2 is upstream of mTORC1 and negatively regulates mTORC1 by inactivating the GTPase Ras homolog enriched in brain (Rheb) [99, 100]. The adenosine monophosphate-activated protein kinase (AMPK) is activated in response to hypoxia or low cellular energy status (high AMP/ATP ratio) and inactivates mTORC1 by phosphorylation of either TSC2 [100] or the raptor component [101]. Amino acid-dependent activation of mTORC1 acts independently of TSC1/2, but requires the Rag GTPases. Rag GTPases interact with mTORC1 through the raptor component causing a translocation of mTORC1 to lysosomes, where the Rag GTPases reside [102, 103].

1.4 *Chlamydomonas* – a convenient model to study TOR function in a photosynthetic organism

The high degree of conservation of TOR proteins throughout the eukaryotic kingdom was leading to the identification of a TOR homolog in plants [104] and a subsequent identification of TOR in *Chlamydomonas reinhardtii* [46]. In addition orthologs of some of the TOR complex components, namely raptor and LST8, were also identified in plants and in the *Chlamydomonas* genome (Table 1) [105]. The group of Crespo demonstrates that CrTOR and CrLST8 exist in high-molecular-mass complexes that associate with microsomal membranes in high abundance in the peri-basal body

region. In contrast to its yeast and mammalian counterparts, there is no clear evidence of TORC2 in *Chlamydomonas* or plants to date, especially because specific components, such as rictor or mSin1 (Table 1), seems to be missing from the genomes of photosynthetic organisms. However, due to the identification of the shared TOR interacting partner, LST8, in *Chlamydomonas* and *Arabidopsis* it might be possible that photosynthetic eukaryotes still possess a functional equivalent of TORC2 [105, 106].

Although TOR was identified in plants more than 10 years ago, the elucidation of the molecular functions and dynamic regulatory mechanisms of this kinase lags strongly behind that of yeast and mammalian systems. This was mainly caused by the lack of molecular and biochemical assays for endogenous TOR kinase activity, the embryo lethality of null *Arabidopsis tor* mutants and the prevailing perceived rapamycin resistance of land plants [104, 107]. Therefore, the finding that growth of *Chlamydomonas* is sensitive to rapamycin, establish this unicellular green alga as an exquisite model system for studying TOR signaling in photosynthetic eukaryotes.

Similar to yeast, *Chlamydomonas* cells that lack FKBP12 (*rap2* mutant) are viable and resistant to rapamycin [43, 46]. This shows on the one hand the unique mode of action of rapamycin and on the other hand that the specific function of FKBP12 as a mediator for rapamycin toxicity is also conserved in *Chlamydomonas*. Phylogenetic analysis demonstrate that the CrTOR kinase is structurally more related to AtTOR than TOR proteins from non-photosynthetic organisms (Figure 2), whereas FKBP12 is more distant to plants than human and yeast homologs [46]. This might explain the higher sensitivity of *Chlamydomonas* to rapamycin in contrast to plants. Only recently it has been shown that, contrary to the long-standing opinion, TOR activity can be inhibited by rapamycin in plants, but only by using very high concentrations (10 μM) and when added to liquid cultures of *Arabidopsis* mesophyll protoplasts or seedlings [108]. In contrast to this, the concentration of rapamycin required to potently inhibit growth of *Chlamydomonas* cells was found to be 0.5 μM [46], which is still about 5 times higher than the concentration employed in yeast [109]. In addition, the growth of *Chlamydomonas* is not fully arrested by rapamycin [46]. The need of a higher concentration and the not fully arrested growth phenotype might be explained in part by the absence of a glutamine residue at position 53 in the drug binding pocket (with respect to the human FKBP12) of the *Chlamydomonas* FKBP12 [46]. It was therefore assumed that this reduces the affinity of FKBP12 to rapamycin. This assumption was supported by several observations. First, expression of the *Chlamydomonas* FKPB12 in the yeast *fpr1* mutant (lacking FKBP12 protein) shows also a reduced sensitivity to rapamycin (a reduced growth with no complete growth arrest). Second, expression of two different mutations of FKBP12 (amino acid substitution at either position 52 and 54 or 52 and 53) displays an increased affinity to rapamycin in both FKBP12 mutant strains, *fpr1* (yeast) and *rap2* (*Chlamydomonas*). But, while these two mutant FKBP12s confer complete sensitivity in yeast, they do not in *Chlamydomonas* [46]. Accordingly, it can be

assumed that either rapamycin-insensitive TOR functions might control *Chlamydomonas* cell growth or that *Chlamydomonas* has regulatory mechanisms that, at least in part, can bypass TOR inhibition to promote cell cycle progression.

Furthermore, it has been suggested that the function of TOR in the regulation of protein synthesis could be also conserved in *Chlamydomonas*, as it was shown that TOR controls phosphorylation of BiP (an endoplasmic reticulum chaperone) through the regulation of protein synthesis [110]. In addition, it has been shown that either rapamycin or nutrient starvation cause an increase in vacuole size that comes along with induced autophagy, which, in turn, suggests that TOR might be an integrator of nutrient availability and as a result modulates autophagy also in this green alga [111, 112]. Only one year ago, the study of Lee and Fiehn presents a first approach to identify the response on primary metabolism of *Chlamydomonas* to inhibition of TOR by rapamycin [113]. Their results showed that treatment of unsychronized *Chlamydomonas* cells with rapamycin induces massive changes in primary metabolism, including an accumulation of TCA cycle intermediates, a strong decrease of phosphorylated sugars and an increase of most amino acids by longer exposure.

Although recent breakthroughs in the plant field, as the rapamycin sensitivity and the existence of inducible RNA interference (RNAi) At*TOR* lines [108, 114], provide invaluable genetic and chemical tools to deciphering the TOR signaling networks in plants, *Chlamydomonas* as the simpler unicellular version of a photosynthetic organism can contribute significantly to elucidate TOR functions in photosynthetic eukaryotes.

1.5 Systems biology for comprehensive analysis of growth

Signaling pathways control almost every aspect of cell life and the response of organisms to their environment. The objective of discovery science is therefore to define all of the components in a biological system to understand all of the genotype-phenotype relationships at the levels of genes, transcripts, proteins and metabolites [115]. Technological breakthroughs in the last years allow simultaneous determination of thousands of genes, transcripts, proteins and metabolites with high-throughput techniques and analytical tools, which have advanced our understanding of biological processes [116]. However, any single ‘omics’ approach might be insufficient to characterize the complexity of biological systems as a ‘whole’ [117]. Therefore, a central task of systems biology is to gather information from each of the distinct levels (genes, transcripts, proteins and metabolites) and integrate the individual ‘omics’ datasets to ultimately formulate mathematical models that describe the structure of the system and its response to several external stimuli [118]. Hence, systems biology combines integrative experimental and theoretical approaches (bioinformatics, computational methods) [115]. Thereby, integration of all these information for a biological

systems to unravel all biological networks, architecture and the principles responsible for its behavior is the most challenging aspect in systems biology [115]. The successful integration of data will depend on a well-designed experiment, statistical analysis and correct interpretation of the results. For the comprehensive analysis of large-scale 'omics' studies the use of bioinformatics tools is inevitable to manage various types of large-scale dataset efficiently and extract valuable knowledge [119]. In the past years many software packages have appeared, which include tools for network visualization, modeling environments, pathway construction and visualization tools and systems biology platforms [120]. The improvement of such integrative analysis is a key to make biological discoveries, which, in turn, lead to the formation of new models, new predictions and new experiments to test them [118].

Aims of the thesis

Understanding the underlying mechanisms of cell growth and proliferation in plants is a key to provide partial solutions for the most daunting problems faced by our world. As cell growth requires the precise temporal and quantitative coordination of the synthesis of cellular components, we decided to use synchronized cell cultures to include cell cycle-dependent regulations in our analyses. Due to the simplicity to achieve synchronized cell cultures of the photosynthetic model organism *Chlamydomonas reinhardtii*, this green alga was chosen to study metabolic changes during the cell cycle. Accordingly, the first aim was the characterization of metabolic responses of a synchronously growing *Chlamydomonas* culture. Therefore, several developments were required:

1. Characterization of the synchronously growing *Chlamydomonas* culture
2. Adaptation and optimization of methods for high throughput screening of metabolites and lipids
3. Development of strategies and methods for data mining, visualization and interpretation

The TOR-kinase, as a sensor of growth stimuli and a central regulator of growth, is an important key to understand growth regulation. The possibility that TOR can be inhibited by the antibiotic rapamycin provides an invaluable chemical tool to study TOR function. Due to its natural sensitivity to rapamycin *Chlamydomonas reinhardtii* provides an optimal model organism to deciphering the TOR signaling network in a photosynthetic eukaryote. The second aim is based on the established synchronized growth system and includes the following points:

4. Investigation of rapamycin stability for the used growth conditions
5. Determination of the rapamycin concentration that is needed to potently inhibit growth of the used *Chlamydomonas* strain without introducing toxic side effects
6. Cytological characterization of changes within the cell cycle caused by rapamycin treatment
7. Characterization of metabolic response to rapamycin inhibition of a synchronously growing *Chlamydomonas* culture

2 Material and Methods

2.1 Material

2.1.1 Chemicals

Unless otherwise stated, all chemicals were of high quality and ordered from the companies Merck (Darmstadt, Germany), Sigma Aldrich (Munich, Germany), Roth (Karlsruhe, Germany), Millipore (Schwalbach, Germany), Biosolve (Valkenswaard, Germany) or VWR (Darmstadt, Germany). All general solutions were prepared with double deionized water (ddH_2O) obtained through a Nano-Pure water purification system (Millipore). Rapamycin was purchased in a high purity degree from LC Laboratories (Boston, USA) and working solutions were always prepared freshly.

2.1.2 Lab equipment

The used lab equipment is listed in Table 2. Standard laboratory equipment (e.g. balance) is not listed.

Table 2. Technical equipment

Equipment	Model/Company
Vacuum Centrifuge	Sartorius CP
UV VIS Photometer	Seiko Ultraspec 2000
NanoDropTM 1000 Spectrophotometer	Thermo Fisher Scientific
Coulter Cell Counter	Beckman Z2 Coulter
Orbital shaker	INFORSYS systems
Absorbance Microplate Reader	ELx808, BioTek
GC and Autosampler	Agilent series 6890/7686
GC Column	DB-35MS
Time-of-flight MS	Leco Pegasus 2
C_8 reverse phase column	Waters, 100mm×2.1mm×1.7µm particles
UPLC	Acquity, Waters
Exactive-FT/MS	Thermo Fischer Scientific
Epi-fluorescence microscope	BX51, Leica
Recirculating temperature control	Julabo FL300
Biostat B-DCU tower	Sartorius

2.1.3 Used *Chlamydomonas reinhardtii* strains

The Chlamydomonas reinhardtii wild type strain CC1690 (mt+; Sager 21 gr) was obtained from the Chlamydomonas Resource Center (University of Minnesota, USA) and was used for all experiments, unless otherwise noted.

2.1.4 Fermenter system for synchronization of *Chlamydomonas* cultures

For synchronization of *Chlamydomonas* with used a custom made fermenter system ("Glasbläserei Müller", Berlin, Germany). A schematic of the fermenters used in these experiments is shown in Figure 6. The advantage of using this system is the constant temperature regulation. For this reason the fermenters consist of double-wall glass vessels, which can be filled with water. Moreover, two glass tubes inside the fermenters serve for exposure to gas and cell harvesting. The glass tube for the cell harvesting is connected to a tube system, which allows, next to the sampling, the dilution of the culture. By using peristaltic pumps culture is first pumped out and afterwards autoclave-sterilized medium is pumped in. In addition to the bubbling by gas supply, the cultures were properly mixed by magnetic stirring.

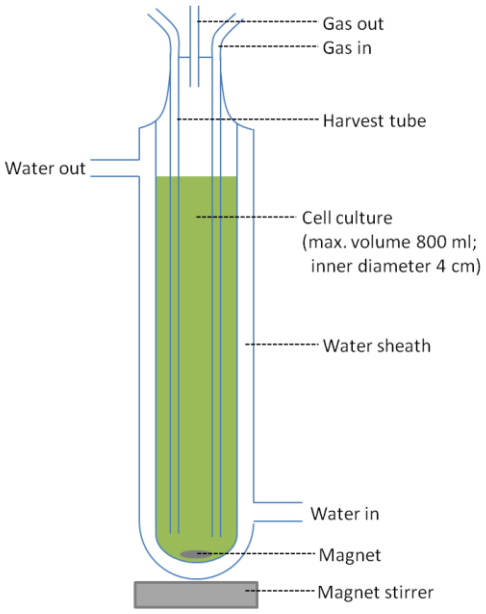

Figure 6. Schematic of a fermenter

2.1.5 Growth media

For cultivation of *Chlamydomonas* pre-cultures and synchronization we used the Sueoka's high salt medium (HSM) [121]. If Chlamydomonas was grown on solid medium, we used either HSM or TRIS-Acetate-Phosphate (TAP) medium [122]. The stock solutions and media were prepared as described in table 3 – 6. In case of solid medium 1.5% agarose and 0.4% Yeast extract were added. Before use the medium was autoclaved and afterwards stored at room temperature and darkness. Medium was always prepared shortly before use. For Hutner's trace solution [123] the advertised solutions were mixed together, heated to 100 °C, and 50 g of EDTA dissolved in 250 ml H_2O was added. After cooling to 70 °C, the pH was adjusted to 6.7 with hot KOH solution. The solution was allowed to cool, and left to oxidize for 1 - 2 weeks with constant stirring. A brown precipitate containing Fe3+ was removed by filtration, and the filtrate stored in the dark at -20 °C.

Table 3. Salts solution (also known as Beijernick's solution)

	TAP salts	HSM salts
NH_4Cl	15 g	100 g
$MgSO_4$ x $7H_2O$	4 g	4 g
$CaCl_2$ x $2H_2O$	2 g	2 g
	Water to 1 liter	Water to 1 liter

Table 4. Phosphate solution

K_2HPO4	288 g
KH_2PO4	144 g
	Water to 1 liter

Table 5. Hutner's trace elements

	amount	water
$ZnSO_4$ x 7 H_2O	22 g	100 ml
H_3BO_3	11.4 g	200 ml
$MnCl_2$ x 4 H_2O	5.06 g	50 ml
$CoCl_2$ x 6 H_2O	1.61 g	50 ml
$CuSO_4$ x 5 H_2O	1.57 g	50 ml
$(NH_4)_6Mo7O_{24}$ x 4 H_2O	1.10 g	50 ml
$FeSO_4$ x 7 H_2O	4.99 g	50 ml

Table 6. Composition of final culture medium

	TAP	HSM
Tris	2.42 g	-
Salts solution	25 ml	5 ml
Phosphate solution	0.375 ml	5 ml
Hutner's trace	1 ml	1 ml
Glacial acetic acid	1 ml	-
	Water to 1 liter	Water to 1 liter

2.1.6 Software

The commercial available software tools that were used for data analysis and visualization are listed in

Table 7. List of used software

Function	Software	Version	Source
Cell counter control	Coulter Multisizer Z2 Accucomp	3.01a	Beckman Coulter
Control and data storage for NanoDrop	NanoDrop ND-1000	3.7.1	NanoDrop Technologies
General data analysis	Office Excel	2007	Microsoft
	SigmaPlot	11.0.0.75	Systat Software
Image analysis	ImageJ	1.44p	[124]
Metabolite analysis	Chroma Tof GC	3.32	LECO, Pegasus
	msMatch		
Lipid analysis	Xcalibur	2.10	Thermo Scientific
	CoMet	2.0	Progenesis
	GoBioSpace		[125]
Statistical analysis and data visualization	MultiExperiment Viewer (MeV)	4.8.1	[126]
Image editing	Inkscape	0.46	http://tavmjong.free.fr/INKSCAPE/

2.2 Methods

2.2.1 Growth conditions

Chlamydomonas reinhardtii cells can be stored for several weeks on solid TAP or HSM plates in continuous light (30 µE m^{-2} s^{-1}) and room temperature (RT).

2.2.1.1 Growing Chlamydomonas pre-culture in flasks

Each experiment was started with preparation of a pre-culture by taking cells from solid plates and transfer them to either HSM or TAP medium under sterile conditions. Pre-cultures were grown on rotary shaker with a speed of 120 rpm at 24 °C under 100 µE m^{-2} s^{-1} continuous light. Under those conditions cells were allowed to grow for several days up to a cell density of 2 – 5 x10^6 cells / ml.

2.2.1.2 Growing of Chlamydomonas on solid plates with rapamycin

For plate experiments, rapamycin was always added shortly before use in the indicated concentrations, unless stated otherwise. If required, rapamycin was added to the medium after agarose was dissolved and the medium had a temperature of 30 – 40 °C. 10 µl of 10-fold dilutions of exponential growing *Chlamydomonas* culture were spotted onto the fresh plates under sterile conditions and allowed to dry. Plates were sealed and cells were grown under continuous light (30 µE m^{-2} s^{-1}) and RT up to 8 days with detailed documentation.

2.2.1.3 Synchronization of Chlamydomonas liquid cultures in fermenters

For synchronization, a pre-culture growing in HSM was diluted in fresh HSM and transferred to the fermenter. Synchronization was achieved by growing the *Chlamydomonas* culture under 12:12 h light-dark regime at 200 µE m^{-2} s^{-1} and a temperature of 34 °C, if not stated otherwise. Furthermore, the cell culture was continuously aerated and mixed vigorously with filtered 2 - 3% CO_2 enriched air and stirred with a magnetic stir bar at the bottom of the fermenter. At the end of each dark phase the culture was diluted to a cell number of 1 x10^6 cells / ml with minimal perturbation by using a tube system in combination with peristaltic pumps, which allows to first pump a distinct amount of culture out and afterwards pump in autoclave-sterilized medium. At the end of the third dark period synchronous experimental cultures were started by diluting the culture to 1 x10^6 cells / ml in fresh HSM and separating the culture to 6 fermenters. Rapamycin was freshly prepared by dissolving in 100% ethanol and added to three of the fermenters in a final concentration of 5 µM (if not stated otherwise) with the onset of light. At the same time an

equivalent volume of 100% ethanol was added to the other three fermenters, which serve as control. Samples were taken at 15 time points (TP) covering the entire cell cycle, starting from 15 min after treatment/onset of light until the end of the dark phase (TP 24 h) to monitor the following parameters: cell number (per ml), cell volume (μm^3),cell size distribution, mitotic state (percent of divided cells), DNA content (µg / ml), chlorophyll (a + b) (µg / ml and µg / 10^6 cells), starch (nmol glucose / ml, nmol glucose / µg chlorophyll and nmol glucose / 10^6 cells), primary metabolites and lipids (**total amount** as peak height / ml and **cellular amount** as peak height / µg chlorophyll).

2.2.2 Harvesting of Chlamydomonas cells

Samples were taken with a syringe through the inner glass tube of the fermenter (Figure 6). To partially compensate the increase of cells during the experiment with synchronized *Chlamydomonas* cultures the sampling volume was lowered with ongoing time of the cell cycle in the following way: 10 ml at TP 0.25 – 4 h, 8 ml at TP 6 – 8 h, 5 ml at TP 10 – 24 h. Cells were distributed to collection tubes or Eppendorf tubes and pelleted by centrifugation for 5 min at 4500 x g. The supernatant was discarded and the cell pellet was immediately frozen in liquid nitrogen and stored at -80 °C.

2.2.3 Determination of cell cycle parameters

For determination of changes in the cell cycle due to TOR inhibition by rapamycin different cell cycle parameters were measured. Cell number and cell volume will give information about growth and cell proliferation and additionally the timing of daughter cell (DC) release. Moreover, DNA content was measured as a marker for S phase and the percentage of divided cells was monitored as a marker the mitotic state.

2.2.3.1 Determination of cell number and cell size

Cell number and cell volume were estimated with a Z2 Coulter Particle Count and Size Analyzer (Beckman Coulter). In principle it measures changes in the electrical conductivity of a small volume of electrolyte as cells displace electrolyte. Depending on the cell density samples were diluted between 1:10 to 1:100 in Isoflow Sheath Fluid (Beckman Coulter) and measured in a size range of 30 – 1900 μm^3.

2.2.3.2 Determination of total DNA content

For determination of the total DNA content, 10 ml cell pellets were extracted using the CTAB method as described by Doyle and Doyle [127]. 800 µl of CTAB buffer (2% CTAB, 1.4 M NaCl, 100 mM Tris-HCl pH 8, 20 mM EDTA, 0.2% β-mercaptoethanol, 0.1 mg/ml proteinase K) was added to the frozen pellet and the samples were incubated for 1 h at 60 °C. 800 µl chloroform:isomylalcohol (24:1) were added and the sample carefully mixed by inversion. Insoluble material was removed by centrifugation at 10 000 x g for 10 min at 4 °C. The upper phase was transferred to a new Eppendorf tube, and 10 mg RNase per ml were added. After incubation at 37 °C for 30 min, samples were stored on ice for 5 min. DNA was precipitated with 600 µl of isopropanol and 50 µl 7.5 M ammonium acetate for 1 h at -20 °C. After centrifugation at 10 000 x g for 10 min, the supernatant was removed carefully and the pellet was washed with 70% ethanol, centrifuged at 10 000 x g for 10 min at 4 °C, and air-dried at room temperature. DNA was finally resuspended in 50 µl sterilized water and quantified using NanoDrop Spectrophotometer and stored at -20 °C.

2.2.3.3 Determination of mitotic state

The mitotic state was determined according to Umen *et al* [128]. Cells were fixed with PBS buffer containing 2% glutaraldehyde and 300 – 500 cells were examined microscopically. The percentage of cells with cleavage furrows was scored as the mitotic fraction.

2.2.3.4 Determination of commitment point

Determination of commitment point was done accordingly to Oldenhof *et al.* [38]. In brief, beside the direct measurement of cell number and cell size at the indicated TPs, aliquots of the culture were taken at distinct TPs and placed in the dark and after 12 -16 h the number and volume of the released DCs was measured. The ratio of DCs per mother cell (MC) was then plotted as a function of time or of the corresponding average of the MC volume. The time point and cell volume at which a ration of two DCs per MC was achieved, was taken as in indicator for when cells had passed the first commitment point.

2.2.4 Extraction of chlorophyll, lipids and primary metabolites

Primary metabolites, chlorophyll and lipids were extracted with minor changes according to a protocol described previously [125]. The frozen cell pellet was resuspended in 1 ml of pre-cooled

(-20 °C) homogenous MTBE-extraction buffer (methanol:methyl-tert-butyl-ether (1:3) mixture, Biosolve, Netherlands). Resuspended cells were incubated for 2 hours in a shaker at 4 °C, followed by 10 min ultrasonication in a water bath on ice. 500 µl of UPLC grade methanol:water (1:3) (Biosolve, Netherlands) was added to the homogenate and subsequent vortexed and centrifuged for 5 min at 4 °C in a table top centrifuge. The addition of the methanol:water mix results in a clear separation of an organic upper phase containing lipids and chlorophyll and an aqueous lower phase containing the polar and semi-polar metabolites. The MTBE-extraction buffer contains ^{13}C-sorbitol as an internal standard for the polar phase and 1,2-diheptadecanoyl-sn-glycero-3-phosphatidylcholine as a standard for the non-polar, organic phase, which were afterwards used for the standardization of technical MS-measurement errors. First the upper organic phase was transferred to a new Eppendorf tube and then the lower polar phase. The solutions were dried down in a SpeedVac concentrator and stored at -80 °C until measurement. The remaining pellet, containing starch and proteins, was frozen in liquid nitrogen and stored at -80 °C until further extraction. In addition, this extraction procedure was always performed with empty, sample-free Eppendorf tubes (method blank) to document contamination resulting from the analytical process.

2.2.5 Metabolite profiling

Mass spectrometry techniques can be coupled to a number of pre-fractionation methods to reduce the complexity of samples. The used combinations here are GC-Tof-MS for primary metabolite profiling and UPLC-FT-MS for lipid profiling.

2.2.5.1 Determination of metabolites using GC-Tof-MS

In a first step carbonyl groups were methoxymized by adding 10 µl of a solution of 40 mg methoxyamine-hydrochloride in 1 ml pyridine to the dried extract and heated for 90 min at 30 °C. In a second step acidic proton moieties are then derivatised with 90 µl N-methyl-N-trimethylsilyltrifloracetamide (MSTFA) for 30 min at 37 °C. The MSTFA contains 13 fatty acid methyl esters (FAMEs) with different chain length as retention time standards. 2 µl of the derivatisation mixture were injected onto the GC-column and measured as described previously [129]. All chromatograms were processed using the Pegasus ChromaTOF software as described by Krall *et al.* [130]. Retention index calculation and peak annotation were performed using msMatch (Steinhauser *et al*.,manuscript in preparation). For the annotation of compounds the exported spectral deconvolutions of peaks were compared with spectra derived authentic chemical standards in highest purity available. This reference library contains about 3100 evaluated spectra of structurally resolved (known) chemical compounds (standards) and more than 250 evaluated

spectra of structurally unresolved (unknown) compounds derived from *Arabidopsis thaliana*. For the peak annotation the following factors have been considered: variations in the retention time, similarity in spectra as well as in the fragment pattern, the peak height and the rank of specific masses. All these processing factors result finally in a so-called "matching factor", which defines how well a spectrum derived from a sample under investigations corresponds to a reference spectrum. For the quantitative comparison the peak height of the unique mass (if existing) was extracted from the spectrum. This value together with the matching factor for each compound was exported as an Excel-file. All compounds were manually checked to address ambiguous assignments and to facilitate high-quality peak annotations.

2.2.5.2 Determination of lipids using UPLC-FT-MS

For lipid analysis [125], the dried pellets were resuspended in a mixture of acetonitrile:isopropanol (7:3) (Biosolve, Netherlands), briefly centrifuged and separated on a reverse phase C_8 column (100mm×2.1mm×1.7µm particles, Waters), using a Waters Acquity UPLC system. The two mobile phases were water with 1% 1 M ammonium acetate, 0.1% acetic acid (Buffer A,), and acetonitrile:isopropanol (7:3) containing 1% 1 M ammoniumacetate, 0.1% acetic acid (Buffer B). The gradient separation, which was performed at a flow rate of 400 µl/min, was: 1 min 45% A, 3 min linear gradient from 45% A to 35% A, 8 min linear gradient from 25% to 11 % Buffer A, and 3 min linear gradient from 11% to 1%Buffer A. After washing the column for 3 min with 1% Buffer A the buffer was set back to 45% Buffer A and the column was re-equilibrated for 4 min (22 min total runtime). The UPLC solvents together with the ESI-source ionize the molecules either positively or negatively and allow them to enter the mass spectrometer after eluting from the column [131]. The mass spectra were acquired by an FT-MS in positive and negative mode (Exactive, Thermo-Fisher, Bremen, Germany). The spectra were recorded using altering full scan and all-ion fragmentation scan mode, covering a mass range from 100 – 1500 m/z [125]. The resolution was set to 10,000 with 1 scan/sec. The capillary voltage was set to 3 kV with a sheath gas flow value of 60 and an auxiliary gas flow of 35. The capillary temperature was set to 150 ˚C, while the drying gas in the heated ESI-source was set to 350˚C. The skimmer voltage was held at 25 V while the tube lens was set to a value of 130 V. The spectra were recorded from min 1 to min 20 of the UPLC gradients. Obtained raw-chromatograms were further processed using Excalibur software version 2.10 (Thermo Fisher) and Progenesis CoMet software (http://www.nonlinear.com/progenesis/qi/). Peaks from raw chromatograms were first picked, then aligned by their parent masses and a final alignment file of all chromatograms was the output, which contains information about m/z-ratio, retention times and retention time deviations for each annotated peak. The assigned peaks were annotated to known compounds with sum formulas, according to retention time and m/z-ratios. On this subject we should note that for some lipid

species we detected more than one peak with the same m/z but different retention times. In this case we named the lipid species with the letter A, B, C, etc. The appearance of different isoforms for those lipid species can result from either a different fatty acid composition or fatty acids with different positions of the double bounds. The obtained data matrix was then further processed for normalizations and statistical analysis.

2.2.6 Determination of the chlorophyll content

The upper organic phase of the MTBE extract as described above contains chlorophyll. An appropriate volume of this phase was mixed with 90% methanol and measured with an UV-VIS spectrometer at a wavelength of 665 nm and 652 nm to distinguish between chlorophyll a and chlorophyll b. The absorption value was kept in the linear range between 0.1 and 1 for valid concentration calculation. The chlorophyll a and b content, and also the total chlorophyll content were calculated according to the following formulas [132].

$$Chl_a = 16.82A_{665} - 9.28A_{652} \quad (3)$$

$$Chl_b = 36.92A_{652} - 16.54A_{665} \quad (4)$$

$$Chl_{a+b} = 0.28A_{665} + 27.64A_{652} \quad (5)$$

2.2.7 Extraction and determination of the starch content

For the determination of the starch content, we optimized the standard protocol from Smith and Zeeman [133] for the use of *Chlamydomonas*. The frozen cell pellet was first washed with 80% ethanol, incubated for 10 min at 80 °C and centrifuged at 5000 rpm for 10 min at room temperature. Afterwards the pellet was dissolved in 250 µl sterile water. Then 250 µl 100 mM sodium acetate was added and starch was hydrolyzed by heating for 3h at 99 °C. The dissolved starch was digested into its glucose monomers over night with an enzyme mix of α-amylase (4.2 units per sample) and α-amyloglucosidase (10 units per sample). The digested extract was centrifuged and the supernatant with the starch-derived glucose monomers was dissolved in 100 mM HEPES-buffer (pH 7) that contained 5 mM $MgCl_2$, 60 mg/ml ATP, 36 mg/ml NADP and glucose-6-phophate-dehydrogenase (1 unit per sample). The baseline was measured at 340 nm and the subsequent addition of hexokinase started the reactions (see below) and the increase of $NADPH+H^+$ was measured at 340 nm with a plate reader in 96-well formats.

1. Glucose + ATP → Glucose-6-Phsophate + ADP (Hexokinase)
2. Glucose-6-Phosphate + NADP + H_2O→ Gluconate-6-Phosphate + NADPH + $2H^+$ (Glucose-6-phosphate-dehydrogenase)

The difference of the maximum value at 340 nm, which should not exceed the linear range of 1, and the baseline is equivalent to the glucose concentration of the digested starch pellet from the MTBE:methanol:water extract. In parallel a glucose calibration curve was measured to determine the glucose concentration in nmol glucose per ml.

2.2.8 Extraction and determination of the protein content

For determination of total protein content, the frozen cell pellet was dissolved in 500 µl IEF buffer (5 M urea, 2 mM thiourea, 2% CHAPS, 15 mM DTT). The samples were incubated for 30 min at room temperature and then centrifuged at 10 000 x g for 5 min. The supernatant, containing the proteins, was transferred to a new Eppendorf tube. Protein concentration was determined by Bradford assay [134].

2.2.9 Determination of rapamycin stability

To test the stability of rapamycin in the used growth medium (HSM), rapamycin concentrations were measured by using UPLC-FT-MS.

2.2.9.1 Experimental procedure

To investigate the rapamycin stability, freshly prepared rapamycin (10 mM in ethanol) was added to HSM to a final concentration of either 0.5 µM or 5 µM. To test the influence of both light and temperature, the rapamycin containing medium (both rapamycin concentrations) was incubated for up to five days at RT and 34 °C and, in addition, in light or dark. Directly after rapamycin addition, five aliquots à 100 µl of the medium from different light and temperature regimes were sampled and directly frozen in liquid nitrogen. The samples were stored at -80 °C until further extraction. The sampling was repeated after 1, 2 and 5 days.

In addition, a dilution series of rapamycin concentration of 500 fM up to 10 µM was prepared. The different concentrations were diluted in acetonitrile:isopropanol (7:3, UPLC grade, Biosolve, Netherlands).

2.2.9.2 Extraction and determination of rapamycin

The frozen 100 µl medium were dissolved in 1 ml of pre cooled (-20 °C) homogenous MTBE-extraction buffer (methanol:MTBE (1:3) mixture) and the further extraction was performed as

described in chapter 2.2.4. After phase separation with methanol:water 500µl of the upper organic phase, which contained the rapamycin, were transferred to a new Eppendorf and dried down in SpeedVac concentrator. The dried pellets were resuspended in a mixture of acetonitrile:isopropanol (7:3), briefly centrifuged and separated on a reverse phase C_8 column using a Waters Acquity UPLC system as described in chapter 2.2.5.2.

2.2.10 Filtering of the raw data

To remove the noise and contaminants from the primary metabolite and lipid data three filtering criteria were applied to the raw data. The first filter concerns contaminants. Therefore, every metabolite or lipid, where the average of the peak height over all samples was lower than the average of the peak height of the method blanks, was removed from data. In a second step, metabolites or lipids where 50% of the values (peak height) were below 5000 (primary metabolite) or 1000 (lipids) counts, respectively, were removed from the data. Third, metabolites or lipids, which had more than one TP with more than 3 missing values in their 6 replicates, were removed.

2.2.11 Normalization of metabolite data

To compare the concentration of different compounds under different growth conditions it is necessary to normalize the data to the same cell amount. In case of plants, especially when whole tissues have been extracted, the fresh weight or dry weight of a sample serves as a standardizing parameter [129, 135]. However, the determination of dry weight or fresh weight of samples of microorganisms from aqueous environments or liquid culture medium, harvested in low amounts, may not be accurate and reliable for data adjustment [136].

In synchronized cell cultures of *Chlamydomonas* normalization to culture volume is often used to determine the increase of various compounds over time [36]. In this study normalization to volume (per ml) was used to analyze the time course of increase of primary and lipid metabolites to identify groups which show a similar temporal pattern within the different conditions.

However, for a quantitative comparison of primary and lipid metabolites between control and rapamycin treatment the normalization to volume is less useful as it does not consider a change in the cell number. Therefore, normalization to cell number would be the most obvious choice. However, during the light phase the cell number remains on a constant level, because newly formed DCs remain surrounded by the MC wall. Only after release of DCs, a difference in cell number is measurable. Therefore, we decided to use the chlorophyll content as a proxy for cell number due to the following reasons:

1. The chlorophyll content increase during the light phase
2. The chlorophyll content increase in the same quantity as the cell number under both, control and rapamycin treatment, conditions

Another advantage of using the chlorophyll content as a standardization parameter is that it can be determined from the same sample as the primary and lipid metabolites by using the MTBE extraction method (see chapter 2.2.4). Therefore it allows also compensating for differences in the sampling volume.

2.2.12 Analysis of the multivariate data

A number of multivariate data analysis tools can be successfully applied for all kinds of -omics data. To facilitate the pattern visualization of large datasets, unpaired t-tests were performed using Excel. Furthermore statistical methods were applied for visualizing changes. In this work, unsupervised statistical methods were used. Unsupervised methods group the samples only according to the information content of the data itself, while supervised methods require a reference data set, where samples are associated with specific features. Among the most commonly used unsupervised data analysis methods are principal component analysis (PCA) and hierarchical clustering analysis (HCA). For PCA and HCA the chlorophyll-normalized data was $\log_2$ transformed.

2.2.12.1 Principal component analysis (PCA)

A PCA analysis is a typical data dimension reduction technique and could be thought of as finding the maximum variance within a large set of samples – also called the principal component. Principal components are formed as linear combinations of the variables to maximize variance of the projected observations [137]. The first principal component describes the largest possible variance. The second principle component is always orthogonal to the first one and describes the second largest variance among the variables. Here, all PCAs were done using the Multiexperiment Viewer [126, 138].

2.2.12.2 Hierachical clustering analysis (HCA)

The hierarchical clustering was done with the Multiexperiment Viewer [126, 139] and is commonly used for analysis of various -omics data. Hierarchical clustering results in creation of a hierarchy of clusters which can be presented as a hierarchical tree. In this work, the Pearson correlation was used. Pearson correlation shows the linear relationship between to data sets. The clustering depends

also on the clustering algorithm which is applied. Here, the average linkage method was used, which defines the distance between groups as the average of the distances between all pairs of individuals in the two groups.

2.2.12.3 Grouping of primary and lipid metabolites according to temporal pattern

To identify the primary and lipid metabolites which start to increase in a similar time frame, the following criteria were used. For each time point the $\log_2$ fold change to the start point TP 0 (TP 0.25 h) was calculated. In addition, the significance of the $\log_2$ fold changes for each time point was determined with an unpaired t-test using Excel. The concentration (per ml) of a compound was considered to be increased in comparison to TP 0 when the $\log_2$ fold change was above 0.5 and the p-value was below 0.05. In addition, it was defined that most of the following time points should meet at least one of previous criteria. Based on the first time point when the compound starts to increase the primary and lipid metabolites were grouped. These groups are referred to as clusters, even though they are not clustered in a classical clustering method.

2.2.12.4 Grouping of primary and lipid metabolites that are shifted in the timing and level of increase after rapamycin treatment

To compare the time course of increase of primary and lipid metabolites under control conditions to that after rapamycin treatment, the same criteria as mentioned above (chapter 2.2.12.3) were used to find the starting point of increase. As a result, we expect three different possibilities for the time factor (T), namely metabolites which show an earlier increase after rapamycin treatment (T-x), metabolites which increase at the same time under both conditions (T0) or metabolites which increase later after rapamycin treatment (T+x).

In addition, we were interested in the total increase, namely the increase between start of the cell cycle (TP 0.25 h) and end of the cell cycle (TP 24 h), of primary and lipid metabolites. Therefore, the $\log_2$ fold changes of the total amount (per ml) between TP 24 h and TP 0.25 h were calculated for rapamycin treated and control cells. Significant differences ($p \leq 0.05$) in the $\log_2$ fold changes between control and rapamycin treatment were determined with an unpaired t-test using Excel. Similar to the time factor we expect three different possibilities for the level factor (L), namely metabolites which increase by a lower level after rapamycin treatment (L-x), metabolites which increase in the same level (L0) or metabolites which increase by a higher level after rapamycin treatment (L+x).

The combination of the three possibilities for each factor (T and L) finally results in nine possible groups (Figure 37 A). These groups are referred to as clusters, even though they are not clustered in a classical clustering method.

3 Results

3.1 Effect of rapamycin on the vegetative cell cycle of *Chlamydomonas*

First research on TOR signaling in *Chlamydomonas* was undertaken by Crespo and coworkers [46]. Within the framework of their studies they showed that rapamycin, a known inhibitor of TOR, causes a clear growth reduction of this unicellular green alga. In contrast to yeast, where the cell cycle is fully arrested in G1 phase upon rapamycin treatment [77], they found that *Chlamydomonas* growth is not fully arrested by this drug. Therefore, we decided to analyze the role of TOR in the *Chlamydomonas* cell cycle in more detail by using a synchronized *Chlamydomonas* cultures.

3.1.1 Establishment of growth conditions for synchronized *Chlamydomonas* cultures

As a first step, we developed growth conditions which allow to achieve a high degree of synchrony and a good reproducibility during repeated life cycles. For this purpose a fermenter system was used. It was known that *Chlamydomonas* can be synchronized by alternating light-dark cycles under photoautotrophic conditions [36]. Important parameters for synchronization are length of light and dark phase, light intensity, temperature and CO_2 concentration. Accordingly, Lien and Knutsen [36] found that at a defined light intensity the temperature is the limiting factor for the exponential increase in biomass. For their system they determined the optimal growth temperature of 35 °C, while a temperature above 36 °C inhibits the process of cytokinesis and sporulation. Additionally, they observed clear differences in growth between two different strains (11-32/90 Gö and 11/32b CCAP). To validate the temperature influence on growth behavior of our experimental *Chlamydomonas* strain (CC1690) we decided to test two different temperatures, 30 °C and 34 °C, while maintaining all the other parameters constant. As a read out for the comparison of those two different temperature settings on growth and synchronization we selected, the cell number, cell size and size distribution. All these parameters were obtained from the 4th synchronized cell cycle using the Z2 Coulter Counter (see chapter 2.2.3.1).

Similar to the results of Lien and Knutsen [36] we found that the higher temperature of 34 °C has a positive influence on strain CC1690 and therefore significantly increases the cell growth (Figure 7 A). We detect a relative increase in cell number of 7.91 ± 0.37 fold at 30 °C whereas the cell number increases 9.71 ± 0.23 fold at 34 °C. The mean cell volume (MCV) does not show a strong difference at the maximum. Comparing each time point (TP) the MCV is lower under 30 °C until 10 h in light. The doubling time (time a cell needs to double in size) for this experiment was 3.51 ± 0.03 h for 30 °C and 3.36 ± 0.12 h for 34 °C. 10 h after onset of light the MCV still increases at 30 °C, whereas it already started to decrease at 34 °C. The decrease in MCV correlates with an

increase in cell number and indicates the sporulation of daughter cells (DCs). The results show that the sporulation is 2 h delayed at 30 °C.

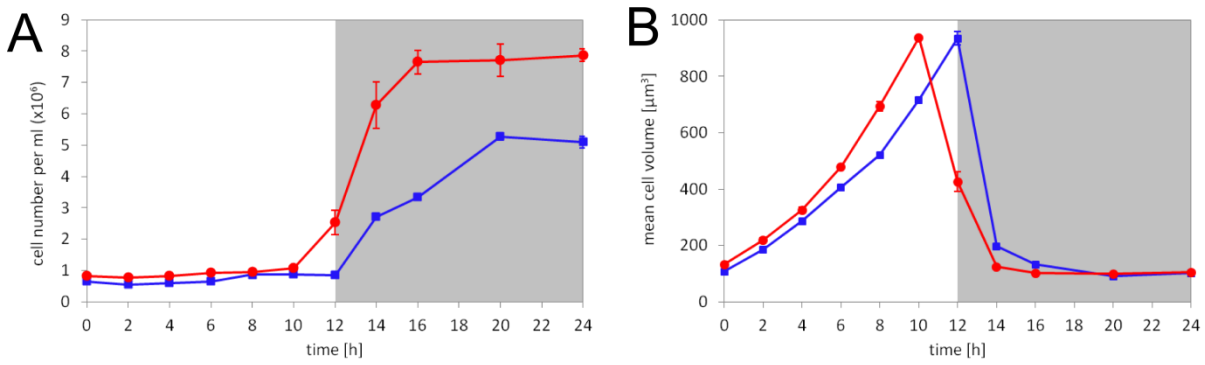

Figure 7. Comparison of cell number and cell size for synchronization at 30 °C and 34 °C
Cell number (A) and mean cell volume (B) measured with Beckman Coulter at indicated TPs for a synchronized culture of *Chlamydomonas* cells. Synchronous cultures were obtained by a 12:12 h light-dark regime at two different temperatures, 30 °C (blue) and 34 °C (red). Dark phase is indicated as a grey background. Data are given as mean ± SD of three biological replicates.

Interestingly, we found a 40% increase in cell number between 6 h and 8 h at 30 °C. To determine if the increase is caused by spontaneous sporulation of DC, accurate cell size distribution data was determined. By using this data, it is possible to distinguish between DC and mother cells (MCs). As can be seen from Figure 8 the synchronized population consists mainly of DCs at the starting- and end point of a 24 h growth cycle. At these TPs the cell size distribution shows a sharp peak at a low cell volume. The dashed line in the plots of Figure 8 displays the border between DCs (left of the dashed line) and MCs (right of the dashed line). Our results show that synchronization at 30 °C indeed leads to a spontaneous early sporulation of a fraction of the cells in the middle of the light phase (6 h and 8 h). Interestingly this phenomenon does not occur at a growth temperature of 34 °C (Figure 8).

This observation is again in full agreement with data from other *Chlamydomonas* strains [30, 36]. Accordingly we confirmed that an intermediate sporulation and a disturbance of the synchronization also occur at lower temperatures for the *Chlamydomonas* strain CC1690. Thus, subsequent experiments were solely conducted at a temperature of 34 °C.

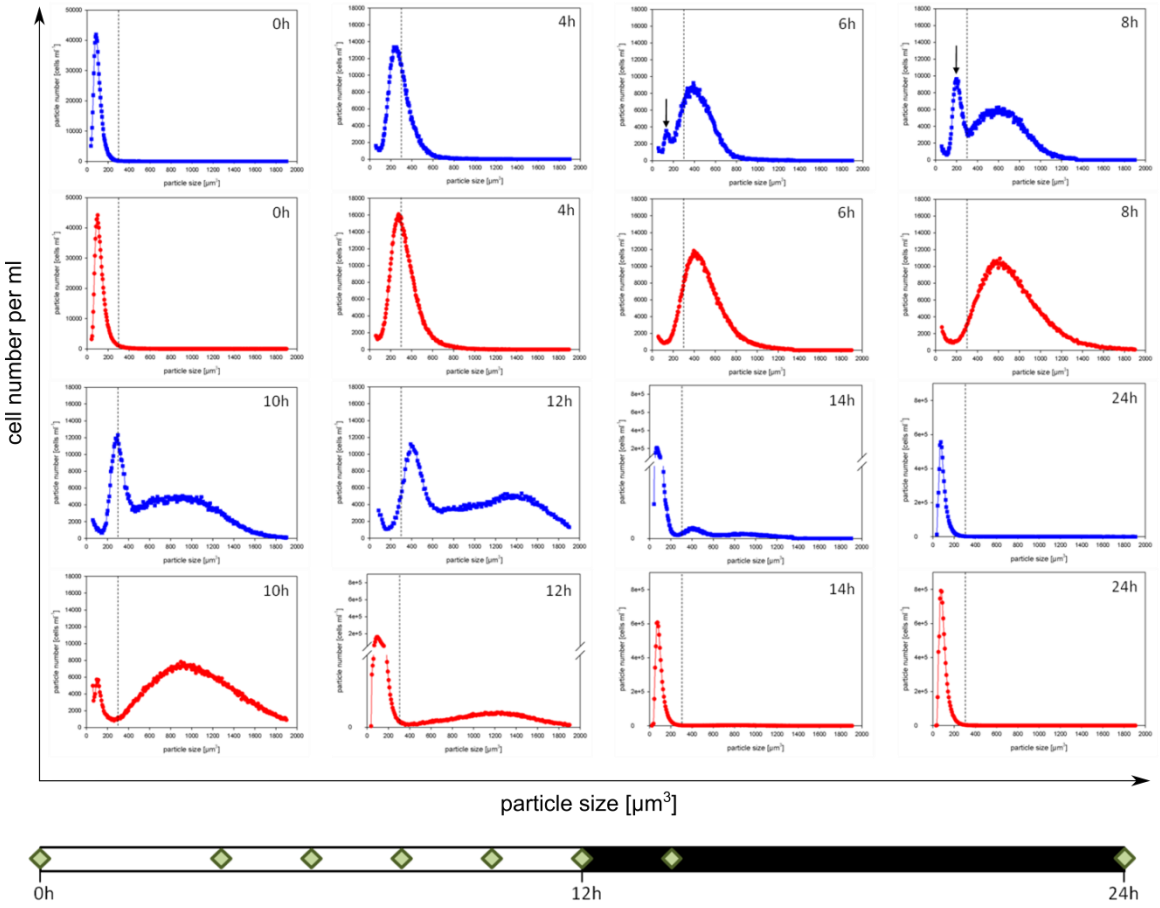

Figure 8. Comparison of cell size distribution between synchronized growth at 30 °C and 34 °C
Cell size distribution measured with Coulter Counter for distinct TP of synchronized culture at 30 °C (blue) and 34 °C (red). The arrow indicates the sporulation of a fraction of cells at 6 h and 8 h. Data represents the mean of three biological replicates. The dashed lines separate the DC and MC. Time line at the bottom displays measured TP (green diamonds) within the 12:12 h light-dark cycle.

3.1.2 Analyzing the physico-chemical properties of rapamycin

The observations of Crespo and coworkers, that the sensitivity and efficiency of *Chlamydomonas* differs from those made in other organisms [46], raised two questions.

1. Is there a concentration which could inhibit the growth of *Chlamydomonas* completely?
2. Is the increased duration of *Chlamydomonas* experiments (days) compared to yeast studies (hours) and therefore the stability of rapamycin the reason for the reduced arrest of *Chlamydomonas* growth?

These issues were investigated by monitoring the growth at different rapamycin concentrations and measuring the rapamycin stability under different conditions.

3.1.2.1 *Higher rapamycin concentrations have a stronger effect on growth inhibition*

To determine if higher concentration of rapamycin might have a stronger effect or can even lead to a full growth arrest, we performed a similar plate experiment as described by Crespo and coworkers [46]. In addition, we investigated the effect of different rapamycin concentration on cultures grown in liquid medium.

3.1.2.1.1 *Influence of rapamycin concentration on plate grown Chlamydomonas cultures*

Serial dilutions of our two lab strains of *Chlamydomonas* (CC1690 and CC503) were spotted on freshly prepared TAP plates containing different concentrations of rapamycin or the drug vehicle (100 % ethanol) alone. Additionally, for better comparison of our results with those already published, Dr. Crespo was so kind to provide us the strains that he used in his initial study (wild type (WT) strain 6C+ and the rapamycin-insensitive *rap2* mutant, which contains a mutation in the rapamycin binding FKBP12 protein coding gene) [46].

Similar to the observations made by Crespo and coworkers [46] we found that incubation with rapamycin inhibited growth efficiently for about 4 days (Figure 9). The highest concentration of rapamycin previously described was 500 nM [46]. We doubled the concentration (1 µM) and additionally tested concentration of 10 µM. Interestingly, even though the extremely high concentration of 10 µM rapamycin cannot fully arrest *Chlamydomonas* growth on plates, we could observe that the higher concentrations clearly increase the inhibitory effect of rapamycin (Figure 9).

Additionally, we also detected different sensitivity to rapamycin for the used strains: The cell-wall deficient strain CC503 displays the strongest growth inhibition, but as this strain also shows a slower growth on control plates (containing ethanol; Figure 9) a clear conclusion for increased rapamycin sensitivity could not be drawn. Besides the cell-wall deficient strain both wild-types and also the *rap2* mutant display an approximately equal growth on the control plates but it became clear that the wild-type strain 6C+ is more sensitive to rapamycin than the strain CC1690 (Figure 9). The finding that both wild-type strains show a different rapamycin-sensitivity was rather unexpected, but might indicate that the uptake in the diverse strains is different. Further we could confirm that the rapamycin insensitive *rap2* mutant shows no sensitivity to rapamycin, even at the highest used concentration (Figure 9).

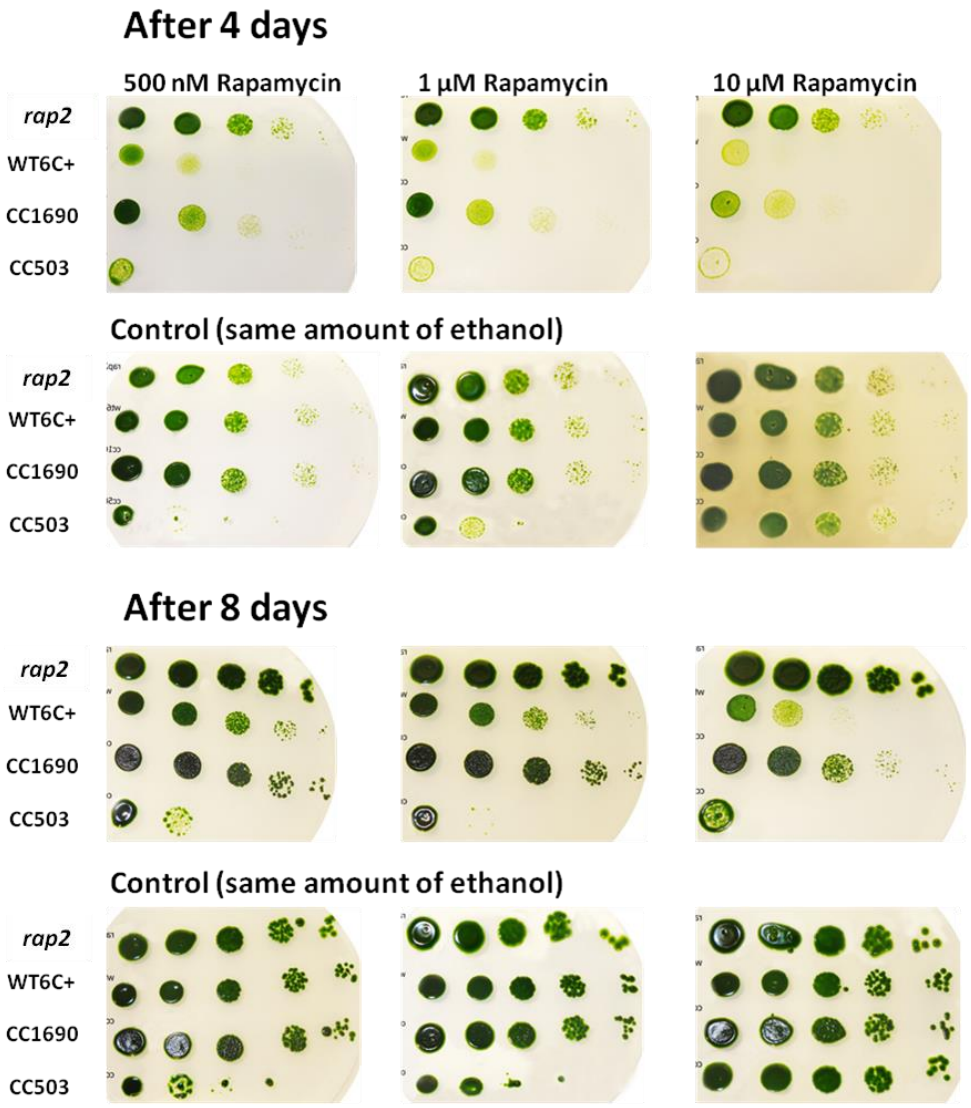

Figure 9. Effect of different rapamycin concentrations on different *Chlamydomonas* strains
All strains were adjusted to the same cell number, subjected to 10-fold serial dilutions and spotted onto TAP plates containing the indicated concentrations of rapamycin or ethanol for the control plates. Plates were incubated at room temperature under continuous light.

3.1.2.1.2 *Influence of rapamycin concentration on liquid grown Chlamydomonas culture*

To monitor the effects of different rapamycin concentrations more precise, we used cultures grown in liquid media, which allow a more accurate and descriptive measurement of cell growth. For these experiments only the preferred *Chlamydomonas* WT lab strain CC1690 was grown in HSM for 9 days at RT at continuous light. During this time, the culture was diluted two times to keep cells in exponential growth. Afterwards, the starting culture was split in several cultures, which contained different concentrations of either rapamycin or the respective drug vehicle as a control. All cultures were adjusted to the same cell number of $5x10^5$ cells / ml. Directly after rapamycin was applied the cell number was measured (TP 0) and again 24 h later (TP 24). The relative

increase in cell number was used to compare the growth inhibitory effect of the different rapamycin concentrations.

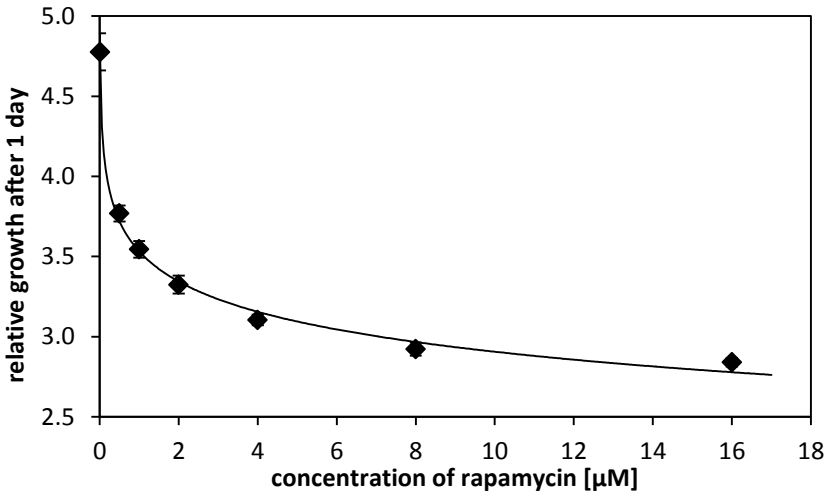

Figure 10. Growth inhibitory effect at different rapamycin concentrations
Here shown is the growth, calculated by cell number measurement, after one day relative to the first measurement, which was made directly after rapamycin addition at different rapamycin concentrations (0 µM, 0.5 µM, 1 µM, 2 µM, 4 µM, 8 µM and 16 µM). Data are given as mean ± SD of 3 technical replicates.

Chlamydomonas shows an exponential response to rapamycin over the tested range of concentrations (Figure 10). The results clearly demonstrate that concentrations higher than 500 nM significantly increase the growth inhibitory effect of the drug, without having obvious negative side effects, as demonstrated by the insensitivity of the rap2 mutant (Figure 9). As a consequence we decided to employ concentration of 5 µM in our further experiments, since this concentration increases the effect more than 2-fold in comparison to 500 nM while concentrations higher than 5 µM do not significantly elevate the growth inhibition.

3.1.2.2 *Rapamycin is degraded in aqueous solutions especially at higher temperatures*

To test the stability of rapamycin a similar plate experiment, as the one described in chapter 3.1.2.1.1, was performed. This time we prepared plates containing rapamycin which were incubated for several days (4 and 10 days) in light at room temperature (RT) before the culture was spotted onto these plates. Results from those plates were than compared to results from freshly prepared plates (0 days, Figure 11).

Incubating rapamycin-containing plates for about 10 days in light, prior to adding *Chlamydomonas*, results in an almost complete loss of the growth inhibitory effect (Figure 11). On the other hand

incubation of cultures on rapamycin-containing plates which have been pretreated for about 4 days (light) shows a similar growth inhibitory effect as can be observed for freshly prepared rapamycin-containing plates (Figure 11). This indicates that between 4 and 10 days something happens to the drug, which clearly affects its activity.

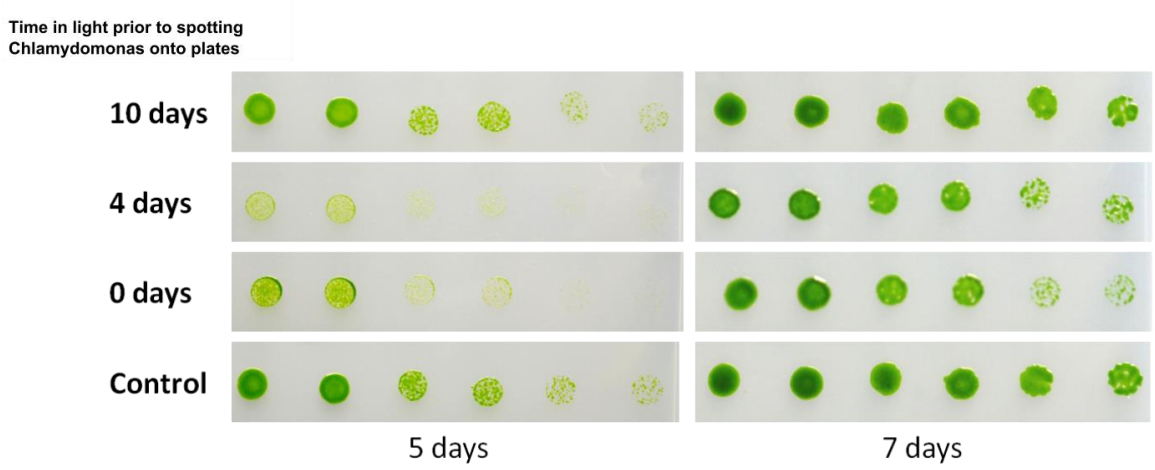

Figure 11. Influence of incubation time on the stability of rapamycin and its growth inhibitory effect
This picture shows the growth of the *Chlamydomonas* strain CC1690 which was spotted in a serial dilution onto TAP plates containing 500 nM rapamycin or the drug vehicle alone (control) after 5 and 7 days. The rapamycin-containing plates were incubated for 0, 4 or 10 days in light at RT before addition of *Chlamydomonas*.

Since the discovery of rapamycin a number of investigators were interested in its quantification. The most common method for quantification of rapamycin is high-performance liquid chromatography (HPLC) using either mass spectrometric or UV detectors.

To set up an accurate quantification procedure we established an UPLC-MS method (see chapter 2.2.9.2). Here we could clearly see that rapamycin can be accurately measured at a retention time of 2.8 min ionizing as two adducts with monoisotopic masses of 931.5895 m/z [M + NH_4] and 936.5449 m/z [M + Na] (Figure 12).

For the quantification assay we prepared and measured a dilution series of rapamycin (500 fM to 10 µM) to determine the linear range of the response curve (Figure 13). A regression coefficient of 0.9963 shows that concentrations from 500 pM (limit of detection, LOD) up to 10 µM are in a good linear range (red line, Figure 13). To test the stability of rapamycin in organic solutions, the diluted samples were stored at 4 °C in the dark and the measurements were repeated. As can be seen from Figure 13 (blue line) similar results were obtained. Thus, rapamycin seems to be stable under these conditions for at least 4 days.

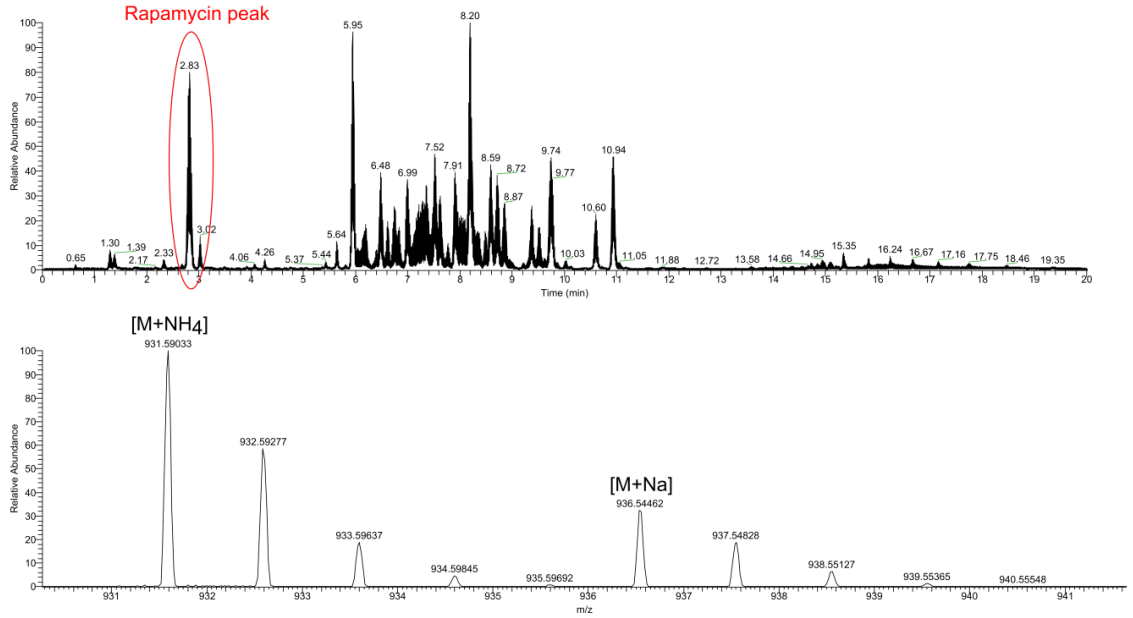

Figure 12. Detection of rapamycin in a LC-MS Chromatogram
Top: Base peak ion chromatogram of a LC run of MTBE extracted *Chlamydomonas* pellet treated with rapamycin. MS run performed in positive mode. Rapamycin peak could be detected at a retention time of 2.83 min. Bottom: Extracted chromatogram showing rapamycin as ammonium and sodium adducts.

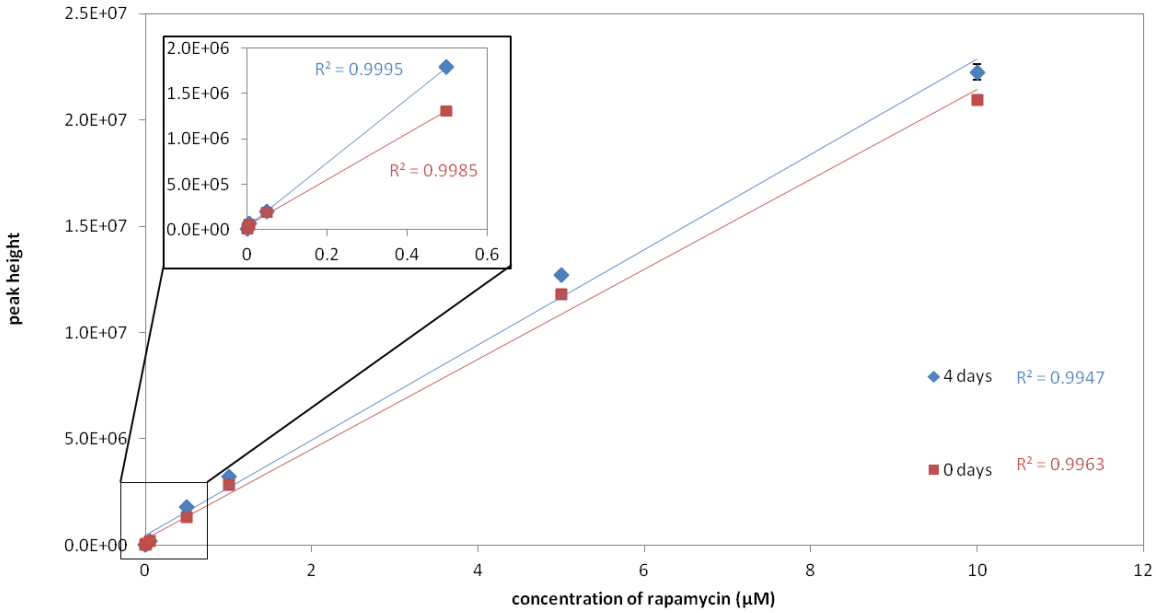

Figure 13. Dilution series of rapamycin
Different rapamycin concentrations (500 pM – 10 µM) were measured with LC-MS. The measurements were performed directly after preparing the dilution series (0 days, red) and then again after 4 days (4 days, blue). Data are given as mean ± SD of 3 technical replicates.

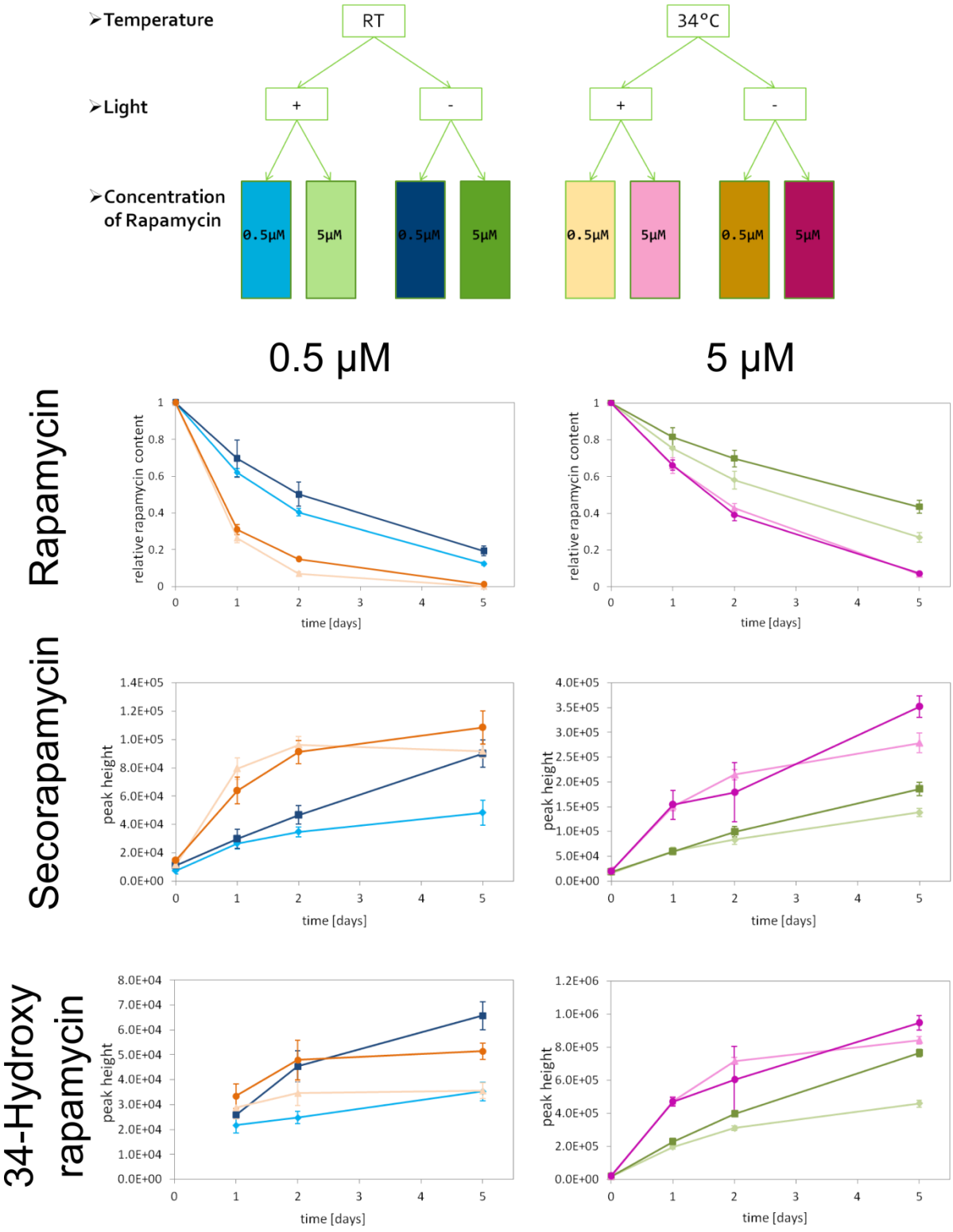

Figure 14. Content of rapamycin and its degradation products over time in HSM
The upper dendrogram shows the different conditions which were used to test rapamycin stability. The diagrams below show the results of LC-MS measurements for rapamycin, secorapamycin and 34-hydroxy rapamycin. In case of rapamycin the concentration is given as relative values based on the first measurement. Results of secorapamycin and 34-hydroxy rapamycin show the peak height per ml at distinct time points. Data are given as mean ± SD of 5 technical replicates.

In a first step, rapamycin stability was determined in the growth medium (HSM) we used for synchronization. To investigate the light sensitivity of rapamycin, we incubated rapamycin containing medium (two different concentrations 0.5 µM and 5 µM) for up to 5 days in light or dark, respectively. As the synchronization experiments were conducted at 34 °C, we additionally tested the influence of temperature on rapamycin stability. Therefore, we performed the same experiments at RT and 34 °C. For better comparison of rapamycin stability we monitored next to the intact molecule the concentration of two known primary degradation products, namely secorapamycin and 34-hydroxy rapamycin [140]

To follow the stability of rapamycin, aliquots from the medium under different light and temperature conditions were taken after 1, 2 and 5 days. Under all conditions a decrease of the rapamycin concentration was visible, but to a different extent in the tested conditions (Figure 14). The results indicate that temperature has a significantly stronger effect on rapamycin degradation than light. The light sensitivity of rapamycin, if at all, is observable at RT, but has only a slight effect at 34 °C. In addition, we observe a proportionally stronger decrease for the more diluted 0.5 µM solution than for the 5 µM solution after 1 day (Figure 14).

As expected, similar to rapamycin the concentrations of secorapamycin and 34-hydroxy rapamycin are stronger effected by temperature than light (Figure 14). Accordingly, higher accumulation of the primary degradation products at 34 °C reflects the stronger decrease of rapamycin at this temperature. An effect of light is not clearly visible for the first two days. After 5 days the two main products exhibit a stronger increase under dark conditions. This is contrary to the observation of rapamycin degradation.

3.1.2.3 *Efficiency of rapamycin decreases with increasing degradation in aqueous media*

For the investigation of the rapamycin effect on synchronous *Chlamydomonas* cells we have to use a temperature of 34 °C to prevent sporulation in the middle of the light phase. Therefore we decided to test the growth inhibitory effect under synchronized conditions for two consecutive synchronization cycles to see if the remaining rapamycin from the first (1^{st}) cycle has still enough activity to cause the same or at least a similar growth inhibition in a second (2^{nd}) cycle. One problem for the investigation of the 2^{nd} cycle was that we had to dilute the culture in the end of the dark phase to avoid cells from stationary phase. With this dilution we would also dilute nearly the whole remaining rapamycin out from the medium. For this reason we decided to split the culture after one synchronization cycle with rapamycin into two cultures after dilution. To one of them we add rapamycin again (Rap+Rap), in the same concentration we used for the 1^{st} cycle and to the other culture we add the drug vehicle alone (Rap+EtOH). For the control culture from the 1^{st} cycle we did the same (Figure 15 A).

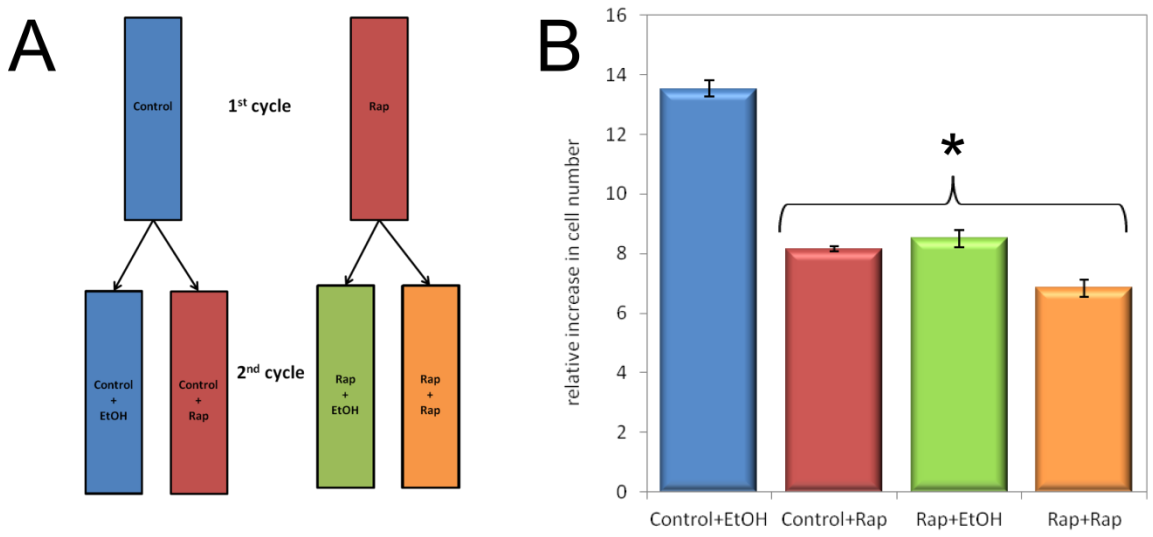

Figure 15. Growth inhibitory effect of rapamycin for two synchronization cycles
(A) Dendrogram shows the experimental design for analyzes of rapamycin effect on two cell cycles. (B) Diagram shows the relative increase in cell number, measured with Beckman Coulter, after 24 h for the 2nd cell cycle. Data are given as mean ± SD for 5 independent, technical replicates. Significant ($p < 0.05$) differences of the rapamycin treated culture to control are indicated with an asterisk.

The data indicate that even after dilution and degradation of rapamycin the remaining rapamycin in the cells is still enough to have a similar growth inhibition in the 2nd cell cycle as in the 1st cell cycle (Figure 15 B). This assumption could be made from the observation that the culture where rapamycin was added the first time (Control+Rap) shows just a slightly stronger reduction in growth of about 2.5% compared to Rap+EtOH. This was interesting as the remaining rapamycin in medium in the Rap+EtOH culture is much less than in the Control+Rap culture due to degradation and dilution of rapamycin. Based on the observed degradation of 40 % after 24 h (Figure 14) and an 8-fold dilution of the culture, we calculated a 90% decrease in the rapamycin concentration. However, this calculation does not include the uptake of rapamycin by the cells. Therefore, we would assume that the remaining rapamycin concentration in the Rap+EtOH culture is less the 0.05 µM. Further we could determine a stronger growth inhibition by adding rapamycin again in the 2nd cycle as the Rap+Rap culture shows the strongest growth reduction, which is about 10% higher compared Control+Rap, indicating that the prolonged application of rapamycin lead to additive growth inhibition

3.1.3 Characterization of the synchronized *Chlamydomonas* culture

After determination of the cellular growth conditions, different cytological parameters were monitored to characterize and validate the synchronized *Chlamydomonas* culture. This is important as the duration of the cell cycle and the degree of synchronization depend on the culture conditions.

As already mentioned above, the cell number increases by a factor of 9.71 ± 0.23 at a temperature of 34 °C. From 0 h to 8 h the culture displays an exponential increase in volume with a doubling time of 3.36 ± 0.12 h (Figure 16 A). The DNA content before replication is approximately 0.2 pg / cell. Nearly 15% of total DNA is synthesized during the first 4 hours of light (Figure 16 B). This DNA fraction has previously been described by Chiang and Sueoka [141] as chloroplast DNA. The rest of the total DNA (~ 85%) is synthesized between 6 and 12 h. Bourguignon and Palade [142] assume that this DNA originates from the nucleus which would mean that the S phase only starts after 6 h in light. To validate this assumption the mitotic state of cells was analyzed microscopically and cells with a cleavage furrow were counted. The cleavage furrow is a visible sign of cytokinesis which directly follows mitosis. The first cells with a cleavage furrow appear at 8 h in the light (Figure 16 B). The release of DCs starts after 10 h in light and is finished approximately 16 h after the onset of light (Figure 16 A). This means the cells require about 6 h for sporulation.

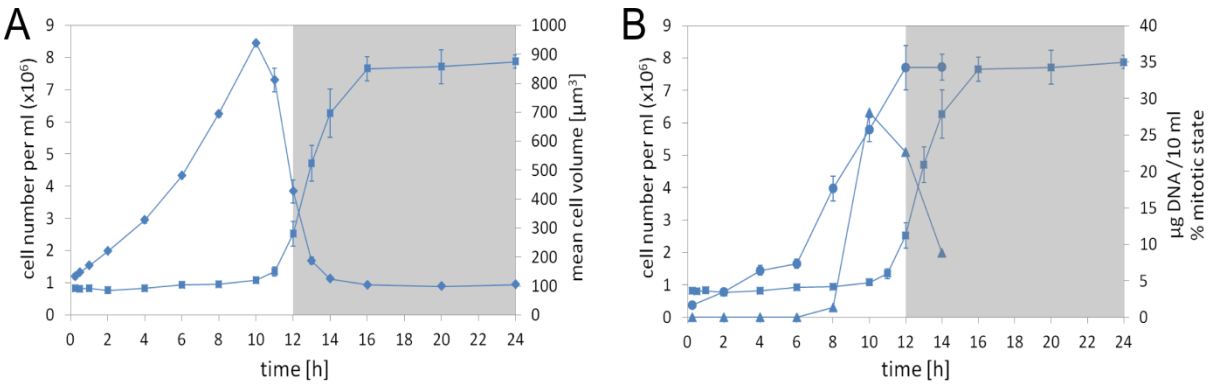

Figure 16. Cell cycle analysis of synchronized *Chlamydomonas* cells
(A) Cell number (square) and mean cell volume (diamond) at different TP for a synchronized culture of *Chlamydomonas*. Cells were synchronized by a 12:12 h light-dark regime. Dark phase is indicated as grey background. (B) Additionally to the cell number (squares), DNA content (circles) and the mitotic state (triangles) were analyzed under the same conditions. Data are given as mean ± SD of three biological replicates.

As the coordination of cell growth and division is an important aspect of cell development, we decided to analyze the cell size distribution more closely. The cell size was measured in a range from 0 µm^3 to 1900 µm^3 at distinct TPs across the entire cell cycle. For a more detailed analyze we divided the whole range in six parts (parts I – VI). The first part, with a size range of 0 to 300 µm^3,

represents the fraction of DC. The value of 300 µm^3 originates from two observations. Under synchronized conditions, *Chlamydomonas* cultures contain mainly DC at the beginning of the light phase (TP 0). This is indicated as a peak in a range of 0 to nearly 300 µm^3 (Figure 17 A and B). Additionally, determination of the critical cell size for cell division revealed also a value of about 300 µm^3 (Figure 17 C).

For determination of the critical cell size, samples of a synchronized culture were probed at several TP during the light phase. Cell volume and cell number were measured using a Beckman Coulter. For each TP, a second sample was placed in the dark. Without any light, only cells that achieved a critical cell size will be able to divide. After incubation of about 20 h in dark the number and volumes of the released DCs were measured. The number of DCs per MC was calculated and plotted as a function of the original MC volume (Figure 17 C). The results show that cells need a critical cell size of about 300 µm^3 to undergo at least one division round.

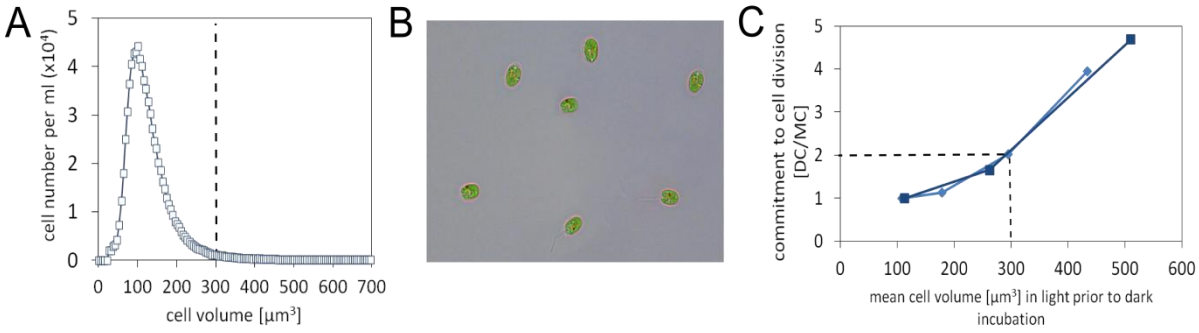

Figure 17. Determination of the size range for daughter cells
Cell size distribution (A) and microscopic picture (B) of a synchronized *Chlamydomonas* culture at TP 0 (start of light phase). (C) Graph of DCs produced per MC as a function of the mean MC volume of which they originated. Results are of two independent experiments. Dotted lines indicate the volume at which cells have doubled their cell number (2 DCs/MC).

According to this result, as described above, a partion size of 300 µm³ was also chosen for the other parts of the cell size distribution (Figure 18 A). Parts II – VI represent the fractions of the divers MCs. At each TP the percentage of cells in the specific size range was calculated. The results are presented in Figure 18 B.

The first part with a range of 0 to 300 µm^3 (fraction of DC) is decreasing in the first 10 h during the light phase. This decrease is a consequence of cellular growth. As the cells become bigger during the light phase, they shift into the next higher size range. This is marked by an increase of the diverse fractions of MCs. During the first 10 h in light parts II – VI show a sequential increase with a time shift of 2 h. After 10 h in the light the release of new DCs starts. This is accompanied by a decrease of all MC fractions (parts II-VI) and a subsequent increase of new DCs (part I). In a

previous study, Craigie and Cavalier-Smith [29] demonstrated that the number of DCs is determined by the volume of MCs. Therefore, we asked if the size distribution at TP 10 h could be used to predict the cell number after complete DC release. To test this hypothesis we initially assumed that each size range could produce a distinct number of DCs (Table 8). Additionally we assumed that the first size range produce no new DCs as the cells do not achieve the critical cell size for division.

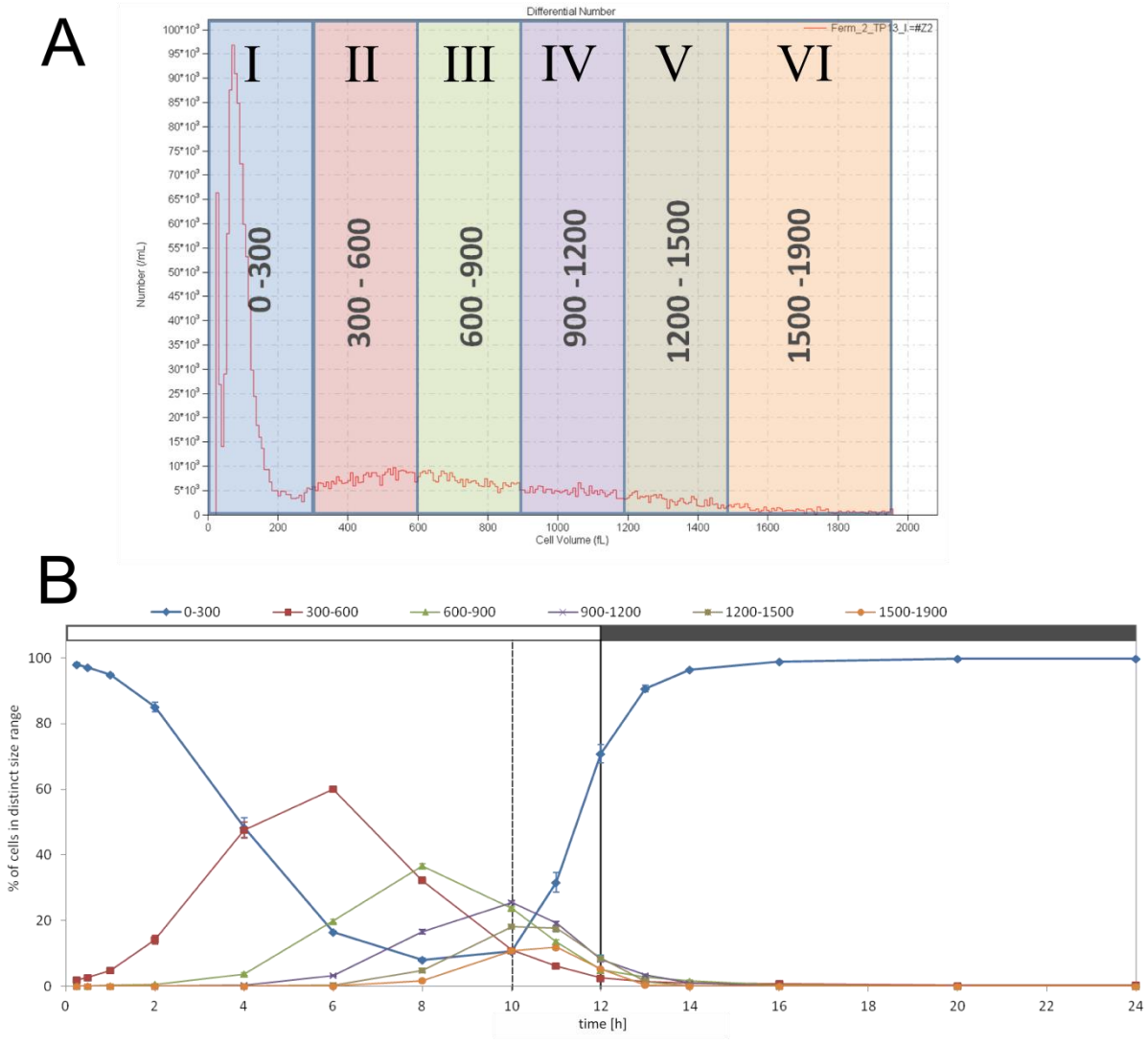

Figure 18. Cell size distribution of synchronized *Chlamydomonas* culture
(A) Diagram shows the defined size ranges (I – VI) for cell size distribution and a graph as an example for the output of the measurement from the Coulter Counter. (B) Graphs present the percentage of cells in the defined size range at distinct time points in synchronously growing *Chlamydomonas* culture during 12:12 h light-dark cycle. The black bar indicates the dark phase. The dashed line displays the time of DC release. Data are given as mean ± SD of three biological replicates.

Chlamydomonas divides by a noncanonical mechanism, termed multiple fission [29]. This means that the cells produce 2^n DCs per division burst. Thus it can be assumed that cells within a size range of 300 – 600 µm^3 (doubling of the size) produce 2 DC, cells within the size range of 600 - 900 µm^3 (tripling of the cell size) produce 4 DC, etc. Cell number of the defined size range was then multiplied by the expected number of DC. The sum of the calculated cell numbers per size range results in the predicted cell number after sporulation. Although we know that this represents a very simplified model, based on an empirical estimation of cell size ranges, the expected cell number and the measured cell number matches, with an error smaller than 4 %, quiet well (Table 8).

Table 8. Calculation of expected cell number

Size Range	0-300	300-600	600-900	900-1200	1200-1500	1500-1900
Expected number of released DC	1	2	4	8	16	32
% of cells in distinct size range	10.6	11.0	23.8	25.6	18.2	10.8

total cell number	8.42E+05

							cell number (10^6 cells / ml)	
cell number in distinct size range	8.97E+04	9.19E+04	2.00E+05	2.16E+05	1.53E+05	9.14E+04	**Predicted**	**Measured**
expected cell number after release of DC	8.97E+04	1.84E+05	8.00E+05	1.73E+06	2.45E+06	2.92E+06	**8.18 ± 0.74**	**7.87 ± 0.15**

3.1.4 Rapamycin treatment results in a delay in cell cycle and a reduction in cell growth

Under the defined growth conditions rapamycin was added with the onset of light and first samples were taken 15 min after rapamycin addition. Cell number and cells size were monitored for one 24 h cycle. The obtained data show that rapamycin treatment reduces the cell number to approximately 50% compared to control (Figure 19 A). Further, we observed that the release of DCs starts with a delay of about 3 - 4 h in rapamycin treated cultures (Figure 20 B).

Additionally, we found that the release of DC is decelerated after rapamycin treatment, especially in the first 2 h after beginning of DC release, with 10% released DC from rapamycin treated cultures compared to 60% release for control cultures (Figure 20 A, B). This is accompanied by a reduced and delayed increase in cell size during the light phase. The cells reach the maximum mean cell volume (MCV) about 2 h later (Figure 19 B). In addition, the maximum MCV is about 10 % reduced in the rapamycin treated cells. This is especially interesting, since we found a similar increase of MCV in the first 4 h in light for rapamycin and control. Cell size distribution shows that during this time cells from the smallest fraction (0-300 µm^3) shifted mainly into the next higher size range (300-600 µm^3) and this does not seem to be strongly affected by the rapamycin treatment (Figure 20 A, B).

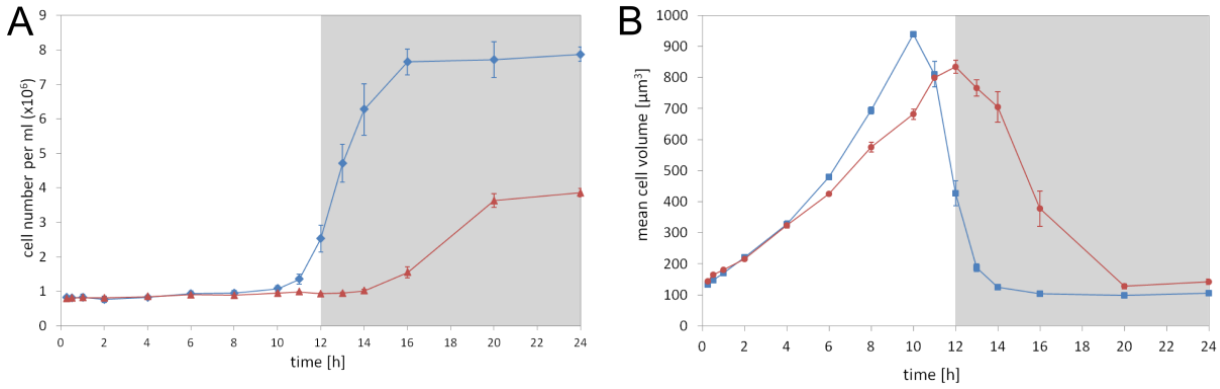

Figure 19. Cell number and cell size after rapamycin treatment
Cell number (A) and mean cell volume (B) were determined at the indicated times for a synchronized culture of *Chlamydomonas*. Cells were synchronized by a 12:12 h light-dark regime. Dark phase is indicated as a grey background. Data are given as mean ± SD of 3 biological replicates.

Interestingly, we also observed that within the first 15 min after rapamycin treatment the MCV increased to a value 7.5% higher than the control. The rapamycin treated cells maintained this slightly stronger increase in MCV until 30 min in the light and only then the control cells cached-up. Afterwards, the increase in cell size of treated cultures is comparable to that of control until 4 h. After TP 4 h rapamycin treated cells start to show a slowing down in their growth, which can be seen in a reduced amount of cells in a size ranges larger than 600 µm^3 and a broader peak (Figure 20 B). It seems that the cells need more time to shift into the next higher size range. This is most likely the reason why fewer cells reach size ranges above 900 µm^3 before DC release. The maximum amount of the cells in the highest size range (1500-1900 µm^3) is more than 50% lower after rapamycin treatment (Figure 20 C). Comparing cell size distribution of rapamycin treated cells to control shows a clear shift to smaller cells. As smaller MCs produce less DCs this explains the reduced cell number of rapamycin treated cells, which was observed at the end of the 24 h cycle.

To validate the strength of this correlation, we used our linear model to predict the expected cell number based on the results of cell size distribution (see Chapter 3.1.2.1). Because of the delay in DC release in the rapamycin treated cells we used the cell size distribution at TP 12 h for these cultures, instead of using TP 10 h which was used for the control. The results demonstrate that contrary to the control cultures (Table 8) the model for rapamycin treated cells overestimates the measured cell number by 56% (Table 9), indicating that the linear relation between cell size and cell number is not maintained in the TOR inhibited *Chlamydomonas* cells

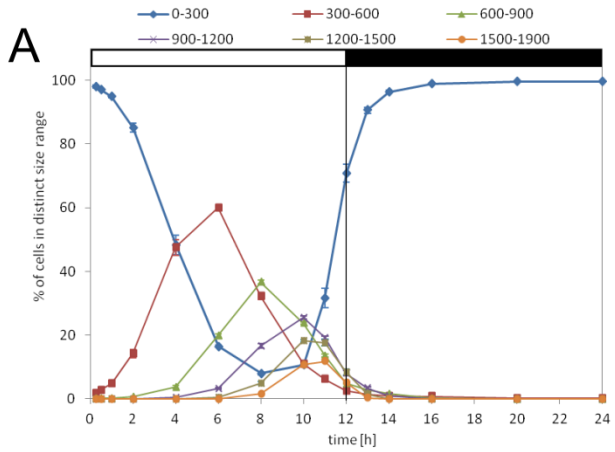

Time [h]	DC 0-300	MC 300-600	MC 600-900	MC 900-1200	MC 1200-1500	MC 1500-1900
0.5	-0.9	0.9	0.1	0.0	0.0	0.0
1	-2.2	2.1	0.1	0.0	0.0	0.0
2	-9.8	9.4	0.3	0.0	0.0	0.0
4	-36.8	33.3	3.1	0.3	0.0	0.0
6	-31.9	12.5	16.1	2.9	0.4	0.0
8	-8.5	-27.8	16.8	13.3	4.4	1.6
10	2.6	-21.3	-12.9	9.0	13.3	9.2
11	21.0	-4.8	-10.2	-6.4	-0.5	1.0
12	39.2	-3.7	-8.6	-11.1	-9.2	-6.6
13	19.8	-1.1	-2.2	-4.7	-7.0	-4.8
14	5.8	-0.5	-1.2	-2.4	-1.4	-0.3
16	2.5	-0.2	-1.3	-0.9	-0.1	0.0
20	0.8	-0.5	-0.2	0.0	0.0	0.0
24	0.0	0.0	0.0	0.0	0.0	0.0

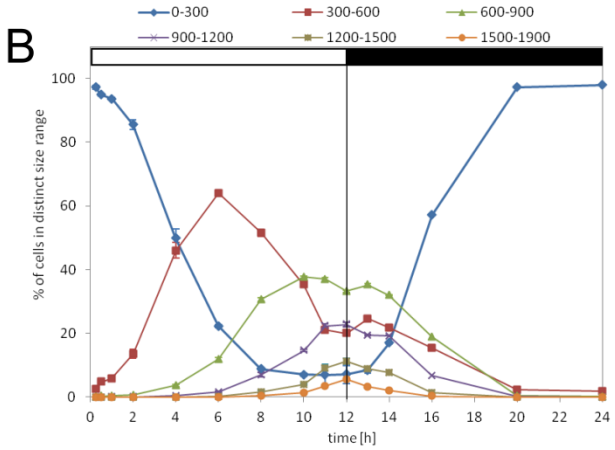

Time [h]	DC 0-300	MC 300-600	MC 600-900	MC 900-1200	MC 1200-1500	MC 1500-1900
0.5	-2.4	2.2	0.2	0.0	0.0	0.0
1	-1.2	1.1	0.1	0.0	0.0	0.0
2	-8.1	7.7	0.3	0.0	0.0	0.0
4	-35.6	32.4	2.9	0.3	0.0	0.0
6	-27.6	18.0	8.3	1.2	0.2	0.0
8	-13.5	-12.5	18.8	5.3	1.4	0.5
10	-1.7	-16.3	7.0	7.7	2.4	0.9
11	-0.2	-14.2	-0.6	7.7	5.2	2.1
12	0.3	-1.0	-3.8	0.4	2.1	2.0
13	1.4	4.7	2.0	-3.3	-2.4	-2.3
14	8.5	-2.8	-3.2	-0.2	-1.1	-1.1
16	40.1	-6.4	-13.0	-12.5	-6.4	-1.8
20	40.1	-13.2	-18.6	-6.7	-1.3	-0.3
24	0.6	-0.4	-0.2	-0.1	0.0	0.0

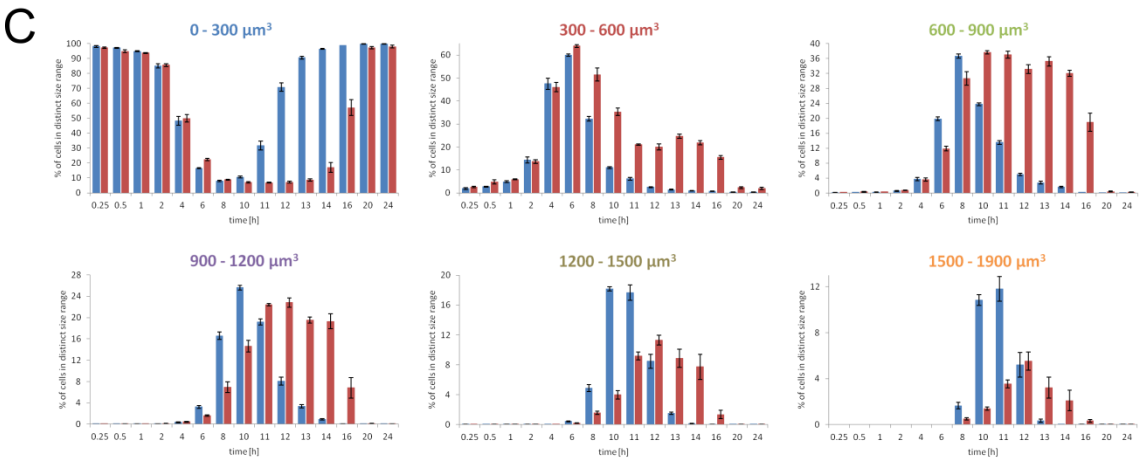

Figure 20. Cell size distribution after rapamycin treatment
Diagrams on the left side present the percentage of cells for control (A) and rapamycin treatment (B) in the defined size range at distinct time points in synchronously growing *Chlamydomonas* culture during 12:12 h light-dark cycle. The black bar indicates the dark phase. Tables next to the diagrams show percentage of increase (yellow background) or decrease (blue background) between two consecutive TP in the defined size range, respectively. (C) Plots display the percentage of cells for certain size ranges for control (blue) and rapamycin treatment (red). Data are given as mean ± SD of 3 biological replicates.

Table 9. Calculation of expected cell number after rapamycin treatment

Size Range	0-300	300-600	600-900	900-1200	1200-1500	1500-1900
Expected number of released DC	1	2	4	8	16	32
% of cells in distinct size range	7.1	20.0	33.2	22.8	11.3	5.5

total cell number	8.36E+05

							cell number (10^6 cells / ml)	
cell number in distinct size range	5.95E+04	1.67E+05	2.78E+05	1.91E+05	9.48E+04	4.64E+04	Expected	Measured
expected cell number after release of DC	5.95E+04	3.34E+05	1.11E+06	1.53E+06	1.52E+06	1.49E+06	**6.03 ± 0.66**	**3.86 ± 0.13**

The reduced growth and delayed cell cycle is also clearly visible comparing photomicrographs of treated and untreated cells (Figure 21 A). Similar to DC release also mitosis is delayed (Figure 21 C). First mitotic cells appear 2 h later in comparison to control. In contrast, DNA synthesis is not delayed (Figure 21 B). The reduced DNA content of rapamycin treated cells reflects, with a fold change of approximately two, exactly the diminished production of new DCs.

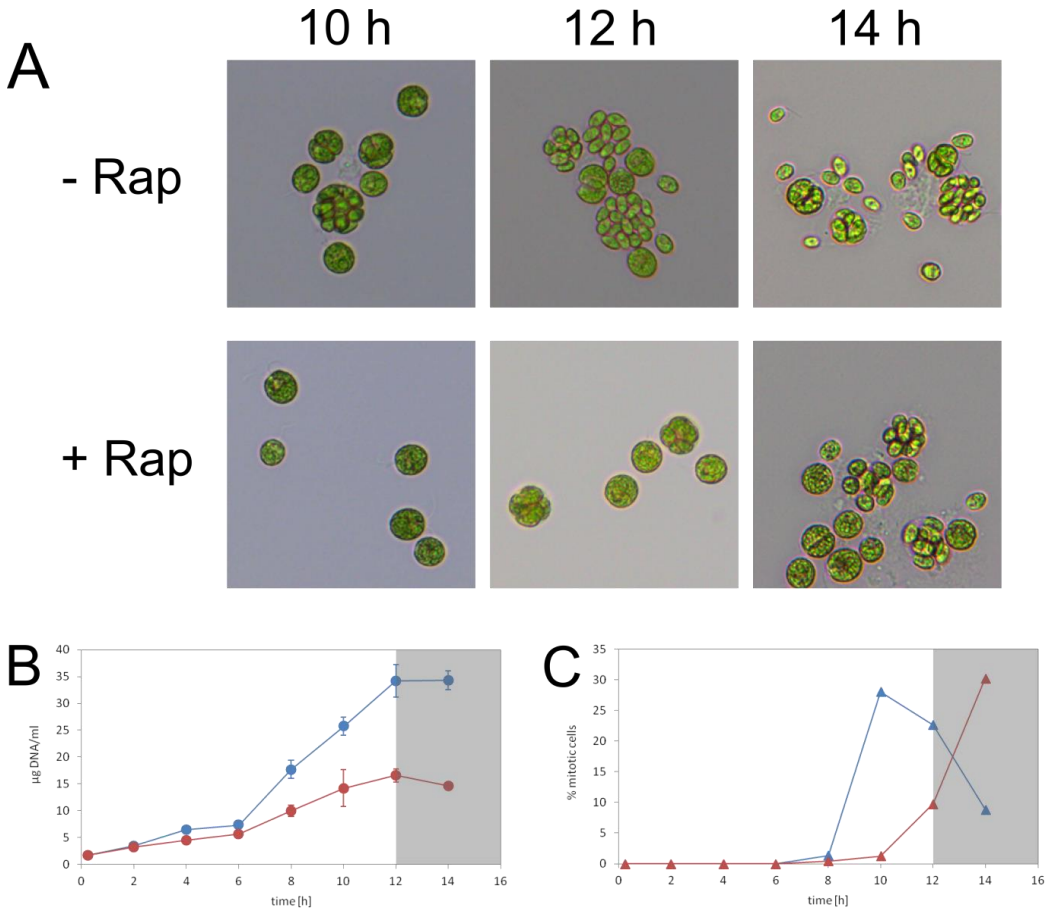

Figure 21. Cell cycle analyzes of synchronized *Chlamydomonas* cells after rapamycin treatment
(A) microscopic images of synchronized cells at distinct TP (10 h, 12 h and 14 h after onset of light) treated with rapamycin (+ Rap) in comparison to control (- Rap). DNA content (B) and mitotic state (C) of synchronized cells were analyzed at the indicated times for rapamycin treated cells (red) and control (blue). Dark phase is indicated as grey background. DNA content is given as mean ± SD of 3 independent, technical replicates.

3.1.5 Addition of rapamycin at later time points during the light phase reduces the growth inhibitory effect

Regulation of cell cycle is an important mechanism of cells to adapt to changing environment. Therefore cells use different regulatory points during the cell cycle. The point, after which cells can be completed with at least one division round independently of light and external energy supply, is called commitment point (CP) in *Chlamydomonas* [32]. As *Chlamydomonas* has several CPs, which were attained consecutively within one cell cycle, we decided to add rapamycin at different TP during the light phase [33].

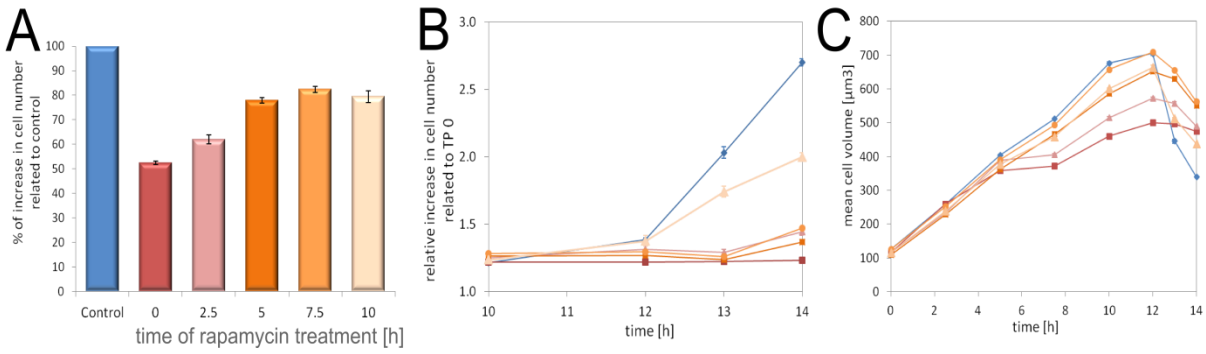

Figure 22. Comparison of cell growth after rapamycin treatment at different time points
Cell number (A, B) and cell size (C) of synchronized *Chlamydomonas* cultures (12:12 h light-dark regime), which were treated with rapamycin at different TPs within the light phase. TPs of rapamycin treatment were: 0 h (onset of light), 2.5 h, 5 h, 7.5 h and 10 h. The growth was compared to the control, which was treated with the drug-vehicle alone at TP 0 h. (A) Percentage of growth reduction after 24 h compared to the control, which was set to 100%. Color code for B and C is the same as for A. Data are given as mean ± SD of 3 independent, technical replicates.

The results show that treatment of synchronized *Chlamydomonas* cultures at later TPs during the light phase and thus later stages in cell cycle decreases the growth inhibitory effect (Figure 22). Comparing the increase in DC number, we found that addition of rapamycin between 0 h and 5 h shows the strongest reduction of growth, whereas addition of rapamycin after 5 h shows almost no additional effect on cell number reduction (Figure 22 A).Nevertheless, it can be seen that even the addition of rapamycin shortly before release of DC (10 h) has still a negative effect on DC number. However, it seems that addition of rapamycin at 10 h in light concerns more the release of DC than the increase in cell size (Figure 22 B and C). Accordingly, we could not observe a difference in the maximum MCV after 10 h in light between rapamycin treatment and the control, even though the DC number is decreased (Figure 22 A, C). On the other hand, addition of rapamycin at 10 h shows no longer a delay in the release of DC (Figure 22 B), but still a reduction. Further, the cultures where rapamycin was added at TP 2.5 h, 5 h and 7.5 h show already a slight increase in cell number after TP 13 h which is 1 h earlier in comparison to the culture where rapamycin was added

at TP 0 h. Therefore it seems that the delay of DC release is shortened if rapamycin is added after TP 0 h. Similar to the results of cell number the effect on cell size is also reduced by a later addition of rapamycin.

3.2 Response dynamics of *Chlamydomonas* to rapamycin treatment in its vegetative cell cycle

Cultivation of synchronously growing cell cultures allows for the analysis of diverse morphological, physiological and biochemical parameters throughout their cellular life cycle. Previous studies concerning the vegetative cell cycle of *Chlamydomonas* were mainly focused on the elucidation of specific changes of few selected compounds. Still there is no comprehensive data-set available describing the vegetative cell cycle on a broader level of metabolites, lipids, transcripts and proteins.

In the frame of this work we will introduce a systems-based approach to characterize the vegetative cell cycle of *Chlamydomonas* under permissive and restrictive growth conditions. In addition, we will use the systems approach for a more detailed characterization of TOR under synchronized conditions.

3.2.1 Adaptation of the MTBE-extraction method for *Chlamydomonas*

For detailed molecular characterization of the synchronized cells, we were interested in measuring as many different compounds, of several different compound classes, at as many as possible TPs. Since every experiment in the closed fermenter system is limited by the sample volume, a method, which allows the full recovery of many different compounds from one single sample, would be favorable. Therefore we decided to adopt a MTBE-extraction method, which was established in our group to the extraction of all major plant metabolite classes, lipids, starch and proteins [131]. The MTBE-extraction method is an optimization of the classical procedure using methanol and chloroform for extraction of lipids and metabolites. The advantage of the MTBE method is the simplified recovering of a solid protein/starch pellet in the bottom of the extraction vial, compared to the obtained interphase using the chloroform-based method. Giavalisco and coworkers could show that the protein quality of the pellet is suitable for proteomics studies, but they do not describe if the starch in this pellet is degraded or native and if the amount is comparable with amounts obtained by the standard methods. Further we asked if it is possible to extract proteins and starch iteratively from the same pellet, without losing too much of either compound class. So initially we tested if the starch amount is the same after the MTBE extraction compared to a

classical methanol extraction [132, 143]. In addition we validated that the obtained chlorophyll content is the same for these two methods.

3.2.1.1 *Extraction efficiency test of chlorophyll, starch and proteins*

2 ml aliquots of non-synchronized culture with 6.5 x10^6 cells were used for the measurements. The methanol extraction of the *Chlamydomonas* cells was performed with 90% methanol and repeated twice. The supernatant of each extraction step, which contains the chlorophyll and other lipids, was transferred to a new collection tube and quantified spectroscopically (see chapter 2.2.6). Similarly another aliquot was extracted using the MTBE-extraction method(see chapter 2.2.4). We again transferred for each step an appropriate volume of the upper (organic) phase, containing lipids and chlorophyll, to a new collection tube to measure the respective chlorophyll content.

The remaining pellets from both methods were further processed for starch extraction. Therefore we used an adapted protocol of Smith and Zeeman [133]. Further we tested if homogenization, using glass beads in a Retch mill before MTBE extraction would increase the amount of extractable chlorophyll and/or starch.

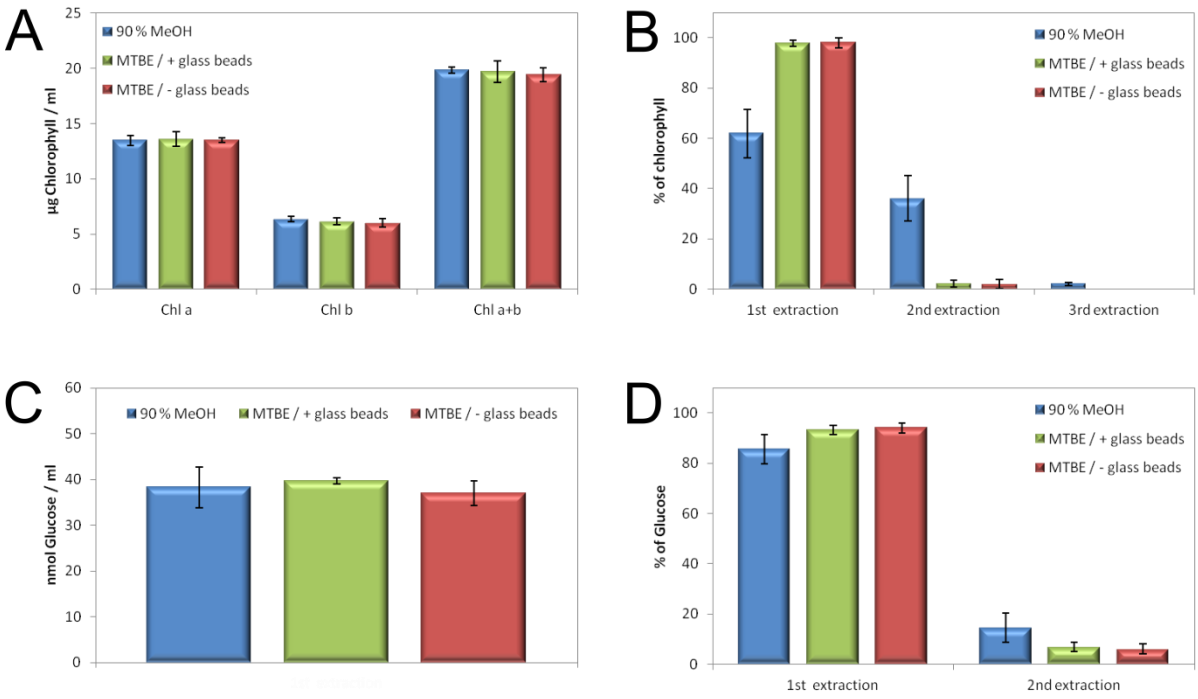

Figure 23. Comparison of methanol and MTBE extraction for chlorophyll and starch
This figure shows the chlorophyll (A, B) and starch (C, D) content of methanol or MTBE extraction. Plot A and C display the sum of chlorophyll content per ml after three extractions and the sum of starch content per ml after two extractions, respectively. The plots on the right side illustrate the percentage of extracted chlorophyll (B) or starch (D) after indicated extraction steps. Additionally, different homogenization methods are shown (green and red). Error bars indicate standard deviation with n=3.

First of all, the results in Figure 23 demonstrate that there is no significant difference in the absolute extractable amount of chlorophyll and starch using the methanol extraction compared to the MTBE-extraction method. It can also be seen that there is no significant difference between the *Chlamydomonas* samples which were physically disintegrated (glass bead treatment) before MTBE extraction. As can be seen from Figure 23 B the extraction of chlorophyll using the 90% MeOH method has to be repeated at least once to extract almost all of the chlorophyll. In contrast, the MTBE-extraction method obtains already 98% of the chlorophyll after a single extraction step.

The starch extraction from the obtained protein/starch pellet was also repeated a second time to exclude extraction deficiencies. 93% of starch could be extracted within the first extraction using the pellets from the MTBE-extraction method, whereas only 86% of starch was obtained within the first extraction step using the pellets from the 90% methanol extraction method. In summary we can conclude that the MTBE method is not only suitable to extract metabolites, lipids, and proteins but also to obtain quantitative amounts of chlorophyll and starch.

3.2.1.2 *Iterative extraction of protein and starch from the MTBE pellet is possible*

As proteins and starch are shown to be extracted from the MTBE pellet the question arises if it would be possible to recover quantitative amounts of starch and proteins from the same pellet. Aliquots of unsynchronized culture with a density of 10^7 cells were used for this purpose. The cells were extracted using the MTBE protocol without mechanical (glass bead) disintegration. The obtained starch/protein pellets were consecutively used for protein followed by the starch extraction and vice versa. The starch and protein extraction were performed as described in the Material and Methods section (chapter 2.2.7 and 2.2.8).

Figure 24 clearly shows that extracting proteins and starch from the same MTBE pellet allows only one order, namely extracting first proteins and use the remaining pellet for starch extraction. As a consequence there is a slight decrease in starch content after protein extraction (7.8%), but this difference is not significant (Figure 24 B). In contrast, as can be seen from Figure 24 A the extraction of proteins after starch extraction results in an almost complete loss of the protein (>90%).

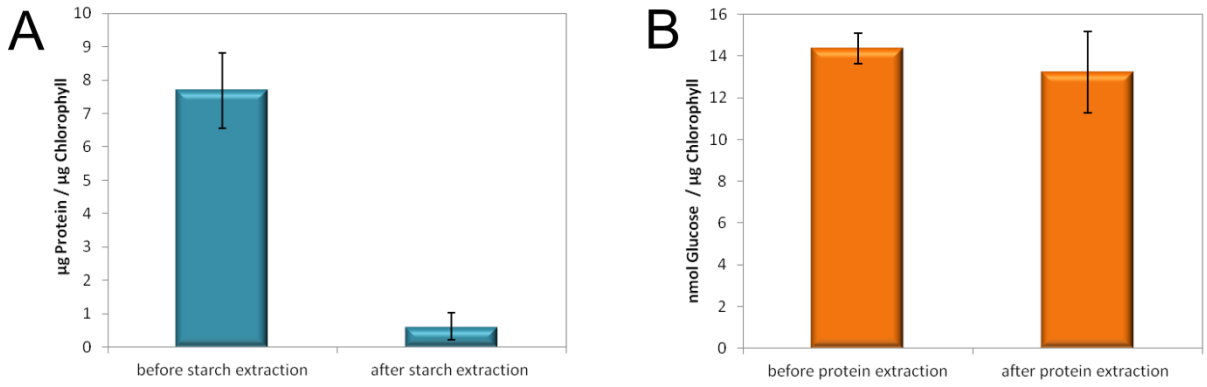

Figure 24. Starch and protein extraction from the same MTBE pellet
(A) Protein content extracted directly after MTBE extraction (before starch extraction, left column) in comparison to the protein content extracted from the remaining pellet after MTBE and starch extraction (right column). The same was done vice versa with starch extraction (B). The column on the left side displays the starch content directly after MTBE extraction whereas the column on the right side shows the amount of starch after MTBE and protein extraction. Error bars indicate standard deviation with n=6.

3.2.1.3 *Optimization of sample preparation steps for primary metabolite analysis*

For measuring primary metabolites, the polar phase of the MTBE extraction has to be dried in a vacuum centrifuge. Before the sample can be measured on GC-Tof/MS the dried pellet has to be derivatized (see chapter 2.2.5.1). This can be a critical step: On the one hand too low volumes could lead to an incompletely resuspension of the pellet. On the other hand a too large volume would decrease the concentrations of the resuspended metabolites. Accordingly we employed two different derivatization volumes. The dried pellets were either derivatized in 100 µl (10 µl of methoxamine-hydrochloride + 90 µl of MSTFA) or 50 µl (5 µl of methoxamine-hydrochloride + 45 µl of MSTFA). From this derivatization mixture either 1 µl or 2 µl were injected into the GC-Tof/MS (see chapter 2.2.5.1). For this test aliquots of unsynchronized *Chlamydomonas* culture with a cell density of about 2 x 10^7 cells were used.

From the detected metabolites only a selection of 8 metabolites, including the internal standard ^{13}C-sorbitol, are presented in Figure 25. These metabolites represent different groups of primary metabolites including organic acids of the TCA cycle, amino acids, sugar and sugar phosphates. The response values (signal intensities) of these compared metabolites are within the dynamic range of the detection system and therefore can be regarded as representative for most of the detectable metabolites.

Generally it can be observed that a derivatization volume of 100 µl provides much better results as under this condition the variance within the replicates is much lower. The explanation for the higher variance in the replicates of the samples derivatized in the smaller volume is an incomplete resuspension of the dried metabolite pellet.

Injecting 1 µl or 2 µl results in no significant difference on the response curve of the selected metabolites. Therefore we decided to use 2 µl for injection as this increases the absolute amount of substances loaded onto the GC column.

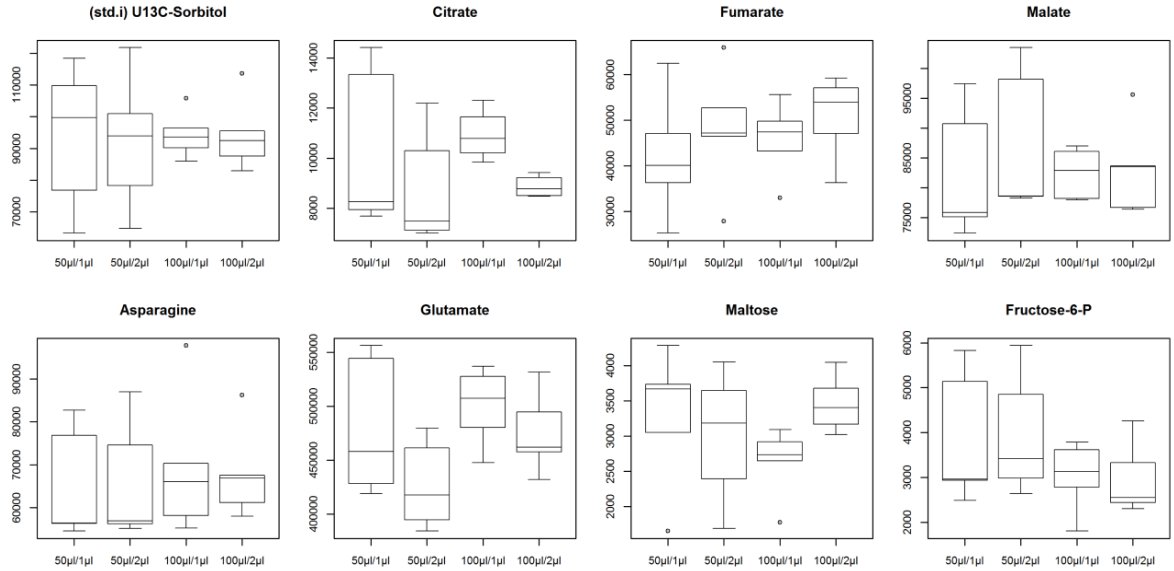

Figure 25. Comparison of derivatization and injected volume for primary metabolites
Primary metabolites from *Chlamydomonas* cell pellets (2 x 10^6 cells) were extracted according to the protocol (see chapter 2.2.4). The dried pellets were derivatized in 50 µl or 100 µl, respectively. From each derivatization mix 1µl and 2µl were injected and measured on GC-Tof/MS (mode). For better comparison the peak intensities were normalized to the same volume (100 µl derivatization volume and 1 µl injected volume). The results are presented in box plots for 5 independent, technical replicates.

3.2.2 Molecular dynamics of starch and chlorophyll in synchronized cells of *Chlamydomonas*

The results in chapter 3.2.1.1 show that the MTBE-extraction method is highly suitable and adapted for the extraction of several different compounds from a single sample. This enables us to monitor changes in chlorophyll, starch, primary and lipid metabolites for a high resolution time series of 15 TP from a single 800 ml fermenter. For each TP we measured 6 replicates, consisting of 2 independent replicates from 3 independent cultures (fermenter systems), which were synchronized under the same conditions. As this experiment was conducted in parallel to the later described rapamycin-treatment, the first samples were taken 15 min after onset of light (TP 0.25 h), because rapamycin was added with the onset of light. However, this TP was defined as TP 0 (starting point) and was used for calculation of relative changes over time.

3.2.2.1 *Chlorophyll dynamics of the synchronized system*

The chlorophylls, namely chl a and chl b, accumulate only in the light phase and remain constant during the dark phase (Figure 26 A). The total chlorophyll content (chl a+b) (per ml) increase by a factor of 8.55 ± 0.72. The accumulation of the chlorophylls during the light phase can be separated in three parts. These parts are marked I, II and III in Figure 26 A and separated by dashed lines. In the first two hours of the light phase (part I) the chl b content does not change whereas the chl a shows a slight increase after 1 h. In the second phase both chlorophylls increase, while chl a shows a stronger increase with a slope of 0.45x compared to a slope of 0.34x for chl b. In phase III both chlorophylls show a stronger increase compared to phase II, but now chl b accumulates faster than chl a (slope of 0.89x for chl a and 0.93x for chl b). During the dark phase neither the chl a nor the chl b level show significant changes.

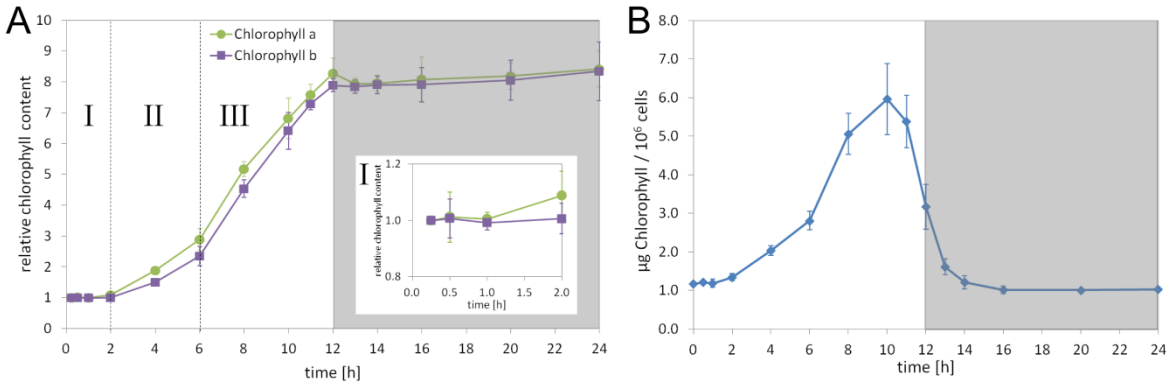

Figure 26. Chlorophyll content of synchronized *Chlamydomonas* cells
The chlorophyll content was analyzed at the indicated times for a *Chlamydomonas* culture synchronized by a 12:12 h light-dark regime. (A) Chlorophyll a (green) and chlorophyll b (purple) are shown as relative values (chlorophyll content per ml) related to the beginning of the cell cycle (TP 0). (B) Chlorophyll a + b content per 10^6 cells. Grey background indicates the dark phase. Data are given as mean ± SD of three biological replicates.

The chlorophyll-to-cell ratio increase during the light, starting from a concentration of 1.16±0.03 pg/cell. This increased chlorophyll-to-cell ratio is explained by the fact that the cells divide without separating. During this process the cells generate a new chloroplast for each DC for which new chlorophyll is synthesized. Still these cells are surrounded by the mother cell wall and therefore count as a single cell. With release of DC (>10 h in light) this ratio starts to decline, although the absolute amount of chlorophyll is still increasing until TP 12 h. The decrease of the ratio during this time period is caused by a stronger increase in cell number than chlorophyll. After completion of DC release the chlorophyll-to-cell ration attains a value of 1.02 ± 0.05 pg/cell, which is corresponding to the value of the DCs of the starting culture (Figure 26 B). This result clearly shows that the accumulation of chlorophyll directly correlates quantitatively with the increase in cell number, even if the DCs are not yet released.

3.2.2.2 *Chlorophyll content per cell is not changed after rapamycin treatment*

As an indicator for photosynthetic activity the chlorophyll content was measured after rapamycin treatment and compared to the control. Interestingly, we found that the chlorophyll content per cell is not affected by rapamycin treatment. Furthermore, we could observe that time course of increase of the chlorophyll content (per ml) during the light phase is not delayed after rapamycin treatment (Figure 27 A). The reduction in chlorophyll (per ml) correlates very well with the reduced cell number. Hence, the chlorophyll content per cell does not change significantly (Figure 27 B).

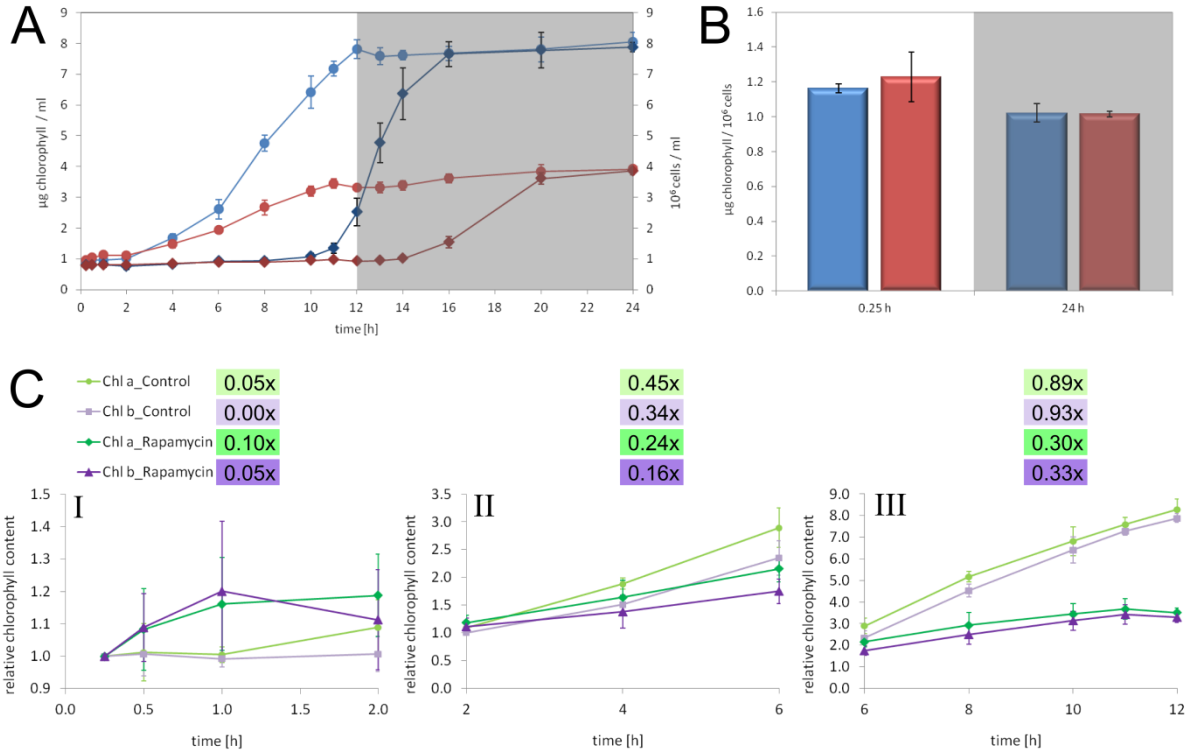

Figure 27. Chlorophyll content after rapamycin treatment
Chlorophyll content was analyzed at the indicated times for a *Chlamydomonas* culture treated with rapamycin (red) in comparison to control (blue). The cells were synchronized by a 12:12 h light-dark regime. (A) Chlorophyll content per ml (circle) and the cell number per ml (diamonds). (B) Chlorophyll content normalized to cell number for the beginning (TP 0.25 h) and the end (TP 24) of the cell cycle. Grey background indicates the dark phase. (C) Comparison of relative chlorophyll a (chl a) and chlorophyll b (chl b) content per ml (fold change to TP 0) of the control and rapamycin treated culture in the three different parts (see 3.2.2.1) Numbers above the plots show the slope value. Data are given as mean ± SD of 3 biological replicates.

The comparison of the increase of chl a and chl b within the three light parts indicate some differences (see 3.2.2.1). In part I (0-2 h) chl a and chl b show a slight but not significant increase in the first hour after rapamycin treatment while under control conditions chl a and chl b remain on a constant level. In the second part (part II, 2-6 h) both, chl a and chl b, show a reduced increase, but similar to control conditions the chl a increases stronger than chl b. In correspondence with the

control, the increase of both chlorophylls is stronger in part III (6-12 h) than in part II with a stronger accumulation of chl b than chl a. Comparison of the slope values show that the reduced increase of chl a and chl b in the rapamycin treated culture is more pronounced in part III than part II. In comparison to the control neither chl a nor chl b show a significant difference until TP 4 h. Only 6 h after rapamycin treatment the chlorophyll content (per ml) is significantly lower compared to the control. In addition, we observed that in contrast to the control where both chlorophylls increase during the whole time period of part III, the chlorophylls of the rapamycin treated culture stop the increase one hour earlier (TP 11 h instead of TP 12 h).

As the total chlorophyll content per cell within one cell cycle is not significantly changes after rapamycin treatment, we decided to use the chlorophyll concentration as a factor for per cell normalization of starch, primary metabolites and lipids. The main advantage of using chlorophyll as a proxy for cell number is that it allows to overcome the normalization problem during the light phase. During the light phase the cells increase in size and subsequently divide while they stay surrounded by the mother cell wall and count therefore as one cell. A difference in DCs is therefore not measurable during this time period and is only detectable after release of DCs. Therefore, under conditions where the growth is changed, normalization to cell number during the light period could lead to misinterpretation of data as the cell number does not reflect the increase in biomass. An example for this problem is presented in Table 10.

Table 10. Comparison of normalization of starch to cell number and chlorophyll
As an example, results of TP 10 h were chosen to display the comparison of normalization to cell number and chlorophyll content.

Starch (nmol Glc/ml)	
Control	Rapamycin
347	344

Cell number (10^6 cells/ml)	
Control	Rapamycin
1.08	0.95

Starch (nmol Glc/10^6 cells)		
Control	Rapamycin	**Foldchange**
320.99	361.23	**1.13**

Chlorophyll (µg/ml)	
Control	Rapamycin
4.90	2.42

Starch (nmol Glc/µg Chl)		
Control	Rapamycin	**Foldchange**
70.89	142.32	**2.01**

3.2.2.3 *Changes in starch content of synchronized Chlamydomonas cultures*

Starch is one of the main products of photosynthetic carbon fixation and serves as a transient carbon reserve for the night. It has already been shown that *Chlamydomonas* cells, grown under a light-dark regime, accumulate starch within the chloroplast during the light and degrade it in the dark [144, 145].

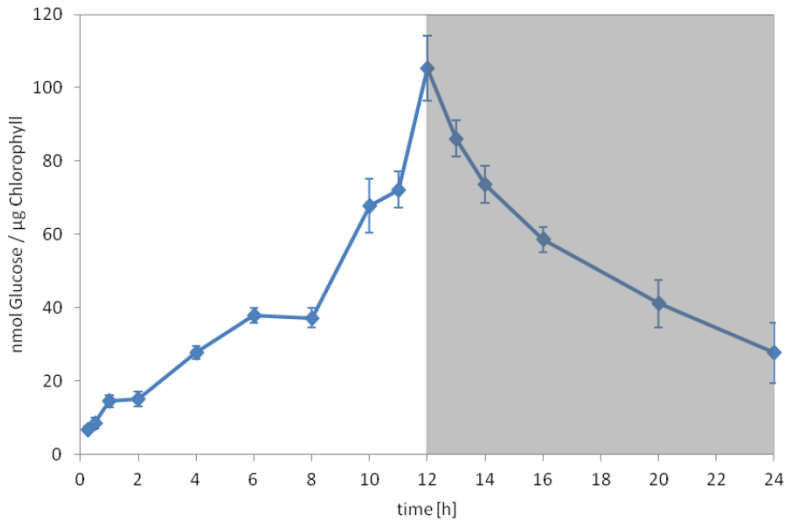

Figure 28. Starch content of synchronized culture
The starch content was analyzed at the indicated times for a *Chlamydomonas* culture synchronized by a 12:12 h light-dark regime. Grey background indicates the dark phase. Data are given as mean ± SD of three biological replicates.

Under our experimental conditions starch accumulates during the entire light period and decreases in the dark (Figure 28). Starch accumulates during the light phase by a factor of 13.14 ± 0.77. In addition our results show that the increase of starch is not fully linear. Between 1 h – 2 h, 6 h – 8 h and 10 h – 11 h the starch content remains almost constant, indicating that during the time periods the fixed carbon might has a stronger flux into other pathways than starch synthesis. The degradation of starch in the dark seems to be more exponential and ends up with an amount that is about 3.4 ± 1.37 times higher than the starting value.

3.2.2.4 *Rapamycin treatment leads to a stronger per cell starch accumulation*

It has been described that inhibition of TOR by rapamycin causes a starvation-like response and accumulation of metabolic reserves in yeast and Arabidopsis [77, 114]. Accordingly, we investigated if rapamycin also increases the amount of storage material in *Chlamydomonas*. Starch

represents the major storage carbohydrate in plants and green algae providing carbon and energy for many cellular processes during periods of darkness [146].

Our results show that rapamycin leads to an increased accumulation of starch, which is up to 2-fold higher per cell than the control (Figure 29 C). Interestingly, we found that the amount of starch per ml is not changed after rapamycin treatment (Figure 29 A).

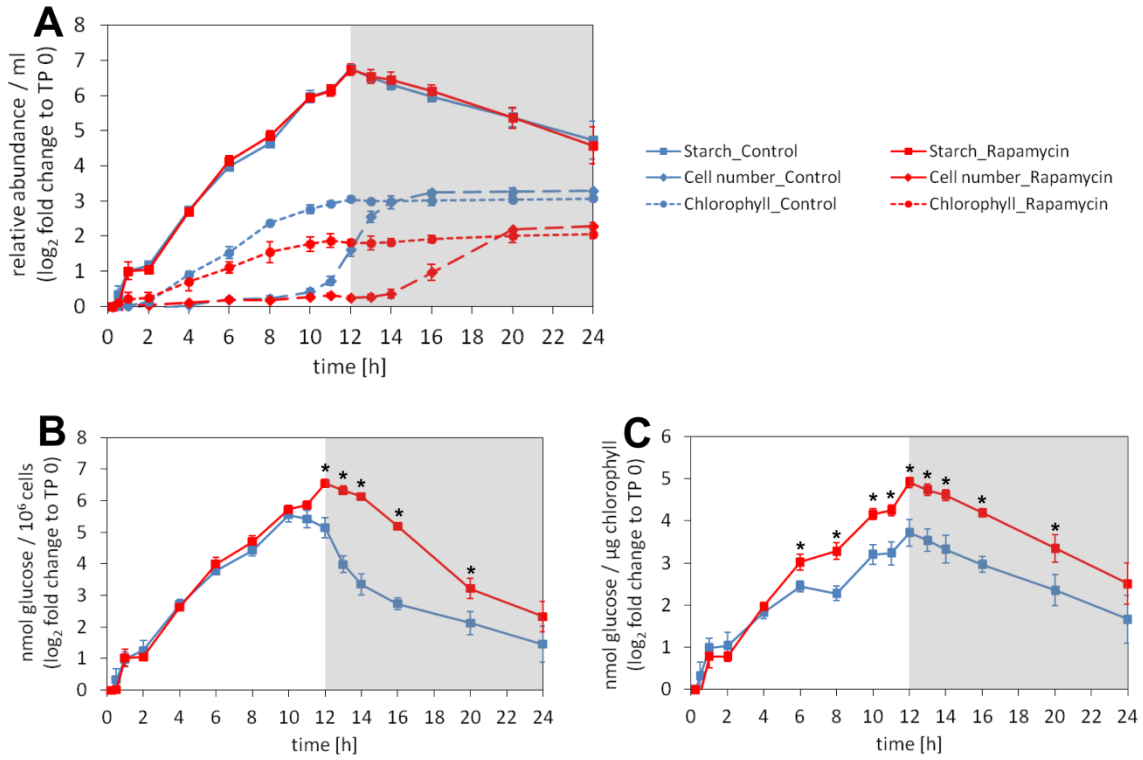

Figure 29. Starch content after rapamycin treatment
Starch content was analyzed at the indicated times for a *Chlamydomonas* culture treated with rapamycin (red) in comparison to control (blue). The cells were synchronized by a 12:12 h light-dark regime. (A) Starch content (nmol glucose/ml), chlorophyll concentration (µg chlorophyll/ml) and cell number (per ml) as indicated by the legend on the right side of the plot. (B) Starch content normalized to cell number. (C) Starch content normalized to chlorophyll contentl. All values are shown as $\log_2$ fold change to TP 0. Grey background indicates the dark phase. Data are given as mean ± SD of 3 biological replicates.

To emphasize once more the difference of normalization to cell number or chlorophyll, we did both for the starch content (Figure 29 B, C). While normalization to cell number displays no difference in the starch content between control and treated culture during the entire light phase, the chlorophyll normalization shows a significant increase of starch 6 hours after rapamycin treatment. In addition, from the data, normalized to cell number, we would assume that the start of starch degradation is shifted in time after rapamycin treatment, while neither the amount per ml nor the chlorophyll normalized data support this observation. The time shift in the decrease of starch is therefore only the result of the time shift in the increase of DCs. For a better comparison of

temporal behavior and quantitative differences it makes sense to consider both the amount per volume and the chlorophyll normalized value of a compound. In the remainder of this study the amount per volume (ml) will be defined as the **total amount** and the chlorophyll normalized value as the **cellular amount**.

Hence, the results suggest that the timing mechanism of starch accumulation/degradation is not affected by rapamycin. Although rapamycin-treated cells accumulate even more starch during the light phase, they seem to mobilize it also much faster than the control cells in the dark phase. While the control degrades about 78 nmol glucose/ µg chlorophyll during the dark, the rapamycin treated culture degrades more than twice, 185 nmol glucose/ µg chlorophyll. At the end of the dark phase the cellular starch content is about 1.75-fold higher than this of the control. Interestingly, we observed that the non-linear increase during the light phase occurs also after rapamycin treatment. Rapamycin treated cells show a reduced increase or even constant level of starch in the same time periods as under control conditions (1 h – 2 h, 6 h – 8 h and 10 h – 11 h).

3.2.3 Analysis of primary metabolites of the synchronized *Chlamydomonas* cells

Primary metabolites were measured by GC-Tof-MS. The data was processed and annotated as described in chapter 2.2.5.1. With this method we were able to unambiguously annotate and quantitatively monitor 68 metabolites over the whole cell cycle of *Chlamydomonas*. The experimental set-up was the same as described in chapter 3.2.2.

3.2.3.1 *Global response description of primary metabolic changes by unsupervised PCA analysis*

First, we used a principal component analysis (PCA) to see if the TPs of the synchronized *Chlamydomonas* cells can be separated due to differences in their metabolic profile and if there is any trend within the dataset. For the PCA we used the average of the two independent aliquots from each fermenter to present the results for the three biological replicates. The PCA is a useful statistical visualization method to reduce a multivariate dataset by transforming the high dimensional dataset into a smaller set of orthogonal variables called principal components [137]. This could help to extract useful information from a complex data set.

The PCA shows a very clear separation of light and dark phase by the first component PC 1 (Figure 30). Furthermore, the light phase can be separated into early light phase (0.25 h – 2 h) and the main light phase (4 h – 12 h) by the second component PC 2. The PC 1 and PC 2 explain together more than 60% of the total variance. The gaps between the three different phases suggest strong

metabolic changes at these transitions. Accordingly during the light phase the samples separate between 0 h and 4 h along PC2 before starting to separate along the maximal variance axes PC1 until 12 - 13 h. With beginning of the dark phase the samples again start to separate along PC2, but now in opposite direction, moving almost back to the origin of TP 0. This meets our expectations that within one cell cycle the metabolic profile should be similar between start and end of the cell cycle.

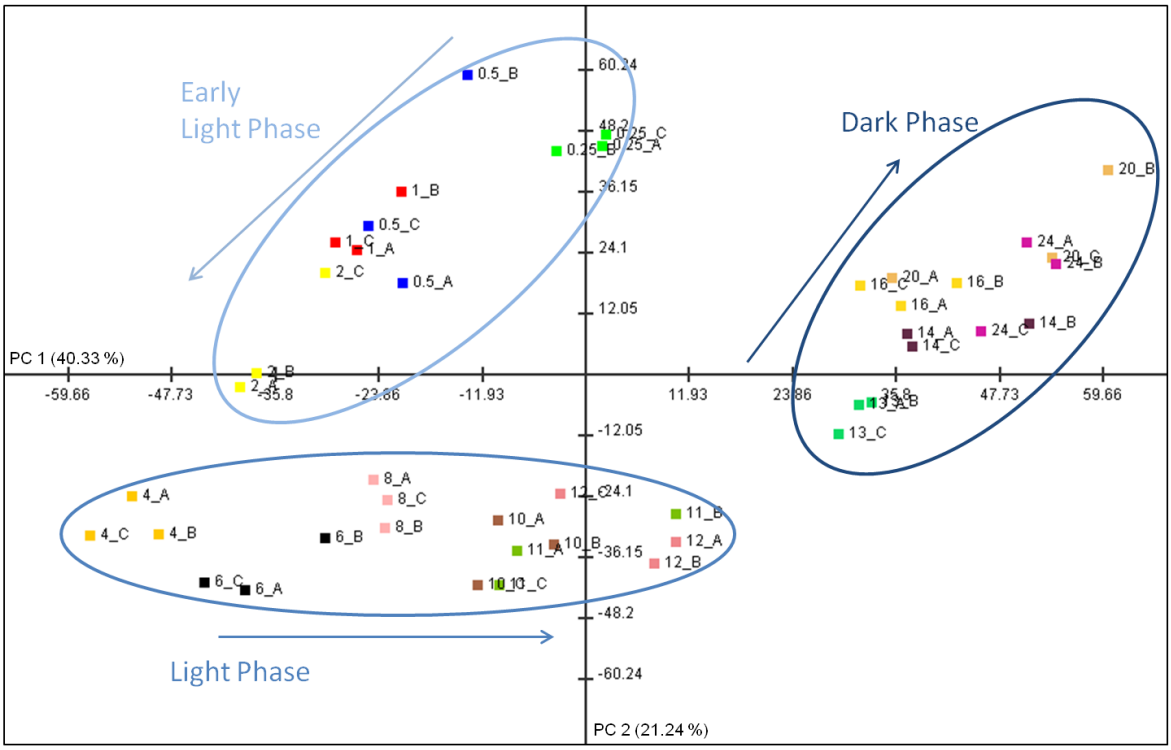

Figure 30. Principal component analysis (PCA) of primary metabolites of a synchronized culture
PCA of primary metabolites, which are chlorophyll normalized and $\log_2$-transformed, of a *Chlamydomonas* culture synchronized by 12:12 h light-dark cycle. The time points in h and replicates are indicated as numbers or letters, respectively. Separation of early light phase (0.25 h – 2 h; light blue), light phase (4 h – 12 h; middle blue) and dark phase (13 h – 24 h; dark blue) is indicated by circles. Arrows next to the different phases display the direction of time course.

3.2.3.2 *Temporal cluster-analysis of primary metabolites during the cell cycle*

As mentioned above we would expect that within one cell cycle the DCs at the end of the dark phase are quite similar in the composition and quantity of their compounds to those cells from the beginning of the light phase. Therefore, we would also assume that each compound has to increase at a certain TP in the same level as the cell number or a cell number equivalent, which is in our case the chlorophyll content. To ensure that this is the case, the cells have to newly synthesize each compound. Thus, the level of each metabolite should increase over time. To find out which metabolites are similarly and which are differently synthesized we decided to group the metabolites

with regard to the TP when their level starts to increase (see chapter 2.2.12.3). For analysis of the temporal behavior we used the total amount of each metabolite (peak height/ml).

To determine the TP at which each metabolite starts to increase we established the following criteria.

- First, the $\log_2$ fold change to TP 0 must be higher than 0.5.
- Second, the p-value of that TP to TP 0 must be lower than 0.05.
- Third, most of following TPs should meet at least one of these criteria.

By using these criteria it was possible to separate the primary metabolites into 4 distinct groups (Figure 31, Supp. table 1). These groups are referred to as cluster, even though they are not clustered in a classical clustering method. Cluster 1 contains metabolites which start to increase 0.5 – 1 h after the onset of light, while metabolites of cluster 2 increase at 2 h in light. Both clusters contain nearly the same amount of annotated metabolites (17 and 18 respectively).

Metabolites of cluster 1 and 2 show an earlier quantitative increase than chlorophyll, while the metabolites of cluster 3 start to increase at the same time as chlorophyll (Figure 31, dotted line in the plots). Metabolites in cluster 4 increase later than chlorophyll. On average the metabolites of cluster 1-3 achieve nearly the same level at the end of the dark phase as chlorophyll, while the average of cluster 4 ends with lower value (Figure 31).

Independently of when the start to increase all metabolites show on average an increase until TP 12 h. With the onset of darkness this pattern switches in either a constant level or a decrease. Further, we could observe a slight increase of most metabolites in the last 4 h of darkness, indicating that they might prepare for the next cell cycle.

In the next step, we focus in more detail on the content of the different clusters to determine if differential functional and/or biochemical groups of metabolites are enriched within the clusters. Therefore, the primary metabolites were presented in their respective pathway (Figure 32).

Except proline, all proteinogenic amino acids could be annotated and most of them (more than 70%) are present in cluster 1 and 2. Within the amino acids, the three aromatic amino acids (tryptophan, phenylalanine, tyrosine), methionine and alanine are present in cluster 1 and therefore show the fastest increase after the light has been switched on. In addition, 4 non-proteinogenic amino acids are in the same cluster, namely homoserine (precursor of methionine), 2-aminobutyrate, beta-alanine and citrulline. Furthermore, pyruvate and spermidine which are precursors of alanine and beta-alanine, belong to cluster 1 (Figure 31 and Figure 32).

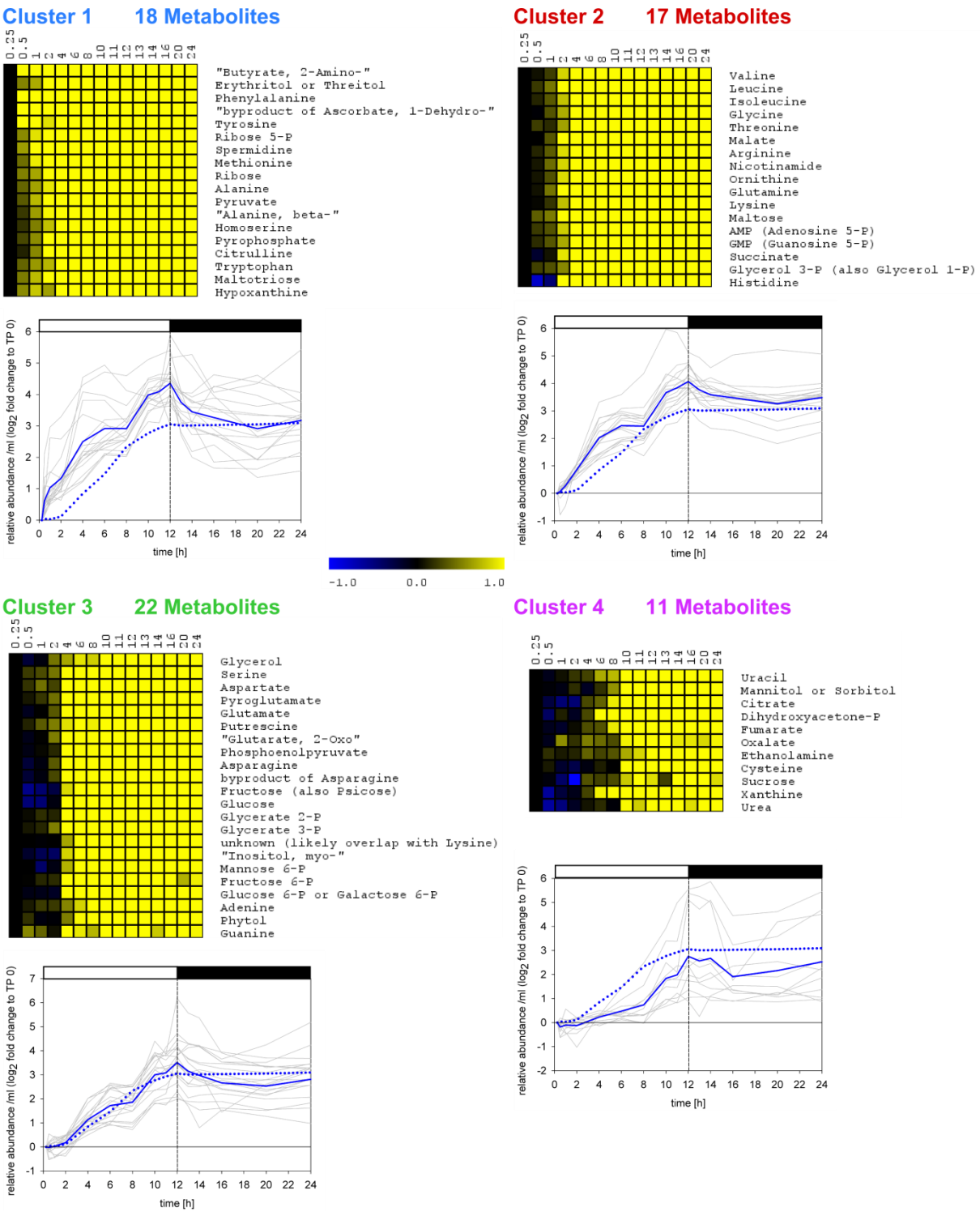

Figure 31. Time related clustering of primary metabolites of synchronized *Chlamydomonas* culture
Primary metabolites were grouped with regard to the TP when their level starts to increase. As a result the data was grouped into 4 clusters. To determine the belonging of each metabolite to one of the 4 clusters specific criteria were established which are explained in detail in the text. For each cluster the log_2-fold changes to TP 0 of absolute values are visualized in heatmaps indicating a decrease (blue) or an increase (yellow). Below the heatmaps the log2 fold changes are plotted as a graph for each metabolite (grey) and the cluster average (blue). In addition the log_2 fold change of chlorophyll is shown (dotted blue line). The results show the median of 6 replicates per TP.

3.2.3.3 *Pathway-mapping of clustered metabolites*

Amino acids which are directly derived from intermediates of the TCA cycle, namely glutamate and aspartate, were found in the same cluster (cluster 3) as well as the precursor of glutamate (2-oxoglutarate). Glutamate and aspartate serve as precursor for most amino acids. Only two of them are present in same cluster (asparagine, pyroglutamate) while all the other amino acids which derive from either aspartate or glutamate are present in cluster 1 or 2. Serine which serves also as precursor for other amino acids clusters together with aspartate and glutamate as well as its precursor 3-phosphoglycerate. The 3 amino acids which need serine as a precursor are glycine, cysteine and tryptophan. All of them are present in different cluster. Within the amino acids, cysteine is the only amino acid which could be found in cluster 4, showing a later increase than all of the other annotated amino acids.

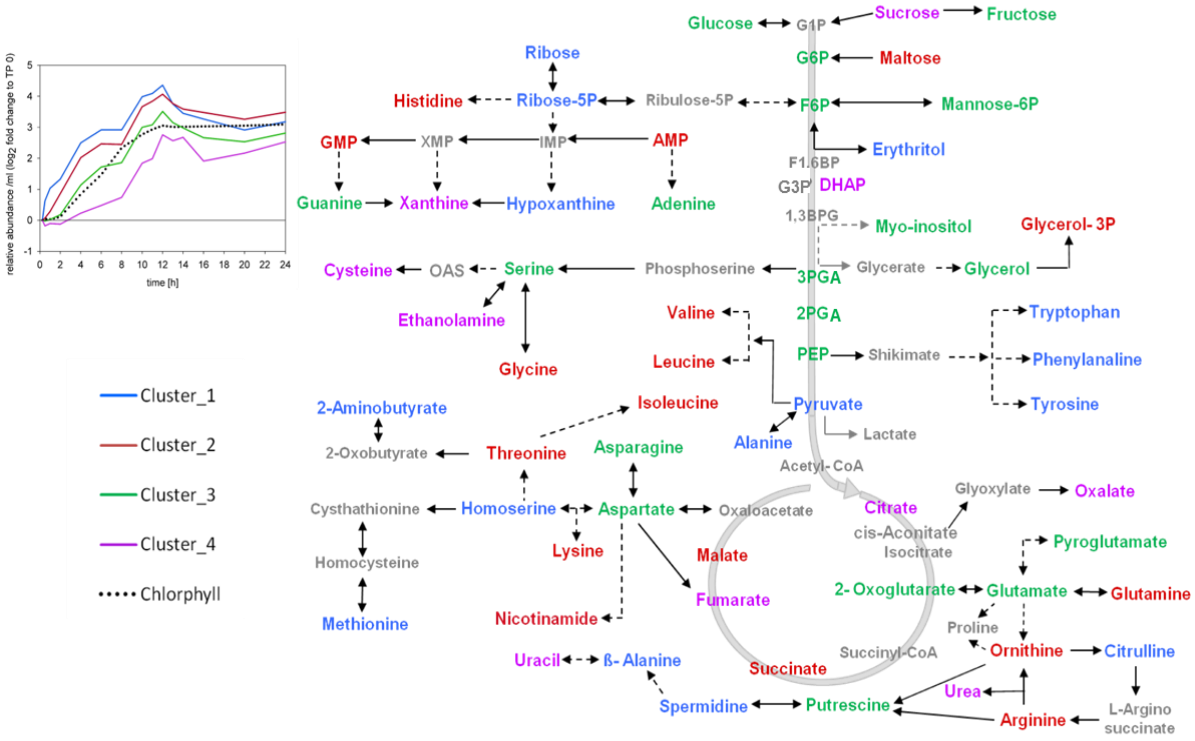

Figure 32. Pathway map of quantitative regulation of primary metabolites during the cell cycle of *Chlamydomonas*
Visualized are central metabolic pathways. The plot (left upper corner) displays the averaged pattern of the 4 different cluster (see Figure 31) and in addition the chlorophyll content of a *Chlamydomonas* culture synchronized by a 12:12 h light-dark cycle. For color code see legend below the plot. Color of each metabolite name within the pathway map indicates the appropriate cluster. Metabolite names in grey display metabolites which were not annotated. G1P – Glucose-1-phosphate; G6P – Glucose-6-phosphate; F6P – Fructose-6-phosphate; F1,6BP – Fructose-1,6-bisphosphate; G3P – Glyceraldehayde-3-phosphate; DHAP – Dihydroxyacetone phosphate; 1,3BPG – Bisphosphoglycerate; 3PGA – Glycerate-3-phosphate; 2PGA – Glycerate-2-phosphate; PEP – Phosphoenolpyruvate; GMP – Guanosine monophosphate; XMP – Xanthosine monophosphate; IMP – Inosine monophosphate; AMP – Adenosine monophosphate; OAS – O-Acetylserine.

Next to amino acids we could annotate two of the major polyamines, namely putrescine and spermidine which are known to play critical roles in cell growth [147]. Earlier experiments have shown that cells undergoing division contain high levels of polyamines and that inhibition of polyamine synthesis lead to an inhibition of cell division [148]. As already mentioned, spermidine belongs to the cluster which shows the fastest increase after onset of light (cluster 1), while putrescine, the precursor of spermidine, increases later and clusters together with the "hub" amino acids glutamate, aspartate and serine (cluster 3).

Intermediates of glycolysis are overrepresented in cluster 3 as well as sugars and sugar derivatives (sugar alcohols and sugar phosphates). In contrast to that organic acids of the TCA cycle show a quite divers timing in their accumulation. The mid to late TCA cycle intermediates, succinate and malate belong to cluster 2 and show the earliest increase among the annotated TCA cycle intermediates. They are followed by 2-oxoglutarate which increases at the same time as chlorophyll (cluster 3). Citrate and fumarate only increase in the middle of the light phase (cluster 4).

Within the purine metabolism, the nucleotides (GMP and AMP) are in the same cluster (cluster 2). They display an earlier increase than their nucleobases (guanine and adenine) which are both in cluster 3. Interestingly, we found that hypoxanthine, which is a degradation product of AMP, shows the earliest increase within the annotated intermediates of purine metabolism while the central metabolite of purine degradation, xanthine [149] display the latest increase.

3.2.3.4 *Several temporal and quantitative changes within the primary metabolism are induced by rapamycin-based TOR inhibition*

Although the TOR signaling pathway is tightly linked to central metabolism investigations on global effects of TOR on the metabolome are quite rare. However, recently, three publications came up, describing metabolic changes after TOR inhibition in mouse, *Arabidopsis* and *Chlamydomonas* [113, 114, 150].

To investigate the response dynamics of the *Chlamydomonas* metabolome to the inhibition of TOR by rapamycin, we used the same experimental set up as described in chapter 3.2.2 which results in total number of 6 replicates and a time series of 15 TP. Rapamycin was added with the onset of light and the first samples were taken 15 min after rapamycin treatment. The 68 annotated metabolites cover fairly the primary metabolism of *Chlamydomonas* cells (see chapter 3.2.3).

The analysis of the primary metabolism of *Chlamydomonas* showed already that the primary metabolites are differentially regulated during the cell cycle (see chapter 3.2.3). The use of the synchronized system and a high-resolution time series enabled us to detect, beside quantitative

changes of primary metabolites, differences in the metabolic pattern. Additionally, this system enabled us to consider the results in the context of the cellular life cycle.

3.2.3.4.1 *Principal component- and hierarchical cluster-analysis reveal a clear separation of control and rapamycin treatment*

Using unsupervised PCA a clear separation of control and rapamycin treatment can be achieved in the first component PC 1 which explains 61% of the variance (Figure 33). The second component PC 2 leads to a separation of different TPs within the two conditions.

The time series of both, control and rapamycin treatment, describes nearly a circle while that of rapamycin treatment is more compressed compared to control (Figure 33). Therefore the separation of early light phase, main light phase and dark phase is not as clear as under control conditions. Especially, TPs of early dark phase (13 h and 14 h) are closer to the light phase after rapamycin treatment.

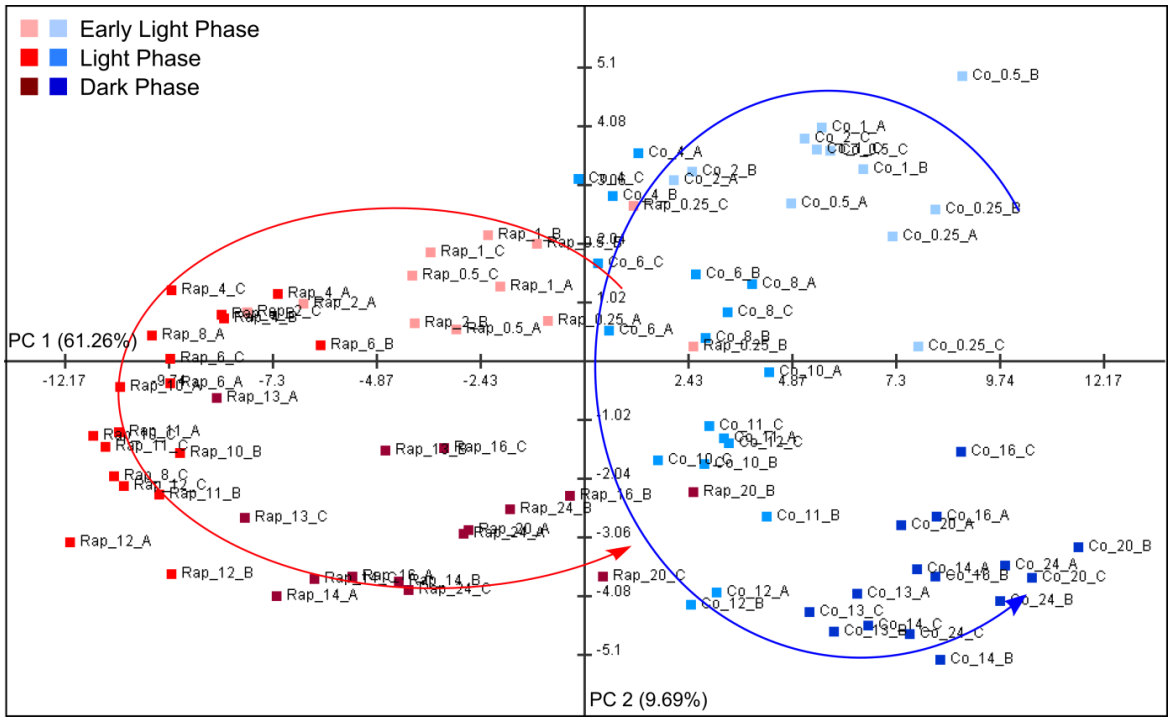

Figure 33. Principal component analysis (PCA) of primary metabolites of synchronized Chlamydomonas cultures for rapamycin treatment and control
PCA of primary metabolites, which are chlorophyll normalized and log_2-transformed, of a *Chlamydomonas* culture synchronized by 12:12 h light-dark regime. The TPs in h and replicates are indicated as numbers or letters, respectively. Separation of early light phase (0.25 h – 2 h), light phase (4 h – 12 h) and dark phase (13 h – 24 h) as indicated. Co = Control; Rap = rapamycin treatment

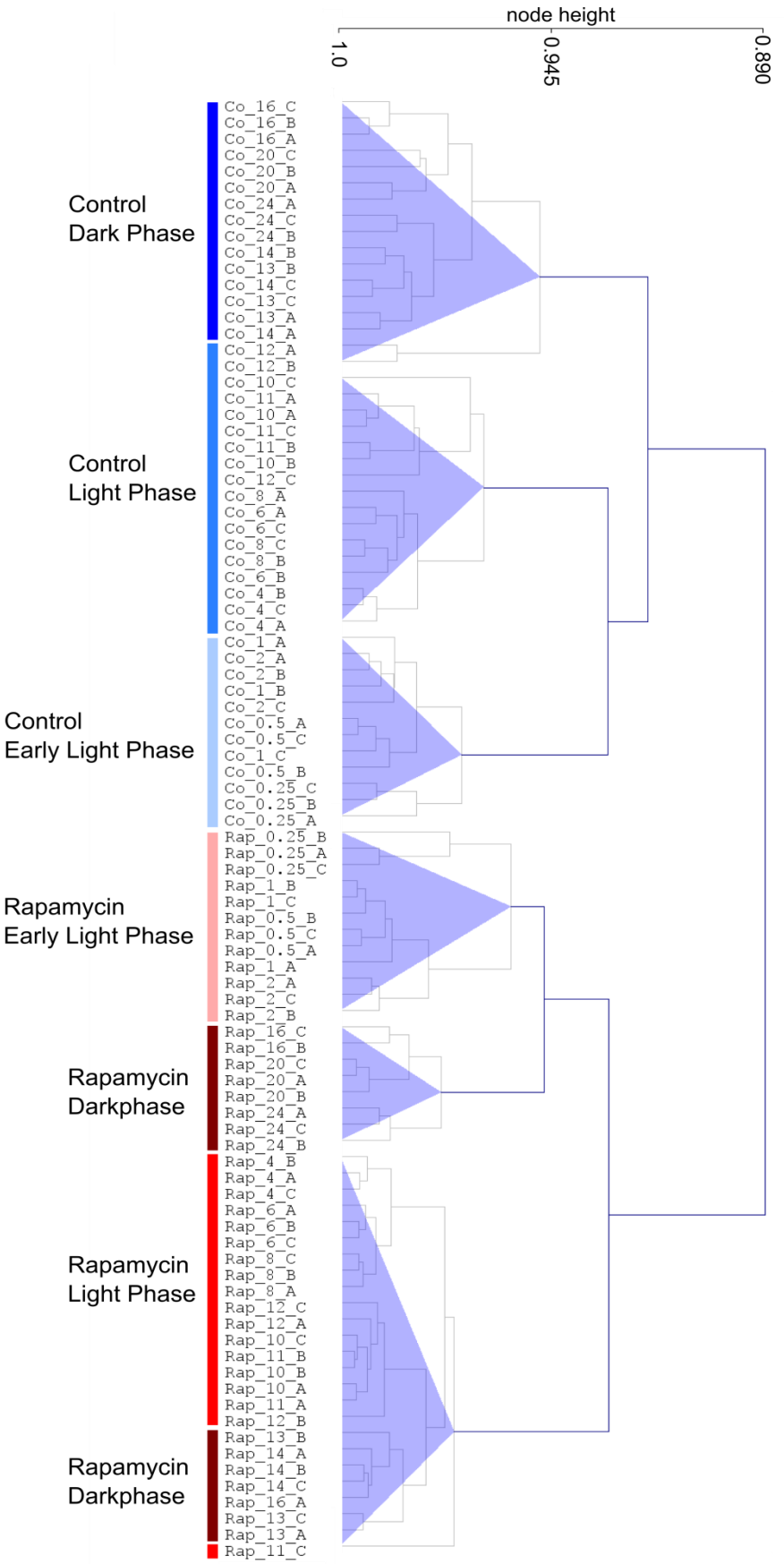

Figure 34. Hierarchical cluster analysis (HCA) of primary metabolites of a synchronized culture for rapamycin treatment and control

Clustering analysis was performed across the samples using Pearson correlation and average linkage method for primary metabolites, which are chlorophyll normalized and log_2-transformed. Separation of early light phase (0.25 h – 2 h), light phase (4 h – 12 h) and dark phase (13 h – 24 h) as indicated.

In addition to the multivariate analysis we applied hierarchical cluster analysis (HCA) using Pearson correlation and an average linkage method [126, 139]. Like the PCA results, the HCA shows a clear separation of control and treated samples while the three biological replicates cluster close together (Figure 34). In addition, we obtained for both conditions 3 representative clusters. Under control conditions the clusters were the same as in the PCA (Figure 30). Only the TP of onset of dark (TP 12 h) could not be assigned precisely to one of the phases by using HCA. One replicate of this TP was found within the cluster of light phase while the other two replicates are in the cluster of dark phase. Nevertheless, within the cluster of dark phase the two replicates of TP 12 h are furthest from all other TP. This is contrary to the results of the PCA where the replicates of TP 12 h are much closer to TP 10 h and TP 11 h compared to the TPs of the dark phase (Figure 30).

Comparing the clusters of rapamycin treatment to that of the control we observed that the cluster of early light phase contain the same TPs under both conditions while the other two cluster differ from that of control. The cluster of light phase includes additionally TPs of the early dark phase (TP 13 h and TP 14 h) confirming metabolically the observed developmental delay of *Chlamydomonas* after rapamycin treatment (see chapter 3.1.4). Interestingly, the critical TP which could not be assigned precisely to one of the clusters under control conditions (TP 12 h) seems to be also time shifted under rapamycin treatment as we found one replicate of TP 16 h in the cluster of light and early dark phase whereas the other two replicates are in the dark phase cluster.

3.2.3.4.2 *Increase of the primary metabolite pool size after rapamycin treatment*

To get a first idea of how the metabolome is changed after rapamycin treatment we compared the total ion count (TIC; summed intensity of all identified metabolites) of the rapamycin treated culture to the control (Figure 35). The results show that the summed pool size of the metabolites is strongly increased throughout the entire cell cycle. Interestingly, we could see that this increase starts already 15 min after rapamycin treatment. In contrast to the measured assimilation product starch content, the TIC of the primary metabolites is not only higher on a cellular level (per cell), but also on the total level (per ml) (Figure 35 A, C). Comparison of the relative increase of the TIC over time shows that the summed metabolic pool size is negatively correlated to the cellular growth and increases about 2 h earlier in the rapamycin culture (Figure 35 B). After 30 min of treatment the TIC has increased by a factor of 4, while this boost is visible for the control only between 2 – 4 h in light.

Generally, we could observe that after TP 4 h the pattern of the TIC distribution on the total level (Figure 30 B) is quite comparable under both conditions in the light. Both show a flattening of the TIC curve between 6 -8 h, followed by a stronger increase between 8 – 10 h. Between 10 – 12 h the TIC of both cultures remains nearly on a constant level. With beginning of the dark phase we could

observe a reduction in the metabolome level under both conditions. Comparison of the TIC pattern on the cellular level shows an increase under both conditions from the onset of light until TP 4 h. Between 4 – 12 h the cellular TIC level of the rapamycin treated culture remains almost constant while that of the control decreases between 4 – 8 h and remains only constant in the last 4 h in light. Under both conditions the cellular TIC level starts to decrease with the onset of darkness. While the control shows only a decrease for 1 h and remains then relatively constant for the remaining dark phase, the cellular TIC of the rapamycin treated culture decreases almost during the entire light phase.

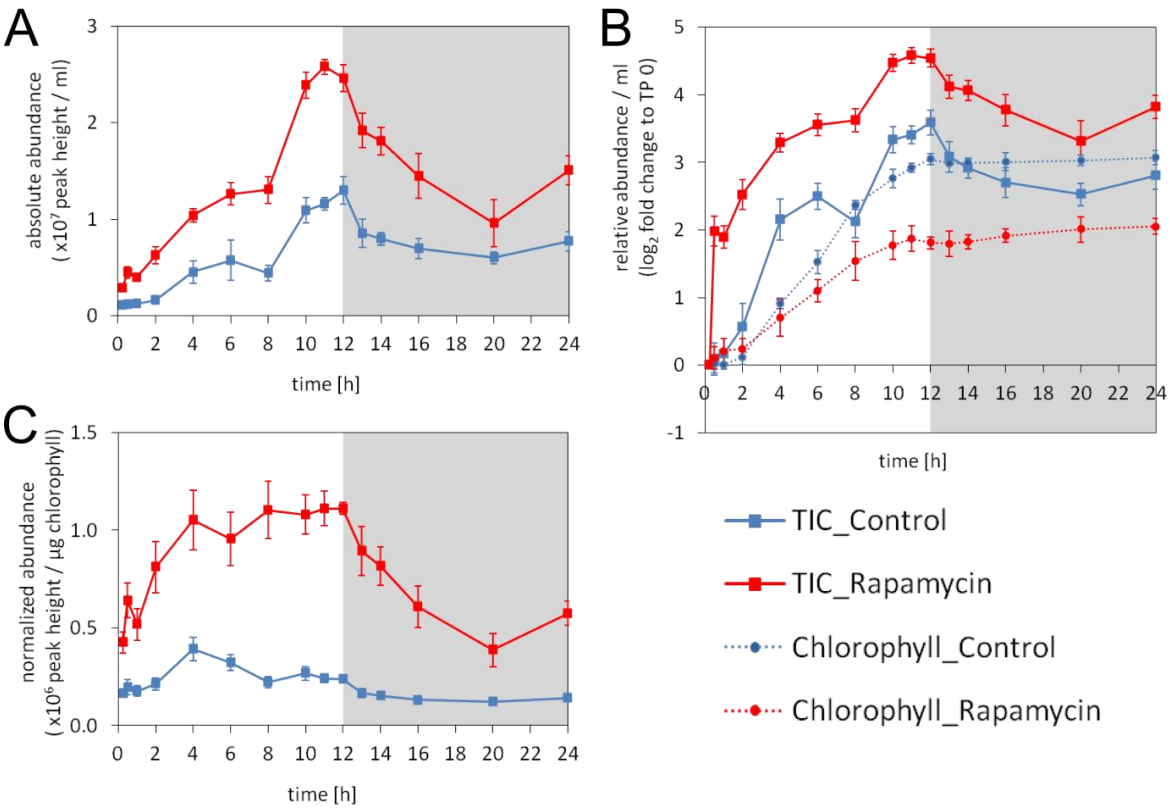

Figure 35. Comparison of the total ion count of primary metabolites for control and rapamycin treatment
Total ion count (TIC) of primary metabolites was analyzed at the indicated times for a *Chlamydomonas* culture treated with rapamycin (red) in comparison to control (blue). The cells were synchronized by a 12:12 h light-dark cycle. (A) TIC per ml. (B) TIC and chlorophyll concentration as $\log_2$ fold change to TP 0. (C) TIC normalized to chlorophyll. Grey background indicates the dark phase. Data are given as mean ± SD of 3 biological replicates.

3.2.3.4.3 *Primary metabolites respond very fast to rapamycin treatment*

The results of multivariate analysis (PCA) and the TIC imply already that inhibition of TOR by rapamycin lead to strong changes of primary metabolism within few minutes. Indeed, 15 min after rapamycin treatment nearly 50% of annotated primary metabolites were significantly changed; in which 29 were increased while 4 were down-regulated (Figure 36). The results demonstrate that

cells in early G1 phase respond very fast to inhibition of TOR by rapamycin. Among the increased metabolites amino acids are highly overrepresented. Except two amino acids (tryptophan and cysteine) all proteinogenic as well as the non-proteinogenic amino acids are significantly increased. However, although not significant, tryptophan and cysteine show a clear increase. More than 70% of the amino acids are increased by a factor of greater than 2 (Figure 36). Glutamine even shows a more than 8-fold increase. Beside the amino acids, the TCA cycle intermediate 2-oxoglutarate, which is the precursor for glutamate, is also significantly increased. Contrary, another intermediate of the TCA cycle, namely malate, is significantly decreased (Figure 36). In addition, we observed that two intermediates of glycolysis (phosphoenolpyruvate and fructose-6-phosphate) are significantly decreased 15 min after rapamycin treatment (Figure 36). Next to these intermediates, also fructose, sucrose, mannose-6-phosphate and glucose-6-phosphate display a reduced cellular amount compared to the control, from which only fructose is significantly decreased. Except mannose-6-phosphate, these sugars and sugar-derivatives are all intermediates of the following pathways glycolysis, sucrose synthesis/degradation and starch synthesis/degradation. Nevertheless, mannose-6-phosphate is not unrelated to these pathways as it can be directly converted to fructose-6-phosphate. A sugar which is neither an intermediate nor very close to these pathways is ribose which shows a 2-fold increase within this short time after rapamycin treatment. On the other hand, we could also observe that maltose which is a product of the hydrolysis of starch display a significant increase.

3.2.3.4.4 *Identification of primary metabolites which are shifted in time and / or their abundance after rapamycin treatment*

In a next step we focused on changes of the metabolic pattern caused by rapamycin treatment. In chapter 3.2.3.2 we could already show that under standardized conditions primary metabolites increase at different TPs within the cell cycle. Now, we wanted to find out if the timing of increase is changed after rapamycin treatment (T-x, earlier increase after treatment; T0, increase at the same time as control; T+x, later increase after treatment). In addition, we are interested if the metabolites after rapamycin treatment achieve a higher (L+x), the same (L0) or a lower (L-x) level at the end of the dark phase (TP 24 h). For the comparison of the timing of increase the total amount (per ml) of each metabolite was used as this value is independent of the increase of chlorophyll and thereby reflects the increase of a compound within the cell culture. This was especially important for metabolites that increase at the same time and in the same quantity as chlorophyll. Those metabolites will therefore show no changes over the entire cell cycle per chlorophyll although they increase per ml.

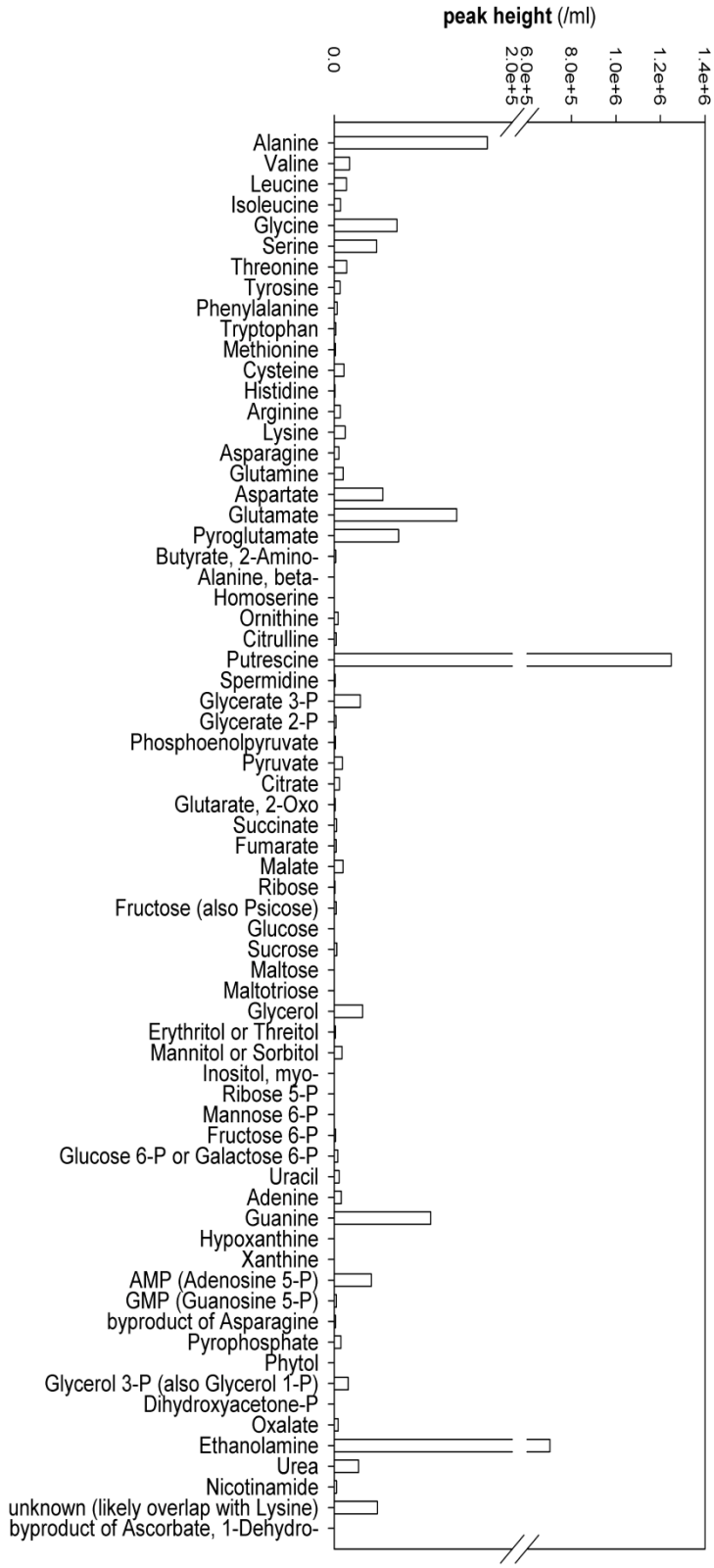

Class	Metabolite	LOG_2 fold change
Amino Acids	**Alanine**	**2.16****
	Valine	1.19**
	Leucine	1.05**
	Isoleucine	1.05**
	Glycine	1.14*
	Serine	1.74**
	Threonine	1.48**
	Tyrosine	0.92**
	Phenylalanine	0.94**
	Tryptophan	0.29
	Methionine	0.45**
	Cysteine	0.52
	Arginine	1.48**
	Lysine	1.23**
	Histidine	**2.04***
	Asparagine	**2.28****
	Glutamine	**4.22****
	Aspartate	1.76**
	Glutamate	**2.05****
Non-protein AA	Pyroglutamate	1.67**
	Butyrate, 2-Amino-	0.46**
	Alanine, beta-	1.19**
	Homoserine	0.91*
	Ornithine	1.03**
	Citrulline	1.71**
Polyamine	Putrescine	0.16
	Spermidine	-0.20
Organic Acids in Glycolysis	Glycerate 3-P	-0.31
	Glycerate 2-P	-0.54
	Phosphoenolpyruvate	**-0.96****
	Pyruvate	0.40
Organic Acids in TCA Cycle	Citrate	-0.36
	Glutarate, 2-Oxo	0.34**
	Succinate	0.13
	Fumarate	0.17
	Malate	-0.27*
Sugars	Ribose	1.06**
	Fructose (also Psicose)	-0.78*
	Glucose	0.27
	Sucrose	-0.54
	Maltose	0.56*
	Maltotriose	0.51
Sugar-Alcohol	Glycerol	0.35
	Erythritol or Threitol	0.06
	Mannitol or Sorbitol	0.22
	Inositol, myo-	0.20
Sugar Phosphates	Ribose 5-P	0.00
	Mannose 6-P	-0.42
	Fructose 6-P	-0.94*
	Glucose 6-P or Galactose 6-P	-0.85
Nucleobases	Uracil	-0.02
	Adenine	0.29
	Guanine	0.75
	Hypoxanthine	0.22
	Xanthine	-0.23
Nucleotides	AMP (Adenosine 5-P)	0.43
	GMP (Guanosine 5-P)	0.36
Other Metabolites	byproduct of Asparagine	1.27**
	Pyrophosphate	0.71*
	Phytol	0.78*
	Glycerol 3-P (also Glycerol 1-P)	0.39
	Dihydroxyacetone-P	1.32
	Oxalate	0.38
	Ethanolamine	0.15
	Urea	-0.20
	Nicotinamide	0.01
	unknown (likely overlap with Lysine)	0.17
	byproduct of Ascorbate, 1-Dehydro-	0.17

Figure 36. Log_2 fold changes of rapamycin treatment to control after 15 min of treatment
Averaged intensities (peak height) of the total amount of primary metabolites at TP 0.25 h are shown in the bar plot (right side; n=6). The table next to the bar plot displays log_2 fold changes of the cellular amount of primary metabolites for the rapamycin treated culture in comparison to the control at TP 0.25 h. Significant ($p < 0.05$) increased (orange) and decreased (blue)and highly significant ($p < 0.01$) increased (red) metabolites are indicated by asterisks.

The combination of the three possibilities for each factor (T and L) finally results in nine possible groups (Figure 37 A). A detailed description for this analysis is given in chapter 0. These groups are referred to as clusters, even though they are not clustered in a classical cluster method. For the analysis of the grouping we used the total amount (per ml) of each metabolite. But due to the rapamycin induced growth reduction (cell size and cell number), a compound which shows the same level in the total amount (per ml) under both conditions should therefore be higher in the cellular amount (per cell). On the other hand a compound which shows a decrease in the total amount can be still higher, the same, but also lower on the cellular level. Although, changes in the cellular amount were not considered in the clustering they need to be taken into account for the interpretation of the data. Therefore, the $\log_2$ fold changes of the cellular amount of rapamycin treatment to control at TP 24 h are additionally presented in the tables for each cluster (Figure 37 B).

In total we found 35 metabolites which show an earlier increase after rapamycin treatment (T-x). Nearly the same amount namely 30 metabolites display no change in the timing of increase (T0) while only 3 metabolites are delayed (T+x). For the quantitative comparison we found the metabolites more evenly distributed; 23 metabolites are higher (L+x), 26 are similar (L0) and 19 are lower (L-x) than the control at the end of the cell cycle.

With the exception of 4 amino acids (tyrosine, phenylalanine, methionine and 2-aminobutyrate) which are not affected in the timing of increase (T0), all amino acids (proteinogenic and non-proteinogenic) show an earlier increase after rapamycin treatment (Figure 37 B). Among the amino acids only cysteine is decreased at the end of the cell cycle in comparison to the control while all the others are increased. Next to amino acids, 4 intermediates of the purine metabolism, namely guanine, hypoxanthine, xanthine and AMP display an earlier increase as well. Guanine and hypoxanthine display also a higher level in the total amount as well as in the cellular amount. Also AMP is significantly increased in the cellular amount while xanthine achieves a similar cellular level as the control at the end of the dark phase.

Furthermore, we found that organic acids of glycolysis are not affected in the timing of increase and in their cellular level after rapamycin treatment. The two annotated poylamines, spermidine and putrescine, are also not affected in the timing of increase, but they are both significantly increased at the cellular level while spermidine is even increased at the total level. Intermediates of the TCA cycle seem to be differentially regulated after rapamycin treatment. In contrast to citrate, 2-oxoglutarate and succinate which are not changed in the timing of increase, fumarate and malate increase earlier than under control conditions. In addition, they are differentially changed in the cellular level at the end of the cell cycle. While citrate and fumarate display no significant change, 2-oxoglutarate and succinate are significantly increased and malate is significantly decreased.

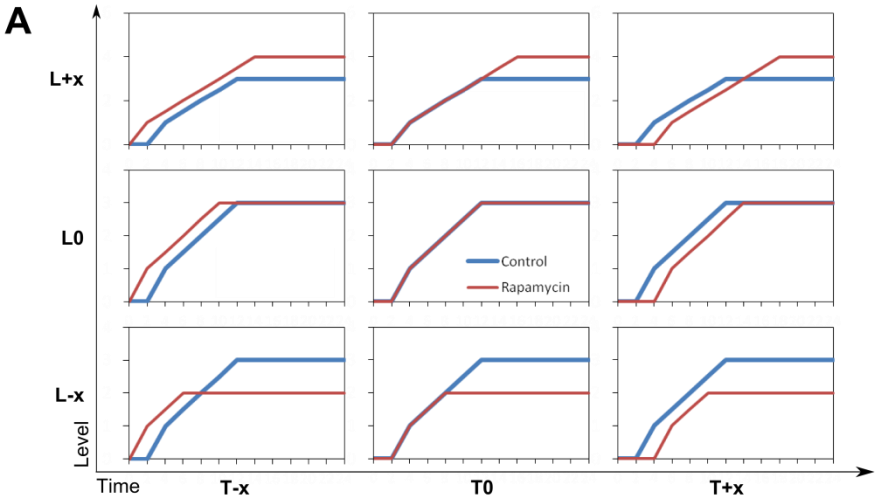

B

T-x/L+x (20 Metabolites)

Class	Metabolite	log_2 fold change TP 24 h
Amino Acids	Alanine	2.94
	Asparagine	3.04
	Aspartate	3.22
	Glutamate	2.23
	Glutamine	3.21
	Glycine	2.21
	Isoleucine	1.95
	Leucine	1.33
	Lysine	1.84
	Serine	2.24
	Threonine	2.27
	Valine	2.02
Non-protein Amino Acids	Alanine, beta-	2.40
	Homoserine	2.29
	Pyroglutamate	1.69
	Ornithine	2.62
Nucleobases	Guanine	3.01
	Hypoxanthine	5.59
Other Metabolites	byproduct of Asparagine unknown (likely overlap with Lysine)	1.84 1.56

T-x/L0 (9 Metabolites)

Class	Metabolite	log_2 fold change TP 24 h
Amino Acids	Arginine	0.88
	Histidine	1.59
	Tryptophan	1.12
Non-protein Amino Acids	Citrulline	1.35
Organic Acid in TCA Cycle	Fumarate	0.61
Sugar	Sucrose	0.34
Sugar-Alcohol	Mannitol or Sorbitol	0.13
Nucleobase	Xanthine	-0.15
Other Metabolites	Urea	0.76

T-x/L-x (6 Metabolites)

Class	Metabolite	log_2 fold change TP 24 h
Amino Acid	Cysteine	-1.02
Organic Acid in TCA Cycle	Malate	-0.40
Sugar	Ribose	-0.06
Sugar-Alcohol	Glycerol	0.18
Nucleotide	AMP (Adenosine 5-P)	0.50

T0/L+x (3 Metabolites)

Class	Metabolite	log_2 fold change TP 24 h
Amino Acid	Tyrosine	1.47
Non-protein Amino Acid	Butyrate, 2-Amino-	1.92
Polyamine	Spermidine	1.87

T0/L0 (16 Metabolites)

Class	Metabolite	log_2 fold change TP 24 h
Amino Acid	Methionine	0.99
	Phenylalanine	1.10
Polyamine	Putrescine	1.11
Organic Acid in Glycolysis	Glycerate 2-P	0.31
Organic Acid in TCA Cycle	Glutarate, 2-Oxo	1.05
	Succinate	0.79
Sugars	Glucose	0.42
	Maltose	0.56
	Maltotriose	1.02
Sugar-Alcohol	Inositol, myo-	0.72
Nucleobases	Adenine	0.58
	Uracil	0.39
Other Metabolites	Ethanolamine	0.81
	Oxalate	0.82
	Phytol	0.01
	Pyrophosphate	0.49

T0/L-x (11 Metabolites)

Class	Metabolite	log_2 fold change TP 24 h
Organic Acids in Glycolysis	Glycerate 3-P	-0.08
	PEP	-0.55
	Pyruvate	0.36
Organic Acids in TCA Cycle	Citrate	0.00
Sugar	Fructose (also Psicose)	0.24
Sugar-Alcohol	Erythritol or Threitol	0.51
Sugar Phosphates	Ribose 5-P	0.45
Nuleotide	GMP (Guanosine 5-P)	0.25
Other Metabolites	byproduct of Ascorbate, 1-Dehydro-	-0.11
	Dihydroxyacetone-P	-1.32
	Glycerol 3-P (also Glycerol 1-P)	0.07

T+x/L+x (-)

T+x/L0 (1 Metabolite)

Class	Metabolite	log_2 fold change TP 24 h
Sugar Phosphate	Fructose 6-P	0.21

T+x/L-x (2 Metabolites)

Class	Metabolite	log_2 fold change TP 24 h
Sugar Phophates	Glucose 6-P or Galactose 6-P	-0.39
	Mannose 6-P	-1.10

z

Figure 37. Clustering of the metabolic response to rapamycin under synchronized conditions
(A) Predicted clusters of the metabolic pattern of the rapamycin treated culture (red) in comparison to control (blue) based on a simplified 2-factorial analysis of time (T) and level (L). A detailed description is given in chapter 0. (B)Tables show the metabolites which belong to the 9 predicted clusters. In addition, the log_2 fold changes of the cellular amount between rapamycin treated culture and control are presented for TP 24 h. Significant ($p < 0.05$) increased and decreased metabolites are indicated in red or blue, respectively.

Interestingly, we could observe that the only 3 metabolites which are delayed after rapamycin treatment are all sugar phosphates. While at the end of the dark phase fructose-6-phosphate and glucose-6-phosphate attain nearly the same level as the control, mannose-6-phosphate is significantly decreased.

3.2.3.4.5 *Visualization of primary metabolites and their respective pathways after treatment with rapamycin under synchronized growth conditions*

As described above, we analyzed quantitative and temporal changes of primary metabolites over the entire cell cycle. Here we now try to integrate and visualize the data within their respective pathways. Therefore, the dynamic $\log_2$ fold changes of chlorophyll normalized data (cellular level) were used (Figure 38; Supp. table 2). The results so far suggest that within the primary metabolism the amino acids are the most consistent group with regard to their dynamic response to the rapamycin treatment. Indeed, we could observe that with minor exceptions all amino acids are strongly up-regulated over the entire cell cycle. This includes also the non-proteinogenic amino acids. Only the aromatic amino acids (tryptophan and phenylalanine) and the sulfur-containing (cysteine and methionine) display a quite different pattern. Cysteine and methionine are even significantly decreased at the end of the dark phase. Additionally, we found that also the amino acid precursors (pyruvate and 2-oxoglutarate) are significantly increased. But interestingly, pyruvate and 2-oxoglutarate show this increase later than their corresponding amino acids (Figure 38).

In particular, intermediates of the purine metabolism, guanine and hypoxanthine, are also significantly up-regulated over the entire cell cycle. Besides the strong up-regulation of amino acids and intermediates of purine metabolism, we noted an intermittently down-regulation of various key intermediates of central metabolism as glycolysis (glucose-6-phosphate, fructose-6-phosphate, mannose-6-phosphate, dihydroxyacetone phosphate, phosphoenolpyruvate), pentose phosphate pathway (ribose-5-phosphate) and TCA cycle (citrate, succinate and malate) (Figure 38). This regulation is much more pronounced within the light phase, the time where the cells increase in size and divide.

Taken together the pathway visualization shows that rapamycin treatment strongly affects the primary metabolism. But beside those strong changes we could identify a small number of metabolites which display no or only minor changes after rapamycin treatment. This includes the purine intermediate GMP, the glycolysis intermediate glycerate-3-phosphate and a precursor of lipid metabolism, namely glycerol-3-phosphate.

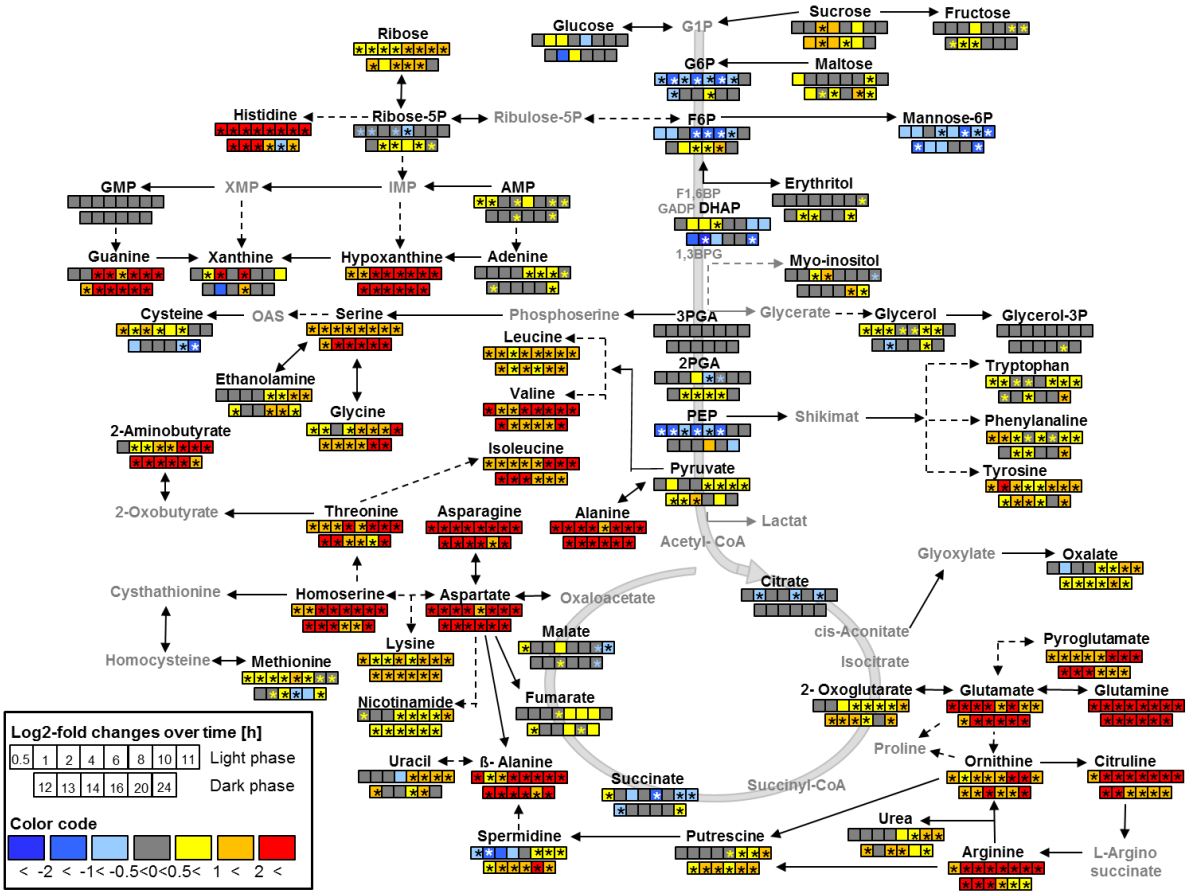

Figure 38. Pathway map with log_2 fold changes of primary metabolites after rapamycin treatment
Visualized are central metabolic pathways. Comparison of primary metabolites of rapamycin treatment versus control for each TP are shown as log_2 fold changes for a *Chlamydomonas* culture synchronized by a 12:12 h light-dark regime. The boxes display changes at the respective TPs according to the color code indicated. Significant changes ($p < 0.05$) for each TP are indicated with an asterisk. Significant log_2 fold changes between 0 - 0.5 are indicated with a yellow asterisk and between -0.5 – 0 with a blue asterisk. Data are medians of 6 independent replicates. G1P – Glucose-1-phosphate; G6P – Glucose-6-phosphate; F6P – Fructose-6-phosphate; F1,6BP – Fructose-1,6-bisphosphate; G3P – Glyceraldehyde-3-phosphate; DHAP – Dihydroxyacetone phosphate; 1,3BPG – Bisphosphoglycerate; 3PGA – Glycerate-3-phosphate; 2PGA – Glycerate-2-phosphate; PEP – Phosphoenolpyruvate; GMP – Guanosine monophosphate; XMP – Xanthosine monophosphate; IMP – Inosine monophosphate; AMP – Adenosine monophosphate; OAS – O-Acetylserine

3.2.4 Lipid profiling of synchronously growing *Chlamydomonas* cultures

In addition to chlorophyll, starch and primary metabolites we further investigated dynamic changes of the lipid metabolism in the vegetative cell cycle of *Chlamydomonas*. The experimental set up was the same as described in chapter 3.2.2. For identification of lipids, samples were measured in positive and negative ion mode on an UPLC-FT-MS and the data was processed and annotated as described in chapter 2.2.5.2. With this method we were able to unambiguously annotate 297 lipids species covering the 10 major lipid classes, namely diacylglycerol (DAG), digalactosyldiacylglycerol (DGDG), monogalactosyldiacylglycerol (MGDG),

sulfoquinovosyldiacylglycerol (SQDG), diacyclglyceryl-N,N,N-trimethylhomoserine (DGTS), triacylglycerol (TAG), phophatidylglycerol (PG), phosphatidylethanolamine (PE), lysophosphatidylethanolamine (lyso-PE) and free fatty acid (FFA).

3.2.4.1 *Distribution of lipid species*

The identified lipid classes with their main functions and their most abundant lipid species and adduct ions are presented in Table 11. The largest number of annotated lipid species belong to the class of structural polar, betaine lipids DGTS and the neutral storage, glycerolipids of the TAG class. Furthermore, we found that with minor exceptions the most abundant lipid species within the membrane lipids consists of 34 carbons in their two fatty acids. This was not surprising as it has already been shown that the dominant chain lengths of the total fatty acid composition in *Chlamydomonas* were C_{16} and C_{18} [151]. Among the few exceptions include the PE, where the most abundant lipid species consist of 36 carbons, and the SQDG, where the most abundant lipid consists of 32 carbons. But also this is consistent with the previous observation of Giroud and coworkers made in 1988 [151].

Table 11. Distribution of identified lipids of *Chlamydomonas reinhardtii*
Identified lipid classes with number (#) of species and their percentage distribution (%) with regard to their abundance in respect of total lipids. In addition, the 3 most abundant lipid species as "carbon:doublebonds" within the lipid class are presented. Among these the most abundant lipid species is underlined.

Lipid class	Localization/Function	# of species / class	Most abundant species	Most abundant ion
FFA	Lipid synthesis precursor	5	18:1, 18:2, <u>18:3</u>	[M-H]
DAG	Plasma membrane/ signaling/ precursor	14	34:1, 34:6_A, <u>34:7</u>	[M+Na]
DGTS	Plasma membrane	68	34:2, <u>34:3_A</u>, 36:5_A	[M+H]
PE/lyso-PE	Plasma membrane	22	<u>36:3</u>, 36:4_B, 36:5	[M+H]
MDGD	Chloroplast membrane	32	34:4_B, 34:6_A, <u>34:7</u>	[M+Na]
DGDG	Chloroplast membrane	35	34:1, 34:2_B, <u>34:3_B</u>	[M+Na]
SQDG	Chloroplast membrane	19	<u>32:0</u>, 34:1, 34:3	[M-H]
PG	Chloroplast membrane	16	34:2_A, <u>34:3</u>, 34:4	[M-H]
TAG	Storage	86	52:4_A, <u>52:6_A</u>, 52:7_A	$[M+NH_4]$

3.2.4.2 *Multivariate analysis of lipids shows a similar temporal behavior as that of primary metabolites*

By using unsupervised PCA we obtained a plot that displays the time course for the different samples describing nearly a circle (Figure 39). This result is in accordance to the previous analysis of primary metabolites (Figure 30).

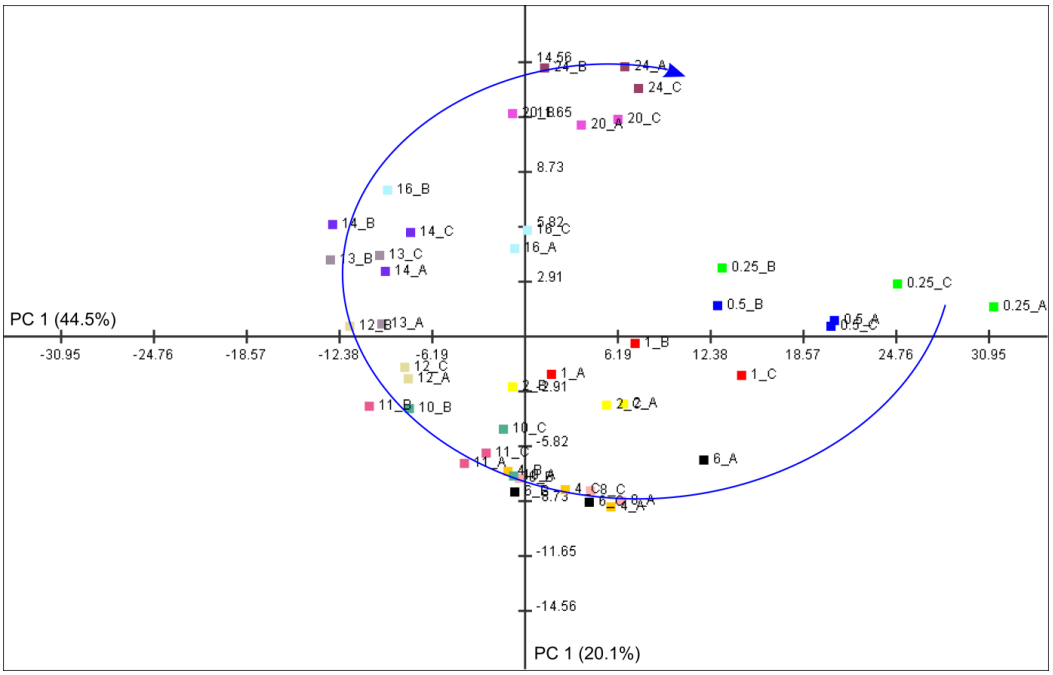

Figure 39. Principal component analysis (PCA) of lipids of a synchronized *Chlamydomonas* culture
PCA of lipids, which are chlorophyll normalized and $\log_2$-transformed, of a *Chlamydomonas* culture synchronized by 12:12 h light-dark regime. The time points in h and replicates are indicated as numbers or letters, respectively.

The obtained result supports our assumption that within one cell cycle the compositions of different compounds should be similar between start and end of the cell cycle. In contrast to the primary metabolite data, different phases within the time course are not as clearly visible. The largest gab was found within the dark phase between 16 h and 20 h in the dark phase. Additionally, we observed that the TPs of 4 – 11 h are closer to each other than the other TPs.

3.2.4.3 *Temporal cluster analysis of lipid species during the cell cycle*

Based on the assumption that within the cell cycle each compound should increase at a certain TP to the same level as the cell number, the temporal dynamics of the total amounts of lipid species were determined. By using the same criteria as described in chapter 3.2.3.2 and 2.2.12.3 five representative clusters were obtained (Figure 40; Supp. table 3).

In cluster 1 and 2 lipid species show an earlier increase than chlorophyll (dotted line). Lipid species in cluster 3 increase after 2 h in light, similar to chlorophyll, while they increase later in cluster 4 and 5. In general, lipid species show, similar to chlorophyll, an increase during the light phase and display only minor changes during the dark phase. On average the increase in cluster 2 – 5 is nearly linear, once the lipid species started to increase.

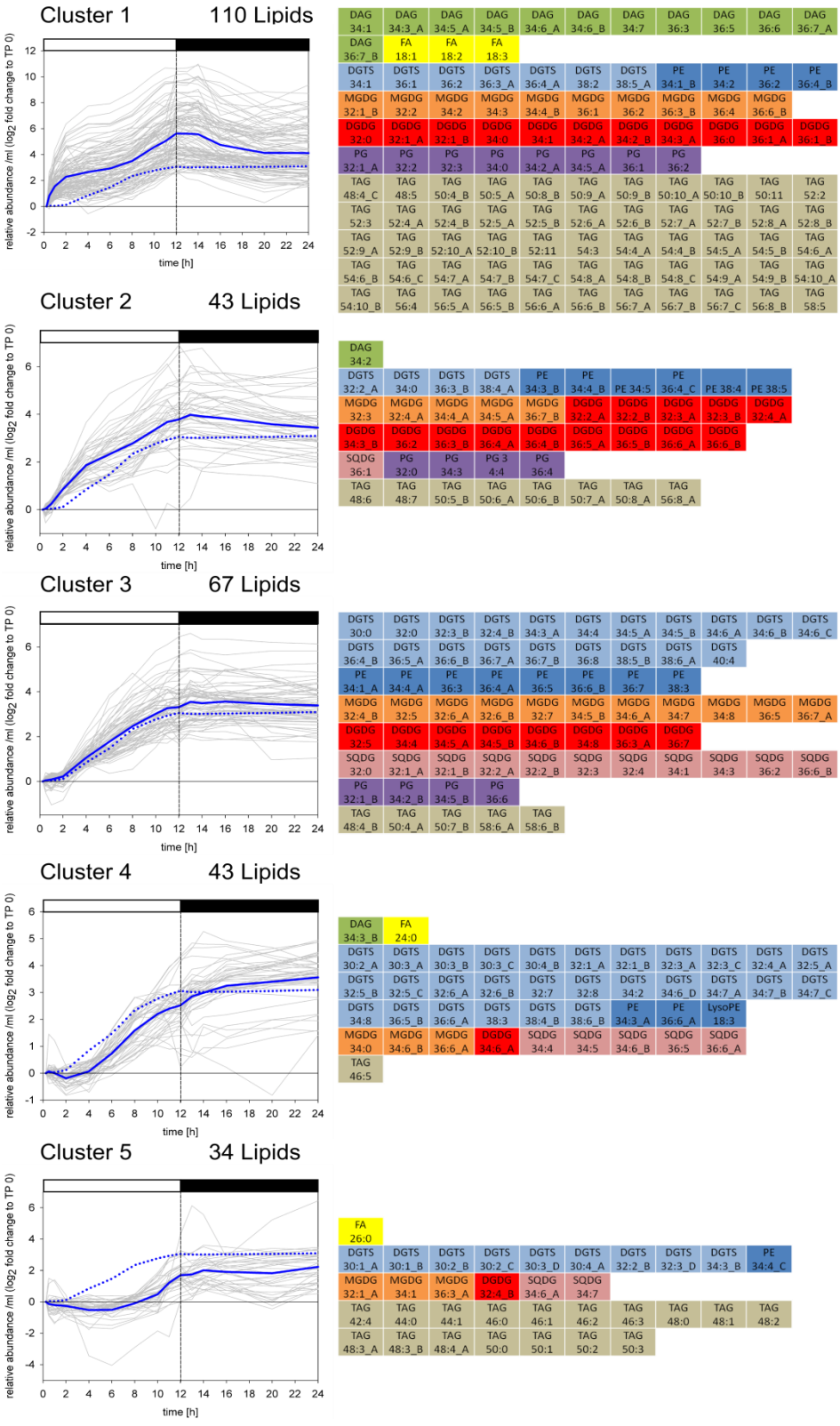

Figure 40. Time related clustering of lipids of a synchronized *Chlamydomonas* culture
Lipid species were grouped with regard to the TP when their level starts to increase. As a result the data was grouped into 5 clusters. To determine the belonging of each lipid species to one of the 5 clusters, specific criteria were established which are explained in detail in chapter 3.2.3.2. For each cluster the log_2-fold changes of the total amount to TP0 are plotted as a graph for each metabolite (grey) and the cluster average (blue). In addition the log_2 fold change of chlorophyll is shown (dotted blue line). The results show the median of 6 replicates per TP.

However, lipid species of cluster 1 show a more stepwise behavior with a flatting of the increase between 2 – 8 h, followed by a stronger increase at the end of the light phase. Further, we could observe that lipids which show an earlier increase than chlorophyll (cluster 1 and 2), usually display also a stronger increase than chlorophyll and therefore end up on a higher level at the end of the light phase. This is followed by a decrease in the total amount during the dark phase. This observation is similar to that of primary metabolites (see chapter 3.2.3.2). Interestingly, we found that lipids species of cluster 4 behave adversatively in the dark phase as they almost double their total amount during this time. On average, lipids of cluster 2 – 4 end up at the same level as chlorophyll while lipids of cluster 1 achieve a higher level and lipids of cluster 5 a lower level as chlorophyll. Contrary to our assumption, but similar to the observations made for primary metabolites, we found that some lipid species show strong differences in their level compared to chlorophyll.

More than one third of the lipid species belong to cluster 1 which shows a significant increase 0.5 – 1 h after the onset of light. With the exception of SQDG species all lipid classes can be found within this cluster. DAGs are the precursor of most lipid species and with the exception of 2 all DAGs belong to cluster 1. In addition, we found FFAs, which are the building blocks of lipids, in the same cluster. Among the FFAs, we found longer chain fatty acids as 24:0 and 26:0 start to increase later and therefore belong to cluster 4 and 5, respectively.

TAGs are next to starch the main storage form of carbon and energy. Different species of TAGs can be found in each cluster while the majority of TAGs belong to cluster 1 and therefore start to increase immediately after the onset of light. Most of the TAGs within cluster 1 contain 52 to 56 carbons in their three fatty acid acyl chains. With one exception these TAGs do not occur in one of the other clusters. Next to those we found also TAGs with 48 and 50 carbons within cluster 1, but only their higher unsaturated species (> 4 double bonds, db). The saturated and lower unsaturated forms (≤ 4 db) of these TAGs can be found in cluster 5 and therefore increase much later than their highly unsaturated forms. In addition, we could observe that TAGs with shorter chain fatty acids (42, 44 and 46 carbons) can only be found in cluster 5.

In general this clustering demonstrates that among the structural lipids the saturated and lower unsaturated forms increase earlier than their higher unsaturated forms. The plasma membrane lipids, DGTS and PE, are represented in all 5 clusters. While the majority of PEs can be found in cluster 3, DGTS are overrepresented in cluster 4. The lower unsaturated forms (≤ 2 db) of PEs and DGTS were found in cluster 1, while their higher unsaturated forms (> 2 db) are overrepresented in cluster 3 and 4. Interestingly, we found that DGTS with shorter chain fatty acids (30 and 32 carbons) can be only found in cluster 3 – 5. Thus, they start to increase later than DGTS with 34 and more carbons. However, they show a similar temporal behavior in their saturation pattern. The

saturated DGTS with 30 and 32 carbons increase earlier (cluster 3) than their unsaturated forms (cluster 4 and 5).

Within the lipids which are exclusively or, as in the case of PGs, mainly synthesized by the chloroplast, MGDGs, DGDGs and PGs are overrepresented in cluster 1 – 3. PGs even appear exclusively in cluster 1-3, with an overrepresentation in cluster 1. While the saturation pattern of DGDGs and PGs corresponds to that observed for plasma membrane lipids MGDGs show in partial a different temporal behavior in their saturation pattern. The monounsaturated forms of MGDGs with less than 36 carbons are in cluster 5 (MGDG 32:1_A and 34:1) and the saturated MGDG 34:0 was found in cluster 4. Thus, in this case the saturated and low unsaturated species increase later than their higher unsaturated (≥2 db) MGDGs which are mainly found in cluster 2 and 3. As already mentioned SQDGs are the only lipid class which was not found in cluster 1. With the exception of SGDG 36:1 (cluster 2), the saturated and low unsaturated (≤ 2 db) SGDG species increase at the same time as chlorophyll (cluster 3), similar to the DGTS with shorter chain fatty acids. This indicates that within the structural lipids the SQDGs are later synthesized. Nonetheless, the temporal behavior of the saturation pattern also corresponds to that observed for structural lipids.

3.2.4.4 *Changes in the lipid profile by rapamycin treatment during the cell cycle of Chlamydomonas*

To investigate the response dynamics of the *Chlamydomonas* lipidome to the inhibition of TOR by rapamycin, we used the same experimental set up as described in chapter 3.2.2 which results in total number of 6 replicates and a time series of 15 TP. Rapamycin was added with the onset of light and the first samples were taken 15 min after rapamycin treatment. For an overview of annotated lipids see Table 11.

3.2.4.4.1 *PCA and HCA reveal a clear separation of control and rapamycin treatment*

By using unsupervised PCA we can see that the cyclic pattern of the time series which was obtained under control conditions can be also observed after rapamycin treatment (Figure 41). This is similar to the observation made for primary metabolites (Figure 33). While under control conditions we could not observe any clear separation of specific time periods within the cell cycle rapamycin treatment leads to a separation of the time series into 3 distinct phases (Figure 41). The time period of the main light phase and early dark phase (TP 4 h – TP 16 h) can be clearly separated by the first component PC 1 from the early light phase (TP 0.25 h – TP 2 h) and the last 4 hours of the dark period (late dark phase; TP 20 h and TP 24 h).

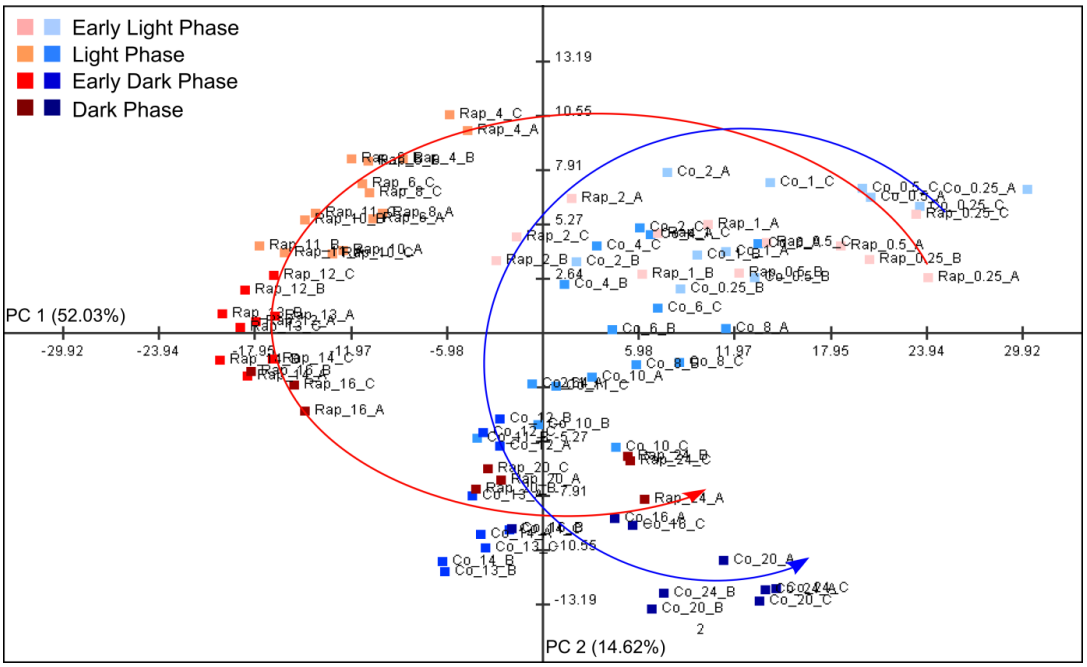

Figure 41. Principal component analysis (PCA) of lipids of a synchronized culture for rapamycin treatment and control
PCA of lipid dataset, which are chlorophyll normalized and $\log_2$-transformed, of a *Chlamydomonas* culture synchronized by 12:12 h light-dark cycle. The time points in h and replicates are indicated as numbers or letters, respectively. Separation of early light phase (0.25 h – 2 h), light phase (4 h – 11 h),early dark phase (12 h – 14 h) and dark phase (13 h – 24 h) as indicated. Co = Control; Rap = rapamycin treatment.

This is contrary to the observations of the primary metabolites where we observed a clear separation of specific time periods under control conditions which are no longer clearly separated after rapamycin treatment (Figure 33). Nevertheless, the separated time phases we obtained after rapamycin treatment differ from those of the primary metabolites under control conditions. However, it can be seen that the separation of the main light phase and early dark phase lead also to a separation of these TPs from those of the control while the TPs of early light phase and late dark phase are close to those of the control.

These observations can be further supported by the application of HCA (Figure 42). Like in the PCA, we can see that within the HCA the rapamycin treated samples from TP 4 h to TP 16 h are clearly separated from all other TPs of rapamycin treatment and control. The HCA also demonstrates that TPs of early light phase from the control and the rapamycin treatment cannot be clearly separated. In contrast, TPs of late dark phase form their own cluster after rapamycin treatment, but they are closely linked to TPs of dark phase of the control.

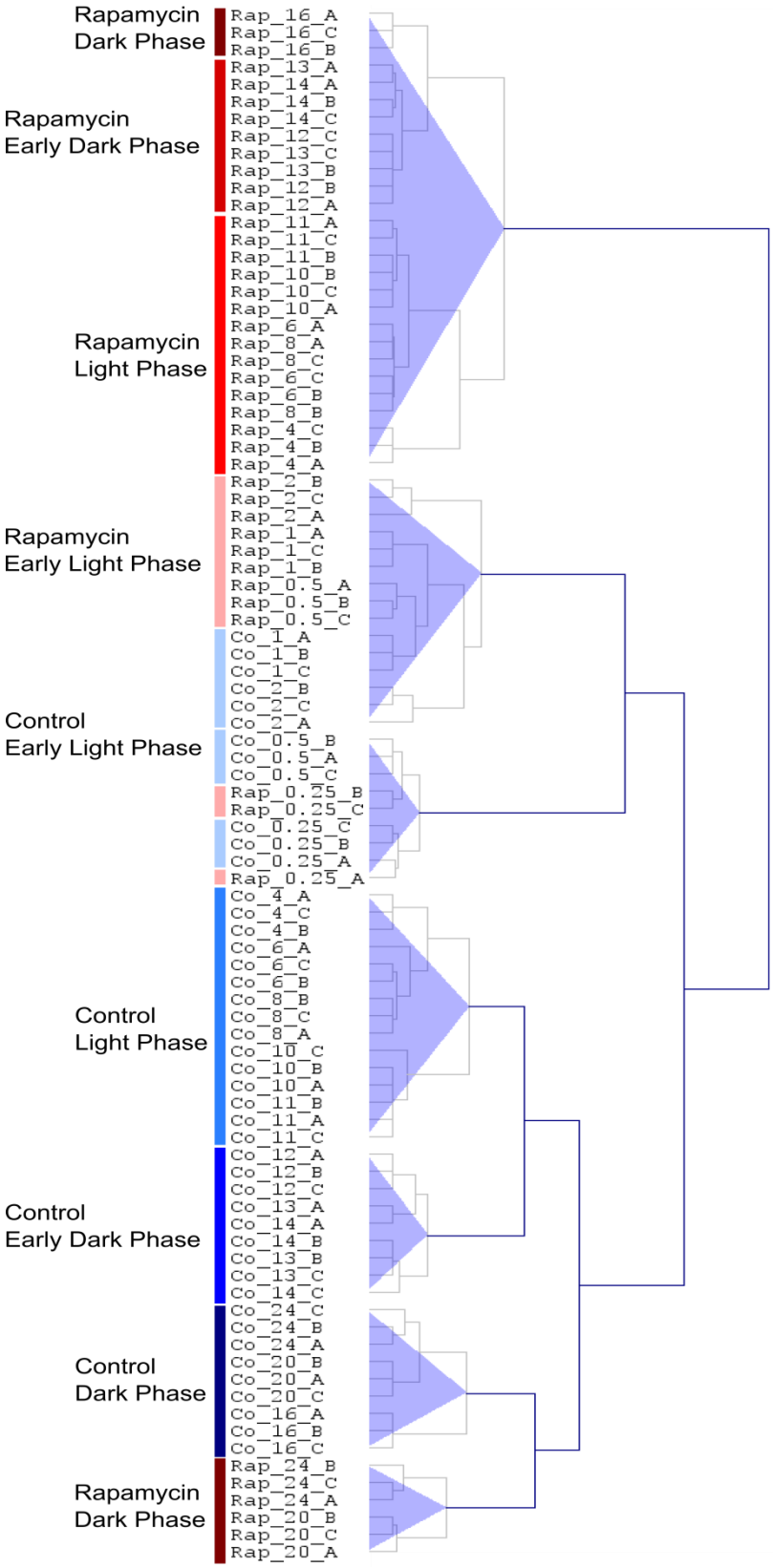

Figure 42. Hierarchical cluster analysis (HCA) of lipids of a synchronized culture for rapamycin treatment and control

Clustering analysis was performed across the samples using Pearson correlation and average linkage method for lipids, which are chlorophyll normalized and $\log_2$-transformed. Separation of early light phase (0.25 h – 2 h), light phase (4 h – 11 h), early dark phase (12 h – 14 h) and dark phase (13 h – 24 h) as indicated.

3.2.4.4.2 *Comparison of the total ion count (TIC) reveals a strong accumulation of storage lipids*

To get a first idea on changes of the lipidome caused by rapamycin treatment we compared the total ion count (TIC) of either structural lipids (DAG, MGDG, DGDG, PG, SQDG, DGTS, PE and FFA) or storage lipids (TAG) of the rapamycin treated culture to that of control (Figure 43). The results show that the total amount (per ml) of structural lipids is significantly reduced from 8 h in light until the end of the dark phase (TP 24 h; Figure 43 A). Interestingly, this demonstrates that the total amount of structural lipids is not affected by rapamycin treatment within the first half of the light phase. However, if considered in relation to chlorophyll (dotted line; Figure 43 B), the reduced amount of structural lipids corresponds approximately to the decline in cell growth after rapamycin treatment.

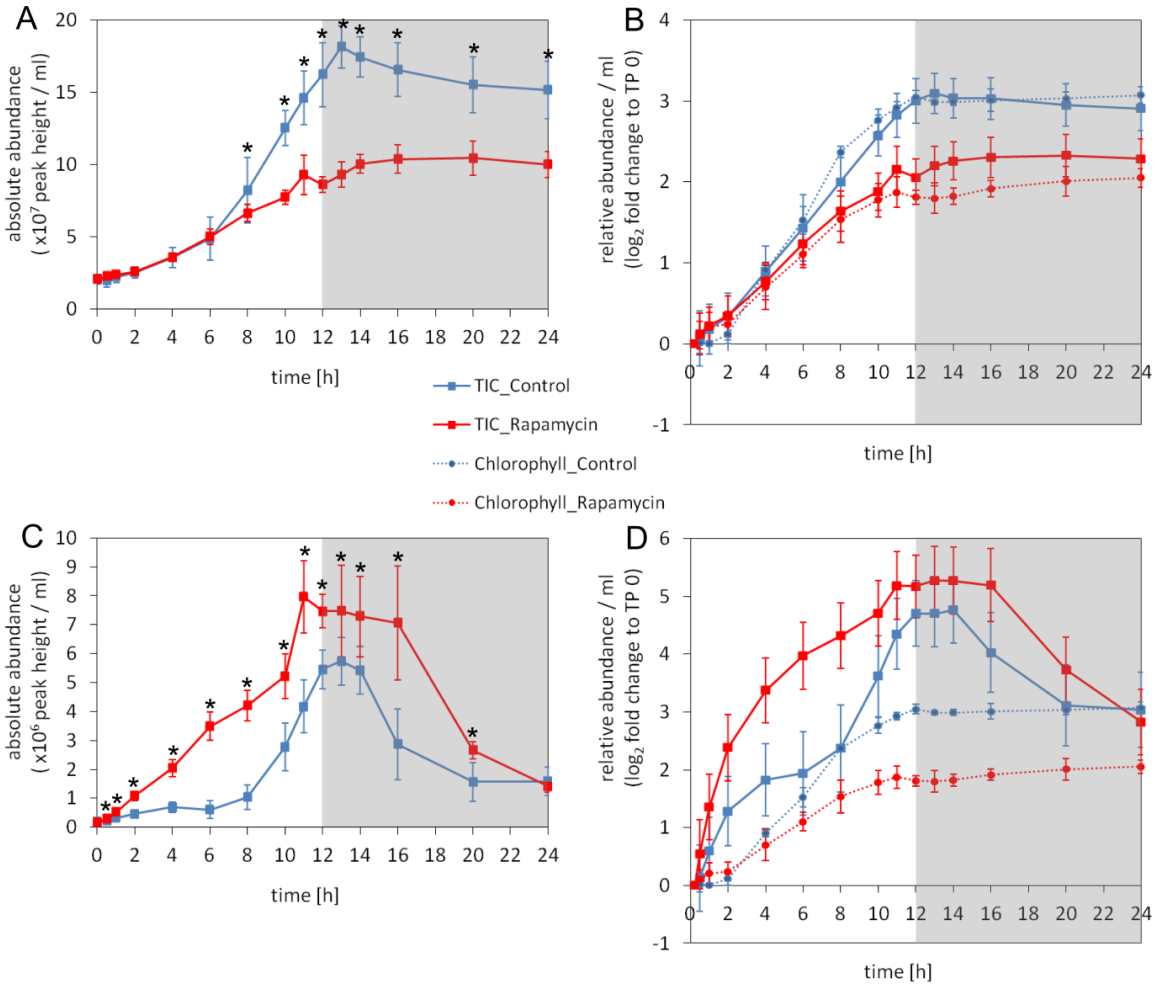

Figure 43. Comparison of the total ion count of lipids for control and rapamycin treatment
Total ion count (TIC) of structural (A, B) and storage (C, D) lipids was analyzed at the indicated times for a *Chlamydomonas* culture treated with rapamycin (red) in comparison to control (blue). The cells were synchronized by a 12:12 h light-dark cycle. (A, C) TIC per ml. Significant ($p < 0.05$) differences in the absolute abundance are indicated by an asterisk. (B, D) TIC and chlorophyll concentration as $\log_2$ fold change to TP 0. Grey background indicates the dark phase. Data are given as mean ± SD of 3 biological replicates.

Similar to starch, we found that storage lipids, namely TAGs, are also accumulated after rapamycin treatment (Figure 43 C, D). But in contrast to starch, the results show that storage lipids are even increased in the total level (amount per ml). Comparison of the pattern shows that under control conditions storage lipids show a weaker increase between 4 – 8 h in light which is followed by a stronger increase from 8 – 12 h. The rapamycin treated culture shows a much stronger increase in the first 6 h of light which is than reduced in the remaining light phase. This results in a 4-fold higher total amount of storage lipids between 6 – 8 h in the rapamycin treated culture while after that the fold change between control and rapamycin treated culture decreases as at the end of the light phase the total amount of storage lipids increases much stronger under control conditions than rapamycin treatment. Further it seems that in the rapamycin treated culture the increase of storage lipids already stops at TP 11 h, while it is increasing until TP 12 h under control conditions. After the onset of dark phase the amount of storage lipids remains on a constant level for about 2 h under control conditions. After which it decreases until TP 20 h where it achieves the same level as chlorophyll and therefore remains constant in the remaining dark phase (Figure 43 D). In contrast to this, storage lipids of the rapamycin treated culture decrease 2 h later and end up on a higher level than chlorophyll, but on the same level as storage lipids under control conditions. However, this leads to a higher cellular amount of TAGs in the rapamycin treated culture at the end of the dark phase.

3.2.4.4.3 *Identification of lipids with changed quantitative temporal dynamics after rapamycin treatment*

As in the case of primary metabolites, we were also interested in changes of the lipid pattern within the cell cycle caused by rapamycin treatment. Therefore, we used the same non-classical clustering analyses as for primary metabolites (Figure 37) which is described in more detail in chapter 0. In short, we compared on one hand the timing of increase (T) and on the other hand the total amount (L) at the end of the cell cycle (TP24) to find groups which show similar changes after rapamycin treatment. In addition, due to the mentioned reason (see chapter 3.2.3.4.4) the $\log_2$ fold changes of the cellular amount (per chlorophyll) of rapamycin treatment to control for TP 24 h are presented in the tables for each cluster (Figure 44 B).

Two thirds of the lipid species (199 of 297 total lipid species) are not affected in their quantitative timing after rapamycin treatment (T0; Table 12 A). From the remaining 98 lipid species which are shifted in their timing about one third (35 lipids) show an earlier increase (T-x) while nearly two third (63 lipids) increase later than the control (T+x).

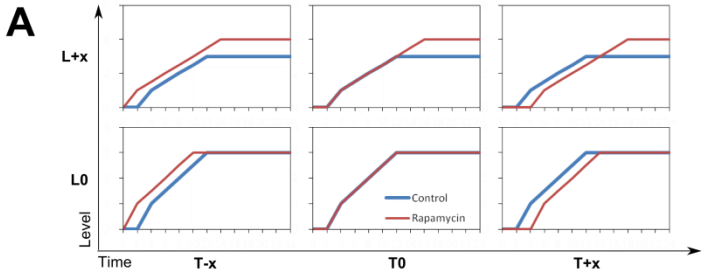

B

T-x/L+x (1 Lipid)

Lipid species	log2 fold change TP 24 h
TAG 46:5	2.22

T0/L+x (1 Lipid)

Lipid species	log2 fold change TP 24 h
PG 34:0	1.69

T+x/L+x (1 Lipid)

Lipid species	log2 fold change TP 24 h
MGDG 34:2	1.50

T-x/L0 (18 Lipids)

Lipid species	log2 fold change TP 24 h
TAG 44:1	0.93
TAG 46:0	0.41
TAG 46:1	0.58
TAG 46:2	0.40
TAG 48:0	0.55
TAG 48:1	0.60
TAG 48:2	0.58
TAG 50:0	0.46
TAG 50:1	0.90
TAG 50:2	0.93
TAG 50:3	0.69
TAG 50:4_A	0.81
TAG 50:5_A	0.57
TAG 50:6_A	0.26
TAG 50:7_A	0.63
TAG 50:7_B	0.24
TAG 56:8_A	1.25
TAG 58:6_B	-0.45

T0/L0 (85 Lipids)

Lipid species	log2 fold change TP 24 h
DAG 34:1	0.85
DAG 34:5_B	0.55
DAG 34:6_A	0.78
DAG 34:6_B	0.89
DAG 36:3	0.61
DAG 36:5	-0.03
DAG 36:7_B	0.07
FA 24:0	0.56
DGTS 34:1	0.72
DGTS 36:2	0.95
DGTS 36:4_A	1.15
DGTS 36:6_A	2.01
DGTS 36:7_A	0.38
DGTS 38:4_A	1.19
DGTS 38:5_A	0.97
DGTS 38:5_B	0.81
PE 34:1_B	0.45
PE 34:2	0.56
PE 34:4_C	0.30
PE 36:4_B	0.93
MGDG 32:3	1.35
MGDG 36:4	1.00
DGDG 32:3_B	0.81
DGDG 34:1	0.86
DGDG 34:3_A	0.63
DGDG 34:3_B	1.02
DGDG 34:5_A	0.74
DGDG 36:0	0.68
DGDG 36:1_A	1.81
DGDG 36:1_B	0.97
DGDG 36:2	1.21
DGDG 36:3_A	1.02
DGDG 36:3_B	1.51
DGDG 36:4_B	1.08
DGDG 36:6_A	1.13
DGDG 36:7	0.74
PG 36:1	0.91
SQDG 34:1	0.76
SQDG 36:1	0.67
SQDG 36:2	0.80

Lipid species	log2 fold change TP 24 h
TAG 42:4	-0.71
TAG 44:0	0.49
TAG 52:2	1.40
TAG 52:3	1.39
TAG 52:4_A	1.98
TAG 52:4_B	1.40
TAG 52:5_A	1.36
TAG 52:5_B	0.85
TAG 52:6_A	1.19
TAG 52:6_B	0.79
TAG 52:7_A	0.85
TAG 52:7_B	0.44
TAG 52:8_A	0.63
TAG 52:8_B	0.89
TAG 52:9_A	1.08
TAG 52:9_B	0.93
TAG 52:10_A	0.69
TAG 52:11	0.11
TAG 54:3	1.31
TAG 54:4_A	1.50
TAG 54:4_B	1.33
TAG 54:5_A	1.09
TAG 54:5_B	1.30
TAG 54:6_A	1.60
TAG 54:6_B	1.01
TAG 54:6_C	1.16
TAG 54:7_A	1.41
TAG 54:7_B	1.00
TAG 54:7_C	1.12
TAG 54:8_A	1.19
TAG 54:8_B	0.89
TAG 54:8_C	1.07
TAG 54:9_A	1.22
TAG 54:9_B	0.88
TAG 54:10_A	1.00
TAG 54:10_B	0.50
TAG 56:4	1.30
TAG 56:5_A	1.42
TAG 56:5_B	1.52
TAG 56:6_A	0.81
TAG 56:6_B	0.90
TAG 56:7_A	1.26
TAG 56:7_B	1.20
TAG 56:7_C	0.98
TAG 58:5	0.63

T+x/L0 (8 Lipids)

Lipid species	log2 fold change TP 24 h
MGDG 32:1_A	1.02
MGDG 32:1_B	1.75
MGDG 34:0	2.38
MGDG 34:1	1.66
MGDG 36:1	1.82
MGDG 36:2	2.01
MGDG 36:6_A	0.64
MGDG 36:6_B	0.73

Figure 44. Clustering according to time and level of changes within the lipids to rapamycin under synchronized conditions

(A) Predicted clusters of the lipid pattern of the rapamycin treated culture (red) in comparison to control (blue) based on a simplified 2-factorial analysis of time (T) and level (L). A detailed description is given in chapter 3.2.3.4.4. (B)Tables show the lipid species which belong to the 9 predicted clusters. In addition, the $\log_2$ fold changes of the cellular amount between rapamycin treated culture and control are presented for TP 24 h. Significant ($p < 0.05$) increased and decreased metabolites are indicated in red or blue, respectively.

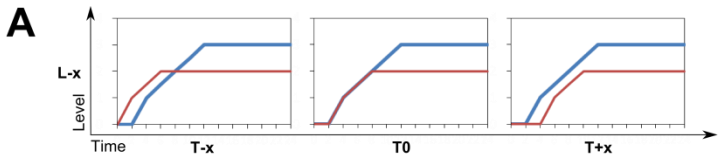

B

T-x/L-x (16 Lipids)

Lipid species	log2 fold change TP 24 h
FA 18:1	0.29
FA 18:2	0.13
DGTS 32:0	-0.28
DGTS 34:0	0.19
DGTS 34:2	0.58
DGTS 38:3	0.59
PE 36:6_A	0.49
LysoPE 18:3	0.51
TAG 48:3_A	0.64
TAG 48:3_B	0.44
TAG 48:4_A	0.42
TAG 50:4_B	0.26
TAG 50:5_B	-0.06
TAG 50:6_B	0.13
TAG 50:8_A	0.48
TAG 50:8_B	-0.14

T0/L-x (113 Lipids)

Lipid species	log2 fold change TP 24 h
DAG 34:2	0.63
DAG 34:5_A	-0.36
DAG 34:7	0.37
DAG 36:6	0.02
DAG 36:7_A	0.51
FA 18:3	0.14
FA 26:0	0.12
DGTS 30:0	-0.24
DGTS 30:1_A	0.03
DGTS 30:2_A	-0.09
DGTS 32:1_A	0.86
DGTS 32:1_B	0.37
DGTS 32:2_A	0.27
DGTS 34:3_A	0.96
DGTS 34:4	0.31
DGTS 34:5_A	-0.06
DGTS 34:6_B	-1.09
DGTS 34:7_A	-0.45
DGTS 36:1	0.34
DGTS 36:3_A	0.71
DGTS 36:3_B	0.64
DGTS 36:4_B	0.43
DGTS 36:5_A	0.69
DGTS 36:5_B	0.35
DGTS 36:6_B	0.38
DGTS 38:2	0.77
DGTS 38:4_B	0.30
DGTS 38:6_A	0.08
PE 34:1_A	-0.76
PE 34:3_B	0.76
PE 34:4_B	0.21
PE 34:5	-0.55
PE 36:2	-1.56
PE 36:3	0.51
PE 36:5	0.03
PE 36:7	-0.31
PE 38:3	0.06
PE 38:4	0.41
PE 38:5	0.62
MGDG 32:4_A	0.00
MGDG 32:4_B	0.34
MGDG 32:5	-0.42
MGDG 32:6_A	-0.27
MGDG 32:7	-0.30
MGDG 34:3	0.73
MGDG 34:4_A	-0.07
MGDG 34:4_B	0.74
MGDG 34:5_A	0.24
MGDG 34:5_B	0.92
MGDG 34:6_A	0.68
MGDG 34:7	0.43
MGDG 34:8	0.09
MGDG 36:3_A	0.07
MGDG 36:3_B	0.48
MGDG 36:5	0.62
MGDG 36:7_A	0.45
MGDG 36:7_B	0.52

Lipid species	log2 fold change TP 24 h
DGDG 32:0	0.21
DGDG 32:1_A	0.34
DGDG 32:1_B	0.44
DGDG 32:2_A	0.49
DGDG 32:2_B	0.81
DGDG 32:3_A	0.04
DGDG 32:4_A	-1.70
DGDG 32:4_B	0.14
DGDG 32:5	-1.00
DGDG 34:0	0.58
DGDG 34:2_A	0.73
DGDG 34:2_B	0.90
DGDG 34:4	0.33
DGDG 34:5_B	0.21
DGDG 34:6_A	0.08
DGDG 34:6_B	0.27
DGDG 34:8	-1.03
DGDG 36:4_A	0.49
DGDG 36:5_A	0.59
DGDG 36:5_B	0.71
DGDG 36:6_B	0.37
PG 32:0	0.31
PG 32:1_A	-0.29
PG 32:2	-0.53
PG 32:3	-0.52
PG 34:2_A	0.15
PG 34:2_B	-0.06
PG 34:3	-0.16
PG 34:4	-0.19
PG 34:5_A	-0.25
PG 34:5_B	-0.86
PG 36:2	0.00
PG 36:4	-0.13
SQDG 32:0	0.45
SQDG 32:1_A	0.05
SQDG 32:1_B	0.61
SQDG 32:2_A	0.51
SQDG 32:2_B	0.45
SQDG 32:3	-0.14
SQDG 32:4	-0.27
SQDG 34:3	0.48
SQDG 36:6_B	-0.01
TAG 46:3	-0.45
TAG 48:4_B	0.22
TAG 48:4_C	-0.22
TAG 48:5	-0.11
TAG 48:6	-1.06
TAG 48:7	0.07
TAG 50:9_A	-0.18
TAG 50:9_B	0.13
TAG 50:10_A	0.08
TAG 50:10_B	0.03
TAG 50:11	0.14
TAG 52:10_B	0.48
TAG 56:8_B	0.41
TAG 58:6_A	-0.46

T+x/L-x (54 Lipids)

Lipid species	log2 fold change TP 24 h
DAG 34:3_A	-0.23
DAG 34:3_B	0.71
DGTS 30:1_B	0.11
DGTS 30:2_B	0.19
DGTS 30:2_C	-0.53
DGTS 30:3_A	-0.46
DGTS 30:3_B	-1.00
DGTS 30:3_C	-0.58
DGTS 30:3_D	-1.37
DGTS 30:4_A	-0.83
DGTS 30:4_B	-1.87
DGTS 32:2_B	0.20
DGTS 32:3_A	0.50
DGTS 32:3_B	0.38
DGTS 32:3_C	0.10
DGTS 32:3_D	0.09
DGTS 32:4_A	0.00
DGTS 32:4_B	-0.39
DGTS 32:5_A	-0.93
DGTS 32:5_B	-1.34
DGTS 32:5_C	-1.09
DGTS 32:6_A	-1.13
DGTS 32:6_B	-1.58
DGTS 32:7	-1.68
DGTS 32:8	-2.06
DGTS 34:3_B	0.54
DGTS 34:5_B	-0.36
DGTS 34:6_A	-0.19
DGTS 34:6_C	-0.77
DGTS 34:6_D	-0.94
DGTS 34:7_B	-1.33
DGTS 34:7_C	-0.91
DGTS 34:8	-1.50
DGTS 36:7_B	-0.58
DGTS 36:8	-1.05
DGTS 38:6_B	-0.55
DGTS 40:4	-0.12
PE 34:3_A	-0.03
PE 34:4_A	0.04
PE 36:4_A	0.01
PE 36:4_C	-0.16
PE 36:6_B	-0.12
MGDG 32:2	0.70
MGDG 32:6_B	0.10
MGDG 34:6_B	0.70
PG 32:1_B	0.48
PG 36:6	0.20
SQDG 34:4	-0.33
SQDG 34:5	0.16
SQDG 34:6_A	-0.14
SQDG 34:6_B	-0.11
SQDG 34:7	-0.42
SQDG 36:5	0.19
SQDG 36:6_A	0.12

Figure 44. *Continued.*

Among the lipid species which increase earlier in rapamycin treatment the TAGs are strongly overrepresented (T-x, Table 12 A) while the cytoplasmic lipid DGTS is most frequently within the lipid species which are delayed in their dynamics after rapamycin treatment (T+x; Table 12). In addition, about 35% of each MGDGs and SQDGs are also delayed after rapamycin treatment.

The quantitative comparison of the total amount shows that the majority of lipid species, namely 183 of 297 total lipid species is decreased at the end of the dark phase (L-x; Table 12 B). More than one third, exactly 111 lipid species display no significant change in the total amount at the end of the dark phase (L0; Table 12 B) while at the same time only 3 lipid species are significantly increased in comparison to the control (L+x; Table 12 B). All structural lipids (MGDG, DGDG, PG SQDG, DGTS, PE) are most frequently within the clusters of a lower amount. With more than 70% of their lipid species, only TAGs are highly overrepresented in the L0 clusters. This is consistent with the results of TIC of structural and storage lipids (Figure 43). If we consider this on the cellular level, we find that the majority of lipid species, namely 144 is significantly increased at the end of dark phase (TP 24 h) after rapamycin treatment (L+x; Table 12 C). Among those lipids, the storage lipids (TAGs) and plastidic lipids (MGDG, DGDG) are represented with each more than 50%. More than one third of the lipid species display no significant change in the cellular amount at the end of the dark phase in comparison to the control (L0; Table 12). This includes the main fraction of the lipid precursor DAG, the plastidic lipid SQDG, the cytoplasmic lipid PE and all of the annotated FFA. With one exception, the remaining TAGs also end up on the same cellular level as under control conditions. Within the 41 lipid species which are decreased at the end of the dark phase the cytoplasmic lipid DGTS is by far the main fraction (L-x; Table 12 C).

Table 12. Summary of the time (T) and level (L) analysis of the rapamycin treated culture in comparison to the control

(A) Number of lipid species with an earlier increase (T-x), same (T0) or later increase (T+x) after rapamycin treatment. (B) Number of lipid species which are lower (L-x), same (L0) or higher (L+x) in the total amount at TP 24 hafter rapamycin treatment. (C) Number of lipid species which are lower (L-x), same (L0) or higher (L+x) in the cellular amount at TP 24 h after rapamycin treatment.

A

	T-x	T0	T+x
DAG	-	12	2
FFA	2	3	-
MGDG	-	20	12
DGDG	-	35	-
SQDG	-	12	7
PG	-	14	2
PE	2	15	5
DGTS	4	29	35
TAG	27	59	-
Sum	35	199	63

B

	L-x	L0	L+x
DAG	7	7	-
FFA	4	1	-
MGDG	21	10	1
DGDG	21	14	-
SQDG	16	3	-
PG	14	1	1
PE	18	4	-
DGTS	60	8	-
TAG	22	63	1
Sum	183	111	3

C

	L-x	L0	L+x
DAG	-	10	4
FFA	-	5	-
MGDG	3	7	22
DGDG	3	6	26
SQDG	-	11	8
PG	4	7	5
PE	3	14	5
DGTS	27	16	25
TAG	1	36	49
Sum	41	112	144

If we take both factors into account we find that the majority, exactly two third of the annotated lipid species only belong to 2 clusters, namely cluster T0/L0 and T0/L-x (Figure 44 B). Apart from that we found two clusters which solely contain 1 lipid class. This is on the one hand cluster T-x/L0 which consists exclusively of TAGs and on the other hand cluster T+x/L0 which only contains MGDGs.

A more detailed view on the lipid species within the different cluster reveals a differential regulation of storage lipids with different fatty acid chain length. TAGs with shorter fatty acids, namely those containing 44 – 50 carbons in their 3 fatty acids show in general an earlier increase and end up on a similar level (per ml) at TP 24 h in comparison to the control (Figure 45 A). In contrast to this, TAGs with longer fatty acids, namely those containing 52 – 56 carbons in their 3 fatty acids show in general no a different in the timing of increase, but they are significantly increased on the cellular level (cluster T0/L0).

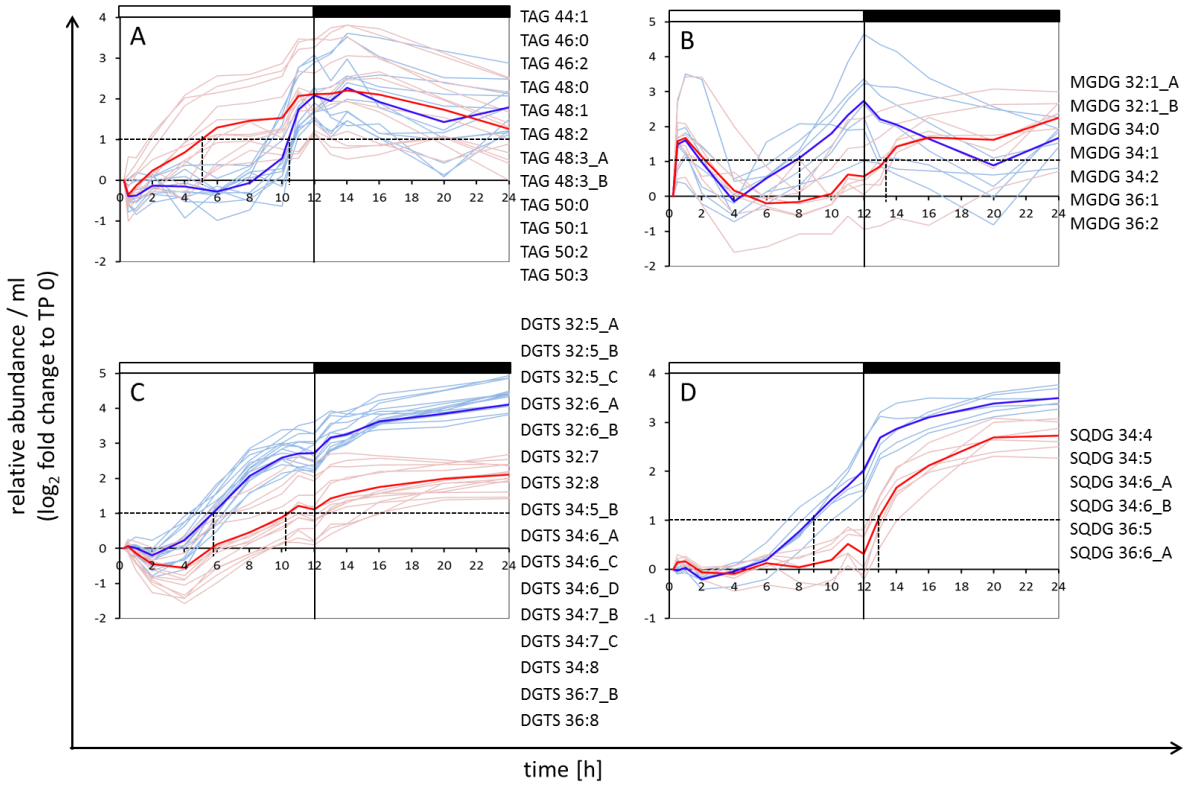

Figure 45. Lipid species with a time shift in their temporal pattern after rapamycin treatment
Time course of specific lipid species for a *Chlamydomonas* culture treated with rapamycin (red) in comparison to the control (blue). In each plot the $\log_2$ fold changes of the total amount (peak height / ml) to TP 0 are plotted as a graph for each metabolite (thin line) and the average (bold line) for control and rapamycin treatment, respectively. To the right of each plot are the lipid species which are presented in the plot. White or black bars above the plot indicate the light or dark phase, respectively. Dotted lines indicate the TP at which the averaged amount of the lipid class for either the control or the rapamycin treatment has doubled. (A) TAG. (B) MGDG. (C) DGTS. (D) SQDG. The results show the median of 6 replicates per TP.

In contrast to the TAGs, we found several lipid species within the membrane lipids that are delayed in their accumulation after rapamycin treatment. This includes plasma membrane lipids (DGTS, PE) as well as chloroplast lipids (MDGD, SQDG, PG) (Figure 44). To our surprise no DGDG seems to be affected in the timing of accumulation. Another difference to storage lipids was the observation that this timing effect occurred on the level of saturation. Whereas DGTS and SQDGs show the delay for their higher unsaturated forms (≥ 4 db) (Figure 45 C, D), MGDGs do this for their saturated and low unsaturated forms (≤2 db) (Figure 45 B). The pattern of the low unsaturated MDGDs, which generally differs from that of the other lipid species, shows two peaks during the light phase. The first peak appears in the first 4 h of the light phase. Interestingly, the rapamycin treated culture shows no differences during this time period in comparison to the control. The obtained delay after rapamycin treatment only concerns the second increase in the second half of the light phase. Moreover, the affected lipid species within the DGTS and SQDG are among those that show a late increase under control conditions (Figure 40 cluster 4 and 5). These observations suggest that mainly lipid species that accumulate later during the light phase are affected by the delay.

3.2.4.4.4 *Quantitative changes within the membrane lipids after rapamycin treatment*

The quantitative comparison of lipids showed a quite similar pattern for membrane lipids in the first 4 hours in light. With minor exceptions, the membrane lipids show a reduced or unchanged cellular content (per chlorophyll) after rapamycin treatment during this period (Table 13). After this time period the different lipid classes and even lipid species within the lipid classes show different changes to TOR inhibition.

The galactoglycerolipids MGDG and DGDG are closely related as MGDG is the metabolic precursor of DGDG [152]. However, their response to TOR inhibition was is some case different. Comparing the pattern of the late light phase (6 -12 h) most DGDGs are significantly increased from 6 h onwards, while only few MGDGs are significantly increased. Among the MGDGs only the high unsaturated (≥ 3 db) forms with 34 and 36 carbons display this increase, while MGDGs with 32 carbons are unchanged or even reduced. However, these observations revealed also a certain resemblance. Both MGDG and DGDG showed the strongest accumulation for species with long chain fatty acids (36 carbons). While in case of DGDG the accumulation in the late light phase mitigate for compounds with shorter chain fatty acids (34 and 32 carbons), this weakening was more pronounced for MGDGs and thereby leading to decreased cellular content for MGDGs with 32 carbons after rapamycin treatment.

Table 13. Changes in the membrane lipids after rapamycin treatment

Log_2 fold changes of the cellular amount (per µg chlorophyll) of membrane lipids for the rapamycin treated *Chlamydomonas* culture in comparison to the control. The header of this table displays the TP in hours after rapamycin treatment. An increase after rapamycin treatment is indicated by reddish colors (yellow: between 0.5 and 1; orange: between 1 and 2; red: above 2) and a decrease is indicated by bluish colors (light blue: between -0.5 and -1; dark blue: between -1 and -2; very dark blue: below -2). Significant changes ($p < 0.05$) are indicated by bold numbers.

	0,25	0,5	1	2	4	6	8	10	11	12	13	14	16	20	24
SQDG 32:0	0,10	-0,15	-0,12	-0,16	**0,25**	**0,38**	**0,44**	**0,46**	**0,39**	**0,58**	**0,64**	**0,53**	**0,51**	**0,57**	**0,53**
SQDG 32:1_A	-0,16	-0,07	0,54	**1,14**	0,02	0,09	-0,03	0,46	**0,84**	-0,01	0,54	0,23	**0,52**	**0,97**	0,20
SQDG 32:1_B	0,08	**-0,21**	-0,23	**-0,31**	0,11	0,31	**0,49**	**0,50**	**0,59**	**0,76**	**0,76**	**0,65**	**0,57**	**0,60**	**0,61**
SQDG 32:2_A	0,10	-0,04	-0,22	-0,28	-0,02	0,23	0,26	0,20	**0,32**	**0,62**	**0,67**	**0,52**	**0,28**	**0,33**	**0,39**
SQDG 32:2_B	0,32	-0,08	-0,22	-0,26	0,36	**0,66**	**0,66**	**0,64**	**0,62**	**0,70**	**0,73**	**0,79**	**0,61**	**0,76**	**0,50**
SQDG 32:3	0,28	-0,08	-0,11	-0,11	0,06	0,30	0,11	-0,15	-0,21	-0,21	-0,14	-0,06	-0,04	0,19	0,13
SQDG 32:4	0,18	-0,12	-0,21	-0,23	0,07	0,17	0,00	**-0,40**	**-0,34**	-0,33	-0,24	-0,17	-0,12	0,06	-0,02
SQDG 34:1	0,12	-0,15	-0,22	-0,10	**0,48**	**0,37**	0,18	-0,08	-0,18	-0,05	0,21	**0,44**	**0,60**	**0,83**	**0,81**
SQDG 34:3	0,10	-0,17	-0,22	**-0,41**	-0,06	0,07	0,16	**0,25**	**0,52**	**0,71**	**0,66**	**0,60**	**0,38**	**0,53**	**0,46**
SQDG 34:4	0,22	-0,08	-0,18	-0,08	**0,34**	**0,57**	**0,51**	**0,25**	0,23	**0,35**	0,14	**0,18**	0,09	-0,02	-0,09
SQDG 34:5	0,24	-0,03	-0,08	-0,07	0,28	**0,59**	**0,57**	**0,33**	**0,30**	**0,52**	**0,49**	**0,59**	**0,62**	**0,57**	0,34
SQDG 34:6_A	0,21	0,04	-0,17	-0,17	0,13	0,32	0,14	-0,23	-0,24	**-0,23**	0,09	**0,24**	0,29	0,32	0,17
SQDG 34:6_B	0,13	-0,11	-0,12	-0,10	0,11	0,33	0,19	-0,18	-0,20	0,05	0,18	**0,38**	**0,51**	**0,55**	0,26
SQDG 34:7	0,21	-0,11	-0,11	-0,05	0,17	0,32	0,26	-0,18	-0,20	0,02	0,06	0,12	0,18	0,05	-0,15
SQDG 36:1	0,22	-0,25	**-0,44**	**-0,48**	**0,39**	**0,58**	**0,60**	**0,78**	**0,79**	0,36	**0,60**	**0,63**	0,41	**0,93**	**0,78**
SQDG 36:2	0,15	-0,40	-0,41	-0,36	0,26	**0,67**	**0,70**	**0,76**	**1,01**	**0,99**	**1,05**	**0,86**	**0,57**	**0,65**	**0,72**
SQDG 36:5	0,23	-0,16	-0,22	-0,30	0,10	**0,53**	0,40	-0,25	**-0,57**	**-1,27**	**-1,07**	**-0,77**	-0,31	**0,53**	0,48
SQDG 36:6_A	0,14	-0,05	-0,15	-0,17	-0,01	0,13	**-0,62**	**-0,86**	**-0,85**	**-1,42**	**-1,42**	**-1,03**	-0,34	0,44	0,46
SQDG 36:6_B	0,19	-0,10	-0,21	-0,24	-0,03	0,30	0,18	-0,18	-0,33	**-0,44**	**-0,51**	**-0,43**	-0,19	0,45	0,46
PG 32:0	0,06	-0,11	**-0,22**	**-0,24**	-0,16	0,22	**0,41**	**0,47**	**0,50**	**0,24**	0,12	0,18	0,15	**0,45**	**0,38**
PG 32:1_A	0,09	**-0,17**	**-0,25**	**-0,56**	**-0,44**	0,08	-0,07	**-0,29**	-0,12	-0,04	-0,14	**-0,23**	**-0,43**	**-0,29**	**-0,22**
PG 32:1_B	0,03	-0,20	-0,23	**-0,52**	**-0,56**	-0,14	0,10	0,05	0,06	-0,05	**-0,57**	**-0,54**	**-0,41**	0,07	**0,52**
PG 32:2	0,14	-0,17	-0,22	**-0,25**	**-0,20**	-0,30	**-0,41**	-0,21	0,06	-0,12	-0,17	-0,32	**-0,77**	**-0,35**	**-0,44**
PG 32:3	0,16	-0,11	-0,23	-0,38	-0,20	0,25	0,05	-0,10	0,05	-0,06	-0,06	0,14	-0,13	-0,20	**-0,50**
PG 34:0	0,06	0,05	-0,16	-0,01	0,25	**0,64**	**1,21**	**1,50**	**1,76**	**2,01**	**2,08**	**2,19**	**2,40**	**2,00**	**1,74**
PG 34:2_A	0,10	-0,07	-0,20	-0,13	**0,37**	0,17	-0,21	**-0,46**	**-0,51**	**-0,61**	**-0,57**	**-0,41**	**-0,41**	-0,11	**0,21**
PG 34:2_B	0,06	**-0,21**	**-0,35**	**-0,91**	**-0,52**	**-0,41**	**-0,49**	**-0,74**	**-0,52**	**-0,40**	**-0,24**	**-0,27**	**-0,45**	**-0,38**	-0,14
PG 34:3	0,09	-0,08	-0,17	**-0,50**	**-0,20**	0,21	**0,27**	**0,24**	**0,38**	**0,43**	**0,38**	**0,38**	0,15	0,03	-0,10
PG 34:4	0,10	-0,15	-0,20	**-0,48**	**-0,56**	**-0,47**	**-0,35**	**-0,28**	-0,03	0,10	0,04	0,03	-0,18	-0,17	**-0,21**
PG 34:5_A	0,28	-0,11	-0,20	-0,17	**-0,41**	-0,14	-0,38	-0,38	-0,17	0,05	0,17	**0,34**	0,24	0,09	0,02
PG 34:5_B	0,26	-0,17	-0,18	-0,21	**-0,50**	-0,51	**-0,63**	**-0,63**	-0,57	-0,34	-0,37	-0,16	-0,33	-0,42	-0,51
PG 36:1	0,38	0,10	-0,01	-0,20	-0,05	**0,40**	**0,27**	0,17	**0,26**	0,26	**0,41**	**0,68**	**0,92**	**0,75**	0,64
PG 36:2	0,25	0,03	**-0,48**	**-0,47**	**-0,83**	-0,08	**-0,65**	**-0,31**	-0,05	0,17	**0,37**	**0,60**	**0,80**	0,21	-0,23
PG 36:4	0,27	0,11	0,07	-0,27	**-0,71**	**-0,39**	**-0,32**	-0,19	0,06	-0,06	0,00	-0,04	-0,11	0,09	-0,33
PG 36:6	0,14	-0,23	**-0,46**	**-1,12**	**-0,91**	**-0,60**	**-1,00**	**-1,16**	**-0,76**	**-0,76**	**-0,56**	**-0,60**	**-0,65**	-0,16	**0,21**
PE 34:1_A	-0,10	-0,20	-0,40	**-0,62**	-0,17	0,10	0,13	0,16	0,10	0,24	-0,03	0,01	**-0,66**	**-0,81**	**-0,75**
PE 34:1_B	0,27	**0,82**	**0,45**	0,09	0,28	**0,72**	**0,56**	0,01	**-0,61**	**-0,81**	**-0,57**	-0,25	**0,59**	**1,12**	**0,79**
PE 34:2	0,00	0,24	0,18	0,82	-0,35	-0,14	-0,14	-0,14	-0,19	-0,15	**-1,21**	-0,30	**0,57**	**2,10**	**0,61**
PE 34:3_A	-0,09	**-0,32**	-0,41	-0,15	-0,20	0,05	0,07	-0,08	-0,07	0,23	-0,09	0,15	**-0,34**	0,09	-0,01
PE 34:3_B	0,00	0,14	0,38	0,92	**-0,53**	-0,30	-0,25	-0,25	-0,21	0,18	**-0,68**	0,02	0,28	**1,43**	0,48
PE 34:4_A	-0,12	-0,15	0,02	**1,01**	-0,32	-0,04	-0,04	-0,16	0,20	0,03	**-1,12**	-0,16	0,10	**1,01**	-0,12
PE 34:4_B	0,06	0,25	0,44	**0,92**	**-0,90**	**-0,60**	**-0,45**	**-0,57**	**-0,37**	-0,01	**-0,62**	-0,03	0,18	**0,85**	0,05
PE 34:4_C	-0,54	-0,51	0,01	**1,83**	0,05	0,72	0,41	0,51	0,67	-0,78	**-2,09**	-0,45	1,89	**2,00**	0,30
PE 34:5	0,18	0,00	-0,20	**-0,41**	**-1,66**	**-1,39**	**-1,15**	**-1,35**	**-1,07**	-0,23	-0,21	0,03	-0,35	-0,34	**-0,49**
PE 36:2	-0,13	-0,31	-0,55	**-1,04**	**-0,46**	-0,31	**-0,57**	**-1,20**	**-1,43**	**-1,68**	**-1,68**	**-1,51**	**-1,79**	**-1,76**	**-1,56**
PE 36:3	-0,09	**-0,27**	-0,33	**-0,63**	0,03	0,34	**0,52**	**0,58**	**0,70**	**1,15**	**1,01**	**1,00**	**0,36**	0,28	**0,51**
PE 36:4_A	-0,12	**-0,36**	**-0,44**	**-0,79**	-0,10	0,15	0,37	0,29	0,12	**0,59**	**0,39**	0,42	-0,29	**-0,42**	-0,07
PE 36:4_B	-0,06	**-0,29**	**-0,44**	**-0,90**	-0,01	0,33	**0,61**	**0,59**	**0,63**	**1,22**	**1,25**	**1,35**	**0,65**	**0,52**	**0,91**
PE 36:4_C	-0,25	**-0,46**	**-0,67**	**-1,40**	**-1,00**	**-0,51**	**-0,35**	**-0,66**	**-0,81**	-0,37	-0,30	-0,21	**-0,57**	-0,28	-0,13
PE 36:5	-0,06	**-0,31**	**-0,45**	**-0,93**	-0,21	0,05	0,40	**0,31**	0,27	**1,02**	**0,93**	**0,89**	-0,08	-0,41	0,11
PE 36:6_A	-0,02	-0,16	0,01	0,07	**0,73**	**0,53**	**0,71**	**0,62**	**0,75**	**1,32**	**0,96**	**1,02**	-0,06	-0,10	0,41
PE 36:6_B	**-0,07**	**-0,33**	**-0,46**	**-1,31**	**-0,95**	**-0,59**	**-0,46**	**-1,02**	**-1,14**	-0,20	-0,04	0,12	**-0,82**	**-0,82**	-0,13
PE 36:7	0,10	**-0,17**	-0,07	-0,48	-0,31	**-0,39**	-0,07	**-0,29**	-0,18	**0,50**	0,16	0,17	**-0,94**	**-1,08**	-0,50
PE 38:3	-0,10	-0,22	**-0,43**	**-0,81**	-0,20	0,11	0,12	0,29	**0,36**	**0,80**	**0,72**	**0,85**	-0,01	-0,24	0,10
PE 38:4	-0,09	**-0,36**	**-0,42**	**-0,73**	0,14	**0,36**	0,34	**0,23**	0,15	0,60	**0,52**	**0,64**	0,07	0,01	0,34
PE 38:5	-0,24	-0,31	**-0,47**	**-1,18**	-0,32	-0,03	0,25	**0,32**	**0,62**	**1,59**	**1,50**	**1,72**	**0,64**	0,08	0,44

Table 13. Continued

	0,25	0,5	1	2	4	6	8	10	11	12	13	14	16	20	24
MGDG 32:1_A	0,00	-0,13	-0,03	-0,32	-0,56	-0,68	-0,57	-0,46	-0,18	-0,45	-0,16	0,03	-0,34	0,95	1,15
MGDG 32:1_B	-0,03	-0,40	-0,21	-0,16	0,34	-0,67	-0,95	-0,99	-1,20	-1,36	-0,25	0,24	0,84	1,96	1,39
MGDG 32:2	0,00	-0,21	-0,15	-0,37	-0,36	-0,55	-0,71	-0,49	-0,54	-0,76	-0,54	-0,54	-0,56	0,46	0,72
MGDG 32:3	0,00	-0,22	-0,41	-0,69	-0,11	0,02	-0,11	0,02	0,19	0,34	0,53	0,12	0,34	1,23	1,21
MGDG 32:4_A	-0,02	-0,18	-0,17	-0,42	-0,46	-0,58	-0,15	-0,08	-0,08	0,39	0,22	0,32	0,04	-0,12	0,07
MGDG 32:4_B	0,05	-0,25	-0,21	-0,60	-0,49	-0,16	-0,14	-0,16	0,05	-0,03	0,22	0,07	-0,07	0,24	0,27
MGDG 32:5	0,07	-0,23	-0,18	-0,43	-0,39	-0,34	-0,28	-0,38	-0,23	-0,30	-0,19	-0,41	-0,49	-0,36	-0,41
MGDG 32:6_A	0,01	-0,27	-0,28	-0,43	-0,31	-0,19	-0,08	-0,04	0,12	0,16	0,29	0,12	-0,16	-0,09	-0,23
MGDG 32:6_B	-0,04	-0,29	-0,37	-0,61	-0,53	-0,41	-0,28	-0,20	0,03	0,06	0,17	-0,02	-0,20	0,05	-0,09
MGDG 32:7	0,01	-0,24	-0,34	-0,55	-0,34	-0,37	-0,16	-0,26	-0,09	-0,16	-0,02	-0,15	-0,39	-0,22	-0,45
MGDG 34:0	0,34	-0,28	-0,20	-0,18	0,93	-0,88	0,30	-1,05	-0,59	-0,02	1,16	2,20	2,61	3,05	2,40
MGDG 34:1	0,29	-0,32	-0,01	0,24	0,24	-0,21	0,07	-0,20	-0,38	-0,63	0,97	2,13	2,58	3,01	1,55
MGDG 34:2	0,03	-0,27	-0,13	-0,11	0,26	-0,08	-0,05	-0,13	-0,14	-0,26	0,16	0,38	0,63	1,42	1,51
MGDG 34:3	0,00	-0,25	-0,18	-0,22	0,31	0,17	0,28	0,26	0,28	0,44	0,67	0,49	0,39	0,70	0,70
MGDG 34:4_A	-0,03	-0,18	-0,19	-0,37	0,51	0,25	0,10	-0,12	-0,19	-0,43	-0,25	-0,33	-0,38	-0,02	-0,01
MGDG 34:4_B	0,00	-0,27	-0,31	-0,43	0,20	0,21	0,27	0,29	0,34	0,44	0,58	0,40	0,26	0,61	0,70
MGDG 34:5_A	0,00	-0,23	-0,21	-0,47	0,24	0,37	0,33	0,32	0,38	0,30	0,42	0,31	0,14	0,32	0,22
MGDG 34:5_B	0,02	-0,25	-0,18	-0,52	0,04	0,18	0,31	0,35	0,53	0,73	0,89	0,69	0,58	0,89	0,92
MGDG 34:6_A	0,04	-0,24	-0,17	-0,41	0,03	0,37	0,66	0,70	0,81	0,90	1,03	0,82	0,67	0,76	0,66
MGDG 34:6_B	0,07	-0,24	-0,21	-0,64	-0,54	-0,32	-0,21	-0,14	0,13	0,36	0,45	0,23	0,27	0,64	0,69
MGDG 34:7	-0,01	-0,28	-0,20	-0,47	-0,14	0,06	0,33	0,36	0,53	0,61	0,77	0,54	0,36	0,51	0,37
MGDG 34:8	0,00	-0,23	-0,29	-0,47	-0,29	-0,11	-0,01	-0,02	0,08	0,13	0,23	0,10	-0,14	0,08	0,00
MGDG 36:1	0,32	-0,27	-0,10	0,05	0,74	-0,31	-0,08	-0,24	-0,37	-0,51	0,43	1,12	1,84	2,46	1,58
MGDG 36:2	0,17	-0,57	-0,36	-0,20	1,97	0,57	-0,26	-0,19	-0,31	-0,76	-0,06	0,12	0,62	1,83	1,93
MGDG 36:3_A	0,26	0,32	0,30	0,41	1,92	1,55	1,43	1,12	1,40	-0,49	-0,62	-1,30	0,50	1,36	0,12
MGDG 36:3_B	0,04	-0,54	-0,62	-0,66	0,33	0,06	-0,26	-0,30	-0,24	-0,38	-0,08	-0,15	-0,12	0,54	0,38
MGDG 36:4	-0,06	-0,74	-0,87	-1,11	0,22	0,62	0,18	-0,25	-0,27	-0,76	-0,48	-0,39	-0,10	0,97	0,90
MGDG 36:5	-0,18	-0,17	-0,18	-0,58	0,03	0,10	0,61	1,05	1,53	1,93	1,66	1,42	1,05	0,89	0,61
MGDG 36:6_A	-0,02	-0,27	-0,10	-0,19	-0,17	0,49	0,78	0,96	1,18	1,86	1,93	1,15	1,10	0,89	0,77
MGDG 36:6_B	-0,02	-0,41	-0,61	-1,14	-0,69	-0,33	-0,35	-0,65	-0,64	-0,93	-0,79	-0,80	-0,58	0,94	0,83
MGDG 36:7_A	-0,13	-0,14	-0,26	-0,41	-0,22	-0,11	0,08	0,11	0,27	0,45	0,67	0,47	0,33	0,47	0,42
MGDG 36:7_B	0,01	-0,23	-0,26	-0,70	-0,39	0,12	0,25	0,43	0,52	0,45	0,60	0,34	0,28	0,61	0,48
DGDG 32:0	0,05	-0,19	-0,04	-0,29	-0,12	-0,08	0,04	0,06	0,06	0,06	0,35	0,32	0,25	0,47	0,17
DGDG 32:1_A	0,05	-0,27	0,00	-0,28	0,16	0,17	0,18	0,05	-0,07	-0,28	-0,01	-0,03	-0,41	0,07	0,36
DGDG 32:1_B	0,03	-0,20	-0,08	-0,26	0,25	0,27	0,31	-0,09	-0,21	-0,43	-0,21	-0,20	-0,12	0,46	0,46
DGDG 32:2_A	0,09	-0,24	0,03	-0,31	-0,16	0,23	0,65	0,71	0,83	0,87	1,04	0,97	0,51	0,71	0,49
DGDG 32:2_B	0,08	-0,18	-0,09	-0,39	0,18	0,59	0,83	0,74	0,82	0,80	0,89	0,91	0,60	1,05	0,78
DGDG 32:3_A	0,09	-0,18	0,00	-0,46	-0,39	-0,33	-0,07	0,06	0,22	0,36	0,52	0,40	0,25	0,30	0,08
DGDG 32:3_B	0,09	-0,22	-0,15	-0,47	-0,30	0,02	0,28	0,23	0,44	0,55	0,71	0,50	0,51	0,84	0,73
DGDG 32:4_A	0,15	0,10	0,35	-0,13	-0,48	-0,21	-0,15	-0,46	-0,36	-0,50	-0,34	-0,60	-0,81	-1,44	-1,58
DGDG 32:4_B	-0,59	0,18	0,60	0,68	0,65	1,71	1,36	1,32	1,25	1,84	1,02	1,30	0,74	0,46	0,17
DGDG 32:5	0,23	0,13	0,36	-0,08	-0,55	-0,03	0,35	0,09	0,31	0,24	0,25	0,22	-0,22	-0,81	-0,79
DGDG 34:0	0,10	-0,26	-0,12	-0,43	-0,06	-0,07	0,15	0,05	-0,14	-0,11	0,33	0,45	0,56	0,91	0,57
DGDG 34:1	0,07	-0,25	-0,07	-0,26	0,34	0,53	0,69	0,58	0,54	0,59	0,71	0,70	0,76	1,04	0,87
DGDG 34:2_A	0,04	-0,19	-0,02	-0,17	0,54	0,75	0,83	0,46	0,32	0,27	0,25	0,25	0,29	0,59	0,77
DGDG 34:2_B	0,09	-0,25	-0,09	-0,29	0,32	0,68	0,98	0,90	0,90	1,07	1,21	1,12	0,98	1,14	0,92
DGDG 34:3_A	0,04	-0,47	-0,68	-0,38	0,08	-0,18	0,28	0,62	0,24	0,18	0,12	0,21	0,07	0,97	0,95
DGDG 34:3_B	0,03	-0,22	-0,12	-0,41	0,05	0,36	0,73	0,87	0,96	1,18	1,27	1,16	1,06	1,21	1,00
DGDG 34:4	0,04	-0,20	-0,07	-0,29	0,21	0,66	0,94	0,77	0,78	0,80	0,86	0,74	0,51	0,52	0,36
DGDG 34:5_A	0,05	-0,40	-0,42	-0,40	-0,05	0,16	0,96	1,61	1,20	1,12	1,05	0,93	0,84	1,45	1,02
DGDG 34:5_B	0,11	-0,13	-0,02	-0,29	0,00	0,50	0,97	0,94	0,97	1,11	1,13	0,83	0,76	0,62	0,34
DGDG 34:6_A	0,03	-0,17	-0,01	-0,17	0,22	0,79	1,23	1,13	1,20	1,33	1,25	1,14	0,81	0,41	0,15
DGDG 34:6_B	0,06	-0,17	-0,18	-0,39	-0,27	0,06	0,37	0,48	0,65	0,83	0,90	0,86	0,51	0,39	0,20
DGDG 34:8	0,53	-0,03	1,00	-0,18	-0,67	0,29	0,63	0,39	0,56	0,58	0,39	0,37	-0,22	-0,74	-0,77
DGDG 36:0	0,47	-0,32	-0,08	-0,73	-0,29	-0,14	-0,06	0,18	-0,03	0,14	0,65	0,69	0,71	1,00	0,60
DGDG 36:1_A	-0,29	-0,19	-0,31	0,00	0,94	1,39	1,66	1,61	1,38	1,84	1,89	1,30	1,85	2,34	1,67
DGDG 36:1_B	0,11	-0,26	-0,07	-0,30	0,40	0,60	0,84	0,68	0,58	0,53	0,71	0,77	0,78	1,13	0,87
DGDG 36:2	0,09	0,00	0,21	-0,15	0,17	0,52	0,94	0,95	1,34	1,23	1,21	1,24	1,32	1,49	1,17
DGDG 36:3_A	0,10	-0,29	-0,25	-0,46	0,18	0,32	0,72	0,96	1,02	1,10	1,19	1,26	0,84	1,02	1,01
DGDG 36:3_B	0,01	-0,21	-0,06	-0,44	0,27	0,56	0,82	1,12	1,56	1,82	1,71	1,65	1,58	1,81	1,48
DGDG 36:4_A	0,03	-0,15	-0,06	-0,36	0,05	0,47	0,67	0,49	0,61	0,51	0,65	0,53	0,31	0,55	0,47
DGDG 36:4_B	-0,01	-0,22	-0,18	-0,64	-0,05	0,61	1,02	1,24	1,35	1,46	1,49	1,28	1,07	1,24	1,15
DGDG 36:5_A	0,06	-0,24	-0,02	-0,20	0,25	0,85	1,27	1,34	1,57	1,52	1,62	1,32	0,99	0,86	0,58
DGDG 36:5_B	0,07	-0,20	-0,13	-0,59	-0,18	0,52	0,84	0,68	0,74	0,55	0,62	0,49	0,28	0,67	0,72
DGDG 36:6_A	0,08	-0,20	-0,07	-0,27	0,13	0,59	1,21	1,39	1,57	1,51	1,60	1,43	1,30	1,37	1,13
DGDG 36:6_B	0,15	-0,18	-0,16	-0,50	-0,53	-0,13	0,26	0,22	0,40	0,30	0,30	0,13	0,04	0,25	0,27
DGDG 36:7	0,06	-0,28	-0,04	-0,20	0,06	0,62	0,99	1,31	1,47	1,43	1,51	1,37	1,27	1,32	0,89

Table 13. Continued

	0,25	0,5	1	2	4	6	8	10	11	12	13	14	16	20	24
DGTS 30:0	-0,09	-0,17	0,00	-0,02	0,37	0,82	1,26	1,30	1,09	0,81	0,76	0,51	0,16	0,15	-0,12
DGTS 30:1_A	-0,13	-0,39	-0,28	-0,43	0,08	0,56	0,80	0,78	0,78	0,67	0,72	0,25	-0,49	-0,05	-0,08
DGTS 30:1_B	-0,20	-0,47	-0,35	-0,54	-0,03	0,45	0,84	0,77	0,61	0,44	0,32	-0,03	-0,39	0,12	0,12
DGTS 30:2_A	0,02	-0,19	-0,14	-0,33	0,09	0,51	0,64	0,32	0,21	0,11	0,19	-0,12	-0,81	-0,08	-0,13
DGTS 30:2_B	-0,08	-0,40	-0,32	-0,50	-0,14	0,16	0,44	0,48	0,58	0,51	0,47	0,28	-0,09	0,22	0,17
DGTS 30:2_C	-0,25	-0,38	-0,25	-0,33	0,22	0,37	0,33	0,06	-0,12	-0,54	-0,47	-0,59	-0,83	-0,44	-0,53
DGTS 30:3_A	-0,01	-0,36	-0,27	-0,47	-0,09	0,02	0,06	-0,22	-0,22	-0,42	-0,37	-0,59	-0,99	-0,33	-0,45
DGTS 30:3_B	-0,12	-0,41	-0,41	-0,68	-0,34	-0,26	-0,34	-0,33	-0,08	-0,19	-0,07	-0,48	-0,87	-0,66	-0,98
DGTS 30:3_C	-0,04	-0,41	-0,33	-0,57	-0,54	-0,39	-0,30	-0,37	-0,19	-0,30	-0,39	-0,64	-0,77	-0,49	-0,61
DGTS 30:3_D	-0,19	-0,35	-0,29	-0,58	-0,72	-0,65	-0,79	-1,20	-1,58	-1,98	-1,86	-1,93	-1,84	-1,38	-1,44
DGTS 30:4_A	-0,13	-0,45	-0,36	-0,58	-0,30	-0,28	-0,18	-0,11	0,04	-0,09	-0,18	-0,43	-0,78	-0,52	-0,80
DGTS 30:4_B	-0,26	-0,49	-0,62	-0,89	-0,76	-0,89	-1,06	-0,84	-0,47	-0,53	-0,61	-1,01	-1,79	-1,54	-1,98
DGTS 32:0	0,07	-0,01	0,28	0,68	1,15	1,33	1,46	1,19	1,00	0,66	0,68	0,66	0,31	0,24	0,00
DGTS 32:1_A	0,03	-0,21	-0,04	-0,21	0,30	0,67	0,86	0,79	0,86	0,85	0,97	0,86	0,72	0,94	0,85
DGTS 32:1_B	0,00	-0,22	-0,12	-0,26	0,27	0,67	0,93	0,66	0,46	0,07	0,10	-0,05	-0,26	0,21	0,28
DGTS 32:2_A	0,20	-0,10	0,09	-0,08	-0,24	0,53	0,95	1,67	1,63	1,88	1,91	0,58	0,32	0,27	0,15
DGTS 32:2_B	-0,13	-0,29	-0,02	-0,16	0,13	0,56	0,70	0,48	0,16	0,07	0,18	-0,01	0,14	0,38	0,23
DGTS 32:3_A	0,01	-0,31	-0,17	-0,27	0,05	0,28	0,44	0,34	0,24	0,19	0,27	0,19	0,18	0,48	0,49
DGTS 32:3_B	-0,07	-0,38	-0,35	-0,58	-0,14	0,23	0,52	0,59	0,71	0,75	0,81	0,65	0,30	0,51	0,38
DGTS 32:3_C	0,06	-0,22	-0,18	-0,38	-0,06	0,05	0,12	-0,14	-0,15	-0,27	-0,13	-0,09	-0,13	0,30	0,15
DGTS 32:3_D	-0,07	-0,37	-0,23	-0,33	-0,18	0,13	0,27	-0,09	-0,25	-0,44	-0,30	-0,22	-0,22	0,05	0,09
DGTS 32:4_A	0,03	-0,20	-0,15	-0,31	0,03	0,07	0,08	-0,20	-0,23	-0,29	-0,10	-0,14	-0,23	0,07	0,02
DGTS 32:4_B	-0,10	-0,41	-0,37	-0,68	-0,38	-0,08	0,05	0,14	0,41	0,51	0,53	0,23	-0,19	-0,19	-0,41
DGTS 32:5_A	0,02	-0,32	-0,31	-0,57	-0,44	-0,40	-0,24	-0,19	0,03	0,15	-0,04	-0,45	-0,72	-0,73	-0,99
DGTS 32:5_B	-0,08	-0,34	-0,42	-0,73	-0,50	-0,58	-0,60	-0,68	-0,57	-0,64	-0,61	-1,01	-1,55	-1,04	-1,32
DGTS 32:5_C	-0,03	-0,27	-0,36	-0,66	-0,67	-0,80	-0,80	-0,64	-0,21	0,02	-0,09	-0,27	-0,63	-0,70	-1,15
DGTS 32:6_A	0,03	-0,25	-0,45	-0,65	-0,72	-0,85	-0,90	-0,62	-0,23	-0,03	-0,12	-0,29	-0,78	-0,85	-1,23
DGTS 32:6_B	0,08	-0,32	-0,55	-0,94	-1,38	-1,69	-1,73	-1,62	-1,25	-1,01	-1,03	-1,34	-1,51	-1,44	-1,71
DGTS 32:7	0,02	-0,33	-0,49	-0,77	-1,03	-1,37	-1,37	-1,02	-0,84	-0,62	-0,80	-1,02	-1,37	-1,32	-1,69
DGTS 32:8	0,07	-0,20	-0,22	-0,49	-0,79	-1,17	-1,21	-1,00	-0,71	-0,76	-1,08	-1,35	-1,76	-1,61	-2,10
DGTS 34:0	0,19	0,50	0,94	0,97	0,92	0,80	0,98	0,94	0,74	0,59	1,37	1,71	1,47	0,70	0,31
DGTS 34:1	0,11	-0,06	0,12	-0,06	0,82	0,94	1,22	0,92	0,79	0,49	0,93	1,12	1,03	1,04	0,81
DGTS 34:2	0,03	-0,14	0,06	0,05	0,60	0,89	1,04	0,55	0,33	0,04	0,21	0,22	0,38	0,60	0,56
DGTS 34:3_A	0,02	-0,24	-0,22	-0,37	0,09	0,46	0,79	0,86	0,89	0,95	1,08	0,99	0,75	0,94	0,88
DGTS 34:3_B	0,01	-0,19	-0,07	-0,11	0,04	0,36	0,51	-0,06	-0,27	-0,44	-0,06	0,09	0,15	0,36	0,53
DGTS 34:4	0,00	-0,23	-0,22	-0,42	-0,02	0,19	0,39	0,39	0,43	0,52	0,64	0,54	0,35	0,49	0,39
DGTS 34:5_A	0,00	-0,26	-0,29	-0,50	-0,21	-0,08	0,09	0,29	0,61	0,80	0,85	0,68	0,38	0,27	-0,07
DGTS 34:5_B	0,00	-0,22	-0,17	-0,45	-0,42	-0,18	-0,24	-0,40	-0,30	-0,19	0,08	0,06	-0,01	-0,13	-0,41
DGTS 34:6_A	0,04	-0,26	-0,25	-0,45	-0,20	-0,14	0,09	0,46	0,84	0,97	1,00	0,88	0,53	0,34	-0,26
DGTS 34:6_B	0,08	-0,30	-0,31	-0,45	-0,62	-0,48	-0,58	-0,74	-0,58	-0,57	-0,30	-0,34	-0,43	-0,73	-1,15
DGTS 34:6_C	0,07	-0,26	-0,32	-0,61	-0,67	-0,68	-0,61	-0,40	0,04	0,24	0,19	-0,04	-0,32	-0,48	-0,85
DGTS 34:6_D	0,09	-0,26	-0,36	-0,67	-0,87	-0,86	-0,97	-1,01	-0,67	-0,52	-0,39	-0,48	-0,76	-0,80	-1,06
DGTS 34:7_A	-0,06	-0,27	-0,17	-0,40	-0,64	-0,28	-0,32	0,12	0,51	0,81	0,77	0,23	0,17	-0,02	-0,55
DGTS 34:7_B	-0,01	-0,35	-0,48	-0,64	-0,81	-0,91	-1,05	-1,05	-0,72	-0,48	-0,37	-0,44	-0,88	-1,07	-1,32
DGTS 34:7_C	-0,08	-0,28	-0,41	-0,73	-0,90	-1,09	-1,20	-0,91	-0,32	-0,02	-0,13	-0,35	-0,62	-0,75	-1,14
DGTS 34:8	0,02	-0,32	-0,55	-0,78	-0,98	-1,24	-1,23	-0,90	-0,49	-0,20	-0,33	-0,54	-0,94	-0,99	-1,42
DGTS 36:1	0,12	-0,03	0,13	0,23	0,82	0,97	1,12	1,05	1,15	0,94	1,25	1,29	1,03	0,74	0,41
DGTS 36:2	0,10	-0,13	-0,13	-0,15	0,65	0,36	0,53	0,66	0,77	0,66	1,07	1,02	1,06	1,15	1,10
DGTS 36:3_A	0,11	-0,05	-0,01	0,04	0,14	0,17	0,32	0,44	0,69	0,78	1,01	1,15	0,90	0,78	0,68
DGTS 36:3_B	0,03	-0,15	0,05	-0,07	0,42	0,53	0,54	0,06	-0,20	-0,42	-0,08	0,14	0,52	0,83	0,74
DGTS 36:4_A	0,01	-0,20	-0,19	-0,36	0,01	0,17	0,37	0,54	0,69	0,73	1,00	1,03	0,92	1,27	1,11
DGTS 36:4_B	-0,01	-0,20	-0,09	-0,22	0,32	0,66	0,74	0,27	0,05	-0,07	0,15	0,21	0,40	0,49	0,43
DGTS 36:5_A	-0,01	-0,23	-0,20	-0,30	0,04	0,29	0,55	0,62	0,75	0,88	0,94	0,78	0,68	0,80	0,63
DGTS 36:5_B	-0,02	-0,23	-0,12	-0,25	0,08	0,38	0,48	0,10	-0,05	-0,10	0,05	0,08	0,21	0,39	0,30
DGTS 36:6_A	0,13	-0,51	-0,41	-0,50	0,50	0,60	1,31	2,26	2,87	4,77	4,66	3,64	3,29	2,41	2,05
DGTS 36:6_B	0,03	-0,22	-0,23	-0,39	-0,08	0,19	0,39	0,40	0,51	0,67	0,68	0,60	0,44	0,54	0,38
DGTS 36:7_A	-0,25	-0,03	-0,31	-0,05	0,67	0,04	-0,01	1,56	2,52	2,82	2,56	1,54	0,99	1,00	0,88
DGTS 36:7_B	0,08	-0,27	-0,33	-0,57	-0,45	-0,34	-0,29	-0,39	-0,13	-0,02	0,00	-0,24	-0,38	-0,41	-0,55
DGTS 36:8	0,11	-0,24	-0,35	-0,53	-0,60	-0,96	-0,89	-0,52	0,17	0,47	0,32	0,14	-0,34	-0,61	-1,09
DGTS 38:2	0,07	-0,20	0,02	-0,10	0,58	0,51	0,48	0,22	0,09	-0,11	0,15	0,16	0,30	0,77	0,77
DGTS 38:3	0,00	-0,20	0,01	0,02	0,59	0,57	0,55	0,06	-0,12	-0,29	-0,07	0,10	0,41	0,75	0,68
DGTS 38:4_A	0,01	-0,20	-0,13	-0,20	0,26	0,32	0,37	0,26	0,38	0,54	0,62	0,60	0,65	1,13	1,16
DGTS 38:4_B	0,03	-0,25	-0,09	-0,27	0,16	0,31	0,23	-0,27	-0,43	-0,58	-0,34	-0,18	0,07	0,32	0,33
DGTS 38:5_A	-0,23	-0,42	-0,63	-0,65	-0,73	-0,57	-0,34	-0,33	0,17	0,81	1,11	1,10	0,69	0,90	0,93
DGTS 38:5_B	0,03	-0,28	-0,30	-0,39	-0,04	0,19	0,23	0,24	0,55	0,76	0,94	0,87	0,75	1,03	0,90
DGTS 38:6_A	0,01	-0,31	-0,31	-0,46	-0,35	-0,38	-0,29	-0,33	-0,07	0,13	0,23	0,12	-0,03	0,27	0,17
DGTS 38:6_B	0,08	-0,27	-0,12	-0,32	-0,15	-0,78	-1,06	-1,51	-1,56	-1,77	-1,61	-1,35	-1,19	-0,48	-0,48
DGTS 40:4	-0,15	-0,25	-0,29	-0,68	-0,83	-0,89	-1,03	-0,98	-0,62	-0,61	-0,49	-0,45	-0,56	-0,20	-0,09

Moreover, the saturated DGDG belong to the few exceptions that are not increased during the late light phase, while MGDG 34:0 showed a significant decrease. During the dark phase the cellular content of most DGDGs remain accumulated. Only the high unsaturated DGDG 32:4_A, DGDG 32:5 and DGDG 34:8 show a reduced cellular content during the dark phase. Similar to this MGDGs with 36 and 34 carbons are significantly increased during the dark phase, while MDGDs with 32 carbons show a different response on the level of unsaturation. While the high unsaturated forms (≥ 4 db) remain unchanged or reduced during the dark phase, the low unsaturated forms increase at the end of the light phase (TP 20 h and TP 24 h).

The sulfolipids (SQDG), which are also of plastidic origin, show an accumulation of their saturated and low unsaturated forms (≤ 4 db) during the late light phase and the dark phase. The high unsaturated SQDG (> 4 db) are mainly reduced during the late light phase and early dark phase (13 – 16 h). This observation was most pronounced for SQDGs with longer chain fatty acids, namely that with 36 carbons in their fatty acids.

Similar to SQDGs, we found that also the cytoplasmic lipid DGTS show an accumulation of saturated and low unsaturated forms and a decrease of high unsaturated species during the late light phase and the dark phase after rapamycin treatment. However, the border between low unsaturated and high unsaturated was dependent on the fatty acid chain length as can be seen in Table 13. Interestingly, the high unsaturated DGTS 36:6_A and DGTS 36:7 display the strongest increase within the DGTS during the late light and following dark phase. In contrast to the DGTS, the phospholipid PE which is also synthesized in the cytoplasm seems to be more affected on level of the fatty acid chain length than the saturation level. PEs with 34 carbons in their two fatty acids are significantly increased 2 h after rapamycin treatment, whereas PEs with 36 carbons are strongly decreased. Between 12 – 14 h this pattern turns to the opposite, showing that PEs with 34 carbons have strongly reduced cellular content while PEs with 36 carbons are significantly accumulated. In the late dark phase this opposite behavior switched again.

Next to PEs we could annotate another phospholipid, namely PGs which derive mainly from the chloroplast. Within the PGs, PG 34:0 shows a strong accumulation during the late light phase and the entire dark phase, while the cellular content of PG 36:6 being strongly reduced during this time. The other PG species displayed less pronounced changes. However, it seems that PGs show a similar response to TOR inhibition as SQDGs and DGTS by accumulating saturated and low unsaturated fatty acids and decrease the amount of high unsaturated species.

4 Discussion

4.1 Effects of TOR inhibition by rapamycin on cell number, cell size and cell cycle progression

The understanding of how cells sense environmental cues and integrate those signals to regulate growth and proliferation is a fundamental aspect in biology. An important protein that responds to this need is the TOR kinase. TOR senses and integrates growth stimuli as nutrient availability and energy status to regulate cell growth. Although yeast cells arrest in G1 phase after TOR inhibition, there was for a long time no clear evidence that TOR has a direct role in the regulation of the cell cycle. This led to the notion that the defect in cell cycle progression upon TOR inhibition is an indirect effect caused by growth inhibition [49]. Only recently the group of Jen Sheen could identify a new substrate of the TOR kinase which indicates a direct link between TOR and the cell cycle [153]. Their results show that TOR directly phosphorylates the transcription factor E2Fa and promotes its activity in transcriptional activation of S-phase genes. Corresponding to the observation in yeast, they found that inhibition of TOR by rapamycin leads to a growth arrest of root meristems in G1 phase.

Cell growth and cell cycle progression are tightly linked processes. Detailed analyses of the relationship between cell growth and cell cycle/cell division require a system that allows to consider both processes. Within a synchronized cell culture ideally all cells are in the same cell cycle phase. Therefore synchronization allows to monitor dynamic changes of various components within different phases of the cell cycle. The simplicity of synchronizing *Chlamydomonas* cells by alternating light-dark regimes make this organism a convenient system to study the role of TOR in the regulation of cell growth and cell proliferation in a photosynthetic eukaryote.

Depending on the strain and culture conditions used for synchronization of *Chlamydomonas* the kinetic of the cell cycle vary and was therefore established under the selected growth conditions. Beside cell number, cell size and size distribution, parameters for different cell cycle phases were monitored, such as the DNA content as a marker for the S phase entry and the percentage of divided cells as marker for the M phase.

4.1.1 Rapamycin stability is not the reason for the different growth phenotype of *Chlamydomonas*

In contrast to yeast and root meristems, *Chlamydomonas* growth is not fully arrested even by using as high rapamycin concentrations as they were used to inhibit growth of *Arabidopsis* (Figure 9)

[153]. The results of this work indicate that this cannot be attributed to rapamycin stability. Although rapamycin degrades very fast, especially at the high temperatures used for synchronization (34 °C) (Figure 14), the growth inhibitory effect of rapamycin can be maintained for at least two cell cycles (48 h) without any further addition of rapamycin (Figure 20). However, the dose-response relationship displays a significant stronger decrease of approximately 20% at a rapamycin concentration of 4 µM compared to 0.5 µM (Figure 10). The results suggest that either the binding of rapamycin to TOR is stable for at least two days or the recovery of *Chlamydomonas* requires more than one additional cell cycle. In addition, the results indicate that obviously the inhibition of TOR is also transferred to the newly produced DCs. Moreover, an additional application of rapamycin in the beginning of the 2nd cell cycle increases the growth inhibitory effect about 10% compared to the first cell cycle, indicating that long-term treatment increases the rapamycin induced growth inhibitory effect. An extension of the experiment for several days, weeks or month would show if the growth inhibitory effect could be further increased and might be lead to a full growth arrest after x rounds of cell cycle. Furthermore, the observations that rapamycin treated *Chlamydomonas* cells are more sensitive for a second rapamycin addition might imply that the TOR inhibited cells become also more sensitive for stresses. Therefore it would be interesting to investigate the response of rapamycin treated cells in combination with different stressors, such as nitrogen depletion.

4.1.2 Inhibition of TOR leads to reduced cell growth and proliferation

A detailed view on the rapamycin effect within one cell cycle revealed a decrease in cell growth and a reduction of approximately 50% in the cell number (Figure 19). In more detail, analysis of the size distribution reveals that rapamycin treatment causes that less cells achieve a cell volume above 1200 µm^3 (Figure 20 C) and thus, those cell sizes which produce the larger number of DCs. However, further investigation of the correlation of cell size and cell number revealed that the reduced increase in cell volume caused by rapamycin treatment can only explain in part the decrease in produced DCs.

4.1.2.1 Correlation of cell size and DC number is changed after rapamycin treatment

For *Chlamydomonas* it has been shown that the number of DCs correlates very well with volume the MC attain during light phase [29]. The coordinated regulation of cell size and cell proliferation has been a topic of interest for cell biologists for over a century. The fact that the cells have to tightly control their cell size to maintain a distinct size also after cell division seems self-evident, but insights into the underlying mechanisms have until recently been relatively sparse [154-157].

Thus, it is also plausible that cells have to increase in size before they divide, because otherwise they will simply divide the same mass into smaller packets, a process that cannot continue indefinitely. However, size control must be defined very careful with respect to the context as cells can increase in size by different mechanisms; a topic that will be discussed in more detail below.

For the analysis of correlation of MC size and DC number, we assumed that the size distribution of MC shortly before release of DC should be sufficient to estimate the number of DCs. After determination of the mean cell volume that is necessary for a doubling of the *Chlamydomonas* cell population (Figure 17), the size distribution curve was divided in equal parts, predicting a linear correlation between cell volume and DC number. The assumption of a linear correlation can be supported by the observation of Craigie and Cavalier-Smith, who showed that for doubling in DC number the MCs needs to achieve the double cell volume [29]. We have to note that this is not comparable with the so called "critical cell size" a cell needs to divide. This value is probably lower and has been shown for different *Chlamydomonas* strains to be between 140 - 178 μm^3 [29, 128, 158]. By using this linear model we estimated the DC number with an error smaller than 4% in comparison to the measured cell number (Table 8). However, using the same model for the rapamycin treated *Chlamydomonas* culture leads to an overestimation of more than 50% in comparison to the measured cell number (Table 9). This implies that in addition to the reduced growth, the correlation of cell volume and produced DCs is changed after rapamycin treatment. The overestimation of cell number indicates that the rapamycin treated cells of the same size range as under control conditions produce less DC.

To validate and precise this model further work is clearly needed. By using a cell sorter it should be possible to divide cell population in different fractions according to their size and determine the produced DC number, similar to the experiment of Craigie and Cavalier-Smith, but using more distinct fractions. As each fraction will not generate a unique population of cells which underwent the same number of division rounds, the model could be précised by plating cells of the distinct size fraction in dark. The dark-plated cells allow to count more precisely the number of undivided and divided cells and further the number of division rounds per cell, leading to a distribution of cells that underwent 0, 1, 2 or more division rounds. Comparing this distribution with the size distribution should yield much clearer results for the correlation of cell volume and cell size.

Furthermore, in eukaryotic cells there is a striking relationship between nuclear DNA content and cell size which suggest that DNA content or nuclear volume plays a conserved role in determining cell size [155, 159]. This idea is mainly supported by observations of cell size changes that correlate with ploidy [160, 161]. However, there are examples where ploidy was altered without a proportional change in cell size [162, 163]. Therefore it is assumed that the ratio between nuclear DNA and cell size is not an absolute dictator of cell size, but is better viewed as a constraint [155]. The finding that the correlation of cell volume and cell number is changed after rapamycin

treatment, might predict also a change in ratio of DNA and cell volume. The measurements we did so far did not allow to determine the ratio of DNA content to cell size. The use of flow cytometric analysis provides a more precise method to determine the DNA content per cell and in addition shows the ratio between DNA-content and cell size [164].

4.1.2.2 Inhibition of TOR leads to a shift of the first commitment point

To further investigate the correlation of cell volume and DC number, the TP and mean cell volume at which a ratio of two DCs per MC has been achieved, was taken as an indicator for when cells had passed the first commitment point for one division round and was determined in an additional experiment for the control and the rapamycin treated culture. The control cells attain the first commitment point at approximately 4 h in light (blue line; Figure 46 B). Interestingly, the results of cell size measurement showed a similar increase in cell size and a similar size distribution in the first 4 h of light of the rapamycin treated culture in comparison to the control (Figure 20). Therefore one could assume that rapamycin treatment has no effect on the first commitment point.

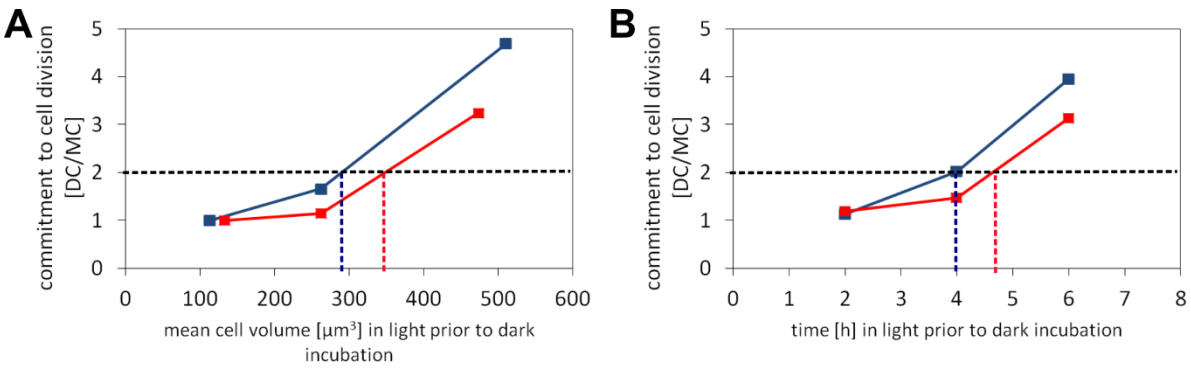

Figure 46. Determination of 1st commitment point after rapamycin treatment in comparison to the control
Number of DCs produced per MC, indicating passage of commitment point, as a function of the average MC volume from which they originated (A) and as a function of time (B). Dotted lines indicate the volume or the time at which cells have doubled their cell number (2DC2/MC) after rapamycin treatment (red) in comparison to the control (blue).

However, although, the cells achieve the same mean cell volume (MCV) after rapamycin treatment within the first 4 h in light, determination of the first commitment point demonstrates that rapamycin treated cells reach this point approximately 1 h later in comparison to the control (Figure 46 B). The time shift of the commitment point was accompanied by a larger cell size necessary for a doubling in cell number (Figure 46 B). This further supports our observation that inhibition of TOR alters the correlation between cell size and cell number. Similar results were obtained when *Chlamydomonas* cells were exposed to blue light before the cells attain a particular

cell size [165]. This might imply that CrTOR is involved in the detection and integration of the spectral composition of light.

4.1.2.3 Inhibition of TOR seems to lead to a cell swelling

Interestingly, our results show that rapamycin treated cells display an increased mean cell volume of approximately 10% directly after rapamycin treatment (Figure 47). The mean cell volume of the rapamycin treated culture remained higher in the first hour after treatment and turned afterwards (from TP 6 h onwards) to the opposite, most likely due to the retarded growth of rapamycin treated cells (Figure 19 B). In a previous study it has been shown that rapamycin treatment of *Chlamydomonas* cells resulted in an up-regulation of the autophagy marker CrATG8, which was accompanied by an increase in vacuole size and an increase in cell size [111]. Analysis of primary metabolites revealed a massive increase of amino acids, which was also observed already 15 min after rapamycin treatment (Figure 36). The strong accumulation of amino acids can derive from a protein breakdown through autophagy Moreover, studies of TOR in *Arabidopsis* revealed that the increase in amino acids of amiR-*tor* lines was accompanied by a significant increase in genes related to autophagy [114]. It is argued that physiological levels of autophagy are required for normal cell size, whereas both insufficient and excessive levels of autophagy lead to retarded growth and a smaller cell size [166]. However, our understanding of the relationship between autophagy and cell growth and cell cycle is still in the beginning. It is therefore also possible that the observed growth retardation of *Chlamydomonas* after rapamycin treatment is caused by an upregulation of autophagy.

A further possible explanation for the fast increase in cell volume after rapamycin treatment, which is probable associated with the rapamycin induced vacuolization [111], might be a hypo-osmotically induced cell swelling caused by the massive increase of the intracellular amino acid pool, It has been shown that some amino acids can cause cell swelling. The amino acids that displayed the strongest increase after rapamycin treatment, namely glutamine, glutamate, asparagine, aspartate and alanine are consistent with those are shown to cause cell swelling [167-170]. Accordingly, we would assume that the initial increase in cell volume in the first hour after rapamycin treatment is rather caused by a cell expansion, possible related to autophagy, than cytoplasmic growth. To confirm the assumption of cell swelling caused by rapamycin treatment it is necessary to determine the intracellular water content by comparing fresh weight and dry weight of cell pellets in further experiments.

In addition, it seems that the cell swelling is continuous and increases within the cell cycle as the newly produced DCs of the rapamycin treated culture display also a larger mean cell volume, which is approximately 30% higher in comparison to the control (Figure 47). The difference in

mean cell volume of DCs of the control culture between TP 0.25 h and TP 24 h is most likely caused by the fact that the cells at TP 0.25 h has already increased in size during the 15 min in light. This can be supported by the observation that the mean cell volume that we obtained from the measurement before the synchronized culture was diluted and separated for the experiment was the same as the mean cell volume at TP 24 h (data not shown).

Especially for plant cells it has been shown that the volume of individual cells can increase by two distinct mechanisms, namely cytoplasmic growth and turgor-driven cell expansion [154]. While cytoplasmic growth is executed by meristems and organ primordia, the increased cell volume of more differentiated tissues resulted mostly from water uptake and vacuole enlargement. Cytoplasmic growth is mainly driven by the net accumulation of macromolecules and cellular components and is often associated with DNA replication. Moreover, cytoplasmic growth is closely linked to energy and nutrient availability, while cell expansion is considered an energetically cheap way to increase in cell size [154]. Until now it is still not certain whether cells measure their volume, mass and/or biosynthetic capacity to regulate cell division and proliferation. Cytoplasmic growth results from macromolecular synthesis and is therefore most likely accompanied with an increase in biosynthetic capacity, whereas an increase in cell volume due to an uptake of water is rather not related to an increase in biosynthetic capacity.

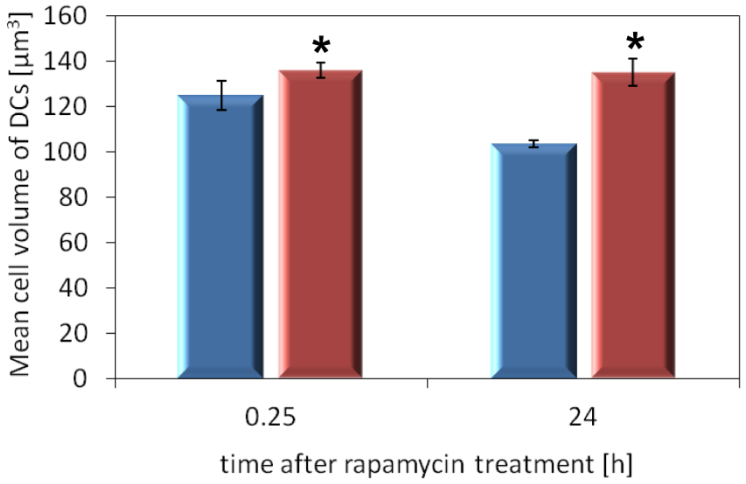

Figure 47. Mean cell volume of DCs after rapamycin treatment in comparison to the control
Mean cell volume of DCs, determined in the size range of 0 - 300 µm^3 at the distinct TPs for control (blue) and rapamycin treatment (red). Data are given as mean ± SD of 3 biological replicates. Significant ($p < 0.05$) differences to control at the distinct TP is indicated with an asterisk.

It is therefore very likely that cells rely not only on their cell volume to make the decision if they divide or not. Accordingly, the assumption that the observed initial higher cell volume after rapamycin treatment is rather caused by an uptake of water, probably accompanied by vacuolization, than cytoplasmic growth can be supported by the observation of a higher size threshold needed for the cell doubling. Therefore, we would assume that cells can differ between cytoplasmic growth and cell enlargement by water uptake.

In the budding yeast there is evidence that the cells assess their size by measuring the overall translation rate (translation rate per ribosome). It is assumed that even cells larger than the critical cell volume do not commit to divide because a critical translation rate is not achieved [156, 171]. In addition, cells growing in sub-lethal doses of cycloheximide (inhibitor of protein synthesis by blocking protein elongation) increased their critical cell volume and delayed the commitment to divide (Start in yeast cells) [4, 172]. Therefore, the larger cell volume and the delay for the 1st commitment point after rapamycin treatment (Figure 46) might be caused by a reduced translation rate. It has long been known that TOR stimulates translation initiation through phosphorylation of S6K1 and contributes to the overall cap-dependent translation by phosphorylating 4E-BPs. Inhibition of TOR with rapamycin leads to a prompt desphosphorylation of its downstream targets, e.g. S6K1 and 4E-BP1 which in consequence downregulate protein production [79]. The observed fast and massive increase of amino acids could be an indication for a decreased translation and thereby a decrease of amino acid incorporation into newly synthesized proteins (Figure 36). An increase of several amino acids was also observed in *Arabidopsis* by downregulation of TOR in inducible amiR-*tor* lines. This observation was accompanied by downregulation of genes coding for cytosolic (80S) and chloroplastic (70S) ribosomal proteins and a decreased synthesis of the 45S rRNA precursor. The authors suggest that this leads to decreased ribosome biogenesis and subsequently reduced translational efficiency and/ or capacity [114]. In addition, transcript data of unsynchronized *Chlamydomonas* culture treated with rapamycin under photoautotrophic growth conditions showed a significant downregulation of genes involved in protein translation within a short time window of 30 min (Susann Irgang, manuscript in preparation).

All in all, one can hypothesize that the increased cell size threshold for the first commitment point is caused by a swelling, whereas the delay in the first commitment point and the resulting prolonged pre-commitment period is most likely the result of a decreased translation rate and/or increased autophagy. Both processes have in common the massive increase of amino acids, albeit in a different context, but still connected. While the reduced translation rate and/or increased autophagy probably caused the increase in amino acids, the swelling of the cells might be in turn the result of the increased amino acids. To confirm this hypothesis further studies need to be conducted as measuring the water content, the translation efficiency (e.g. ribosomal loading) and autophagy marker of rapamycin treated cells.

Moreover, there is evidence that cell cycle regulators such as cyclin D, cyclin-dependent kinase 4 (CDK4), the transcription factor E2F and the retinoblastoma tumor suppressor protein (RB) can influence growth rates [155]. For *Chlamydomonas* it has been shown that mutations in MAT3/RB, E2F1 or DP1, dimeric partner of E2F, lead to altered cell size phenotypes, which are similar to the cell size phenotypes of animal and plant cells that have perturbations in the RB pathway [158, 173-176]. Whereas *mat3* mutants pass commitment at a smaller size and produce smaller DCs than wild type (WT) cells, *dp1* and *e2f1* mutants have the opposite phenotype. Next to affect the cell size in an opposite way, *dp1* and *e2f1* were found to suppress *mat3* by alternating the size checkpoint function that controls how many S/M cycles are initiated rather than simply slowing cell cycle progression [158]. The recent discovery of E2F as a direct substrate of TOR in root meristems [153], might also suggest that the observed growth phenotype of larger DCs is caused more directly by TOR through E2F.

4.1.3 Timing of the distinct cell cycle phases

Under the used growth conditions (see chapter 2.2.1.3) *Chlamydomonas* cells enter the S phase in the middle of the light phase (TP 6 h) (Figure 16 B). First mitotic cells could be observed after 8 h in light (Figure 16), showing that the cells enter the M phase 2 h after they start to synthesize nuclear DNA. As mentioned above the release of DCs starts after 10 h in light (Figure 16 A). In consistence with the obtained 2 h time interval for the peaking of the distinct size ranges, this pattern is also reflected by timing of the cell cycle phases and supports therefore the chosen separation of the size distribution. Interestingly, we could observe that DNA synthesis occurs until the onset of dark phase (TP 12 h). This shows that DC release starts before all cells have been completed their division. This overlap of cell division and DC release can be in part explained by the spread in cell size of the starting cell population and the intercellular variation in growth during the light period [29]. Accordingly, the size distribution data supports this idea as it shows that with progressing time the curve becomes broader. The obtained increasing heterogeneity in cell size might be explained by the increasing cell density during the light phase and the concomitant changes in light intensity and probable also nutrient availability. Therefore, it is suggested that the maximum attainable synchrony is limited by the intercellular variation in growth, which is mainly influenced by the light intensity [29]. This assumption was supported, by the observation that an increased light intensity reduced the temporal spread of cell division [29, 36]. A further optimization would be a synchronization of chemostat cultures by using bioreactors which automatically control and regulate the density of a cell culture to maintain a nearly constant cell density. This would make the growth conditions more stable during the entire cell cycle.

4.1.4 TOR inhibition leads to a prolonged cell cycle

Next to the shift of commitment timing and size our results indicate that also the length of the entire cell cycle is affected by rapamycin treatment (Figure 48). As the release of DCs marks the end of the cell cycle [38], TOR inhibition by rapamycin increases the length of the cell cycle by 3 h. In more detail, we observed that the mitotic phase is delayed by 2 h and the time span between mitotic phase and release of DCs is prolonged by 1 h. Interestingly, we found that DNA synthesis was not delayed and therefore it seems that the transition of G1 to S phase is not affected by rapamycin treatment in *Chlamydomonas*.

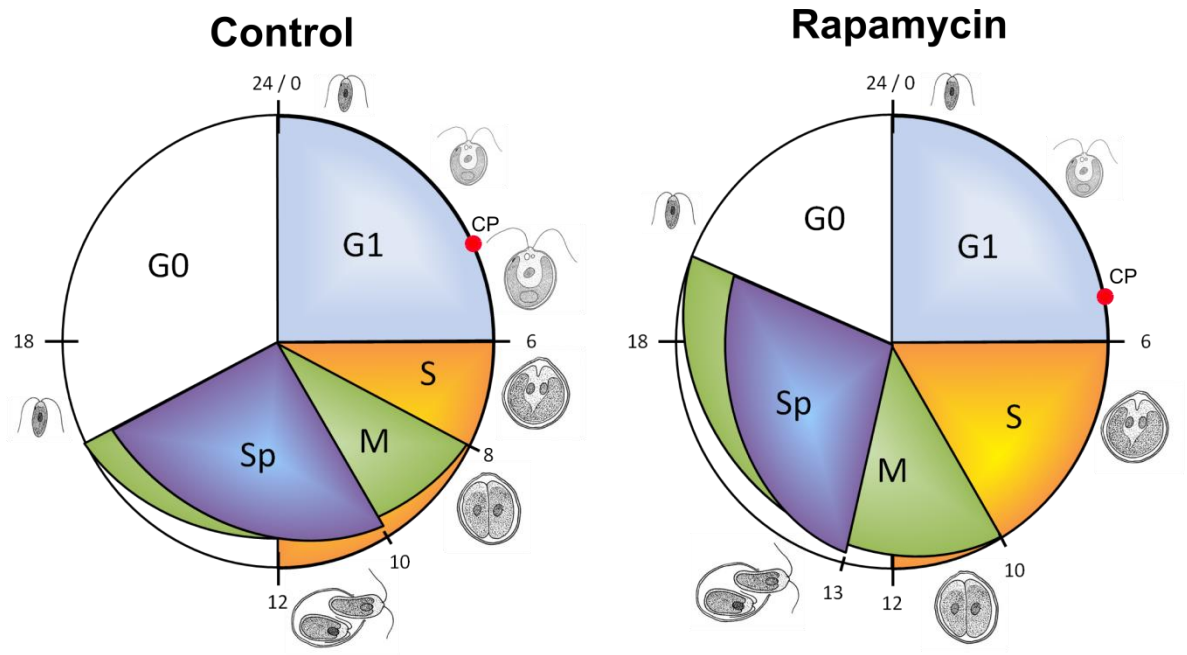

Figure 48. Schematic of cell cycle phases of synchronized *Chlamydomonas* culture after rapamycin treatment in comparison to the control

The observation that rapamycin treatment delays the CP by 1 h, mitosis by 2 h and DC release by 3 h in comparison to the control, might indicate an effect that accumulates over time. As most cell cycle regulators are synthesized only within specific cell cycle phases and are needed to induce the transcription and/or translation of the following cell cycle regulators [1, 25], downregulation on either the transcript level or the protein level might explain the delay and also the accumulation of this effect. Nevertheless, this fails also to explain why DNA synthesis is not shifted in timing.

Furthermore, the delay of CP, but not DNA synthesis leads to shortened time period between first CP and S phase. This might imply that TOR inhibition by rapamycin treatment leads to an

uncoupling of growth control and DNA synthesis. In *Arabidopsis* root meristems it has been shown that DNA synthesis is completely inhibited upon rapamycin treatment due to the direct regulation of the transcription factor E2Fa [153]. As this mechanism has so far only been shown for a specific cell type in *Arabidopsis*, it needs to be elucidated if the impact of TOR on E2F regulation is a conserved or tissue-specific effect. Nevertheless, we found that the DNA synthesis was reduced after rapamycin treatment, but in the same quantity as the cell number. The observation that the DNA synthesis is downregulated in correlation with cell growth and cell proliferation and is not affected in the timing, might imply that TOR is not directly involved in the regulation of DNA replication. Another protein that is suggested to regulate DNA synthesis is the retinoblastoma (RB) protein [177]. In mammalian cells, E2F4 and RB co-localize at foci that are the sites of DNA synthesis in early S phase [178, 179]. RB belongs to a family of so-called pocket proteins and interacts with specific DNA-binding proteins and chromatin remodeling complexes [177]. The RB tumor suppressor pathway is conserved in most eukaryotic lineages, including animals, plants and green algae, while it has been lost from yeast and other fungi [158]. RB proteins interact with transcriptions factor heterodimers in the E2F and DP families [180]. Through a combination of activator and repressor complexes, EF2 and RB family members regulate, next to cell size [158], the timing of expression of diverse sets of genes, involved in S phase entry, mitotic progression, the maintenance of DNA integrity and, potentially, differentiation and development [177]. Mammalian genomes encode at least six E2F proteins, from which five (E2F1-5) are transcriptional activators that interact with RB, while E2F6 does not associate with any pocket protein and is believed to repress transcription [181, 182]. In contrast, *Chlamydomonas* contains only single copy genes encoding E2F and RB [158]. Beside the direct interaction of TOR and E2F [153], it has been shown that rapamycin treatment inhibits the phosphorylation of RB, which is probably mediated by TOR through deficiency of active cyclin D/ Cdk 4 complexes [183, 184]. Phosphorylation and inactivation of RB is required for cell cycle progression, as phosphorylated RB can no longer bind to E2F, thus allowing the expression of E2F targets [185]. In *Chlamydomonas*, it has been shown that similar to animals and plants MAT3/RB is also phosphorylated as the cell cycle progresses, with maximum phosphorylation occurring during S/M phase, while in contrast to metazoans this phosphorylation causes the release E2F-DP from RB, MAT3/RB remains bound to E2F1/DP1 and associates with chromatin at all stages of the cell cycle [186]. This regulatory difference in the RB pathway might be an explanation of the different growth phenotype of TOR inhibited *Chlamydomonas* cells, if indeed there is a correlation between TOR and the RB pathway.

Moreover, the observed delay of mitotic entry can also be attributed to E2F as it regulates also the expression of several genes with mitotic functions, such as *cyclin B1* [187, 188]. However, *Chlamydomonas e2f1* mutants showed a similar pattern of repression and induction of cell cycle genes, including cyclin B, with peak expression levels comparable to WT [158]. In contrast to our

observation, *e2f* mutants did not display any delay of mitosis after passing commitment. This might imply that E2F is not involved in the mitotic delay after rapamycin treatment.

Although there is some evidence that TOR is involved in the regulation of the RB and E2F family members and thereby regulating the cell cycle progression, there are certain discrepancies, such as the results that TOR inhibition by rapamycin does not induce a growth arrest in G1 and, furthermore, initiation of S phase is not altered, which make the direct regulation of E2F and RB by TOR questionable. Nevertheless, the interaction of TOR and the RB pathway is an interesting field and should be further investigated. With its natural sensitivity to rapamycin and the presence of different mutants of the RB pathway *Chlamydomonas* is valuable candidate to elucidate the connection of both, TOR and RB pathway.

4.2 Effect of TOR inhibition on primary and lipid metabolism of synchronized *Chlamydomonas* cells

Transition from a growing state to a resting state or vice versa profoundly changes the metabolism of cells. Broadly speaking, there is a metabolic shift from anabolic processes for the *de novo* synthesis of macromolecules (growing or proliferating cells) towards catabolic processes for breakdown of macromolecules to release energy (resting cells). The TOR kinase has emerged as a signaling node that promotes cell growth and proliferation by the activation of key anabolic processes [189]. The aim of this study was to describe the metabolic changes within the cell cycle of *Chlamydomonas* cells and compare these results to cells where the TOR signaling pathway was inhibited by rapamycin.

4.2.1 Dynamics of the metabolism over the cell cycle of *Chlamydomonas*

The decision of a cell to enter the cell cycle depends most fundamentally on the metabolic status, meaning the coordination between extracellular nutrients and intracellular metabolite concentrations. The metabolic status of a cell has to ensure that it provides both energy and sufficient biosynthetic precursors in the form of carbon, nitrogen, sulfur, phosphate and oxygen sources for the synthesis of macromolecules to produce new DCs [190].

The increase in cell volume during the light phase is accompanied by an accumulation of primary metabolites, which provide the building blocks of most essential macromolecular structures including ribonucleotides, deoxyribonucleotides, proteins and lipids. The majority of primary and lipophilic metabolites achieve the maximum content per volume at the end of the light phase (Figure 31; Figure 40; Supp. table 1). Moreover, the results show that in general primary and lipid

metabolites that show a faster increase than chlorophyll, display also a stronger accumulation during the light phase (Figure 31, Figure 40, cluster 1 and 2). As to be expected, those metabolites have to decrease also stronger during the dark phase to end-up at the same level as chlorophyll. Analysis of the time point at which the metabolite content per volume starts to increase allowed to reveal different clusters of coordinated but also sequentially increasing metabolites. Moreover, it confirmed that functionally and biochemically related groups could be identified within these clusters (see chapter 3.2.3.3 and 3.2.4.3). These results showed that despite their different timing the majority of metabolites start to increase within the G1 phase (between 0 – 6 h in light) and at least doubled their amount per volume within this period. Nevertheless, within both primary and lipophilic metabolites there are compounds which showed a constant or even reduced level within the first half of the light phase (Figure 31 cluster 4, Figure 40 cluster 5). While a reduced level of those metabolites could be caused by a reduced biosynthesis or by either an increased transformation into other intermediates or an increased incorporation into macromolecules, the constant level is most likely due to a steady state between biosynthesis and transformation/incorporation. Within the lipid profiles, we found that especially DGTS and TAGs with shorter fatty acids (30 and 32 carbons in case of DGTS and 42 to 50 carbons in case of TAGs) and a lower degree of unsaturation (≤ 3 db) are overrepresented within the cluster that shows no increase during the G1 phase (Figure 40, cluster 5). This might imply that those lipid species are converted in the same quantity as they are synthesized for either membrane or storage lipid biosynthesis within the G1 phase and thereby support the rapid growth. Quantitative modeling of TAG homeostasis in yeast demonstrated that lipolysis is important for the initiation of growth [191]. While our results might be the first indication that in addition to TAGs also specific membrane lipids are degraded to provide precursors within the G1 phase, the results also indicate that this concerns only TAGs and DGTS with short fatty acids. This could lead to a further hypothesis, namely, that the FA derived from the mobilization of those lipid species are subjected to elongation and are therefore used for a rapid synthesis of lipids with longer chain FA. This idea is supported by the observation that DGTS with 38 carbons in their two FAs and TAGs with 56 carbons in their three FAs display a very rapid increase during the progression of the cell cycle of *Chlamydomonas* (Figure 40, cluster 1).

Moreover, our results show that the increase of most primary metabolites is attenuated in their accumulation rate between 6 – 8 h (Figure 31). A similar pattern was also found for starch (Figure 28) and TAGs (Figure 43 D, blue line). Interestingly, the attenuation of TAGs starts already 2 h earlier. These observations coincide with the nuclear DNA synthesis (Figure 16). Since DNA replication is costly in terms of energy and nutrient consumption it is likely that the increase in energy demand for DNA biosynthesis directly impacts on other pathways by slowing them down or even leads to a degradation of specific metabolites. This observation raises the question whether the observed attenuation is caused by DNA-synthesis or whether a reduction in specific

biosynthetic processes is required to start DNA synthesis. The earlier attenuation of TAGs might therefore be the first indication of a requirement of a reduction in biosynthesis. An increase of the temporal resolution of the data by including more TPs for this time frame would provide further insights into the sequence of processes.

Next to their DNA content cells duplicate all of their components during the growth phase and divide them into two nearly identical DCs, so that each DC receives the machinery and information necessary to successfully grow and proliferate [192]. As *Chlamydomonas* cells can divide by multiple fission to generate more than two DCs (in principle 2^n DCs, were n is the number of division rounds), the cells have therefore to increase their components by the same factor as the number of DCs. To our surprise, the obtained results show that not all components that we measured increase at the same level as the cell number and therefore display a higher or lower cellular amount (amount per chlorophyll) at the end of the dark phase (TP 24 h) compared to the beginning of the light phase (TP 0.25 h). This discrepancy between effectively very closely related developmental stages (TP 0.25 h and TP 24 h contain almost only freshly liberated DCs) can also be observed in the PCA analysis of primary and lipid metabolites (Figure 30; Figure 39). Next to the significant changes in the metabolic profile of TP 0.25 h and TP 24 h in the primary and lipid metabolites we could also observe that the starch content per µg chlorophyll was increased at TP 24 h in comparison to TP 0.25 h. Possible explanations for these somewhat unexpected observations could in part be given by the fact that the start- and end-point cultures are not absolutely identical. While the first samples (TP 0.25 h) were taken 15 min after onset of light, the last TP was sampled in the dark, shortly before the onset of light. As light has a strong influence on cells, especially when they grow photoautotrophically, we assume that a number of metabolites and lipids respond very fast to the onset of light. This assumption is further supported by a clear separation of TP 0.25 h and TP 0.5 h in the PCA, especially for the primary metabolite data (Figure 30). We found that metabolites, which show a fast increase after the onset of light, show a lower value at TP 24 h in comparison to TP 0.25 h, while it was vice versa for metabolites which decrease after the onset of light (Table 14 A). However, not all the metabolic differences could be explained by their immediate light responsiveness (Table 14 B). In addition, we could also observe quantitative differences between start and end of the cell cycle for metabolites that do not display those fast changes after the onset of light (Table 14 C).

Neverthelesss, the differences of these compounds could be either explained by the linear dynamic range and the sensitivity of the employed mass spectrometric measurements, or they simply might be caused by the increasing density of the culture and the consequent decrease in light intensity and nutrient availability. An optimization of the whole analysis system would be a synchronization of *Chlamydomonas* cultures using bioreactors which automatically control and regulate the density of a cell culture, the nutrient composition and the pH within the system allowing to maintain a nearly

constant cell density in a constant environment. This chemostat-based system would make the growth conditions more stable during the entire cell cycle and lead to a lower variance between the replicated samples [14].

Table 14. Comparison of TP 0.25 h and TP 24 h for distinct primary metabolites

	median peak height /µg chlorophyll at distinct TP [h]			Fold change	
	0.25	0.5	24	TP 0.5/TP 0.25	TP 24/TP 0.25
A					
2-Aminobutyrate	2.89E+02	5.91E+02	1.39E+02	2.04	0.48
Hypoxanthine	7.35E+01	1.24E+02	2.82E+01	1.69	0.38
Spermidine	1.67E+02	2.71E+02	8.48E+01	1.62	0.51
Guanine	1.20E+04	1.93E+04	3.01E+03	1.62	0.25
Glucose	1.09E+02	7.73E+01	1.38E+02	0.71	1.27
Dihydroxyacetone-P	4.27E+01	2.89E+01	1.72E+02	0.68	4.03
B					
Phytol	6.93E+01	1.08E+02	3.90E+02	1.56	5.63
Ribose	1.36E+02	2.06E+02	6.68E+02	1.52	4.93
Uracil	9.73E+02	7.23E+02	5.19E+02	0.74	0.53
Fructose	3.06E+02	1.98E+02	1.82E+02	0.65	0.59
C					
Oxalate	6.05E+02	6.34E+02	1.53E+02	1.05	0.25
Fructose 6-P	2.65E+02	2.84E+02	3.61E+01	1.07	0.14
Cysteine	1.74E+03	1.83E+03	4.51E+02	1.05	0.26
Histidine	5.67E+01	5.25E+01	3.05E+02	0.93	5.38

4.2.2 Regulation of primary and lipid metabolism by TOR in *Chlamydomonas*

Under photoautotrophic growth conditions *Chlamydomonas* does fix carbon (CO_2) by the Calvin cycle using light energy. The absorbed energy from the photons are subsequently converted into chemical energy (adenosine triphosphate (ATP)) and reducing power in form of nicotinamide adenine dinucleotide phosphate (NADPH). The photosynthetic carbon fixation further provides carbon skeletons for all molecules and biochemical reactions within the living cell. Accordingly, photoautotrophic cells rely on photosynthesis for promoting growth and require antenna complexes to capture light for an optimal conversion of photons to energy [193].

Our metabolic analysis showed that the observed growth reduction of TOR inhibited *Chlamydomonas* cells is accompanied by strong changes in both primary metabolites and lipids, leading to a clear separation of control and rapamycin treatment by PCA and HCA (Figure 33, Figure 34, Figure 41, Figure 42). However, those analyses also revealed that the response of primary metabolites, which are closer to the Calvin cycle, respond much faster to TOR inhibition

than the more complex lipids. In the following chapters the effect of TOR inhibition on primary metabolites and lipids within the *Chlamydomonas* cell cycle will be discussed in more detail.

4.2.3 Chlorophyll homeostasis is not affected by TOR inhibition

Chlorophylls are critical components of both the light-harvesting and reaction center complexes of the photosynthetic apparatus and they are absolutely essential for photosynthesis [194]. While in angiosperm plants light is absolutely required for the chlorophyll synthesis [195, 196], *Chlamydomonas* cells can synthesize chlorophyll also in the dark [194]. Nevertheless, light/dark-synchronized *Chlamydomonas* cells do accumulate chlorophyll only during the light phase [36], even though it is still unclear how this is mechanistically regulated [197]. Our results are in agreement with those observations, showing an accumulation of chlorophyll during the light phase and a constant chlorophyll level over the entire dark phase (Figure 26). Moreover, the increase in chlorophyll represents a proxy for the increase in cell number, since the total amount of chlorophyll seems to be constant per DCs. This chlorophyll to DC ratio is actually equal at the beginning of the cell cycle and at the end (Figure 27 B, blue column).

TOR inhibition by rapamycin treatment decreases the chlorophyll content per suspension volume, but this reduction is matched by the decrease in the cell number (Figure 27 A). Consequently, we can assume that the chlorophyll content per cell is not changed after rapamycin treatment (Figure 27 B). The interesting question that arises from here and which needs to be further investigated is, if a reduction in chlorophyll biosynthesis and photosynthesis leads to a reduced cellular growth or if the reduced cellular growth, which is a consequence of TOR inhibition by rapamycin simply leads to less cells and less chlorophyll per suspension volume. However, given the result that the rapamycin treated cells produce DC with the same amount of chlorophyll as under control conditions, there is substantial evidence to suggest that TOR is not involved in the regulation of chlorophyll homeostasis. This result was quite unexpected, as TOR is an integrator of nutrient and growth factor signals and several changes in nutrient availability have been shown to alter the chlorophyll content of cells [198, 199]. Chlorophyll biosynthesis represents a very complex pathway and requires at least 17 steps [200]. The regulation of chlorophyll biosynthesis is extremely important since several of the intermediates, like prochlorophyllide, can, if illuminated, produce harmful reactive oxygen species (ROS) causing oxidative damage or cell death [201]. Although it seems that rapamycin treated cells maintain chlorophyll homeostasis, it cannot be excluded that the decrease in chlorophyll biosynthesis might lead to an accumulation of intermediates of the chlorophyll pathway and thereby an increase in ROS. However, first measurements of ROS by staining H_2O_2 and O_2- of rapamycin treated cells showed no dramatically changes in the abundance of ROS under photoautotrophic conditions (Susann Irgang; manuscript in

preparation). Moreover, the observation that cells maintain the cellular chlorophyll level constant after growth reduction by rapamycin treatment, suggest that chlorophyll biosynthesis and growth are tightly linked processes. Thus far it is still unclear how chlorophyll biosynthesis and growth are correlated and how they influence each other.

Concomitant to the results of chlorophyll content, measurements of photosynthesis parameters within our group showed that the maximum quantum yield (Fv/Fm-value) and the electron transport rate of photosystem II (PS II) are also not significantly changed within 8 h of rapamycin treatment of *Chlamydomonas* cells, grown under photoautotrophic conditions (Susann Irgang, manuscript in preparation). In addition, we found that 3-phosphoglycerate (3PGA), which is the first product of CO_2 fixation within the Calvin cycle, showed a similar behavior after TOR inhibition as chlorophyll. The 3PGA content per suspension volume of rapamycin treated cells is significantly decreased after 8 h in the light in comparison to the control (Figure 49 A), resulting in no significant changes on the cellular level (per µg chlorophyll) (Figure 49 B). Interestingly, we observed that the chlorophyll content was significantly reduced two hours earlier (TP 6 h) than the 3PGA content, which might provide a first indication of the order in which the growth reduction events happen. Meaning that TOR inhibition first leads to a reduced chlorophyll biosynthesis (directly or indirectly) and this in consequence results in a reduced photosynthetic rate and reduced CO_2 fixation in the Calvin cycle. However, this assumption needs to be further validated by measurements of the oxygen evolution, carbon fixation and activity of the electron transport chain of synchronized *Chlamydomonas* cells.

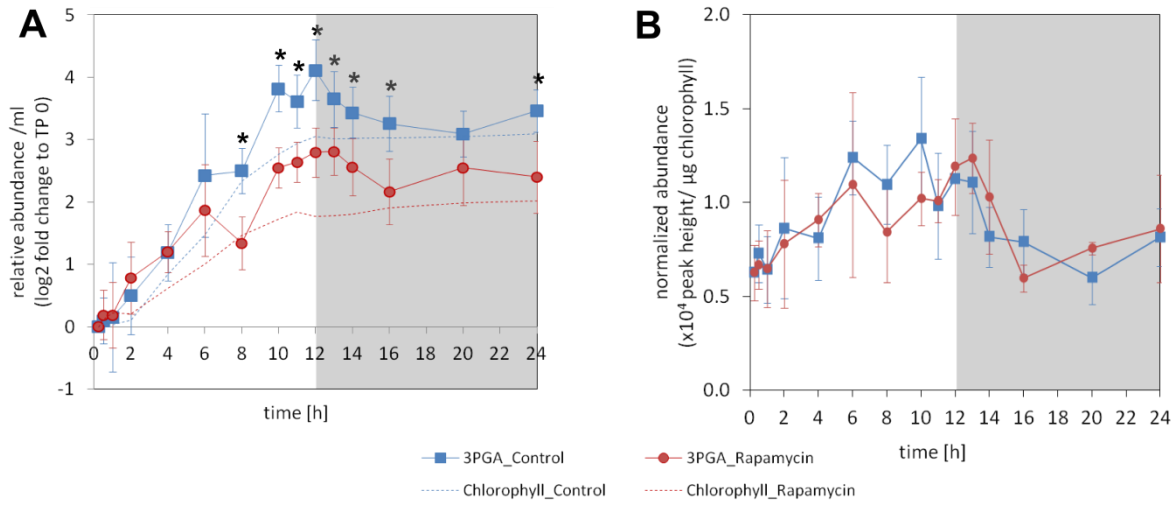

Figure 49. 3PGA content after rapamycin treatment
3-phosphoglycerate (3PGA) content was analyzed at the indicated times for a *Chlamydomonas* culture treated with rapamycin (red) in comparison to the control (blue). The cells were synchronized by a 12:12 h light-dark cycle. (A) 3PGA and chlorophyll content per suspension volume as log2 fold change to TP 0. (B) 3PGA content per µg chlorophyll. Grey background indicates the dark phase. Data are given as mean ± SD of 3 biological replicates.

4.2.4 TOR inhibition by rapamycin changes the carbon partitioning

Under photoautotrophic conditions with CO_2 as sole carbon source the synthesis of starch is an efficient way to store carbon during the light phase [193]. Under the used growth conditions the starch content of the synchronized *Chlamydomonas* cells increased during the entire light phase. With the onset of the dark phase the starch content reaches its maximum and starts to continuously decrease (Figure 28). After starch, neutral, non-membrane forming lipids as the triacylglycerols (TAGs) represent a major storage for highly reduced carbon and energy [193]. It has been shown that plant leaves typically do not accumulate high amounts of storage lipids, but they do in fact synthesize significant amounts of TAGs during the day and degrade them during the night [202]. The results show that similar to starch TAGs can increase during the light phase. Although both starch and TAG content increase within the light, they do not increase with the same factor. The cellular starch amount increases by a factor of 15.7 ± 1.8, while the cellular TAG content increases only by a factor of 2.3 ± 0.5 (Table 15). However, to compare the amount of starch with this of TAGs an absolute quantification of the TAG concentration needs to be determined.

Table 15. Maximum increase of starch and Triacylglycerol content in light
Total (per suspension volume) and cellular (per µg chlorophyll, Chl) content of starch and triacylglycerol at time point (TP) 12 h and their fold change to TP 0. Data are given as mean ± SD of three biological replicates.

	Starch				Triacylglycerol			
	nmol Glucose / ml (TP 12 h)	Fold change (TP 12 h / TP 0)	nmol Glucose / µg Chl (TP 12 h)	Fold change (TP 12 h / TP 0)	x10^6 Peakheight / ml (TP 12 h)	Fold change (TP 12 h / TP 0)	x10^6 Peakheight / µg Chl (TP 12 h)	Fold change (TP 12 h / TP 0)
Control	604 ± 78	110 ± 21	107 ± 9	16 ± 2	5.4 ± 0.8	29 ± 11	0.9 ± 0.1	2.3 ± 0.5
Rapamycin	594 ± 47	109 ± 19	224 ± 31	33 ± 5	7.3 ± 1.4	46 ± 13	3.4 ± 0.3	7.4 ± 1.6

In agreement with results from yeast [77, 203], fruit fly [204, 205] and *Arabidopsis* [114], we found that the inhibition of TOR in *Chlamydomonas* leads to an increased accumulation of starch (Figure 29) and TAGs (Figure 43 C and D).

Interestingly, we found that the starch content per volume of the rapamycin treated *Chlamydomonas* culture is not changed over the entire cell cycle in comparison to the control (Figure 29 A). This shows that the *Chlamydomonas* cell culture, which is severely reduced in cell number, produces the same amount of starch during the light phase and, maybe even more interesting, degrades the same amount of starch during the dark phase as the control culture. However, taken into account that the rapamycin treated culture produced less cells within one cell cycle and, moreover, less chlorophyll per volume, the starch content per µg chlorophyll was significantly increased after 6 h in light (Figure 29 C). The accumulation of starch was

accompanied by a decrease of phosphorylated carbohydrates, namely glucose-6-phosphate (G6P), fructose-6-phosphate (F6P), mannose-6-phosphate and ribose-5-phosphate (ribose-5P) during the light phase (Figure 38). This is in agreement with observation made by Lee and Fiehn in *Chlamydomonas* after TOR inhibition [113] and was also reported for artificial micro RNA lines of TOR (amiR-*tor*) in *Arabidopsis* [114]. Except of mannose-6-phospahte, the phosphorylated carbohydrates show an inverted pattern during the dark phase, being significantly increased. As the decrease in the starch content per volume during the dark phase is the same after rapamycin treatment as under control conditions, but the cell number is reduced by 50% after rapamycin treatment, the amount of starch degraded per cell is much higher. Therefore, the increase of the phosphorylated carbohydrates might be linked to the increased degradation of starch. In addition, we found that maltose, a product of the starch breakdown [206], was significantly increased during the dark phase (Figure 38).

In contrast to starch the TAG content per suspension volume is already increased 30 min after rapamycin treatment (Figure 43 C) leading to a stronger increase of the cellular TAG content (per chlorophyll) in comparison to starch as can be seen in Table 15. These results show that during the light phase the accumulation rate of the cellular starch content is about twice as high after TOR inhibition, while that of the cellular TAG content is about three times higher. Moreover the results show that TAGs start to increase much earlier than starch. These results were initially rather unexpected as it has been shown in *Chlamydomonas* cells subjected to nitrogen starvation that the TAG accumulation lags behind that of starch. Interestingly, it was also reported that rapid TAG synthesis occurs only when carbon supply exceeds the capacity of starch synthesis [207]. Therefore our results might imply that TOR has a more dominant role in the regulation of TAG biosynthesis than in the regulation of starch.

Among those TAGs, which are significantly increased already after 30 min, are solely polyunsaturated species (≥ 4 db) with 52 – 56 carbons in their three fatty acids (Supp. table 4). This result is in full agreement with results from TOR inhibition in *Arabidopsis* [114]. Beside the accumulation of TAGs we found that 15 min after rapamycin treatment low unsaturated (≤ 3 db) TAG species with 46 – 50 carbons in their three fatty acids are significantly reduced in comparison to the control (Supp. table 4). This is might be correlated with the increase of glycerol, a degradation product of glycerolipids, from 30 min after rapamycin treatment until the end of the light phase (Figure 38). This might indicate that after TOR inhibition TAG species with short chain fatty acids are mobilized during the initial growth phase to provide precursors for the rapid synthesis of TAGs with longer chain fatty (see chapter 4.2.1). Studies in mammalian systems, indeed reported that inhibition of TOR signaling by rapamycin stimulates lipolysis, primarily via activation of adipose triacylglycerol lipase (ATGL) [208].

Concomitant with the decrease of those TAG species we found that the FFA 18:3 shows an approximately 4-fold increase already 15 min after rapamycin treatment (Supp. table 4). This was further accompanied by strong reduction in the cellular phosphoenolpyruvat (PEP) content (Figure 38). Although much less is known about the pathway from CO_2 to acetyl-CoA in *Chlamydomonas,* it is assumed that the products of CO_2 fixation, namely triosephosphate (glyceraldehyde-3-phosphate and DHAP) and the 3-carbon sugar acid (3PGA) are transferred to the cytoplasm. In the cytoplasm they are converted to PEP and subsequently pyruvate which is transferred to mitochondria, where it is transformed into acetyl-CoA [193]. However, it has been also shown that the chloroplast fractions contain a pyruvate phosphate dikinase that catalyzes the reversible conversion of PEP and pyruvate [209]. The decrease of PEP could therefore be linked to an increased *de novo* FA biosynthesis, by an increased flux of fixed carbon through PEP. On the other hand PEP could be used for the synthesis of longer-carbon-chain compounds through gluconeogenesis which are then used for starch synthesis. It is therefore possible that the strong decrease of PEP during the light phase results from both increased starch and fatty acid synthesis. In contrast to the decrease of PEP, pyruvate shows no significant changes in the first 4 h after rapamycin treatment (Figure 38). After 4 h the cellular pyruvate content of the rapamycin treated culture is increased until the middle of the dark phase. It is therefore most likely that other pathways support the synthesis of pyruvate. An additional route for pyruvate synthesis is through the decarboxylation of malate by the plastidial NADP-dependent malic enzyme [193]. Although the cellular malate content shows only slight changes after rapamycin treatment, the significant decrease in the cellular malate content at the end of the light phase might potentially be related with the accumulation of pyruvate. Furthermore pyruvate can be produced by the degradation of the amino acids glycine, alanine, tryptophan, threonine, serine and cysteine [210]. As the amino acids are strongly accumulated after rapamycin treatment they might support the accumulation of pyruvate. Ketogenic amino acids, as leucine, lysine, isoleucine, phenylalanine, tryptophan, tyrosine and threonine can be converted to acetyl-CoA [193]. Among these, leucine, lysine and the aromatic amino acids (phenylalanine, tryptophan, tyrosine) show a weaker accumulation after rapamycin treatment compared to other amino acids. This might indicate that breakdown of ketogenic amino acids contribute to pools for fatty acid synthesis.

Next to being a precursor for fatty acid synthesis, acetyl-CoA is also an intermediate of the TCA cycle. The observation that the cellular citrate level is slightly reduced during the light phase, may suggest that the flux of acetyl-CoA is shifted to fatty acid synthesis. This observation is in agreement with metabolite profiling analysis in yeast under nitrogen starvation which also showed a decrease of citrate [12]. However, beside the massive changes in the cellular TAG and FFA content, it was quite surprising that the cellular glycerol-3-phosphate content shows no significant changes over the entire cell cycle. It remains therefore to be determined if the flux through glycerol-3-phosphat is might be changed after TOR inhibition. Therefore, additional flux analysis

would be helpful for a better understanding of the data. In addition, the compartmentalization of metabolites is also an important factor in the regulation of metabolic pathways. In green microalgae such as *Chlamydomonas* the glycolytic pathway is highly compartmentalized. The "upper half" of the glycolysis (from glucose to glyceraldehyde-3-phospahte (G3P)) takes exclusively place in the chloroplast and the "lower half" (from 3PGA to pyruvate) being localized in the cytosol. G3P and 3PGA are present in the chloroplast and the cytosol and their concentration within these different compartments is mainly determined by the concentration of ATP and NAD(P)H in these compartments [193]. It would be therefore interesting to analyze the concentration of each metabolite in the different compartments of *Chlamydomonas* cells to determine changes in the compartmentalization of metabolites during the cell cycle and after TOR inhibition.

4.2.5 TOR inhibition affects membrane lipid composition

Studies published over the last few years have shown that TOR controls lipogenesis through the regulation of the transcription factor sterol regulatory element-binding protein1 (SREBP1) and the phosphatidic acid phosphatase LIPIN1 [83, 211, 212]. Beside the strong accumulation of TAG, the analysis of membrane lipids revealed that TOR inhibition in *Chlamydomonas* strongly affects the composition of membrane lipids on the level of saturation and fatty acid chain length. In addition, the desaturation of specific lipid species was delayed after TOR inhibition.

4.2.5.1 TOR inhibition in Chlamydomonas leads to a decrease in membrane lipids during the initial growth phase

The early increase of storage lipids was accompanied by a reduction of several membrane lipid species during the first 4 h after rapamycin treatment (Table 13). Within those MGDGs, DGTS and PEs display the strongest decrease. These results may indicate that during the initial growth phase a breakdown of membrane lipids, next to that proposed for TAGs with short chain fatty acids, fuels the rapid synthesis of TAGs by shuffling fatty acids from membrane lipids to TAGs. The remodeling of membrane lipids to TAGs under nitrogen starvation has been proposed in several publications [152, 207, 213]. Furthermore, it has been shown that a lipase-encoding gene (CrLIP1) is required for rapid TAG turnover in *Chlamydomonas* [214]. *In vitro*, the CrLIP1 protein has been shown to hydrolyze DAG and phospholipids but not TAG. In addition, we observed a strong increase of DAGs directly after rapamycin treatment, which reached a significant level 1 h after treatment (Supp. table 4). This result may support the idea of an increased breakdown of membrane lipids during the initial growth phase after TOR inhibition. As these observed responses occur very

fast after rapamycin treatment (within 1 h) we assume that TOR signaling pathway may directly regulate the activation of specific lipases.

4.2.5.2 TOR inhibition affects the desaturation of membrane lipids

After an initial decrease in their cellular content several lipid species, covering all lipid classes of the membrane lipids, show an increased accumulation during the late light phase (6 – 12 h) and the dark phase (Table 13). However, in case of DGTS, SQDG and PG this accumulation concerned only saturated and lowly unsaturated species, while highly unsaturated species are decreased, whereby the border between low and high unsaturated depends on the lipid class and the fatty acid chain length. Changes in the saturation level of membrane lipids often occur in response to environmental stresses, including temperature stress and may help to maintain membrane integrity [215]. Under heat stress the levels of saturated fatty acids does increase in both thylakoid membranes [216] and in the plasma membranes [217]. The desaturation of fatty acids has accordingly been discussed as an adjustment strategy to stabilize thylakoid membranes in order to avoid a reduction in photosynthetic efficiency [218, 219]. The obtained results from this data might therefore indicate that *Chlamydomonas* cells tend to stabilize their membranes after TOR inhibition. Furthermore the changes in the degree of saturation after rapamycin treatment might cause changes in the lipid fluidity and thereby lead to changes in the membrane permeability. How these changes in the saturation level are regulated in detail, if it is directly or indirectly regulated by TOR and what are the consequences for the membrane fluidity needs to be further investigated, possibly by applying brought scale proteomic and/or transcriptomic analysis on these synchronized cell cultures.

4.2.5.3 The desaturation of membrane lipids with shorter fatty acid chain length seems to be stronger affected by TOR inhibition

Interestingly, MGDGs and DGDGs show this accumulation of lowly unsaturated fatty acids and decrease of highly unsaturated fatty acids only for lipid species with 32 carbons. MDGDs and DGDGs with 34 and 36 carbons are increased at the end of the dark phase independent of the degree of unsaturation. In addition we found that the decrease of highly unsaturated fatty acids within the DGTS is more pronounced for those with 30 to 34 carbons. Analysis of the fatty acid composition in *Chlamydomonas* showed that C 16 and C 18 fatty acids are the dominant chain lengths [151]. Therefore, we assume that the lipid species with less than 36 carbons contain at least one C 16 fatty acid, while those with 36 and more carbons contain most likely no C 16 fatty acid. Early studies in higher plants revealed that according to the position of fatty acids glycerolipids can

be divided into two groups [220-222]. Glycerolipids with C 16 fatty acids at the sn2 position are called prokaryotic as this fatty acid pattern corresponds to that of cyanobacteria. The other group with the eukaryotic pattern is exclusively esterified with C 18 fatty acids at the sn2 position. While the eukaryotic pattern is characteristic for glycerolipids from extraplastidic membranes, the glycerolipids of plastidial membranes contain both types of fatty acid distribution. In *Chlamydomonas* it has been proposed that MGDG, DGDG and SQDG are exclusively synthesized by the chloroplast due to their prokaryotic pattern [151]. The annotation of MDGD, DGDG and SQGD with 36 carbons either indicates that they contain C 20 fatty acids at the sn1 position or they are of eukaryotic origin. Furthermore, it was assumed that DGTS are exclusively synthesized in the cytoplasm, while the same publication showed that 14% of the DGTS are prokaryotic [151]. This is consistent with our finding of DGTS with 30 and 32 carbons. The observation that the effect on the saturation level was more pronounced within lipid species containing less than 36 carbons, might therefore indicate that TOR inhibition affects the desaturation of C 16 fatty acids much stronger than that of the C 18 fatty acids. Furthermore, this might suggest that mainly glycerolipids of plastidic (prokaryotic) origin respond to TOR inhibition by a change in the saturation level. To answer these questions the determination of the positional distribution of fatty acids of the different lipid species would be needed, which unfortunately requires more sophisticated analysis.

4.2.5.4 TOR inhibition seems to result in an accumulation of membrane lipids with longer fatty acid chain length

Among the DGDGs and DGTS, those with 36 and 38 carbons in their two fatty acids show the strongest accumulation after rapamycin treatment. This might imply an accumulation of the longer chain fatty acid C 18 within these lipid classes and furthermore an increased ratio of C 16 to C 18 within the membranes. The observation of the strong accumulation of DGDG with 36 carbons, which are most likely of eukaryotic origin, can also lead to another assumption. In higher plants it has been shown that phosphate limitation leads to an accumulation of DGDG in extraplastidic membranes and thereby replaces a large proportion of phosphatidylcholine [223, 224]. Although it is argued that the phosphate-inducible pathway of DGDG may not exists in *Chlamydomonas* due to the presence of phosphate-free DGTS [225], our data indicate that a similar pathway may exist in *Chlamydomonas*. Concomitant to the strong increase of the eukaryotic DGDGs we also found that several phospholipids display a strong decrease after TOR inhibition (Table 13). In addition, it has been reported that phosphate homeostasis is altered due to TOR inhibition by rapamycin [226]. Furthermore, the simultaneous reduction of endogenous phosphorylated metabolites (Figure 38) may indicate that phosphate homeostasis is also affected by TOR inhibition in *Chlamydomonas*. To shed more light on the question if and how the concentration of the different lipid classes in relation to each other is changed after TOR inhibition, the absolute quantification of lipids of

isolated plasma membranes needs to be analyzed. Ideally these results are also compared to nutrient (nitrate, phosphate, sulfate) starvation experiments performed in the same experimental system.

4.2.5.5 Desaturation of specific membrane lipids is delayed after TOR inhibition

Finally, our lipidomic results also indicate that desaturation of fatty acids from DGTS and SQDG is not only reduced but also delayed after rapamycin treatment (Figure 45 C, D). In addition, saturated and low unsaturated MGDGs display also a strong delay (Figure 45 B). Interestingly, this delay was most pronounced in the second half of the light phase and might imply a correlation to the observed delay in mitosis. However, if and how this might be correlated with the cell cycle remains to be further investigated. A good candidate for the direct connection between lipid synthesis and TOR signaling is the sterol regulatory element-binding protein1 (SREBP1), which in mammalian systems has been shown to be a fundamental regulator of fatty acid desaturation [227-229]. Moreover, studies on mTORC1 revealed that SREBP activation is promoted by the mTORC1 signaling [230, 231], namely it seems that SREBP1 is stimulated by S6K1, which is a direct downstream target of from mTORC1 signaling [232]. Although a SREBP1 homologue in *Chlamydomonas* has not been identified so far it should be further investigated if the decrease in desaturation of membrane lipids might be regulated by TOR signaling through possible SREBP homologs in *Chlamydomonas*.

4.2.6 Regulation of nitrogen metabolism by TOR

Concomitant with the massive increase of carbon reserves, TOR inhibition in *Chlamydomonas* leads to a strong accumulation of nitrogen-containing compounds, including proteinogenic and non-proteinogenic amino acids, polyamines and purine and pyrimidine derivatives (Figure 38). In yeast it has been shown that among the genes that are affected when TOR signaling is inhibited by rapamycin, the most affected ones are the nitrogen-regulated genes [96]. Furthermore, it was found that the phosphorylation of the nitrogen-regulated kinase NPR1 is regulated by TOR [233]. Thus, downregulation of TOR has been suggested to mimic nitrogen starvation-like responses [234].

4.2.6.1 Amino acids of the nitrogen assimilation pathway are increased after TOR inhibition

Chlamydomonas can utilize a number of different nitrogen sources, both inorganic (nitrate, nitrite and ammonium) and organic (purines, urea and amino acids) [235-238]. As the assimilation of

nitrogen requires carbon, their metabolism must be intimately coordinated to sustain optimal growth. The CO_2 which is assimilated through photosynthesis will be converted through glycolysis and TCA cycle to 2-oxoglutarate, which serves as the carbon skeleton for nitrogen assimilation. Ammonium, either directly taken-up or produced by nitrate and nitrite reductase, is ultimately incorporated into carbon skeletons by the activity of two enzymes glutamine synthetase (GS) and glutamine-2-oxoglutarate aminotransferase (GOGAT) to generate glutamine and glutamate. The same enzymes are also responsible for the reassimilation of ammonium released in photorespiration.[239]. The nitrogen atoms of glutamine and glutamate are used to synthesize other amino acids. This includes aspartate and alanine which are synthesized through a direct transfer of the amino group from glutamate to oxaloacetate and pyruvate by aspartate and alanine amino transferase, respectively. In higher plants, asparagine and glutamine are the primary nitrogen-transport compounds. Nitrogen assimilated into glutamine is transferred to asparagine, catalyzed by asparagine synthetase [240]. These amino acids were found to show the strongest accumulation 15 min after rapamycin treatment (Figure 36) and remain increased during the progression of the cell cycle (Figure 38). These results might imply that TOR inhibition in *Chlamydomonas* leads to increased nitrogen assimilation possibly also due to increased photorespiration. However, the observation that almost all amino acids increase 15 min after rapamycin treatment, suggests that the increase of those amino acids is rather correlated with the previously described processes of TOR signaling such as translation and autophagy [79, 241] than, solely with an increased nitrogen assimilation. Indeed, it has been shown that under carbon starvation in maize root tips the nitrogen released by protein degradation was partly stored in asparagine. This was accompanied by a decrease of enzymes of nitrogen assimilation whereas the enzyme activity of asparagine synthetase was increased [242]. The observation that 2-oxoglutarate accumulates from 4 h onwards after rapamycin treatment, therefore might indicate a reduced flow through GS and GOGAT. In cyanobacteria it has been shown that the 2-oxoglutarate pool is intimately linked to nitrogen assimilation [243-245]. Therefore, measurements of activities of the enzymes involved in nitrogen assimilation and amino acid biosynthesis would be helpful to determine the source of the increase of those amino acids. In addition, it would be interesting to measure the intra- and extracellular ammonium and nitrogen levels to find out if the total nitrogen content of the cells is changed after rapamycin treatment and if nitrogen taken-up at higher rates or if it is released into the medium. Moreover, it is suggested that the expression of the asparagine synthethase gene is under metabolic control of the nitrogen to carbon ratio. Therefore, it would be interesting to determine the nitrogen to carbon ratio after TOR inhibition in *Chlamydomonas*.

4.2.6.2 Arginine and its intermediates accumulate as a result of TOR inhibition

Next to asparagine, arginine is a major storage form of nitrogen in plants, because it is with four nitrogen atoms the proteinogenic amino acid with the highest nitrogen content [246]. Arginine is synthesized from glutamate via the two non-proteinogenic amino acids ornithine and citrulline [247]. All these amino acids are strongly increased 15 min after rapamycin treatment and remain increased during the entire cell cycle (Figure 36; Figure 38). Given the available data, it cannot be assessed whether this accumulation results from an increased degradation or decreased translation of proteins or an increased biosynthesis of arginine. However, the observation that also the intermediates of arginine biosynthesis are increased after TOR inhibition might imply an increase in the biosynthesis of arginine. Phosphate deficiency in plants has been shown to increase *de novo* arginine biosynthesis which was accompanied by an accumulation of ammonia. The authors suggest that the increased activity of the arginine de novo biosynthetic pathway provides a mechanism for detoxifying leaf tissue of excess ammonia [248]. In addition, it has been shown that arginine and the arginine pathway intermediates accumulate in leaves during several nutrient deficiencies [249-252]. The rate limiting step in arginine biosynthesis is catalyzed by N-acetylglutamate kinase (NAGK), and its activity is feedback-inhibited by arginine [247]. In cyanobacteria and plants NAGK activity is regulated by the PII protein [253, 254]. The PII protein controls a wide range of processes related to nitrogen metabolism by coordinating the regulation of nitrogen assimilation in response to nitrogen, carbon and energy supply. In oxygenic phototrophs PII protein can form a complex with the NAGK enzyme and thereby enhancing the catalytic activity of NAGK and strongly reducing the feedback inhibition by arginine, which leads to increased arginine levels. When nitrogen is scarce PII protein dissociates from NAGK. The released NAGK is then highly sensitive to feedback inhibition by arginine [255]. In cyanobacteria, the dissociation of the PII-NAGK complex occurs upon binding of ADP to PII and 2-oxoglutarate-promoted PII phosphorylation [253, 256, 257]. It has been further shown that the complex formation between PII and NAGK is conserved in higher plants and in accordance with this PII controls arginine biosynthesis [254], while the detailed mechanism of the PII-NAGK interaction remains to be clarified. Only recently, the PII protein has been identified and characterized in *Chlamydomonas reinhardtii* [258]. Although structural analysis revealed that most of the residues in the PII protein, which are known to be important for the formation of the complex with NAGK, are conserved in *Chlamydomonas* it remains to be investigated if the complex formations also occurs in *Chlamydomonas*. The identification of the PII protein in *Chlamydomonas* may provide a possible candidate through which TOR could nitrogen metabolism and assimilation through the regulation of arginine biosynthesis.

4.2.6.3 Compounds deriving from arginine metabolism accumulate later during the cell cycle

To access the nitrogen stored in arginine, it must be hydrolyzed by mitochondrial arginase to regenerate ornithine and thereby release urea [259]. Urea can leave the mitochondrion and can then be hydrolyzed to release ammonium, which is reassimilated into glutamine and glutamate. In most organisms this reaction is catalyzed by urease. However, urease is not present in species of yeast [260] and green algae [261]. *Chlamydomonas* contains an adaptive enzyme activity the urea amidolyase, which consists of two enzyme activities, namely urea carboxylase and allophanate hydrolase [237]. While arginine, ornithine and citrulline show a rapid increase after TOR inhibition, the accumulation of urea is lagging behind them and occurred only from 6 h onwards (Figure 38). In addition, we found that the diamine putrescine, which can derive from both arginine and ornithine, displays the same timing of accumulation as urea, being continuously increased 6 h after rapamycin treatment (Figure 38). Comparison of the concentrations of all annotated metabolites showed that putrescine was the most abundant metabolite (Figure 36). This could be explained by the use of ammonium as nitrogen source in the medium as it has been shown that plants strongly accumulate putrescine when they are grown in ammonium instead of nitrate [262]. Putrescine can be further converted into the triamine spermidine by the addition of an aminopropyl group derived from decarboxylated S-adenosylmethionine [263]. With a delay of 2 h, spermidine was accumulated as well from 8 h onwards after rapamycin treatment. Due to the delayed accumulation of urea and polyamines, it can be suggested that this might only result from the significant increase of arginine and ornithine and a possible increase in the free ammonia level rather than being a direct result of the TOR inhibition.

In higher plants polyamines, especially putrescine, play important roles in the response to abiotic stress [264]. In most studies concerning polyamines and stress responses, these metabolites have not been associated with nitrogen metabolism. However, studies on osmotic shock showed that putrescine increase was strongly dependent on their metabolic precursor (arginine) availability [265]. In addition, Slocum and Weinstein have found that osmotic stress in oat leaf segments leads to a parallel increase of both putrescine and ammonium level. However, an inhibition of putrescine biosynthesis by DL-α- difluoromethylarginine (DFMA) under osmotic stress conditions leads to a reduced accumulation of putrescine and a stronger accumulation of ammonia. Due to these results they suggest that the stress-induced putrescine accumulation has at least a partial role in sequestering ammonia for ammonia detoxification [266]. The obtained results could therefore lead to the hypothesis that the observed increase in amino acids might be accompanied by an increase in the ammonia level and that the observed increase in arginine and polyamine metabolism occurred to reduce the level of free ammonia, resulting first in an increase of arginine and arginine intermediates and as a latter consequence an accumulation of polyamines. It would therefore be

interesting to see if inhibition of putrescine biosynthesis by DFMA in rapamycin treated cells would also lead to an increase of the ammonia level. However, it remains to be further investigated if the observed accumulation of arginine and polyamines is only the consequence of an increase in the ammonia level or if their accumulation is a direct effect of TOR inhibition.

In contrast to putrescine, spermidine was reduced from 30 min to 4 h after rapamycin treatment (Figure 38). Next to being important for the response to abiotic stress, polyamines are required for cell growth and cell division in eukaryotic and prokaryotic organisms [267, 268]. In *Chlamydomonas* it has been shown that a decrease in the spermidine level during the G1 phase by either addition of spermine or inhibition of spermidine synthase prevented cell division [269]. Therefore, the observed decrease of spermidine during the G1 phase might be a cause for the observed delay in mitosis and DC relaease. Furthermore, it has been shown that the spermin-induced cell cycle arrest was overcome by subsequent addition of spermidine [269]. It would be therefore interesting to test if the addition or spermidine to rapamycin treated cells would affect the delay in mitosis and DC release.

4.2.7 TOR inhibition leads to an increase of degradation products of the nucleotide metabolism

Our data shows that rapamycin treatment yields a massive increase of hypoxanthine, guanine and β-alanine (Figure 38). Guanine and hypoxanthine are degradation products of purine nucleotides, which can serve for the regeneration of plant nucleotide pools, while β-alanine is the degradation product of pyrimidine nucleotides [149]. Interestingly, hypoxanthine, which is a degradation product of AMP, is already significantly increased 30 min after the light was turned on, while guanine, which is derived from GMP, displays a significant increase only from 2 h in the light onwards. Beside the earlier increase of hypoxanthine this metabolite also shows a much stronger increase of up to 15-fold in comparison to guanine, which displays an up to 5-fold increase after rapamycin treatment. β-alanine, which is the degradation product of uracil, is already significantly increased 15 min after rapamycin treatment (Figure 36) and remains increased during the entire cell cycle.

The purine base adenine shows a significant increase only at the end of the light phase, which might imply that AMP is converted to IMP, which is then dephosphorylated to inosine and subsequently hydrolyzed to hypoxanthine. This may also explain the stronger increase of hypoxanthine in comparison to guanine. More surprisingly was the observation that the xanthine level was not dramatically changed after rapamycin treatment as the further degradation of both guanine and hypoxanthine converge on xanthine, which is the central metabolite in purine degradation [149]. This leads to two hypotheses; either nucleotide degradation runs on a normal

level, while the activity of the hypoxanthine-guanine phosphoribosyltransferase is strongly reduced or xanthine is very fast converted into the subsequent degradation products. In most plants the degradation of purines appears to perform special functions related to the storage and translocation of nitrogen. In contrast to animals, where the final product of purine degradation is uric acid, plants can further metabolize uric acid to finally produce NH_3, CO_2 and glyoxylate [149]. In addition, the degradation of uracil to β-alanine produces NH_3 and CO_2. Those end products may be reused in photosynthesis (CO_2) or reassimilated by the photorespiratory glycolate and glutamine oxoglutarate aminotransferase (GOGAT) pathway. It is therefore possible that TOR inhibition in *Chlamydomonas* leads to a strong degradation of purine and pyrimidine nucleotides to refill the nitrogen and carbon pools.

The source for the accumulation of nucleotide degradation products might come from degradation of RNAs. This assumption is supported by the observation that rapamycin treatment of transgenic Arabidopsis lines expressing yeast FKBP12 resulted in strong reduction in the total RNA content [270]. Whether this assumption is also valid in *Chlamydomonas* needs to be further investigated.

As *de novo* synthesis of nucleotides is very energy consuming the increase of guanine and hypoxanthine could also indicate an increase of the salvage pathway to provide sufficient nucleotides for the DNA synthesis and transcription. In Yeast, rapamycin treatment leads to a downregulation of transcripts of purine biosynthesis [271]. Furthermore, only recently it has been shown that mTOR regulates the *de novo* pyrimidine synthesis through S6K1 by posttranslational regulation of CAD (carbamoyl-phosphate synthetase2, aspartate transcarbamoylase, dihydroorotatase) [272]

From our thus far obtained results it is not possible to determine if the strong accumulation of guanine and hypoxanthine results from an increased degradation or an increased purine salvage. It is also possible that a combination of both leads to the obtained accumulation of guanine and hypoxanthine.

4.3 Conclusion and Outlook

In this study a high resolution kinetic metabolomic characterization of *Chlamydomonas* cell cultures during a fully cell cycle was performed. These analyses clearly showed that the transition of G1 to S phase was accompanied by attenuation in the accumulation rate of various primary metabolites and carbon reserves, which indicates a massive re-allocation of energy and nutrient resources. The obtained results therefore provide initial experimental evidence of the whole cell metabolism and therefore a good basis for further investigation on metabolomic, transcriptomic and proteomic dynamics during this transition point. In addition, metabolic flux analysis could be performed to identify biosynthetic precursors of DNA synthesis and other important biosynthetic processes (e.g. membrane lipid biosynthesis) which might be important for S phase entry.

In a second project, which represents an extension of the initial project, the synchronized Chlamydomonas cells were used to analyze the impact of TOR inhibition on cell cycle, proliferation and growth. The results from this study clearly show that TOR inhibition causes a severely reduced growth, leading to a reduction of newly produced DCs by 50%. A closer look into the size distribution data revealed that the correlation between cell size and produced DCs was clearly changed after TOR inhibition. In addition, we found that mitosis and DC release was delayed after TOR inhibition. However, while the reduction in cell number was accompanied by a reduction in DNA content, DNA synthesis was not delayed, which might imply that at least the transition of G1 to S phase was not affected by TOR inhibition. It is therefore likely that the observed delay in mitosis and DC release is rather a result of growth reduction caused by TOR inhibition than a direct result of TOR regulation. The present data therefore reveals that TOR is involved in the regulation of both, cell growth and proliferation in *Chlamydomonas*, while the impact of TOR on the cell cycle remains to be clarified.

Next to the direct cell cycle related results our data reveals that the obtained growth-phenotype was accompanied by strong accumulation of carbon (starch and TAGs) and nitrogen (arginine, glutamine and asparagine) reserves. Moreover, the most rapid changes that occur within 15 - 30 min after rapamycin treatment were an increase of proteinogenic and non-proteinogenic amino acids and a reduction of phosphate-containing compounds (PEP, G6P and F6P), membrane lipids and spermidine. Due to synchronization and the high resolution time series, the data provides next to quantitative changes additional information concerning the sequence of the obtained changes. Thereby, we found that TOR inhibition leads to a faster accumulation of TAGs (already 30 min after rapamycin treatment) than starch (6 h after rapamycin treatment) and moreover a stronger increase of TAGs in comparison to the increase of starch, which is contrary to results obtained under nutrient starvation. This could lead to the assumption that TOR has a more dominant or direct role in the regulation of TAG biosynthesis. These results therefore provide an excellent starting point for further investigations in the field of biotic resources, such as biofuels.

Furthermore, we observed that the accumulation of a major storage form of nitrogen, namely arginine, occurred already 15 min after TOR inhibition and was followed by an accumulation of urea and polyamines 6 h after rapamycin treatment, which might result from an overflow in the arginine pool due to increased free ammonia level.

Taken together, the present data reveals strong changes in carbon and nitrogen portioning in response to TOR inhibition. At the same time the present data clearly demonstrates the major benefit of using synchronized cell cultures. Based on the observed changes in the metabolism, which are mostly result from the regulation of enzymes on transcriptional, translational or even post-translational level, we will use the established system for further investigations including targeted but also untargeted transcriptomic and proteomic analysis. The so developed data matrices and their contained information will then be used for integrative analysis hopefully leading to the mechanistic understanding of the *Chlamydomonas* TOR signaling network.

References

1. Bisova K, Krylov DM, Umen JG: **Genome-wide annotation and expression profiling of cell cycle regulatory genes in Chlamydomonas reinhardtii**. *Plant physiology* (**2005**), 137(2): p. 475-491.
2. Slaninova M, Nagyova B, Galova E, Hendrychova J, Bisova K, Zachleder V, Vlcek D: **The alga Chlamydomonas reinhardtii UVS11 gene is responsible for cell division delay and temporal decrease in histone H1 kinase activity caused by UV irradiation**. *DNA Repair* (**2003**), 2(6): p. 737-750.
3. Su TT, O'Farrell PH: **Size control: cell proliferation does not equal growth**. *Current biology : CB* (**1998**), 8(19): p. R687-689.
4. Jorgensen P, Rupes I, Sharom JR, Schneper L, Broach JR, Tyers M: **A dynamic transcriptional network communicates growth potential to ribosome synthesis and critical cell size**. *Genes & development* (**2004**), 18(20): p. 2491-2505.
5. Shaul O, VanMontagu M, Inze D: **Cell cycle control in Arabidopsis**. *Ann Bot-London* (**1996**), 78(3): p. 283-288.
6. Johnson A, Skotheim JM: **Start and the restriction point**. *Curr Opin Cell Biol* (**2013**), 25(6): p. 717-723.
7. Ishidate T, Elewa A, Kim S, Mello CC, Shirayama M: **Divide and differentiate: CDK/Cyclins and the art of development**. *Cell Cycle* (**2014**), 13(9).
8. Bertoli C, Skotheim JM, de Bruin RA: **Control of cell cycle transcription during G1 and S phases**. *Nature reviews Molecular cell biology* (**2013**), 14(8): p. 518-528.
9. Arellano M, Moreno S: **Regulation of CDK/cyclin complexes during the cell cycle**. *The international journal of biochemistry & cell biology* (**1997**), 29(4): p. 559-573.
10. Pir P, Gutteridge A, Wu J, Rash B, Kell DB, Zhang N, Oliver SG: **The genetic control of growth rate: a systems biology study in yeast**. *Bmc Syst Biol* (**2012**), 6: p. 4.
11. Gutteridge A, Pir P, Castrillo JI, Charles PD, Lilley KS, Oliver SG: **Nutrient control of eukaryote cell growth: a systems biology study in yeast**. *BMC biology* (**2010**), 8: p. 68.
12. Castrillo JI, Zeef LA, Hoyle DC, Zhang N, Hayes A, Gardner DC, Cornell MJ, Petty J, Hakes L, Wardleworth L *et al*: **Growth control of the eukaryote cell: a systems biology study in yeast**. *Journal of biology* (**2007**), 6(2): p. 4.
13. van Uden N: **Yield and maintenance analysis in the chemostat; a tool for metabolic studies of growing cells**. *Arch Mikrobiol* (**1968**), 62(1): p. 34-40.
14. Hoskisson PA, Hobbs G: **Continuous culture--making a comeback?** *Microbiology* (**2005**), 151(Pt 10): p. 3153-3159.
15. Ferenci T: **A cultural divide on the use of chemostats**. *Microbiology* (**2006**), 152(Pt 5): p. 1247-1248.
16. Jandt U, Platas Barradas O, Portner R, Zeng AP: **Mammalian cell culture synchronization under physiological conditions and population dynamic simulation**. *Appl Microbiol Biotechnol* (**2014**), 98(10): p. 4311-4319.
17. Nurse P: **Systems biology: understanding cells**. *Nature* (**2003**), 424(6951): p. 883.
18. Merchant SS, Prochnik SE, Vallon O, Harris EH, Karpowicz SJ, Witman GB, Terry A, Salamov A, Fritz-Laylin LK, Marechal-Drouard L *et al*: **The Chlamydomonas genome reveals the evolution of key animal and plant functions**. *Science* (**2007**), 318(5848): p. 245-250.
19. Grossman AR, Harris EE, Hauser C, Lefebvre PA, Martinez D, Rokhsar D, Shrager J, Silflow CD, Stern D, Vallon O *et al*: **Chlamydomonas reinhardtii at the crossroads of genomics**. *Eukaryot Cell* (**2003**), 2(6): p. 1137-1150.
20. Gutman BL, Niyogi KK: **Chlamydomonas and Arabidopsis. A dynamic duo**. *Plant physiology* (**2004**), 135(2): p. 607-610.
21. Rochaix JD: **Chlamydomonas reinhardtii as the photosynthetic yeast**. *Annu Rev Genet* (**1995**), 29: p. 209-230.
22. Goodenough UW: **Green Yeast**. *Cell* (**1992**), 70(4): p. 533-538.

23. Vandepoele K, Raes J, De Veylder L, Rouze P, Rombauts S, Inze D: **Genome-wide analysis of core cell cycle genes in Arabidopsis**. *The Plant cell* (**2002**), 14(4): p. 903-916.
24. Joubes J, Chevalier C, Dudits D, Heberle-Bors E, Inze D, Umeda M, Renaudin JP: **CDK-related protein kinases in plants**. *Plant Mol Biol* (**2000**), 43(5-6): p. 607-620.
25. Mironov VV, De Veylder L, Van Montagu M, Inze D: **Cyclin-dependent kinases and cell division in plants- the nexus**. *The Plant cell* (**1999**), 11(4): p. 509-522.
26. Donnan L, Carvill EP, Gilliland TJ, John PCL: **The Cell-Cycles of Chlamydomonas and Chlorella**. *New Phytologist* (**1985**), 99(1): p. 1-40.
27. Coleman AW: **The Nuclear-Cell Cycle in Chlamydomonas (Chlorophyceae)**. *J Phycol* (**1982**), 18(2): p. 192-195.
28. Jones RF: **Physiological and Biochemical Aspects of Growth and Gametogenesis in Chlamydomonas-Reinhardtii**. *Annals of the New York Academy of Sciences* (**1970**), 175(2): p. 648-&.
29. Craigie RA, Cavalier-Smith T: **Cell-Volume and the Control of the Chlamydomonas Cell-Cycle**. *Journal of cell science* (**1982**), 54(Apr): p. 173-191.
30. Schlösser U: **Enzymatisch Gesteuerte Freisetzung Von Zoosporen Bei Chlamydomonas Reinhardii Dangeard in Synchronkultur**. *Arch Mikrobiol* (**1966**), 54(2): p. 129-159.
31. Kubo T, Kaida S, Abe J, Saito T, Fukuzawa H, Matsuda Y: **The Chlamydomonas hatching enzyme, sporangin, is expressed in specific phases of the cell cycle and is localized to the flagella of daughter cells within the sporangial cell wall**. *Plant & cell physiology* (**2009**), 50(3): p. 572-583.
32. Spudich JL, Sager R: **Regulation of the Chlamydomonas cell cycle by light and dark**. *The Journal of cell biology* (**1980**), 85(1): p. 136-145.
33. Zachleder V, Vandenende H: **Cell-Cycle Events in the Green-Alga Chlamydomonas-Eugametos and Their Control by Environmental-Factors**. *Journal of cell science* (**1992**), 102: p. 469-474.
34. Donnan L, John PCL: **Cell-Cycle Control by Timer and Sizer in Chlamydomonas**. *Nature* (**1983**), 304(5927): p. 630-633.
35. Bernstein E: **Synchronous division in Chlamydomonas moewusii**. *Science* (**1960**), 131(3412): p. 1528-1529.
36. Lien T, Knutsen G: **Synchronous Growth of Chlamydomonas-Reinhardtii (Chlorophyceae) - Review of Optimal Conditions**. *J Phycol* (**1979**), 15(2): p. 191-200.
37. Harris EH: ***Chlamydomonas* in the Laboratory**. In: *The Chlamydomonas Sourcebook.* Edited by Harris EH, vol. 1, Second edn: Elsevier (**2009**).
38. Oldenhof H, Zachleder V, Van den Ende H: **The cell cycle of Chlamydomonas reinhardtii: the role of the commitment point**. *Folia microbiologica* (**2007**), 52(1): p. 53-60.
39. Sehgal SN, Baker H, Vezina C: **Rapamycin (AY-22,989), a new antifungal antibiotic. II. Fermentation, isolation and characterization**. *The Journal of antibiotics* (**1975**), 28(10): p. 727-732.
40. Vezina C, Kudelski A, Sehgal SN: **Rapamycin (AY-22,989), a new antifungal antibiotic. I. Taxonomy of the producing streptomycete and isolation of the active principle**. *The Journal of antibiotics* (**1975**), 28(10): p. 721-726.
41. Martel RR, Klicius J, Galet S: **Inhibition of the immune response by rapamycin, a new antifungal antibiotic**. *Canadian journal of physiology and pharmacology* (**1977**), 55(1): p. 48-51.
42. Houchens DP, Ovejera AA, Riblet SM, Slagel DE: **Human brain tumor xenografts in nude mice as a chemotherapy model**. *European journal of cancer & clinical oncology* (**1983**), 19(6): p. 799-805.
43. Heitman J, Movva NR, Hall MN: **Targets for Cell-Cycle Arrest by the Immunosuppressant Rapamycin in Yeast**. *Science* (**1991**), 253(5022): p. 905-909.
44. Wullschleger S, Loewith R, Hall MN: **TOR signaling in growth and metabolism**. *Cell* (**2006**), 124(3): p. 471-484.

45. Crespo JL, Hall MN: **Elucidating TOR signaling and rapamycin action: lessons from Saccharomyces cerevisiae**. *Microbiology and molecular biology reviews : MMBR* (**2002**), 66(4): p. 579-591, table of contents.
46. Crespo JL, Diaz-Troya S, Florencio FJ: **Inhibition of target of rapamycin signaling by rapamycin in the unicellular green alga Chlamydomonas reinhardtii**. *Plant physiology* (**2005**), 139(4): p. 1736-1749.
47. Laplante M, Sabatini DM: **mTOR signaling in growth control and disease**. *Cell* (**2012**), 149(2): p. 274-293.
48. Hall MN: **The TOR signalling pathway and growth control in yeast**. *Biochem Soc Trans* (**1996**), 24(1): p. 234-239.
49. Loewith R, Hall MN: **Target of rapamycin (TOR) in nutrient signaling and growth control**. *Genetics* (**2011**), 189(4): p. 1177-1201.
50. Perry J, Kleckner N: **The ATRs, ATMs, and TORs are giant HEAT repeat proteins**. *Cell* (**2003**), 112(2): p. 151-155.
51. Dames SA, Mulet JM, Rathgeb-Szabo K, Hall MN, Grzesiek S: **The solution structure of the FATC domain of the protein kinase target of rapamycin suggests a role for redox-dependent structural and cellular stability**. *The Journal of biological chemistry* (**2005**), 280(21): p. 20558-20564.
52. Bosotti R, Isacchi A, Sonnhammer EL: **FAT: a novel domain in PIK-related kinases**. *Trends Biochem Sci* (**2000**), 25(5): p. 225-227.
53. Alarcon CM, Heitman J, Cardenas ME: **Protein kinase activity and identification of a toxic effector domain of the target of rapamycin TOR proteins in yeast**. *Mol Biol Cell* (**1999**), 10(8): p. 2531-2546.
54. Benjamin D, Colombi M, Moroni C, Hall MN: **Rapamycin passes the torch: a new generation of mTOR inhibitors**. *Nature reviews Drug discovery* (**2011**), 10(11): p. 868-880.
55. Wedaman KP, Reinke A, Anderson S, Yates J, 3rd, McCaffery JM, Powers T: **Tor kinases are in distinct membrane-associated protein complexes in Saccharomyces cerevisiae**. *Mol Biol Cell* (**2003**), 14(3): p. 1204-1220.
56. Reinke A, Anderson S, McCaffery JM, Yates J, 3rd, Aronova S, Chu S, Fairclough S, Iverson C, Wedaman KP, Powers T: **TOR complex 1 includes a novel component, Tco89p (YPL180w), and cooperates with Ssd1p to maintain cellular integrity in Saccharomyces cerevisiae**. *The Journal of biological chemistry* (**2004**), 279(15): p. 14752-14762.
57. Loewith R, Jacinto E, Wullschleger S, Lorberg A, Crespo JL, Bonenfant D, Oppliger W, Jenoe P, Hall MN: **Two TOR complexes, only one of which is rapamycin sensitive, have distinct roles in cell growth control**. *Mol Cell* (**2002**), 10(3): p. 457-468.
58. Kim DH, Sarbassov DD, Ali SM, Latek RR, Guntur KV, Erdjument-Bromage H, Tempst P, Sabatini DM: **GbetaL, a positive regulator of the rapamycin-sensitive pathway required for the nutrient-sensitive interaction between raptor and mTOR**. *Mol Cell* (**2003**), 11(4): p. 895-904.
59. Jacinto E, Loewith R, Schmidt A, Lin S, Ruegg MA, Hall A, Hall MN: **Mammalian TOR complex 2 controls the actin cytoskeleton and is rapamycin insensitive**. *Nature cell biology* (**2004**), 6(11): p. 1122-1128.
60. Peterson TR, Laplante M, Thoreen CC, Sancak Y, Kang SA, Kuehl WM, Gray NS, Sabatini DM: **DEPTOR is an mTOR inhibitor frequently overexpressed in multiple myeloma cells and required for their survival**. *Cell* (**2009**), 137(5): p. 873-886.
61. Kaizuka T, Hara T, Oshiro N, Kikkawa U, Yonezawa K, Takehana K, Iemura S, Natsume T, Mizushima N: **Tti1 and Tel2 are critical factors in mammalian target of rapamycin complex assembly**. *The Journal of biological chemistry* (**2010**), 285(26): p. 20109-20116.
62. Kim DH, Sarbassov DD, Ali SM, King JE, Latek RR, Erdjument-Bromage H, Tempst P, Sabatini DM: **mTOR interacts with raptor to form a nutrient-sensitive complex that signals to the cell growth machinery**. *Cell* (**2002**), 110(2): p. 163-175.
63. Hara K, Maruki Y, Long X, Yoshino K, Oshiro N, Hidayat S, Tokunaga C, Avruch J, Yonezawa K: **Raptor, a binding partner of target of rapamycin (TOR), mediates TOR action**. *Cell* (**2002**), 110(2): p. 177-189.

64. Wang L, Harris TE, Roth RA, Lawrence JC, Jr.: **PRAS40 regulates mTORC1 kinase activity by functioning as a direct inhibitor of substrate binding**. *The Journal of biological chemistry* (**2007**), 282(27): p. 20036-20044.
65. Vander Haar E, Lee SI, Bandhakavi S, Griffin TJ, Kim DH: **Insulin signalling to mTOR mediated by the Akt/PKB substrate PRAS40**. *Nature cell biology* (**2007**), 9(3): p. 316-323.
66. Thedieck K, Polak P, Kim ML, Molle KD, Cohen A, Jeno P, Arrieumerlou C, Hall MN: **PRAS40 and PRR5-like protein are new mTOR interactors that regulate apoptosis**. *PloS one* (**2007**), 2(11): p. e1217.
67. Sancak Y, Thoreen CC, Peterson TR, Lindquist RA, Kang SA, Spooner E, Carr SA, Sabatini DM: **PRAS40 is an insulin-regulated inhibitor of the mTORC1 protein kinase**. *Mol Cell* (**2007**), 25(6): p. 903-915.
68. Sarbassov DD, Ali SM, Kim DH, Guertin DA, Latek RR, Erdjument-Bromage H, Tempst P, Sabatini DM: **Rictor, a novel binding partner of mTOR, defines a rapamycin-insensitive and raptor-independent pathway that regulates the cytoskeleton**. *Current biology : CB* (**2004**), 14(14): p. 1296-1302.
69. Frias MA, Thoreen CC, Jaffe JD, Schroder W, Sculley T, Carr SA, Sabatini DM: **mSin1 is necessary for Akt/PKB phosphorylation, and its isoforms define three distinct mTORC2s**. *Current biology : CB* (**2006**), 16(18): p. 1865-1870.
70. Jacinto E, Facchinetti V, Liu D, Soto N, Wei S, Jung SY, Huang Q, Qin J, Su B: **SIN1/MIP1 maintains rictor-mTOR complex integrity and regulates Akt phosphorylation and substrate specificity**. *Cell* (**2006**), 127(1): p. 125-137.
71. Pearce LR, Huang X, Boudeau J, Pawlowski R, Wullschleger S, Deak M, Ibrahim AF, Gourlay R, Magnuson MA, Alessi DR: **Identification of Protor as a novel Rictor-binding component of mTOR complex-2**. *Biochem J* (**2007**), 405(3): p. 513-522.
72. Pearce LR, Sommer EM, Sakamoto K, Wullschleger S, Alessi DR: **Protor-1 is required for efficient mTORC2-mediated activation of SGK1 in the kidney**. *Biochem J* (**2011**), 436(1): p. 169-179.
73. Kunz J, Henriquez R, Schneider U, Deuter-Reinhard M, Movva NR, Hall MN: **Target of rapamycin in yeast, TOR2, is an essential phosphatidylinositol kinase homolog required for G1 progression**. *Cell* (**1993**), 73(3): p. 585-596.
74. Helliwell SB, Wagner P, Kunz J, Deuter-Reinhard M, Henriquez R, Hall MN: **TOR1 and TOR2 are structurally and functionally similar but not identical phosphatidylinositol kinase homologues in yeast**. *Mol Biol Cell* (**1994**), 5(1): p. 105-118.
75. Brown EJ, Albers MW, Shin TB, Ichikawa K, Keith CT, Lane WS, Schreiber SL: **A mammalian protein targeted by G1-arresting rapamycin-receptor complex**. *Nature* (**1994**), 369(6483): p. 756-758.
76. Sabatini DM, Erdjument-Bromage H, Lui M, Tempst P, Snyder SH: **RAFT1: a mammalian protein that binds to FKBP12 in a rapamycin-dependent fashion and is homologous to yeast TORs**. *Cell* (**1994**), 78(1): p. 35-43.
77. Barbet NC, Schneider U, Helliwell SB, Stansfield I, Tuite MF, Hall MN: **TOR controls translation initiation and early G1 progression in yeast**. *Mol Biol Cell* (**1996**), 7(1): p. 25-42.
78. Jastrzebski K, Hannan KM, Tchoubrieva EB, Hannan RD, Pearson RB: **Coordinate regulation of ribosome biogenesis and function by the ribosomal protein S6 kinase, a key mediator of mTOR function**. *Growth factors* (**2007**), 25(4): p. 209-226.
79. Ma XM, Blenis J: **Molecular mechanisms of mTOR-mediated translational control**. *Nature reviews Molecular cell biology* (**2009**), 10(5): p. 307-318.
80. Mayer C, Zhao J, Yuan X, Grummt I: **mTOR-dependent activation of the transcription factor TIF-IA links rRNA synthesis to nutrient availability**. *Genes & development* (**2004**), 18(4): p. 423-434.
81. Kantidakis T, Ramsbottom BA, Birch JL, Dowding SN, White RJ: **mTOR associates with TFIIIC, is found at tRNA and 5S rRNA genes, and targets their repressor Maf1**. *Proceedings of the National Academy of Sciences of the United States of America* (**2010**), 107(26): p. 11823-11828.

82. Laplante M, Sabatini DM: **An emerging role of mTOR in lipid biosynthesis**. *Current biology : CB* (**2009**), 19(22): p. R1046-1052.
83. Peterson TR, Sengupta SS, Harris TE, Carmack AE, Kang SA, Balderas E, Guertin DA, Madden KL, Carpenter AE, Finck BN *et al*: **mTOR complex 1 regulates lipin 1 localization to control the SREBP pathway**. *Cell* (**2011**), 146(3): p. 408-420.
84. Wang BT, Ducker GS, Barczak AJ, Barbeau R, Erle DJ, Shokat KM: **The mammalian target of rapamycin regulates cholesterol biosynthetic gene expression and exhibits a rapamycin-resistant transcriptional profile**. *Proceedings of the National Academy of Sciences of the United States of America* (**2011**), 108(37): p. 15201-15206.
85. Duvel K, Yecies JL, Menon S, Raman P, Lipovsky AI, Souza AL, Triantafellow E, Ma Q, Gorski R, Cleaver S *et al*: **Activation of a metabolic gene regulatory network downstream of mTOR complex 1**. *Mol Cell* (**2010**), 39(2): p. 171-183.
86. Robitaille AM, Christen S, Shimobayashi M, Cornu M, Fava LL, Moes S, Prescianotto-Baschong C, Sauer U, Jenoe P, Hall MN: **Quantitative phosphoproteomics reveal mTORC1 activates de novo pyrimidine synthesis**. *Science* (**2013**), 339(6125): p. 1320-1323.
87. Ben-Sahra I, Howell JJ, Asara JM, Manning BD: **Stimulation of de novo pyrimidine synthesis by growth signaling through mTOR and S6K1**. *Science* (**2013**), 339(6125): p. 1323-1328.
88. Semenza GL, Roth PH, Fang HM, Wang GL: **Transcriptional regulation of genes encoding glycolytic enzymes by hypoxia-inducible factor 1**. *The Journal of biological chemistry* (**1994**), 269(38): p. 23757-23763.
89. Laughner E, Taghavi P, Chiles K, Mahon PC, Semenza GL: **HER2 (neu) signaling increases the rate of hypoxia-inducible factor 1alpha (HIF-1alpha) synthesis: novel mechanism for HIF-1-mediated vascular endothelial growth factor expression**. *Mol Cell Biol* (**2001**), 21(12): p. 3995-4004.
90. Hudson CC, Liu M, Chiang GG, Otterness DM, Loomis DC, Kaper F, Giaccia AJ, Abraham RT: **Regulation of hypoxia-inducible factor 1alpha expression and function by the mammalian target of rapamycin**. *Mol Cell Biol* (**2002**), 22(20): p. 7004-7014.
91. Jung CH, Ro SH, Cao J, Otto NM, Kim DH: **mTOR regulation of autophagy**. *FEBS letters* (**2010**), 584(7): p. 1287-1295.
92. Hosokawa N, Hara T, Kaizuka T, Kishi C, Takamura A, Miura Y, Iemura S, Natsume T, Takehana K, Yamada N *et al*: **Nutrient-dependent mTORC1 association with the ULK1-Atg13-FIP200 complex required for autophagy**. *Mol Biol Cell* (**2009**), 20(7): p. 1981-1991.
93. Ganley IG, Lam du H, Wang J, Ding X, Chen S, Jiang X: **ULK1.ATG13.FIP200 complex mediates mTOR signaling and is essential for autophagy**. *The Journal of biological chemistry* (**2009**), 284(18): p. 12297-12305.
94. Jewell JL, Russell RC, Guan KL: **Amino acid signalling upstream of mTOR**. *Nature reviews Molecular cell biology* (**2013**), 14(3): p. 133-139.
95. Gasch AP, Werner-Washburne M: **The genomics of yeast responses to environmental stress and starvation**. *Functional & integrative genomics* (**2002**), 2(4-5): p. 181-192.
96. Cardenas ME, Cutler NS, Lorenz MC, Di Como CJ, Heitman J: **The TOR signaling cascade regulates gene expression in response to nutrients**. *Genes & development* (**1999**), 13(24): p. 3271-3279.
97. Urban J, Soulard A, Huber A, Lippman S, Mukhopadhyay D, Deloche O, Wanke V, Anrather D, Ammerer G, Riezman H *et al*: **Sch9 is a major target of TORC1 in Saccharomyces cerevisiae**. *Mol Cell* (**2007**), 26(5): p. 663-674.
98. Binda M, Peli-Gulli MP, Bonfils G, Panchaud N, Urban J, Sturgill TW, Loewith R, De Virgilio C: **The Vam6 GEF controls TORC1 by activating the EGO complex**. *Mol Cell* (**2009**), 35(5): p. 563-573.
99. Zhang Y, Gao X, Saucedo LJ, Ru B, Edgar BA, Pan D: **Rheb is a direct target of the tuberous sclerosis tumour suppressor proteins**. *Nature cell biology* (**2003**), 5(6): p. 578-581.
100. Inoki K, Li Y, Xu T, Guan KL: **Rheb GTPase is a direct target of TSC2 GAP activity and regulates mTOR signaling**. *Genes & development* (**2003**), 17(15): p. 1829-1834.

101. Gwinn DM, Shackelford DB, Egan DF, Mihaylova MM, Mery A, Vasquez DS, Turk BE, Shaw RJ: **AMPK phosphorylation of raptor mediates a metabolic checkpoint**. *Mol Cell* (**2008**), 30(2): p. 214-226.
102. Sancak Y, Peterson TR, Shaul YD, Lindquist RA, Thoreen CC, Bar-Peled L, Sabatini DM: **The Rag GTPases bind raptor and mediate amino acid signaling to mTORC1**. *Science* (**2008**), 320(5882): p. 1496-1501.
103. Sancak Y, Bar-Peled L, Zoncu R, Markhard AL, Nada S, Sabatini DM: **Ragulator-Rag complex targets mTORC1 to the lysosomal surface and is necessary for its activation by amino acids**. *Cell* (**2010**), 141(2): p. 290-303.
104. Menand B, Desnos T, Nussaume L, Berger F, Bouchez D, Meyer C, Robaglia C: **Expression and disruption of the Arabidopsis TOR (target of rapamycin) gene**. *Proceedings of the National Academy of Sciences of the United States of America* (**2002**), 99(9): p. 6422-6427.
105. Diaz-Troya S, Florencio FJ, Crespo JL: **Target of rapamycin and LST8 proteins associate with membranes from the endoplasmic reticulum in the unicellular green alga Chlamydomonas reinhardtii**. *Eukaryot Cell* (**2008**), 7(2): p. 212-222.
106. Mahfouz MM, Kim S, Delauney AJ, Verma DP: **Arabidopsis TARGET OF RAPAMYCIN interacts with RAPTOR, which regulates the activity of S6 kinase in response to osmotic stress signals**. *The Plant cell* (**2006**), 18(2): p. 477-490.
107. Ren M, Qiu S, Venglat P, Xiang D, Feng L, Selvaraj G, Datla R: **Target of rapamycin regulates development and ribosomal RNA expression through kinase domain in Arabidopsis**. *Plant physiology* (**2011**), 155(3): p. 1367-1382.
108. Xiong Y, Sheen J: **Rapamycin and glucose-target of rapamycin (TOR) protein signaling in plants**. *The Journal of biological chemistry* (**2012**), 287(4): p. 2836-2842.
109. Koltin Y, Faucette L, Bergsma DJ, Levy MA, Cafferkey R, Koser PL, Johnson RK, Livi GP: **Rapamycin sensitivity in Saccharomyces cerevisiae is mediated by a peptidyl-prolyl cis-trans isomerase related to human FK506-binding protein**. *Mol Cell Biol* (**1991**), 11(3): p. 1718-1723.
110. Diaz-Troya S, Perez-Perez ME, Perez-Martin M, Moes S, Jeno P, Florencio FJ, Crespo JL: **Inhibition of protein synthesis by TOR inactivation revealed a conserved regulatory mechanism of the BiP chaperone in Chlamydomonas**. *Plant physiology* (**2011**), 157(2): p. 730-741.
111. Perez-Perez ME, Florencio FJ, Crespo JL: **Inhibition of target of rapamycin signaling and stress activate autophagy in Chlamydomonas reinhardtii**. *Plant physiology* (**2010**), 152(4): p. 1874-1888.
112. Perez-Perez ME, Crespo JL: **Autophagy in the model alga Chlamydomonas reinhardtii**. *Autophagy* (**2010**), 6(4): p. 562-563.
113. Lee do Y, Fiehn O: **Metabolomic response of chlamydomonas reinhardtii to the inhibition of target of rapamycin (TOR) by rapamycin**. *Journal of microbiology and biotechnology* (**2013**), 23(7): p. 923-931.
114. Caldana C, Li Y, Leisse A, Zhang Y, Bartholomaeus L, Fernie AR, Willmitzer L, Giavalisco P: **Systemic analysis of inducible target of rapamycin mutants reveal a general metabolic switch controlling growth in Arabidopsis thaliana**. *Plant Journal* (**2013**), 73(6): p. 897-909.
115. Castrillo JI, Oliver SG: **Yeast systems biology: the challenge of eukaryotic complexity**. *Methods in molecular biology* (**2011**), 759: p. 3-28.
116. Sheth BP, Thaker VS: **Plant systems biology: insights, advances and challenges**. *Planta* (**2014**).
117. Gygi SP, Rochon Y, Franza BR, Aebersold R: **Correlation between protein and mRNA abundance in yeast**. *Mol Cell Biol* (**1999**), 19(3): p. 1720-1730.
118. Ideker T, Galitski T, Hood L: **A new approach to decoding life: systems biology**. *Annual review of genomics and human genetics* (**2001**), 2: p. 343-372.
119. Shinozaki K, Sakakibara H: **Omics and bioinformatics: an essential toolbox for systems analyses of plant functions beyond 2010**. *Plant & cell physiology* (**2009**), 50(7): p. 1177-1180.

120. Joyce AR, Palsson BO: **The model organism as a system: integrating 'omics' data sets**. *Nature reviews Molecular cell biology* (**2006**), 7(3): p. 198-210.
121. Sueoka N: **Mitotic Replication of Deoxyribonucleic Acid in Chlamydomonas Reinhardi**. *Proceedings of the National Academy of Sciences of the United States of America* (**1960**), 46(1): p. 83-91.
122. Gorman DS, Levine RP: **Cytochrome f and plastocyanin: their sequence in the photosynthetic electron transport chain of Chlamydomonas reinhardi**. *Proceedings of the National Academy of Sciences of the United States of America* (**1965**), 54(6): p. 1665-1669.
123. Hutner SH: **Anaerobic and aerobic growth of purple bacteria (Athiorhodaceae) in chemically defined media**. *Journal of general microbiology* (**1950**), 4(3): p. 286-293.
124. Schneider CA, Rasband WS, Eliceiri KW: **NIH Image to ImageJ: 25 years of image analysis**. *Nature methods* (**2012**), 9(7): p. 671-675.
125. Hummel J, Segu S, Li Y, Irgang S, Jueppner J, Giavalisco P: **Ultra performance liquid chromatography and high resolution mass spectrometry for the analysis of plant lipids**. *Frontiers in plant science* (**2011**), 2: p. 54.
126. Saeed AI, Sharov V, White J, Li J, Liang W, Bhagabati N, Braisted J, Klapa M, Currier T, Thiagarajan M *et al*: **TM4: A free, open-source system for microarray data management and analysis**. *Biotechniques* (**2003**), 34(2): p. 374-+.
127. Doyle J, Doyle JL: **A rapid DNA isolation procedure for small quantities of fresh leaf tissue**. *Phytochemical Bulletin* (**1987**), 19: p. 11-15.
128. Umen JG, Goodenough UW: **Control of cell division by a retinoblastoma protein homolog in Chlamydomonas**. *Genes & development* (**2001**), 15(13): p. 1652-1661.
129. Lisec J, Schauer N, Kopka J, Willmitzer L, Fernie AR: **Gas chromatography mass spectrometry-based metabolite profiling in plants**. *Nature protocols* (**2006**), 1(1): p. 387-396.
130. Krall L, Huege J, Catchpole G, Steinhauser D, Willmitzer L: **Assessment of sampling strategies for gas chromatography-mass spectrometry (GC-MS) based metabolomics of cyanobacteria**. *Journal of chromatography B, Analytical technologies in the biomedical and life sciences* (**2009**), 877(27): p. 2952-2960.
131. Giavalisco P, Li Y, Matthes A, Eckhardt A, Hubberten HM, Hesse H, Segu S, Hummel J, Kohl K, Willmitzer L: **Elemental formula annotation of polar and lipophilic metabolites using (13) C, (15) N and (34) S isotope labelling, in combination with high-resolution mass spectrometry**. *The Plant journal : for cell and molecular biology* (**2011**), 68(2): p. 364-376.
132. Bar-Nun S, Ohad I: **[34] Chloroplast membrane polypeptides**. In: *Methods in enzymology*. Edited by Anthony San P, vol. Volume 69: Academic Press; (**1980**): p. 363-374.
133. Smith AM, Zeeman SC: **Quantification of starch in plant tissues**. *Nature protocols* (**2006**), 1(3): p. 1342-1345.
134. Bradford MM: **A rapid and sensitive method for the quantitation of microgram quantities of protein utilizing the principle of protein-dye binding**. *Analytical biochemistry* (**1976**), 72: p. 248-254.
135. Allwood JW, Erban A, de Koning S, Dunn WB, Luedemann A, Lommen A, Kay L, Loscher R, Kopka J, Goodacre R: **Inter-laboratory reproducibility of fast gas chromatography-electron impact-time of flight mass spectrometry (GC-EI-TOF/MS) based plant metabolomics**. *Metabolomics : Official journal of the Metabolomic Society* (**2009**), 5(4): p. 479-496.
136. Huege J, Krall L, Steinhauser MC, Giavalisco P, Rippka R, Tandeau de Marsac N, Steinhauser D: **Sample amount alternatives for data adjustment in comparative cyanobacterial metabolomics**. *Analytical and bioanalytical chemistry* (**2011**), 399(10): p. 3503-3517.
137. Pearson K: **On lines and planes of closest fit to systems of points in space.** *Philos Mag* (**1901**), 2(7-12): p. 559-572.

138. Raychaudhuri S, Stuart JM, Altman RB: **Principal components analysis to summarize microarray experiments: application to sporulation time series**. *Pacific Symposium on Biocomputing Pacific Symposium on Biocomputing* (**2000**): p. 455-466.
139. Eisen MB, Spellman PT, Brown PO, Botstein D: **Cluster analysis and display of genome-wide expression patterns**. *Proceedings of the National Academy of Sciences of the United States of America* (**1998**), 95(25): p. 14863-14868.
140. Il'ichev YV, Alquier L, Maryanoff CA: **Degradation of rapamycin and its ring-opened isomer: role of base catalysis**. *Arkivoc* (**2007**): p. 110-131.
141. Chiang KS, Sueoka N: **Replication of Chloroplast DNA in Chlamydomonas Reinhardi during Vegetative Cell Cycle - Its Mode and Regulation**. *Proceedings of the National Academy of Sciences of the United States of America* (**1967**), 57(5): p. 1506-1513.
142. Bourguignon LYW, Palade GE: **Incorporation of Polypeptides into Thylakoid Membranes of Chlamydomonas-Reinhardtii - Cyclic Variations**. *Journal of Cell Biology* (**1976**), 69(2): p. 327-344.
143. Porra RJ, Thompson WA, Kriedemann PE: **Determination of Accurate Extinction Coefficients and Simultaneous-Equations for Assaying Chlorophyll-a and Chlorophyll-B Extracted with 4 Different Solvents - Verification of the Concentration of Chlorophyll Standards by Atomic-Absorption Spectroscopy**. *Biochimica et biophysica acta* (**1989**), 975(3): p. 384-394.
144. Klein U: **Intracellular Carbon Partitioning in Chlamydomonas-Reinhardtii**. *Plant physiology* (**1987**), 85(4): p. 892-897.
145. Thyssen C, Schlichting R, Giersch C: **The CO2-concentrating mechanism in the physiological context: lowering the CO2 supply diminishes culture growth and economises starch utilisation in Chlamydomonas reinhardtii**. *Planta* (**2001**), 213(4): p. 629-639.
146. Smith AM, Stitt M: **Coordination of carbon supply and plant growth**. *Plant Cell and Environment* (**2007**), 30(9): p. 1126-1149.
147. Tiburcio AF, Campos JL, Figueras X, Besford RT: **Recent Advances in the Understanding of Polyamine Functions during Plant Development**. *Plant Growth Regul* (**1993**), 12(3): p. 331-340.
148. Walker MA, Roberts DR, Shih CY, Dumbroff EB: **A requirement for polyamines during the cell division phase of radicle emergence in seeds of *Acer saccharum***. *Plant & cell physiology* (**1985**), 26: p. 967-972.
149. Zrenner R, Stitt M, Sonnewald U, Boldt R: **Pyrimidine and purine biosynthesis and degradation in plants**. *Annu Rev Plant Biol* (**2006**), 57: p. 805-836.
150. Tucci P, Porta G, Agostini M, Antonov A, Garabadgiu AV, Melino G, Willis AE: **Rapamycin regulates biochemical metabolites**. *Cell Cycle* (**2013**), 12(15): p. 2454-2467.
151. Giroud C, Gerber A, Eichenberger W: **Lipids of Chlamydomonas-Reinhardtii - Analysis of Molecular-Species and Intracellular Site(S) of Biosynthesis**. *Plant and Cell Physiology* (**1988**), 29(4): p. 587-595.
152. Li X, Moellering ER, Liu B, Johnny C, Fedewa M, Sears BB, Kuo MH, Benning C: **A galactoglycerolipid lipase is required for triacylglycerol accumulation and survival following nitrogen deprivation in Chlamydomonas reinhardtii**. *The Plant cell* (**2012**), 24(11): p. 4670-4686.
153. Xiong Y, McCormack M, Li L, Hall Q, Xiang C, Sheen J: **Glucose-TOR signalling reprograms the transcriptome and activates meristems**. *Nature* (**2013**), 496(7444): p. 181-186.
154. Sablowski R, Carnier Dornelas M: **Interplay between cell growth and cell cycle in plants**. *J Exp Bot* (**2013**).
155. Umen JG: **The elusive sizer**. *Curr Opin Cell Biol* (**2005**), 17(4): p. 435-441.
156. Jorgensen P, Tyers M: **How cells coordinate growth and division**. *Current biology : CB* (**2004**), 14(23): p. R1014-1027.
157. Rupes I: **Checking cell size in yeast**. *Trends in genetics : TIG* (**2002**), 18(9): p. 479-485.
158. Fang SC, de los Reyes C, Umen JG: **Cell size checkpoint control by the retinoblastoma tumor suppressor pathway**. *Plos Genet* (**2006**), 2(10): p. e167.

159. Gregory TR: **Coincidence, coevolution, or causation? DNA content, cell size, and the C-value enigma**. *Biological reviews of the Cambridge Philosophical Society* (**2001**), 76(1): p. 65-101.
160. Sugimoto-Shirasu K, Roberts K: **"Big it up": endoreduplication and cell-size control in plants**. *Curr Opin Plant Biol* (**2003**), 6(6): p. 544-553.
161. Kondorosi E, Roudier F, Gendreau E: **Plant cell-size control: growing by ploidy?** *Curr Opin Plant Biol* (**2000**), 3(6): p. 488-492.
162. Leiva-Neto JT, Grafi G, Sabelli PA, Dante RA, Woo YM, Maddock S, Gordon-Kamm WJ, Larkins BA: **A dominant negative mutant of cyclin-dependent kinase A reduces endoreduplication but not cell size or gene expression in maize endosperm**. *The Plant cell* (**2004**), 16(7): p. 1854-1869.
163. Schnittger A, Weinl C, Bouyer D, Schobinger U, Hulskamp M: **Misexpression of the cyclin-dependent kinase inhibitor ICK1/KRP1 in single-celled Arabidopsis trichomes reduces endoreduplication and cell size and induces cell death**. *The Plant cell* (**2003**), 15(2): p. 303-315.
164. Cully M, Downward J: **Assessing cell size and cell cycle regulation in cells with altered TOR activity**. *Methods in molecular biology* (**2012**), 821: p. 227-237.
165. Oldenhof H, Zachleder V, van den Ende H: **Blue light delays commitment to cell division in Chlamydomonas reinhardtii**. *Plant biology* (**2004**), 6(6): p. 689-695.
166. Vellai T, Bicsak B, Toth ML, Takacs-Vellai K, Kovacs AL: **Regulation of cell growth by autophagy**. *Autophagy* (**2008**), 4(4): p. 507-509.
167. Meijer AJ: **Amino acids as regulators and components of nonproteinogenic pathways**. *The Journal of nutrition* (**2003**), 133(6 Suppl 1): p. 2057S-2062S.
168. Krause U, Bertrand L, Maisin L, Rosa M, Hue L: **Signalling pathways and combinatory effects of insulin and amino acids in isolated rat hepatocytes**. *European journal of biochemistry / FEBS* (**2002**), 269(15): p. 3742-3750.
169. Lang F, Busch GL, Ritter M, Volkl H, Waldegger S, Gulbins E, Haussinger D: **Functional significance of cell volume regulatory mechanisms**. *Physiological reviews* (**1998**), 78(1): p. 247-306.
170. Haussinger D: **The role of cellular hydration in the regulation of cell function**. *Biochem J* (**1996**), 313 (Pt 3): p. 697-710.
171. Unger MW, Hartwell LH: **Control of cell division in Saccharomyces cerevisiae by methionyl-tRNA**. *Proceedings of the National Academy of Sciences of the United States of America* (**1976**), 73(5): p. 1664-1668.
172. Popolo L, Vanoni M, Alberghina L: **Control of the yeast cell cycle by protein synthesis**. *Experimental cell research* (**1982**), 142(1): p. 69-78.
173. Sage J, Mulligan GJ, Attardi LD, Miller A, Chen S, Williams B, Theodorou E, Jacks T: **Targeted disruption of the three Rb-related genes leads to loss of G(1) control and immortalization**. *Genes & development* (**2000**), 14(23): p. 3037-3050.
174. Park JA, Ahn JW, Kim YK, Kim SJ, Kim JK, Kim WT, Pai HS: **Retinoblastoma protein regulates cell proliferation, differentiation, and endoreduplication in plants**. *The Plant journal : for cell and molecular biology* (**2005**), 42(2): p. 153-163.
175. Herrera RE, Sah VP, Williams BO, Makela TP, Weinberg RA, Jacks T: **Altered cell cycle kinetics, gene expression, and G1 restriction point regulation in Rb-deficient fibroblasts**. *Mol Cell Biol* (**1996**), 16(5): p. 2402-2407.
176. Dannenberg JH, van Rossum A, Schuijff L, te Riele H: **Ablation of the retinoblastoma gene family deregulates G(1) control causing immortalization and increased cell turnover under growth-restricting conditions**. *Genes & development* (**2000**), 14(23): p. 3051-3064.
177. Stevaux O, Dyson NJ: **A revised picture of the E2F transcriptional network and RB function**. *Curr Opin Cell Biol* (**2002**), 14(6): p. 684-691.
178. Kennedy BK, Barbie DA, Classon M, Dyson N, Harlow E: **Nuclear organization of DNA replication in primary mammalian cells**. *Genes & development* (**2000**), 14(22): p. 2855-2868.
179. Lai A, Kennedy BK, Barbie DA, Bertos NR, Yang XJ, Theberge MC, Tsai SC, Seto E, Zhang Y, Kuzmichev A *et al*: **RBP1 recruits the mSIN3-histone deacetylase complex to**

the pocket of retinoblastoma tumor suppressor family proteins found in limited discrete regions of the nucleus at growth arrest. *Mol Cell Biol* (**2001**), 21(8): p. 2918-2932.

180. Nevins JR: **Toward an understanding of the functional complexity of the E2F and retinoblastoma families**. *Cell growth & differentiation : the molecular biology journal of the American Association for Cancer Research* (**1998**), 9(8): p. 585-593.
181. Trimarchi JM, Fairchild B, Wen J, Lees JA: **The E2F6 transcription factor is a component of the mammalian Bmi1-containing polycomb complex**. *Proceedings of the National Academy of Sciences of the United States of America* (**2001**), 98(4): p. 1519-1524.
182. Trimarchi JM, Lees JA: **Sibling rivalry in the E2F family**. *Nature reviews Molecular cell biology* (**2002**), 3(1): p. 11-20.
183. Mita MM, Mita A, Rowinsky EK: **The molecular target of rapamycin (mTOR) as a therapeutic target against cancer**. *Cancer biology & therapy* (**2003**), 2(4 Suppl 1): p. S169-177.
184. Popowski M, Ferguson HA, Sion AM, Koller E, Knudsen E, Van Den Berg CL: **Stress and IGF-I differentially control cell fate through mammalian target of rapamycin (mTOR) and retinoblastoma protein (pRB)**. *The Journal of biological chemistry* (**2008**), 283(42): p. 28265-28273.
185. DeCaprio JA: **How the Rb tumor suppressor structure and function was revealed by the study of Adenovirus and SV40**. *Virology* (**2009**), 384(2): p. 274-284.
186. Olson BJ, Oberholzer M, Li Y, Zones JM, Kohli HS, Bisova K, Fang SC, Meisenhelder J, Hunter T, Umen JG: **Regulation of the Chlamydomonas cell cycle by a stable, chromatin-associated retinoblastoma tumor suppressor complex**. *The Plant cell* (**2010**), 22(10): p. 3331-3347.
187. Muller H, Bracken AP, Vernell R, Moroni MC, Christians F, Grassilli E, Prosperini E, Vigo E, Oliner JD, Helin K: **E2Fs regulate the expression of genes involved in differentiation, development, proliferation, and apoptosis**. *Genes & development* (**2001**), 15(3): p. 267-285.
188. Ishida S, Huang E, Zuzan H, Spang R, Leone G, West M, Nevins JR: **Role for E2F in control of both DNA replication and mitotic functions as revealed from DNA microarray analysis**. *Mol Cell Biol* (**2001**), 21(14): p. 4684-4699.
189. Howell JJ, Ricoult SJ, Ben-Sahra I, Manning BD: **A growing role for mTOR in promoting anabolic metabolism**. *Biochem Soc Trans* (**2013**), 41(4): p. 906-912.
190. Cai L, Tu BP: **Driving the cell cycle through metabolism**. *Annual review of cell and developmental biology* (**2012**), 28: p. 59-87.
191. Zanghellini J, Natter K, Jungreuthmayer C, Thalhammer A, Kurat CF, Gogg-Fassolter G, Kohlwein SD, von Grunberg HH: **Quantitative modeling of triacylglycerol homeostasis in yeast--metabolic requirement for lipolysis to promote membrane lipid synthesis and cellular growth**. *Febs J* (**2008**), 275(22): p. 5552-5563.
192. Mitchison JM, Creanor J: **Further measurements of DNA synthesis and enzyme potential during cell cycle of fission yeast Schizosaccharomyces pombe**. *Experimental cell research* (**1971**), 69(1): p. 244-247.
193. Johnson X, Alric J: **Central carbon metabolism and electron transport in Chlamydomonas reinhardtii: metabolic constraints for carbon partitioning between oil and starch**. *Eukaryot Cell* (**2013**), 12(6): p. 776-793.
194. Grossman AR, Lohr M, Im CS: **Chlamydomonas reinhardtii in the landscape of pigments**. *Annu Rev Genet* (**2004**), 38: p. 119-173.
195. Ilag LL, Kumar AM, Soll D: **Light regulation of chlorophyll biosynthesis at the level of 5-aminolevulinate formation in Arabidopsis**. *The Plant cell* (**1994**), 6(2): p. 265-275.
196. Beale SI: **Biosynthesis of the Tetrapyrrole Pigment Precursor, delta-Aminolevulinic Acid, from Glutamate**. *Plant physiology* (**1990**), 93(4): p. 1273-1279.
197. Nogaj LA, Srivastava A, van Lis R, Beale SI: **Cellular levels of glutamyl-tRNA reductase and glutamate-1-semialdehyde aminotransferase do not control chlorophyll synthesis in Chlamydomonas reinhardtii**. *Plant physiology* (**2005**), 139(1): p. 389-396.

198. Wase N, Black PN, Stanley BA, DiRusso CC: **Integrated Quantitative Analysis of Nitrogen Stress Response in Chlamydomonas reinhardtii Using Metabolite and Protein Profiling**. *Journal of proteome research* (**2014**), 13(3): p. 1373-1396.
199. Collier JL, Grossman AR: **Chlorosis Induced by Nutrient Deprivation in Synechococcus Sp Strain Pcc-7942 - Not All Bleaching Is the Same**. *Journal of bacteriology* (**1992**), 174(14): p. 4718-4726.
200. Beale SI: **Enzymes of chlorophyll biosynthesis**. *Photosynthesis research* (**1999**), 60(1): p. 43-73.
201. Vavilin DV, Vermaas WF: **Regulation of the tetrapyrrole biosynthetic pathway leading to heme and chlorophyll in plants and cyanobacteria**. *Physiol Plant* (**2002**), 115(1): p. 9-24.
202. Lin WL, Oliver DJ: **Role of triacylglycerols in leaves**. *Plant Sci* (**2008**), 175(3): p. 233-237.
203. Schmelzle T, Beck T, Martin DE, Hall MN: **Activation of the RAS/cyclic AMP pathway suppresses a TOR deficiency in yeast**. *Mol Cell Biol* (**2004**), 24(1): p. 338-351.
204. Bjedov I, Toivonen JM, Kerr F, Slack C, Jacobson J, Foley A, Partridge L: **Mechanisms of Life Span Extension by Rapamycin in the Fruit Fly Drosophila melanogaster**. *Cell metabolism* (**2010**), 11(1): p. 35-46.
205. Teleman AA, Chen YW, Cohen SM: **Drosophila Melted modulates FOXO and TOR activity**. *Dev Cell* (**2005**), 9(2): p. 271-281.
206. Weise SE, Weber AP, Sharkey TD: **Maltose is the major form of carbon exported from the chloroplast at night**. *Planta* (**2004**), 218(3): p. 474-482.
207. Fan J, Yan C, Andre C, Shanklin J, Schwender J, Xu C: **Oil accumulation is controlled by carbon precursor supply for fatty acid synthesis in Chlamydomonas reinhardtii**. *Plant & cell physiology* (**2012**), 53(8): p. 1380-1390.
208. Chakrabarti P, English T, Shi J, Smas CM, Kandror KV: **Mammalian target of rapamycin complex 1 suppresses lipolysis, stimulates lipogenesis, and promotes fat storage**. *Diabetes* (**2010**), 59(4): p. 775-781.
209. Terashima M, Specht M, Hippler M: **The chloroplast proteome: a survey from the Chlamydomonas reinhardtii perspective with a focus on distinctive features**. *Curr Genet* (**2011**), 57(3): p. 151-168.
210. Bhatnagar D, Xu S, Fischer C, Arechederra RL, Minteer SD: **Mitochondrial biofuel cells: expanding fuel diversity to amino acids**. *Phys Chem Chem Phys* (**2011**), 13(1): p. 86-92.
211. Porstmann T, Santos CR, Griffiths B, Cully M, Wu M, Leevers S, Griffiths JR, Chung YL, Schulze A: **SREBP activity is regulated by mTORC1 and contributes to Akt-dependent cell growth**. *Cell metabolism* (**2008**), 8(3): p. 224-236.
212. Lamming DW, Sabatini DM: **A Central role for mTOR in lipid homeostasis**. *Cell metabolism* (**2013**), 18(4): p. 465-469.
213. Sakurai K, Moriyama T, Sato N: **Detailed Identification of Fatty Acid Isomers Sheds Light on the Probable Precursors of Triacylglycerol Accumulation in Photoautotrophically Grown Chlamydomonas reinhardtii**. *Eukaryot Cell* (**2014**), 13(2): p. 256-266.
214. Li X, Benning C, Kuo MH: **Rapid triacylglycerol turnover in Chlamydomonas reinhardtii requires a lipase with broad substrate specificity**. *Eukaryot Cell* (**2012**), 11(12): p. 1451-1462.
215. Iba K: **Acclimative response to temperature stress in higher plants: approaches of gene engineering for temperature tolerance**. *Annu Rev Plant Biol* (**2002**), 53: p. 225-245.
216. Vigh L, Gombos Z, Horvath I, Joo F: **Saturation of Membrane-Lipids by Hydrogenation Induces Thermal-Stability in Chloroplast Inhibiting the Heat-Dependent Stimulation of Photosystem-I-Mediated Electron-Transport**. *Biochimica et biophysica acta* (**1989**), 979(3): p. 361-364.
217. Vigh L, Los DA, Horvath I, Murata N: **The Primary Signal in the Biological Perception of Temperature - Pd-Catalyzed Hydrogenation of Membrane-Lipids Stimulated the Expression of the Desa Gene in Synechocystis-Pcc6803**. *Proceedings of the National Academy of Sciences of the United States of America* (**1993**), 90(19): p. 9090-9094.

218. Pearcy RW: **Effect of Growth Temperature on Fatty-Acid Composition of Leaf Lipids in Atriplex-Lentiformis-(Torr)-Wats**. *Plant physiology* (**1978**), 61(4): p. 484-486.
219. Raison JK, Roberts JKM, Berry JA: **Correlations between the Thermal-Stability of Chloroplast (Thylakoid) Membranes and the Composition and Fluidity of Their Polar Lipids Upon Acclimation of the Higher-Plant, Nerium-Oleander, to Growth Temperature**. *Biochimica et biophysica acta* (**1982**), 688(1): p. 218-228.
220. Roughan PG, Slack CR: **Cellular-Organization of Glycerolipid Metabolism**. *Annu Rev Plant Phys* (**1982**), 33: p. 97-132.
221. Roughan G, Slack R: **Glycerolipid Synthesis in Leaves**. *Trends Biochem Sci* (**1984**), 9(9): p. 383-386.
222. Frentzen M: **Biosynthesis and Desaturation of the Different Diacylglycerol Moieties in Higher-Plants**. *Journal of plant physiology* (**1986**), 124(3-4): p. 193-209.
223. Dormann P, Benning C: **Galactolipids rule in seed plants**. *Trends in plant science* (**2002**), 7(3): p. 112-118.
224. Andersson MX, Stridh MH, Larsson KE, Lijenberg C, Sandelius AS: **Phosphate-deficient oat replaces a major portion of the plasma membrane phospholipids with the galactolipid digalactosyldiacylglycerol**. *FEBS letters* (**2003**), 537(1-3): p. 128-132.
225. Riekhof WR, Sears BB, Benning C: **Annotation of genes involved in glycerolipid biosynthesis in Chlamydomonas reinhardtii: Discovery of the betaine lipid synthase BTA1(Cr)**. *Eukaryot Cell* (**2005**), 4(2): p. 242-252.
226. Tataranni T, Biondi G, Cariello M, Mangino M, Colucci G, Rutigliano M, Ditonno P, Schena FP, Gesualdo L, Grandaliano G: **Rapamycin-Induced Hypophosphatemia and Insulin Resistance Are Associated With mTORC2 Activation and Klotho Expression**. *Am J Transplant* (**2011**), 11(8): p. 1656-1664.
227. Shimano H, Horton JD, Hammer RE, Shimomura I, Brown MS, Goldstein JL: **Overproduction of cholesterol and fatty acids causes massive liver enlargement in transgenic mice expressing truncated SREBP-1a**. *Journal of Clinical Investigation* (**1996**), 98(7): p. 1575-1584.
228. Hannah VC, Ou JF, Luong A, Goldstein JL, Brown MS: **Unsaturated fatty acids down-regulate SREBP isoforms 1a and 1c by two mechanisms in HEK-293 cells**. *Journal of Biological Chemistry* (**2001**), 276(6): p. 4365-4372.
229. Yang FJ, Vought BW, Satterlee JS, Walker AK, Sun ZYJ, Watts JL, DeBeaumont R, Saito RM, Hyberts SG, Yang S *et al*: **An ARC/Mediator subunit required for SREBP control of cholesterol and lipid homeostasis**. *Nature* (**2006**), 442(7103): p. 700-704.
230. Li SJ, Brown MS, Goldstein JL: **Bifurcation of insulin signaling pathway in rat liver: mTORC1 required for stimulation of lipogenesis, but not inhibition of gluconeogenesis**. *Proceedings of the National Academy of Sciences of the United States of America* (**2010**), 107(8): p. 3441-3446.
231. Yecies JL, Zhang HH, Menon S, Liu SH, Yecies D, Lipovsky AI, Gorgun C, Kwiatkowski DJ, Hotamisligil GS, Lee CH *et al*: **Akt Stimulates Hepatic SREBP1c and Lipogenesis through Parallel mTORC1-Dependent and Independent Pathways**. *Cell metabolism* (**2011**), 14(1): p. 21-32.
232. Duvel K, Yecies JL, Menon S, Raman P, Lipovsky AI, Souza AL, Triantafellow E, Ma QC, Gorski R, Cleaver S *et al*: **Activation of a Metabolic Gene Regulatory Network Downstream of mTOR Complex 1**. *Mol Cell* (**2010**), 39(2): p. 171-183.
233. Schmidt A, Beck T, Koller A, Kunz J, Hall MN: **The TOR nutrient signalling pathway phosphorylates NPR1 and inhibits turnover of the tryptophan permease**. *Embo J* (**1998**), 17(23): p. 6924-6931.
234. Matsuo T, Otsubo Y, Urano J, Tamanoi F, Yamamoto M: **Loss of the TOR kinase Tor2 mimics nitrogen starvation and activates the sexual development pathway in fission yeast**. *Mol Cell Biol* (**2007**), 27(8): p. 3154-3164.
235. Pineda M, Cardenas J: **Transport and assimilation of purines in Chlamydomonas reinhardtii**. *Sci Mar* (**1996**), 60: p. 195-201.
236. Kirk DL, Kirk MM: **Carrier-Mediated Uptake of Arginine and Urea by Chlamydomonas-Reinhardtii**. *Plant physiology* (**1978**), 61(4): p. 556-560.

237. Hodson RC, Williams SK, Davidson WR: **Metabolic Control of Urea Catabolism in Chlamydomonas-Reinhardi and Chlorella-Pyrenoidosa**. *Journal of bacteriology* (**1975**), 121(3): p. 1022-1035.
238. Florencio FJ, Vega JM: **Utilization of Nitrate, Nitrite and Ammonium by Chlamydomonas-Reinhardii - Photoproduction of Ammonium**. *Planta* (**1983**), 158(4): p. 288-293.
239. Nunes-Nesi A, Fernie AR, Stitt M: **Metabolic and signaling aspects underpinning the regulation of plant carbon nitrogen interactions**. *Molecular plant* (**2010**), 3(6): p. 973-996.
240. Urquhart AA, Joy KW: **Use of Phloem Exudate Technique in the Study of Amino-Acid-Transport in Pea-Plants**. *Plant physiology* (**1981**), 68(3): p. 750-754.
241. Jung CH, Ro SH, Cao J, Otto NM, Kim DH: **mTOR regulation of autophagy**. *FEBS letters* (**2010**), 584(7): p. 1287-1295.
242. Brouquisse R, James F, Pradet A, Raymond P: **Asparagine Metabolism and Nitrogen Distribution during Protein-Degradation in Sugar-Starved Maize Root-Tips**. *Planta* (**1992**), 188(3): p. 384-395.
243. Coronil T, Lara C, Guerrero MG: **Shift in Carbon Flow and Stimulation of Amino-Acid Turnover Induced by Nitrate and Ammonium Assimilation in Anacystis-Nidulans**. *Planta* (**1993**), 189(3): p. 461-467.
244. Tapia MI, deAlda JAGO, Llama MJ, Serra JL: **Changes in intracellular amino acids and organic acids induced by nitrogen starvation and nitrate or ammonium resupply in the cyanobacterium Phormidium laminosum**. *Planta* (**1996**), 198(4): p. 526-531.
245. Tapia MI, Llama MJ, Serra JL: **Regulation of nitrate assimilation in the cyanobacterium Phormidium laminosum**. *Planta* (**1996**), 198(1): p. 24-30.
246. Llacer JL, Fita I, Rubio V: **Arginine and nitrogen storage**. *Curr Opin Struc Biol* (**2008**), 18(6): p. 673-681.
247. Slocum RD: **Genes, enzymes and regulation of arginine biosynthesis in plants**. *Plant Physiol Bioch* (**2005**), 43(8): p. 729-745.
248. Rabe E, Lovatt CJ: **Increased Arginine-Biosynthesis during Phosphorus Deficiency - a Response to the Increased Ammonia Content of Leaves**. *Plant physiology* (**1986**), 81(3): p. 774-779.
249. Gilfilla.Im, Jones WW: **Effect of Iron and Manganese Deficiency on Chlorophyll Amino Acid and Organic Acid Status of Leaves of Macadamia**. *P Am Soc Hortic Sci* (**1968**), 93(Dec): p. 210-&.
250. Mertz ET, Matsumoto H: **Further studies on the amino acids and proteins of sulfur-deficient alfalfa**. *Archives of biochemistry and biophysics* (**1956**), 63(1): p. 50-63.
251. Freney JR, Delwiche CC, Johnson CM: **The effect of chloride on the free amino acids of cabbage and cauliflower plants**. *Aust J Biol Sci* (**1959**), 12: p. 160-166.
252. Possingham JV: **The effect of mineral nutrition on the content of free amino acids and amides in tomato plants. I. A comparison of the effects of deficiencies of copper, zinc, manganese, iron and molybdenum.** *Aust J Biol Sci* (**1956**), 9: p. 539-551.
253. Burillo S, Luque I, Fuentes I, Contreras A: **Interactions between the nitrogen signal transduction protein PII and N-acetyl glutamate kinase in organisms that perform oxygenic photosynthesis**. *Journal of bacteriology* (**2004**), 186(11): p. 3346-3354.
254. Ferrario-Mery S, Besin E, Pichon O, Meyer C, Hodges M: **The regulatory PII protein controls arginine biosynthesis in Arabidopsis**. *FEBS letters* (**2006**), 580(8): p. 2015-2020.
255. Forchhammer K: **P(II) signal transducers: novel functional and structural insights**. *Trends in microbiology* (**2008**), 16(2): p. 65-72.
256. Heinrich A, Maheswaran M, Ruppert U, Forchhammer K: **The Synechococcus elongatus P signal transduction protein controls arginine synthesis by complex formation with N-acetyl-L-glutamate kinase**. *Mol Microbiol* (**2004**), 52(5): p. 1303-1314.
257. Maheswaran M, Urbanke C, Forchhammer K: **Complex formation and catalytic activation by the PII signaling protein of N-acetyl-L-glutamate kinase from Synechococcus elongatus strain PCC 7942**. *The Journal of biological chemistry* (**2004**), 279(53): p. 55202-55210.

258. Ermilova E, Lapina T, Zalutskaya Z, Minaeva E, Fokina O, Forchhammer K: **PII signal transduction protein in Chlamydomonas reinhardtii: localization and expression pattern**. *Protist* (**2013**), 164(1): p. 49-59.
259. Goldraij A, Polacco JC: **Arginine degradation by arginase in mitochondria of soybean seedling cotyledons**. *Planta* (**2000**), 210(4): p. 652-658.
260. Whitney PA, Cooper T: **Urea Carboxylase from Saccharomyces-Cerevisiae - Evidence for a Minimal 2-Step Reaction Sequence**. *Journal of Biological Chemistry* (**1973**), 248(1): p. 325-330.
261. Hattori A: **Studies on the Metabolism of Urea and Other Nitrogenous Compounds in Chlorella-Ellipsoidea .3. Assimilation of Urea**. *Plant and Cell Physiology* (**1960**), 1(2): p. 107-115.
262. Leruduli.D, Goas G: **Presentation and Determination of Some Amines in Seedlings of Soja-Hispida Moench Deprived of Cotyledons and Cultivated in Presence of Nitrates, Urea and Ammonium Chloride**. *Cr Acad Sci D Nat* (**1971**), 273(13): p. 1108-&.
263. Slocum RD: **Tissue and subcellular localization of polyamines and enzymes of polyamine metabolism**. In: *Biochemstry and Physiology of Polyamines in Plants*. Edited by Slocum RD, Flores HE. Boca Raton, FL: CRC Press; (**1991**): p. 23-40.
264. Galston AW, KaurSawhney R, Altabella T, Tiburcio AF: **Plant polyamines in reproductive activity and response to abiotic stress**. *Bot Acta* (**1997**), 110(3): p. 197-207.
265. Flores HE, Galston AW: **Osmotic Stress-Induced Polyamine Accumulation in Cereal Leaves .2. Relation to Amino-Acid Pools**. *Plant physiology* (**1984**), 75(1): p. 110-113.
266. Slocum RD, Weinstein LH: **Stress-induced putrescine accumulation as a mechanism of ammonia detoxification in cereal leaves**. In: *Polyamines and Ethylene: Biochemistry, Physiology, and Interaction.* Edited by Flores HE, Arteca RN, Shannon JC. Boca Raton, FL: CRC Press; (**1990**): p. 157-165.
267. Kusano T, Berberich T, Tateda C, Takahashi Y: **Polyamines: essential factors for growth and survival**. *Planta* (**2008**), 228(3): p. 367-381.
268. Takahashi T, Kakehi J: **Polyamines: ubiquitous polycations with unique roles in growth and stress responses**. *Ann Bot* (**2010**), 105(1): p. 1-6.
269. Theiss C, Bohley P, Voigt J: **Regulation by polyamines of ornithine decarboxylase activity and cell division in the unicellular green alga Chlamydomonas reinhardtii**. *Plant physiology* (**2002**), 128(4): p. 1470-1479.
270. Ren M, Venglat P, Qiu S, Feng L, Cao Y, Wang E, Xiang D, Wang J, Alexander D, Chalivendra S *et al*: **Target of rapamycin signaling regulates metabolism, growth, and life span in Arabidopsis**. *The Plant cell* (**2012**), 24(12): p. 4850-4874.
271. Shamji AF, Kuruvilla FG, Schreiber SL: **Partitioning the transcriptional program induced by rapamycin among the effectors of the Tor proteins**. *Current biology : CB* (**2000**), 10(24): p. 1574-1581.
272. Ben-Sahra I, Howell JJ, Asara JM, Manning BD: **Stimulation of de Novo Pyrimidine Synthesis by Growth Signaling Through mTOR and S6K1**. *Science* (**2013**), 339(6125): p. 1323-1328.

Supplementary tables

Supp. table 1. Changes of primary metabolites during the cell cycle

Changes of the total amount (per ml) of primary metabolites are shown as log_2 fold changes for each TP to TP 0 for a *Chlamydomonas* culture synchronized by a 12:12 h light-dark regime. The header of this table displays the TP in hours after onset of light. The dark phase (TP 13 – TP24 h) is indicated as grey background. Log_2 fold changes above 0.5 are indicated by reddish colors (orange and red), while red indicates a significant ($p < 0.005$) increase. Yellow background indicates the three highest values for log_2 fold changes. Primary metabolites were grouped with regard to the TP when their level starts to increase. This results in 4 cluster indicated by blue, red, green and purple background.

	0.5	1	2	4	6	8	10	11	12	13	14	16	20	24
Butyrate. 2-Amino-	0.99	1.49	1.99	4.08	3.97	3.65	4.47	4.54	4.49	2.71	2.01	1.66	1.63	2.17
Erythritol or Threitol	0.52	0.68	1.11	2.05	2.67	3.20	4.52	4.64	4.64	4.05	3.73	3.89	3.62	3.81
Phenylalanine	1.36	1.54	1.33	1.75	2.40	2.84	4.19	4.27	4.29	4.02	3.81	3.45	3.33	3.32
byproduct of Ascorbate.														
1-Dehydro-	2.12	2.96	3.29	4.30	4.72	4.60	5.11	5.26	5.40	4.11	3.10	1.85	1.95	3.18
Tyrosine	1.10	1.06	0.89	1.26	2.12	2.07	3.40	3.75	3.97	3.68	3.59	3.54	3.37	3.24
Ribose 5-P	0.55	0.90	1.23	2.49	3.20	3.23	3.90	3.71	3.77	3.41	3.13	3.01	2.67	2.90
Spermidine	0.63	2.62	2.58	3.37	3.09	2.57	3.72	3.61	3.74	3.24	2.72	2.75	1.91	2.04
Methionine	0.44	0.93	1.36	2.04	2.29	2.57	4.08	4.41	4.53	4.06	4.05	4.63	4.39	4.05
Ribose	0.51	0.66	1.23	1.91	2.51	2.71	3.98	4.04	5.16	5.22	5.27	4.07	4.35	5.43
Alanine	0.40	0.65	0.91	3.82	3.82	3.10	4.39	4.49	4.38	3.12	2.98	2.71	2.63	2.71
Pyruvate	0.36	0.74	1.21	1.92	2.40	2.54	3.90	3.77	3.95	3.47	3.38	3.19	2.99	3.24
Alanine. beta-	0.23	0.62	0.98	4.55	4.94	4.13	3.91	4.25	4.52	3.86	3.49	2.88	1.92	3.33
Homoserine	0.20	0.50	0.76	1.42	2.07	2.02	3.49	3.59	3.64	3.23	2.93	2.70	2.25	2.55
Pyrophosphate	0.29	0.56	1.01	2.04	2.53	2.55	3.76	4.04	3.04	3.07	3.13	4.26	3.97	3.41
Citrulline	0.13	0.54	1.19	2.19	3.02	2.89	4.14	4.12	4.76	4.08	3.77	3.60	2.82	3.37
Tryptophan	0.40	0.61	0.73	1.22	2.05	2.54	3.78	3.91	4.24	4.11	3.92	4.24	4.61	3.77
Maltotriose	0.49	0.74	1.46	2.38	2.49	3.08	3.87	4.14	5.90	5.31	4.92	3.97	2.66	3.09
Hypoxanthine	0.55	0.79	0.63	2.18	2.24	2.20	3.13	3.10	4.05	2.80	2.18	2.40	1.35	1.57
Valine	0.07	0.24	0.84	2.26	2.33	2.00	3.28	3.41	3.70	3.62	3.50	3.30	3.04	3.35
Leucine	0.23	0.48	1.06	2.75	2.92	2.71	3.90	3.97	4.22	3.88	3.80	3.51	3.22	3.62
Isoleucine	0.15	0.35	0.77	2.51	2.85	2.59	3.79	3.81	3.83	3.39	3.36	3.50	3.28	3.17
Glycine	-0.02	0.33	0.69	1.39	1.80	1.36	2.49	2.58	3.09	2.63	2.37	2.28	1.81	2.23
Threonine	0.25	0.17	0.64	2.73	2.99	2.81	4.02	4.18	3.98	3.67	3.63	3.26	3.14	3.02
Malate	0.01	0.34	1.09	2.39	3.09	3.13	4.25	4.67	4.75	4.06	3.82	3.57	3.37	3.74
Arginine	0.15	0.37	0.88	1.88	2.73	2.74	4.34	4.19	4.71	4.01	3.66	3.72	3.29	3.53
Nicotinamide	0.09	0.43	0.84	1.82	2.02	2.10	2.88	3.04	3.40	3.49	3.51	3.42	3.30	3.55
Ornithine	0.08	0.32	0.87	1.99	2.39	2.16	3.52	4.00	4.22	3.64	3.20	3.17	2.62	3.03
Glutamine	0.07	0.47	1.03	1.45	1.90	1.93	3.37	3.54	3.89	3.27	3.01	2.80	2.28	2.62
Lysine	0.03	0.21	0.76	1.85	2.67	2.53	3.61	3.85	3.84	3.33	3.09	3.06	3.07	3.53
Maltose	0.37	0.49	1.09	2.05	2.41	2.48	3.49	3.69	4.32	4.04	4.21	3.84	3.44	3.74
AMP (Adenosine 5-P)	0.23	0.33	0.82	1.43	1.95	2.07	3.42	3.53	4.06	4.12	4.06	3.91	3.85	4.00
GMP (Guanosine 5-P)	0.17	0.34	0.68	1.25	1.55	1.82	3.10	3.23	3.62	3.80	3.49	3.68	3.56	3.56
Succinate	-0.18	0.08	0.92	1.98	2.84	2.82	3.93	4.40	4.59	4.22	3.83	3.56	3.30	3.64
Glycerol 3-P (also														
Glycerol 1-P)	0.26	0.33	0.54	1.29	1.89	1.99	2.94	3.34	3.81	3.89	3.91	3.53	3.61	3.84
Histidine	-0.78	-0.45	1.13	3.32	3.60	4.36	5.97	5.85	5.13	4.94	4.57	5.04	5.23	5.07

Supp.table 1. Continued

	0.5	1	2	4	6	8	10	11	12	13	14	16	20	24
Glycerol	-0.22	-0.06	0.46	0.67	0.91	0.82	1.99	2.22	3.81	4.13	4.19	3.53	3.36	3.23
Serine	0.24	0.30	0.47	2.02	2.58	2.49	3.76	3.81	3.75	3.06	2.85	2.43	2.18	2.58
Aspartate	0.21	0.45	0.27	2.02	2.40	2.12	3.32	3.25	2.92	2.50	2.51	2.78	2.39	2.57
Pyroglutamate	0.09	0.22	0.45	1.16	1.71	1.49	2.86	3.26	3.42	2.98	2.79	2.68	2.31	2.82
Glutamate	-0.12	0.01	0.35	1.28	1.93	1.69	3.22	3.36	3.48	2.96	2.74	2.39	2.13	2.84
Putrescine	0.14	0.36	0.50	0.89	1.06	0.95	1.80	1.82	1.99	1.89	1.86	1.89	1.55	1.62
Glutarate. 2-Oxo	-0.09	0.01	0.50	1.44	2.08	1.88	3.20	2.94	3.00	2.64	2.55	2.57	2.79	2.80
Phosphoenolpyruvate	-0.08	0.03	0.16	1.11	1.47	2.22	2.35	2.58	3.13	2.60	3.14	1.45	2.61	3.25
Asparagine	-0.22	-0.06	0.36	1.83	2.65	2.51	3.79	3.97	4.08	3.68	3.49	3.46	3.35	3.29
byproduct of Asparagine	-0.21	-0.06	0.29	1.04	1.44	1.71	2.72	3.13	3.43	3.09	3.21	3.03	2.56	3.14
Fructose (also Psicose)	-0.54	-0.43	-0.26	0.86	1.27	1.49	2.38	2.40	2.66	2.04	2.15	2.22	1.99	2.07
Glucose	-0.47	-0.45	-0.06	1.10	2.58	1.96	4.40	3.86	6.19	5.57	5.36	3.91	3.30	3.44
Glycerate 2-P	0.05	0.19	0.15	1.40	2.45	2.60	3.92	3.78	4.21	3.50	3.12	2.83	2.80	3.28
Glycerate 3-P	0.09	0.16	0.50	1.19	2.43	2.50	3.82	3.61	4.11	3.65	3.44	3.26	3.09	3.46
unknown (likely overlap with Lysine)	0.01	-0.02	0.00	0.66	1.08	1.03	1.91	2.02	2.07	1.79	1.54	1.61	1.51	1.83
Inositol. myo-	-0.17	-0.33	-0.38	0.84	1.85	2.35	3.57	3.84	4.45	4.30	4.16	3.53	3.51	4.23
Mannose 6-P	0.00	-0.41	-0.07	0.71	1.39	2.26	3.32	4.14	4.72	4.30	4.19	3.94	3.70	3.68
Fructose 6-P	0.01	0.16	0.18	1.44	2.11	2.47	2.90	3.06	3.34	2.67	1.88	1.36	0.71	0.95
Glucose 6-P or Galactose 6-P	-0.08	-0.10	-0.14	1.23	1.69	2.37	2.78	3.34	3.68	3.48	2.81	2.23	1.85	2.13
Adenine	0.11	0.24	0.23	0.53	0.84	1.20	2.21	2.49	2.70	2.49	2.51	2.32	2.47	2.51
Phytol	0.20	-0.06	-0.03	0.50	0.98	2.05	3.93	3.15	3.81	4.26	4.22	3.65	4.25	5.18
Guanine	0.54	0.40	0.07	1.08	0.93	0.72	1.83	1.74	2.30	1.69	0.80	1.54	1.27	0.97
Uracil	-0.10	0.07	0.21	0.27	0.69	0.74	1.50	1.46	2.59	2.31	2.46	1.34	1.13	2.28
Mannitol or Sorbitol	-0.03	-0.08	0.18	-0.14	0.20	0.59	2.50	2.09	5.11	4.72	5.09	3.23	3.58	4.69
Citrate	-0.25	-0.45	-0.45	0.29	0.39	0.94	1.81	1.79	1.74	1.67	1.84	2.35	2.54	2.19
Dihydroxyacetone-P	-0.38	0.13	-0.13	0.29	1.45	2.48	3.93	4.98	5.55	5.65	5.87	4.45	4.62	5.45
Fumarate	-0.12	-0.17	0.05	0.31	0.33	0.93	1.96	2.37	2.31	2.68	2.56	1.95	1.90	2.58
Oxalate	-0.11	0.57	0.20	0.50	0.42	0.31	0.96	1.03	1.36	1.18	0.92	0.91	0.86	0.97
Ethanolamine	0.19	0.10	0.14	0.39	0.27	0.33	0.68	0.85	1.98	1.84	2.08	1.23	1.18	1.86
Cysteine	0.10	-0.18	-0.29	-0.06	0.12	-0.01	1.72	1.87	2.38	1.62	1.41	1.37	1.06	1.37
Sucrose	-0.04	-0.40	-1.02	0.33	0.26	0.29	0.80	1.23	0.89	0.25	1.12	1.54	1.50	0.87
Xanthine	-0.60	-0.24	-0.10	0.27	0.96	1.55	3.40	3.38	5.38	5.25	5.01	1.76	4.19	4.51
Urea	-0.62	-0.49	-0.14	0.08	0.18	-0.03	0.98	0.81	1.05	1.06	1.07	0.88	1.25	1.05

Supp. table 2 Changes of primary metabolites after rapamycin treatment

Log_2 fold changes of the cellular amount (per µg chlorophyll) of primary metabolites for the rapamycin treated *Chlamydomonas* culture in comparison to the control. The header of this table displays the TPs in hours after rapamycin treatment. An increase after rapamycin treatment is indicated by reddish colors (yellow: between 0.5 and 1; orange: between 1 and 2; red: above 2) and a decrease is indicated by bluish colors (light blue: between -0.5 and -1; dark blue: between -1 and -2; very dark blue: below -2). Significant changes ($p < 0.05$) are indicated by bold numbers.

	0.25	0.5	1	2	4	6	8	10	11	12	13	14	16	20	24
Alanine	**2.14**	**2.54**	**2.29**	**2.84**	**3.30**	**1.64**	**2.72**	**2.39**	**2.57**	**2.84**	**3.65**	**3.70**	**3.51**	**2.56**	**2.94**
Valine	**1.21**	**2.14**	**1.84**	**1.68**	**2.52**	**2.46**	**2.88**	**2.62**	**2.93**	**2.28**	**1.06**	**1.24**	**1.14**	**1.21**	**2.02**
Leucine	**1.01**	**1.39**	**1.28**	**0.96**	**1.66**	**1.19**	**1.30**	**1.28**	**1.35**	**1.29**	**1.00**	**1.12**	**0.88**	**1.02**	**1.34**
Isoleucine	**1.07**	**1.56**	**1.38**	**1.43**	**1.84**	**1.62**	**2.03**	**2.08**	**2.35**	**2.47**	**2.10**	**2.03**	**1.38**	**1.06**	**1.95**
Glycine	**1.10**	**0.66**	**0.69**	0.39	**0.69**	**1.03**	**1.86**	**1.91**	**2.03**	**1.33**	**1.61**	**1.91**	**1.85**	**2.31**	**2.21**
Serine	**1.74**	**1.70**	**1.54**	**1.49**	**1.80**	**1.22**	**1.83**	**1.67**	**1.92**	**1.91**	**2.30**	**2.50**	**2.54**	**2.38**	**2.24**
Threonine	**1.47**	**1.89**	**1.66**	**1.83**	**2.73**	**1.91**	**2.45**	**2.23**	**2.40**	**2.65**	**2.03**	**1.97**	**1.58**	**0.91**	**2.27**
Tyrosine	**0.95**	**1.57**	**2.21**	**1.28**	**0.64**	**0.66**	**1.29**	**1.56**	**1.69**	**0.70**	**1.02**	**1.10**	**0.98**	0.45	**1.47**
Phenylalanine	**0.92**	**1.26**	**1.80**	**0.94**	0.17	**0.50**	0.49	**0.54**	**0.65**	0.38	**0.75**	**0.88**	0.34	0.26	**1.10**
Tryptophan	0.23	**0.67**	**0.85**	0.49	0.43	0.47	**0.52**	**0.62**	**0.62**	0.49	0.48	**0.65**	-0.14	-0.37	**1.12**
Methionine	0.47	**0.72**	**0.81**	**0.76**	**0.56**	**1.09**	**0.62**	0.40	0.45	0.31	0.40	**0.60**	**-0.73**	-0.52	**0.99**
Cysteine	0.47	**1.24**	**0.94**	**1.05**	**0.55**	0.50	**0.51**	-0.01	0.03	-0.60	0.37	0.36	-0.03	**-0.52**	**-1.02**
Arginine	**1.39**	**1.79**	**2.08**	**2.03**	**2.89**	**2.49**	**3.04**	**2.73**	**2.90**	**2.56**	**2.13**	**2.15**	**1.38**	**0.61**	**0.88**
Lysine	**1.27**	**1.31**	**0.78**	**0.59**	**1.33**	**0.63**	**1.18**	**1.08**	**1.03**	**1.45**	**1.50**	**1.64**	**1.33**	**1.28**	**1.84**
Histidine	**2.02**	**3.79**	**3.04**	**2.93**	**3.52**	**2.26**	**2.68**	**2.48**	**2.75**	**3.27**	**2.23**	**2.72**	**1.08**	**-0.50**	**1.59**
Asparagine	**2.25**	**3.72**	**3.59**	**3.90**	**3.84**	**2.92**	**3.75**	**3.73**	**3.83**	**4.12**	**3.25**	**2.89**	**2.39**	**1.83**	**3.04**
Glutamine	**4.23**	**3.86**	**3.88**	**3.37**	**2.62**	**3.45**	**4.18**	**4.40**	**4.45**	**3.52**	**3.98**	**4.20**	**4.00**	**3.74**	**3.21**
Aspartate	**1.80**	**2.66**	**2.01**	**2.70**	**2.74**	**1.98**	**2.74**	**2.84**	**3.12**	**3.71**	**3.18**	**3.10**	**2.55**	**2.20**	**3.22**
Glutamate	**2.00**	**2.31**	**2.06**	**2.31**	**2.27**	**1.78**	**2.50**	**1.95**	**1.93**	**1.98**	**2.31**	**2.49**	**2.57**	**2.39**	**2.23**
Pyroglutamate	**1.67**	**1.48**	**1.49**	**1.55**	**1.72**	**1.66**	**2.29**	**2.36**	**2.24**	**2.36**	**2.01**	**2.26**	**1.99**	**1.75**	**1.69**
Butyrate, 2-Amino-	**0.52**	0.36	**0.50**	**0.78**	**1.81**	**1.42**	**2.26**	**2.36**	**2.55**	**2.73**	**4.27**	**4.63**	**4.24**	**2.25**	**1.92**
Alanine, beta-	**1.15**	**2.11**	**0.99**	**1.84**	**3.42**	**2.30**	**3.82**	**4.07**	**4.62**	**4.60**	**3.61**	**2.97**	**2.53**	**1.93**	**2.40**
Homoserine	0.82	**1.66**	**1.35**	**2.23**	**2.94**	**2.39**	**2.55**	**2.38**	**2.73**	**2.94**	**2.19**	**2.46**	**1.87**	**1.73**	**2.29**
Ornithine	**1.06**	**1.01**	**0.98**	**1.20**	**1.69**	**1.48**	**2.15**	**2.16**	**1.82**	**1.93**	**1.92**	**2.14**	**1.75**	**1.76**	**2.62**
Citrulline	**1.55**	**1.73**	**2.10**	**2.19**	**2.81**	**2.33**	**2.98**	**3.05**	**3.06**	**2.56**	**2.03**	**1.95**	**1.49**	**1.52**	**1.35**
Putrescine	0.19	0.02	-0.03	-0.08	-0.19	0.37	**0.89**	**0.94**	**1.14**	**0.97**	**1.18**	**1.14**	**0.98**	**1.23**	**1.11**
Spermidine	-0.06	**-0.50**	**-1.13**	-1.12	-0.72	0.43	**0.58**	**0.97**	**0.94**	**0.88**	**1.29**	**1.54**	**1.32**	**2.10**	**1.87**
Glycerate 3-P	-0.29	-0.07	0.01	0.15	0.08	-0.18	-0.34	-0.37	0.13	0.06	0.21	0.33	-0.32	0.33	-0.08
Glycerate 2-P	-0.41	-0.12	0.12	0.39	0.81	**-0.83**	**-0.49**	-0.34	0.05	0.16	**0.56**	**0.84**	**0.76**	**0.57**	0.31
Phosphoenolpyruvate	**-0.92**	**-1.29**	**-1.23**	**-0.98**	**-1.35**	**-0.78**	**-1.14**	-0.24	-0.36	-0.31	-0.26	0.43	1.46	-0.45	-0.55
Pyruvate	0.33	0.42	0.64	0.04	-0.14	**0.76**	**0.76**	**0.68**	**0.89**	**0.82**	**0.95**	**1.00**	0.48	0.57	0.36
Citrate	-0.23	-0.17	**-0.53**	-0.48	-0.06	**-0.78**	-0.42	**-0.61**	-0.22	0.07	0.42	0.41	-0.19	-0.45	0.00
Glutarate, 2-Oxo	0.35	0.35	0.48	0.69	**0.66**	**0.51**	**0.62**	**0.83**	**1.04**	**1.43**	**1.24**	**1.61**	**0.61**	0.09	**1.05**
Succinate	0.13	**0.70**	-0.02	-0.76	0.48	**-1.30**	-0.17	**-0.59**	**-0.96**	**-0.52**	-0.31	0.07	0.04	0.07	**0.79**
Fumarate	0.23	0.16	0.04	0.09	**0.35**	0.53	0.54	0.53	-0.11	**0.75**	0.10	0.47	0.56	**0.49**	0.61
Malate	**-0.39**	**0.62**	0.11	-0.25	0.69	-0.27	-0.15	**-0.42**	**-0.52**	-0.15	0.08	**0.30**	0.32	0.05	**-0.40**
Ribose	**1.16**	**0.96**	**0.77**	**0.69**	**0.63**	**1.05**	**1.05**	**1.22**	**1.25**	**1.45**	0.58	**1.12**	**1.18**	**1.02**	-0.06
Fructose (also Psicose)	**-0.72**	0.12	0.33	0.06	0.67	0.07	0.24	**0.46**	**0.42**	**0.49**	**0.63**	**0.80**	0.45	0.15	0.24
Glucose	0.27	0.45	0.75	0.94	0.10	-0.60	0.10	-0.01	0.38	0.22	-1.05	0.87	0.23	0.48	0.42
Sucrose	-0.59	-0.41	0.19	**1.39**	1.01	0.19	0.67	0.34	0.19	1.15	**1.62**	1.26	**0.71**	0.78	0.34
Maltose	**0.54**	0.54	0.19	-0.04	0.00	0.12	0.31	**0.54**	0.33	0.64	**0.42**	**0.73**	0.11	**1.20**	**0.56**
Maltotriose	0.37	**0.48**	0.32	**0.78**	0.19	**0.79**	0.51	**2.46**	**1.35**	**1.94**	**1.46**	**2.29**	0.42	**2.19**	**1.02**
Glycerol	0.29	**0.52**	**0.69**	**0.94**	**0.33**	**0.46**	**0.93**	**0.75**	0.31	0.05	**-0.96**	-0.45	0.27	**0.64**	0.18
Erythritol or Threitol	0.04	0.05	-0.01	-0.11	0.44	0.27	0.28	0.21	**0.30**	0.25	**0.57**	**0.71**	0.36	0.14	**0.51**
Mannitol or Sorbitol	0.33	**0.39**	**0.88**	**0.97**	0.21	**1.07**	**0.63**	0.30	0.55	-0.55	-1.41	-0.44	0.08	**0.64**	0.13
Inositol, myo-	0.11	0.37	0.29	**0.61**	**1.04**	-0.13	0.14	-0.18	**-0.39**	-0.48	-0.20	0.27	0.05	**1.20**	**0.72**
Ribose 5-P	-0.17	**-0.30**	**-0.44**	-0.24	**-0.13**	**-0.99**	-0.46	-0.23	0.17	0.26	**0.71**	**0.88**	0.68	**0.51**	**0.45**
Mannose 6-P	-0.28	-0.72	-0.68	-0.30	**-0.70**	-0.65	**-1.18**	**-0.56**	**-1.43**	**-1.47**	-0.52	-0.52	0.07	-0.46	**-1.10**
Fructose 6-P	-0.90	-0.77	-0.53	-0.14	**-1.22**	**-1.42**	**-1.57**	**-0.59**	-0.14	0.00	0.57	**0.68**	**0.86**	**1.42**	0.21
Glucose 6-P or Galactose 6-P	-0.58	**-0.75**	**-1.17**	**-0.76**	**-1.07**	**-0.90**	**-1.57**	**-0.53**	-0.36	**-0.79**	0.00	0.03	**0.68**	0.49	-0.39

Supp.table 2. Continued

	0.25	0.5	1	2	4	6	8	10	11	12	13	14	16	20	24
Uracil	-0.02	-0.05	0.13	-0.04	-0.99	1.05	1.20	1.53	1.07	1.11	0.09	0.19	0.83	1.55	0.39
Adenine	0.23	0.02	-0.01	-0.09	-0.09	0.59	0.62	0.56	0.34	0.34	0.29	0.23	0.29	0.48	0.58
Guanine	0.75	0.03	0.36	2.07	2.53	1.49	2.47	2.74	2.49	1.91	2.84	3.23	2.56	2.87	3.01
Hypoxanthine	0.18	1.01	1.22	2.74	4.07	2.90	3.96	4.28	4.15	3.09	4.42	4.41	4.22	4.51	5.59
Xanthine	-0.23	0.16	0.83	2.20	0.47	2.04	0.17	0.28	0.50	0.03	-1.86	-0.25	1.96	-0.48	-0.15
AMP (Adenosine 5-P)	0.37	0.54	0.55	0.29	0.27	0.51	0.43	0.42	0.31	0.26	-0.19	0.28	0.08	0.36	0.50
GMP (Guanosine 5-P)	0.23	0.35	0.22	-0.06	0.01	0.19	0.17	-0.02	0.04	-0.07	-0.19	0.21	-0.31	-0.19	0.25
byproduct of Ascorbate, 1-Dehydro-	0.22	0.21	-0.20	-0.12	0.16	-0.63	-0.33	-0.08	0.03	-0.23	0.29	0.61	0.92	-0.02	-0.11
byproduct of Asparagine	1.34	2.22	2.71	2.78	2.84	2.30	2.67	2.94	3.20	3.14	2.22	2.02	1.47	1.63	1.84
Pyrophosphate	0.50	0.51	-0.20	-0.59	-0.26	-0.48	-0.15	-0.21	-0.01	0.97	1.13	0.76	-0.64	-1.01	0.49
Phytol	0.75	0.17	0.19	0.15	-0.01	0.53	-0.47	-0.71	-0.04	0.00	-0.27	0.46	1.36	0.96	0.01
Glycerol 3-P (also Glycerol 1-P)	0.40	0.08	0.15	0.07	0.28	-0.01	-0.06	0.09	-0.12	-0.23	-0.32	-0.06	0.29	0.32	0.07
Dihydroxyacetone-P	1.07	0.10	-0.97	-0.79	0.62	0.22	-0.23	-0.79	-0.53	-1.09	-2.76	-0.89	-0.49	0.07	-1.32
Oxalate	0.23	-0.37	-0.63	-0.12	-0.47	0.99	0.69	1.01	1.07	0.98	0.89	0.89	0.99	1.50	0.82
Ethanolamine	0.07	-0.28	-0.24	-0.17	-0.34	0.50	0.93	1.27	1.20	0.58	0.33	0.39	1.10	1.62	0.81
Urea	-0.19	0.31	0.20	0.25	0.08	0.54	0.71	1.08	1.28	1.33	0.48	1.11	1.01	0.74	0.76
Nicotinamide	0.11	0.28	0.34	0.34	0.78	0.69	0.60	0.88	1.01	0.98	0.73	0.71	0.73	0.61	0.67
unknown (likely overlap with Lysine)	0.17	0.20	0.02	0.11	0.42	0.47	0.98	1.01	1.08	1.33	1.35	1.50	1.23	1.16	1.56

Supp. table 3 Changes of lipids during the cell cycle

Changes of the total amount (per ml) of lipids are shown as log_2 fold changes for each TP to TP 0 for a *Chlamydomonas* culture synchronized by a 12:12 h light-dark regime. The header of this table displays the TP in hours after onset of light. The dark phase (TP 13 – TP24 h) is indicated as grey background. Log_2 fold changes above 0.5 are indicated by reddish colors (orange and red), while red indicates a significant ($p < 0.005$) increase. Yellow background indicates the three highest values for log_2 fold changes. Lipids were grouped with regard to the TP when their level starts to increase. This results in 5 cluster indicated by blue, red, green, purple and orange background.

	0,5	1	2	4	6	8	10	11	12	13	14	16	20	24
DAG 34:1	0,60	0,99	1,07	1,16	1,62	2,16	3,16	3,54	4,27	3,99	3,93	3,39	3,27	3,45
DAG 34:3_A	-0,21	1,27	2,37	2,64	3,08	3,50	4,19	4,29	5,37	5,44	5,83	5,11	5,10	5,29
DAG 34:5_A	1,45	3,10	4,71	2,01	1,76	2,83	5,86	5,55	8,82	8,70	9,04	5,54	7,42	8,12
DAG 34:5_B	2,00	3,12	4,71	4,45	5,10	6,10	8,06	7,66	9,67	9,74	10,06	8,49	8,85	8,71
DAG 34:6_A	1,96	2,72	3,76	2,27	3,03	4,41	5,80	4,45	7,30	7,35	7,59	5,12	6,53	7,61
DAG 34:6_B	1,60	2,31	2,50	0,76	1,33	3,11	5,53	4,67	7,50	7,20	7,67	6,24	7,06	7,50
DAG 34:7	1,64	2,50	3,13	1,32	2,55	4,08	5,71	4,48	7,58	7,45	7,72	5,42	6,70	7,73
DAG 36:3	0,82	0,71	1,30	0,78	1,38	1,45	2,82	2,43	6,81	7,22	8,23	3,75	5,37	7,04
DAG 36:5	2,69	2,47	4,58	4,03	4,20	4,35	6,44	6,30	10,44	10,39	10,99	7,02	7,92	9,36
DAG 36:6	2,19	3,31	4,58	5,03	4,93	5,18	6,82	7,14	9,38	9,35	10,04	7,93	7,65	7,93
DAG 36:7_A	0,24	0,53	1,01	1,96	2,20	2,30	2,95	3,14	4,72	4,82	5,27	3,99	3,57	3,60
DAG 36:7_B	1,02	1,93	2,90	3,10	2,66	2,84	4,42	4,72	6,39	6,27	6,78	5,19	4,32	3,42
DGDG 32:0	0,46	0,75	1,18	2,06	2,83	3,35	3,75	3,99	4,09	4,00	3,84	3,65	3,33	3,30
DGDG 32:1_A	0,33	0,83	1,01	1,18	1,47	1,72	2,30	2,71	3,06	2,94	2,78	2,74	2,38	2,36
DGDG 32:1_B	0,46	0,96	1,39	1,48	1,93	2,40	3,29	3,76	4,49	4,40	4,22	4,03	3,61	3,35
DGDG 34:0	0,70	1,08	1,67	2,33	2,91	3,30	3,75	4,14	4,37	4,12	3,89	3,65	3,23	3,21
DGDG 34:1	0,49	0,76	1,02	1,14	1,38	1,94	2,46	2,73	3,09	3,04	3,04	2,85	2,71	2,61
DGDG 34:2_A	0,23	0,56	0,79	0,58	0,68	1,12	2,01	2,57	3,12	3,37	3,33	3,36	3,49	3,45
DGDG 34:2_B	0,32	0,72	1,44	2,17	2,49	3,00	3,47	3,61	3,76	3,63	3,51	3,34	2,97	2,74
DGDG 34:3_A	0,71	1,18	1,43	1,74	2,41	2,66	3,19	4,02	4,13	4,12	3,91	3,95	3,24	3,08
DGDG 36:0	2,09	3,07	4,40	5,22	5,74	6,02	6,14	6,62	6,55	6,44	6,21	6,05	5,29	5,76
DGDG 36:1_A	0,58	2,23	2,41	2,39	2,16	1,96	2,11	2,48	2,94	3,07	3,19	2,56	2,00	2,43
DGDG 36:1_B	0,60	1,10	1,72	1,98	2,38	2,67	3,22	3,63	4,00	3,95	3,69	3,50	3,01	3,06
DGTS 34:1	0,66	1,37	2,17	1,70	2,24	2,82	3,62	4,12	4,70	4,34	3,96	3,83	3,85	3,95
DGTS 36:1	0,36	0,64	0,77	1,15	1,93	2,66	3,21	3,50	4,02	4,00	3,75	3,58	3,58	3,65
DGTS 36:2	0,41	0,64	0,64	0,27	1,94	3,09	3,81	4,14	4,52	4,35	4,20	3,92	3,69	3,48
DGTS 36:3_A	0,41	0,59	0,43	1,03	2,18	3,13	3,71	3,87	4,06	4,23	3,99	3,73	3,68	3,64
DGTS 36:4_A	0,22	0,50	0,82	1,55	2,59	3,69	4,19	4,37	4,57	4,45	4,28	4,07	3,69	3,45
DGTS 38:2	0,25	0,54	0,95	0,81	1,42	2,46	3,34	3,81	4,37	4,10	3,99	3,87	3,57	3,29
DGTS 38:5_A	0,08	1,09	1,40	2,72	3,95	4,94	5,53	5,55	5,15	4,88	4,40	3,77	2,88	2,44
FA 18:1	0,46	0,88	0,91	0,81	1,06	1,86	3,32	2,85	4,98	4,60	4,50	2,76	3,27	3,68
FA 18:2	0,60	0,97	1,29	1,67	2,26	3,37	4,83	4,17	6,25	5,85	5,89	3,73	4,47	5,06
FA 18:3	1,23	1,86	2,50	1,76	3,36	3,97	5,78	5,07	7,01	6,89	6,83	5,12	5,68	6,10
MGDG 32:1_B	1,67	1,82	1,44	0,51	0,89	1,59	2,38	2,92	3,36	2,89	2,62	2,11	1,10	1,53
MGDG 32:2	0,41	0,66	0,76	0,58	0,99	1,62	1,92	2,27	2,64	2,58	2,51	2,26	1,85	1,82
MGDG 34:2	0,76	1,12	0,78	0,06	0,56	1,26	2,16	2,78	3,24	3,15	3,13	2,90	2,50	2,27
MGDG 34:3	0,57	1,04	1,42	1,34	1,86	2,58	3,24	3,56	3,67	3,38	3,21	3,03	2,67	2,44
MGDG 34:4_B	0,28	0,63	0,91	1,00	1,46	2,31	2,80	3,07	3,22	3,15	3,10	3,06	2,76	2,55
MGDG 36:1	1,90	1,97	1,15	-0,57	0,13	0,72	1,43	2,11	2,65	2,14	2,00	1,31	0,29	1,85
MGDG 36:2	2,70	3,51	3,36	0,43	0,58	1,33	2,77	3,86	4,65	4,35	4,14	3,40	2,56	1,93
MGDG 36:3_B	1,33	2,43	3,58	4,09	4,38	5,04	5,47	5,65	5,83	5,66	5,36	4,82	3,87	3,19
MGDG 36:4	1,02	1,85	2,62	2,90	2,69	3,23	3,75	4,08	4,67	4,52	4,28	3,81	3,17	2,27
MGDG 36:6_B	0,40	0,70	1,36	2,28	2,35	2,67	2,93	3,12	3,41	3,54	3,40	3,36	2,82	2,57
PE 34:1_B	1,09	1,58	2,33	2,78	2,87	2,86	4,03	5,42	5,36	4,61	4,37	3,62	3,29	3,92
PE 34:2	0,17	0,62	1,79	2,57	3,19	3,51	4,36	5,05	5,23	6,40	6,16	5,27	5,59	6,47
PE 36:2	1,28	2,32	3,44	3,89	4,68	4,80	5,96	6,55	6,35	6,91	6,13	6,54	5,68	4,90
PE 36:4_B	0,18	0,57	1,04	1,64	2,02	2,37	3,02	3,36	2,73	3,05	2,75	3,24	3,09	2,81
PG 32:1_A	0,31	0,71	0,75	0,94	1,36	2,04	3,15	3,45	3,66	3,57	3,55	3,64	3,60	3,54
PG 32:2	0,54	1,16	1,37	1,71	2,05	2,33	2,38	2,36	2,72	2,63	2,67	2,76	3,01	3,95
PG 32:3	-0,05	0,55	1,65	3,39	3,79	4,13	4,42	4,40	4,33	4,31	4,05	3,85	3,77	3,77
PG 34:0	0,44	0,60	1,07	1,60	1,79	1,84	2,02	2,58	2,46	2,80	2,80	2,58	2,81	2,87
PG 34:2_A	0,51	1,29	1,46	0,80	0,62	0,95	1,70	2,25	2,67	2,96	2,82	2,94	3,09	3,30
PG 34:5_A	0,21	0,57	0,77	1,76	2,52	3,48	3,99	4,07	3,91	3,96	3,76	3,56	3,56	3,75
PG 36:1	1,46	1,22	0,56	1,08	1,63	1,90	2,97	3,45	3,70	3,64	3,42	3,28	2,95	3,04
PG 36:2	0,90	1,63	1,37	2,00	2,76	3,57	4,27	4,75	4,59	4,61	4,44	4,28	3,99	3,59

Supp.table 3. Continued

	0,5	1	2	4	6	8	10	11	12	13	14	16	20	24
TAG 48:4_C	0,58	1,22	1,64	1,41	0,80	0,50	1,98	2,83	3,00	3,34	3,53	3,62	3,28	3,29
TAG 48:5	0,76	1,47	1,88	2,05	1,43	1,29	2,50	3,20	3,39	3,88	4,01	3,55	3,19	3,36
TAG 50:10_A	2,32	2,68	2,75	4,49	5,05	5,57	6,82	7,41	7,74	7,82	7,56	6,56	5,53	5,53
TAG 50:10_B	0,54	0,81	1,67	2,84	3,17	3,97	5,55	6,17	6,78	7,12	7,04	6,38	6,06	6,37
TAG 50:11	1,25	1,38	1,56	2,60	3,06	4,01	5,61	6,16	6,75	6,74	6,54	5,29	4,39	5,11
TAG 50:4_B	0,27	0,77	1,02	1,32	0,77	1,03	2,45	3,32	3,54	3,80	4,06	3,92	3,47	3,32
TAG 50:5_A	0,41	1,02	1,52	1,86	1,64	1,99	3,42	4,21	4,39	4,61	4,52	3,80	3,18	3,21
TAG 50:8_B	0,28	1,07	2,33	3,56	3,64	4,07	5,04	5,70	6,10	6,33	6,18	6,05	5,60	5,50
TAG 50:9_A	0,23	1,34	2,47	3,73	4,06	4,55	5,66	6,26	6,77	6,87	6,59	5,99	5,10	5,00
TAG 50:9_B	0,32	0,90	1,98	3,65	4,00	4,50	5,65	6,29	6,65	6,91	6,76	6,27	5,40	5,45
TAG 52:10_A	1,03	1,22	2,56	3,44	4,01	4,71	6,20	6,62	7,60	7,82	8,09	6,41	5,82	6,86
TAG 52:10_B	0,64	0,92	1,95	2,70	2,92	3,76	5,29	5,79	6,60	6,91	6,99	5,87	5,26	6,23
TAG 52:11	1,03	1,07	2,44	2,97	3,41	4,30	5,84	6,17	7,39	7,41	7,66	6,02	5,50	6,32
TAG 52:2	0,68	1,21	1,38	1,35	1,00	1,41	2,28	3,31	3,73	2,97	3,20	2,19	1,38	1,93
TAG 52:3	0,57	0,81	1,12	1,62	1,31	1,60	2,71	3,70	4,10	3,79	3,72	2,84	2,09	2,28
TAG 52:4_A	1,05	2,15	2,86	3,48	3,34	4,02	5,57	6,36	6,68	6,33	5,85	4,51	3,38	3,38
TAG 52:4_B	0,74	1,13	1,44	1,88	1,51	1,75	3,17	4,05	4,40	4,47	4,50	3,70	2,73	2,43
TAG 52:5_A	1,10	2,24	3,10	3,85	3,62	4,19	5,76	6,48	6,62	6,96	7,09	6,24	4,79	4,13
TAG 52:5_B	0,57	1,15	1,63	2,24	1,91	2,22	3,70	4,51	4,83	5,32	5,50	4,94	3,83	3,21
TAG 52:6_A	0,63	1,45	2,36	3,32	3,25	3,91	5,33	5,98	6,19	6,75	6,91	6,43	5,16	4,45
TAG 52:6_B	0,36	1,24	2,08	2,73	2,42	2,79	4,40	5,03	5,33	5,73	5,87	5,37	4,42	3,95
TAG 52:7_A	0,49	1,37	2,40	3,29	3,23	3,89	5,32	5,98	6,20	6,52	6,61	6,04	4,92	4,40
TAG 52:7_B	1,50	3,61	4,53	5,13	4,89	5,43	6,75	7,53	7,83	8,01	8,06	7,40	6,34	6,25
TAG 52:8_A	1,90	3,70	5,06	6,06	6,20	6,96	8,09	8,70	8,79	8,80	8,87	8,00	6,75	6,91
TAG 52:8_B	0,78	2,07	3,40	4,43	4,64	5,28	6,66	7,24	7,59	7,80	7,76	6,80	5,71	5,44
TAG 52:9_A	0,80	1,62	3,04	4,46	4,81	5,48	6,77	7,25	7,79	7,87	7,97	6,78	5,60	6,02
TAG 52:9_B	0,78	1,42	2,72	4,05	4,21	4,87	6,24	6,83	7,53	7,82	7,92	6,81	5,89	6,25
TAG 54:10_A	2,19	4,36	6,35	7,75	7,93	8,83	10,16	10,69	10,62	10,68	10,88	10,32	8,61	7,68
TAG 54:10_B	1,06	3,55	5,60	6,37	6,33	7,10	8,72	9,50	9,59	9,48	9,81	9,56	7,79	6,83
TAG 54:3	0,70	0,99	1,58	1,19	0,95	1,30	2,02	2,97	3,19	3,00	3,35	2,36	1,62	1,71
TAG 54:4_A	0,39	0,75	0,92	1,56	1,66	2,14	3,11	3,57	3,85	3,91	3,75	2,78	2,09	2,29
TAG 54:4_B	0,75	1,16	1,84	1,78	1,62	2,02	2,70	3,45	3,79	3,48	3,39	2,59	1,82	1,57
TAG 54:5_A	0,93	2,05	2,83	2,93	2,90	3,58	4,71	5,27	5,67	5,15	4,85	3,73	2,90	2,88
TAG 54:5_B	0,64	1,26	1,84	1,93	1,82	2,23	3,07	3,80	4,17	3,84	3,49	2,60	1,86	1,71
TAG 54:6_A	0,84	1,13	1,51	2,07	2,00	2,57	3,57	4,15	5,00	5,72	6,52	5,26	4,77	4,88
TAG 54:6_B	0,77	1,95	3,17	3,71	3,73	4,33	5,43	6,17	6,66	6,14	5,79	4,24	3,26	3,25
TAG 54:6_C	0,45	0,85	1,49	1,93	1,80	2,31	3,32	4,16	4,33	4,30	3,91	2,86	1,86	1,69
TAG 54:7_A	1,07	2,17	3,21	3,99	4,11	4,90	5,94	6,45	6,89	7,20	7,32	6,05	5,11	5,11
TAG 54:7_B	1,63	3,42	4,95	5,63	5,73	6,41	7,78	8,51	8,84	8,51	8,12	6,67	4,76	4,33
TAG 54:7_C	0,65	1,35	1,96	2,54	2,45	2,98	4,28	5,12	5,33	5,28	5,06	4,10	2,45	1,88
TAG 54:8_A	0,71	1,52	2,57	3,43	3,63	4,19	5,30	5,98	6,30	6,29	6,34	5,28	3,81	3,39
TAG 54:8_B	1,62	3,64	5,42	6,34	6,32	7,00	8,68	9,42	9,57	9,57	9,41	8,32	6,34	5,37
TAG 54:8_C	0,70	1,50	2,57	3,36	3,18	3,81	5,41	6,25	6,45	6,74	6,88	5,89	4,13	3,28
TAG 54:9_A	1,03	2,34	3,75	5,14	5,38	6,16	7,62	8,18	8,26	8,48	8,51	7,70	6,03	5,16
TAG 54:9_B	1,44	3,50	5,39	6,35	6,41	7,34	8,91	9,62	9,61	9,82	9,94	9,27	7,38	6,39
TAG 56:4	0,97	1,73	2,76	3,02	3,30	3,78	4,73	5,43	5,77	5,52	5,13	4,01	2,54	2,52
TAG 56:5_A	1,50	2,56	3,51	4,13	4,47	5,03	5,72	6,57	6,83	6,60	6,29	5,51	4,38	4,34
TAG 56:5_B	0,78	1,84	2,99	3,49	3,74	4,14	5,09	5,93	6,07	5,93	5,30	4,33	2,74	2,51
TAG 56:6_A	0,24	1,03	2,03	3,01	3,37	4,06	5,02	5,58	6,00	5,84	5,52	4,47	3,17	2,97
TAG 56:6_B	0,17	0,65	1,58	2,23	2,37	2,94	3,88	4,65	5,28	5,05	4,74	3,66	1,99	2,00
TAG 56:7_A	0,33	1,08	1,97	2,76	3,13	3,53	4,60	5,33	6,18	6,21	6,25	5,35	4,28	4,10
TAG 56:7_B	1,05	3,94	5,66	6,90	7,21	8,04	9,35	9,85	10,17	10,24	9,70	8,39	6,63	5,90
TAG 56:7_C	0,72	1,30	2,40	3,15	3,67	4,06	5,38	6,23	6,36	6,42	6,28	5,41	3,33	2,92
TAG 56:8_B	0,13	0,63	2,55	4,05	4,77	5,51	7,02	7,70	7,94	8,05	7,62	6,50	4,54	4,03
TAG 58:5	0,25	1,68	3,17	4,12	4,99	5,82	7,02	7,79	8,15	7,89	7,43	6,15	3,58	3,13
DAG 34:2	0,04	0,37	0,61	1,07	1,11	1,66	2,79	3,28	4,19	4,51	4,90	4,36	3,85	3,70
DGDG 32:2_A	0,20	0,39	0,63	1,49	2,10	2,39	2,85	2,92	2,99	2,79	2,62	2,55	2,26	2,02
DGDG 32:2_B	0,16	0,47	1,13	2,18	2,65	3,15	3,72	3,83	4,01	4,01	3,66	3,64	2,97	2,59
DGDG 32:3_A	0,17	0,29	0,91	1,76	2,38	3,20	3,71	3,71	3,83	3,81	3,69	3,51	3,26	3,00
DGDG 32:3_B	0,08	0,29	0,74	1,88	2,73	3,44	4,02	4,07	4,20	4,24	4,11	3,84	3,35	2,86
DGDG 32:4_A	-0,13	-0,10	0,51	1,96	3,32	3,92	4,99	5,12	5,37	5,34	5,31	5,30	5,57	5,50
DGDG 34:3_B	0,09	0,31	0,81	1,74	2,27	2,95	3,18	3,31	3,35	3,36	3,22	3,03	2,66	2,37
DGDG 36:2	0,25	0,42	0,91	1,90	2,62	2,94	3,64	3,54	3,85	3,90	3,84	3,30	2,99	2,90
DGDG 36:3_B	0,11	0,34	0,94	1,80	2,44	3,09	3,32	3,05	3,13	3,25	3,11	2,85	2,44	2,10
DGDG 36:4_A	0,11	0,39	0,82	1,41	1,78	2,16	2,84	3,04	3,40	3,47	3,45	3,39	3,33	3,36
DGDG 36:4_B	0,07	0,30	0,88	1,62	1,86	2,21	2,39	2,47	2,61	2,67	2,61	2,58	2,46	2,20
DGDG 36:5_A	0,19	0,31	0,57	1,11	1,19	1,36	1,66	1,53	1,88	1,81	1,74	1,84	2,12	2,41
DGDG 36:5_B	0,11	0,21	0,62	1,25	1,45	1,78	2,52	2,59	3,12	3,20	3,14	3,11	3,06	2,84
DGDG 36:6_A	0,09	0,24	0,54	1,10	1,36	1,55	1,79	1,86	2,12	2,07	1,98	1,88	1,95	2,00
DGDG 36:6_B	0,08	0,35	0,60	1,63	2,20	2,71	3,30	3,41	3,69	3,80	3,63	3,47	3,27	3,04
DGTS 32:2_A	0,26	0,24	0,61	1,31	0,76	1,09	-0,81	0,26	-0,01	0,48	1,69	2,38	3,07	3,39
DGTS 34:0	-0,15	-0,14	1,37	3,66	4,87	5,38	5,75	6,30	6,91	6,25	5,47	5,15	5,26	5,34
DGTS 36:3_B	0,09	0,16	0,58	0,89	1,45	2,39	3,41	3,99	4,53	4,42	4,27	4,13	3,76	3,50
DGTS 38:4_A	0,17	0,35	0,63	1,65	2,78	3,83	4,56	4,81	4,94	4,97	4,77	4,50	3,94	3,43

Supp.table 3. Continued

	0,5	1	2	4	6	8	10	11	12	13	14	16	20	24
MGDG 32:3	0,11	0,30	0,84	1,63	2,07	2,57	2,60	2,56	2,53	2,56	2,52	2,37	2,01	1,78
MGDG 32:4_A	0,06	0,19	0,82	2,09	2,40	2,67	2,69	2,50	2,07	1,86	1,60	1,51	1,40	1,09
MGDG 34:4_A	0,02	0,24	0,87	1,11	1,42	1,96	2,55	2,99	3,48	3,64	3,60	3,57	3,50	3,43
MGDG 34:5_A	0,09	0,25	0,85	1,24	1,47	2,13	2,44	2,67	2,90	3,00	2,95	3,03	2,93	2,86
MGDG 36:7_B	0,20	0,36	0,90	2,10	2,43	2,81	2,85	2,94	2,98	3,03	2,97	2,75	2,60	2,56
PE 34:3_B	-0,26	-0,12	0,95	2,42	2,92	3,32	3,73	4,28	4,19	5,04	4,82	4,48	4,87	5,33
PE 34:4_B	-0,10	0,00	0,85	2,55	3,51	3,97	4,83	5,24	5,14	6,04	5,97	5,40	5,61	5,97
PE 34:5	-0,19	0,31	0,89	2,84	4,03	4,79	5,63	6,12	5,33	6,00	5,67	5,74	5,52	5,83
PE 36:4_C	0,17	0,49	1,30	2,53	2,98	3,20	3,96	4,56	4,01	4,30	4,06	4,16	3,72	3,37
PE 38:4	0,18	0,42	0,88	1,77	2,34	2,88	3,58	4,10	3,51	4,03	3,82	4,04	3,58	2,88
PE 38:5	-0,18	0,06	0,54	1,72	2,95	3,77	4,41	4,64	3,76	4,18	4,03	4,52	4,18	3,52
PG 32:0	0,21	0,41	1,01	1,90	2,39	2,54	2,91	3,34	3,67	3,94	3,85	4,06	3,89	3,95
PG 34:3	0,16	0,41	1,27	2,42	2,81	3,01	3,27	3,32	3,30	3,29	3,08	3,06	3,01	2,95
PG 34:4	0,15	0,28	0,56	1,86	2,84	3,42	3,85	3,73	3,65	3,85	3,64	3,58	3,47	3,41
PG 36:4	0,13	0,34	1,13	2,80	3,72	4,04	4,41	4,33	4,37	4,43	4,32	4,13	4,05	4,13
SQDG 36:1	0,20	0,36	0,63	1,05	1,54	2,21	2,61	3,02	3,40	3,36	3,28	3,19	2,87	2,95
TAG 48:6	-0,56	-0,22	1,22	2,28	1,87	1,40	2,71	3,42	3,52	4,09	4,32	4,29	3,78	3,84
TAG 48:7	-0,27	0,14	0,88	1,75	1,78	1,79	3,38	4,16	4,32	4,88	4,88	5,02	4,76	4,73
TAG 50:5_B	-0,15	0,37	0,88	1,72	1,18	1,50	2,88	3,73	3,89	4,56	4,70	4,75	4,16	3,67
TAG 50:6_A	-0,22	0,01	0,63	1,69	1,64	1,99	3,12	3,92	4,06	4,69	4,69	4,67	4,11	3,77
TAG 50:6_B	-0,17	0,20	0,65	1,30	0,98	1,45	2,78	3,55	3,64	4,35	4,49	4,74	4,26	3,78
TAG 50:7_A	0,11	0,18	1,16	2,56	2,87	3,26	4,10	4,63	4,93	5,28	5,21	5,24	4,73	4,61
TAG 50:8_A	-0,31	0,18	1,56	2,76	3,12	3,53	4,71	5,28	5,44	5,73	5,82	5,71	5,18	5,18
TAG 56:8_A	0,06	0,25	1,39	2,63	3,15	4,04	5,45	5,99	6,58	6,69	6,78	5,63	4,32	3,80
DGDG 32:5	-0,11	-0,26	-0,23	0,72	2,30	2,96	4,26	4,43	4,84	4,95	4,88	4,92	5,18	5,26
DGDG 34:4	0,07	0,16	0,41	0,81	1,04	1,56	2,28	2,57	2,90	3,02	3,00	3,04	3,09	3,04
DGDG 34:5_A	0,14	0,30	0,35	1,37	1,55	1,86	1,71	2,18	2,17	2,28	2,21	2,23	1,82	2,15
DGDG 34:5_B	0,02	0,20	0,31	1,11	1,61	2,21	2,85	3,03	3,27	3,30	3,13	3,13	3,04	2,95
DGDG 34:6_B	0,08	0,19	0,49	1,44	2,19	2,91	3,55	3,67	3,72	3,80	3,71	3,69	3,54	3,42
DGDG 34:8	0,16	0,24	0,49	2,25	3,87	4,63	5,82	6,11	6,45	6,61	6,34	6,35	6,20	6,14
DGDG 36:3_A	0,18	0,26	0,18	0,73	1,07	1,64	1,82	1,91	1,91	1,93	1,83	1,87	1,81	1,77
DGDG 36:7	0,06	0,20	0,30	0,68	0,97	1,48	1,74	1,70	2,11	2,08	1,96	1,87	2,00	2,02
DGTS 30:0	-0,15	-0,29	0,16	0,99	1,43	1,83	2,06	2,38	2,88	3,15	3,34	3,82	4,32	4,56
DGTS 32:0	-0,37	-0,42	0,35	2,06	3,23	3,80	4,40	4,86	5,61	5,88	5,75	5,64	5,82	5,82
DGTS 32:3_B	0,20	0,34	0,35	0,74	1,15	1,61	1,96	2,14	2,27	2,41	2,37	2,68	2,72	2,81
DGTS 32:4_B	0,21	0,31	0,37	0,84	1,33	1,91	2,15	2,28	2,33	2,52	2,54	2,82	2,96	3,23
DGTS 34:3_A	0,10	0,19	0,25	0,83	1,21	1,87	2,29	2,49	2,67	2,74	2,71	2,74	2,70	2,68
DGTS 34:4	0,15	0,28	0,41	0,90	1,40	2,09	2,68	2,99	3,15	3,31	3,20	3,14	3,10	3,14
DGTS 34:5_A	0,10	0,18	0,23	0,91	1,76	2,56	2,90	3,02	3,05	3,24	3,24	3,33	3,51	3,66
DGTS 34:5_B	0,04	-0,02	-0,01	0,92	1,57	2,52	3,16	3,51	3,61	3,92	3,84	3,83	3,88	4,08
DGTS 34:6_A	0,04	-0,03	-0,14	0,75	1,85	2,67	2,97	3,05	3,05	3,32	3,24	3,39	3,47	3,83
DGTS 34:6_B	0,02	-0,09	-0,29	1,08	2,32	3,42	4,13	4,44	4,49	4,94	4,78	4,73	4,58	4,73
DGTS 34:6_C	0,09	0,10	-0,11	0,64	1,77	2,85	3,39	3,41	3,27	3,80	3,76	3,98	4,20	4,41
DGTS 36:4_B	0,06	0,15	0,32	0,84	1,22	1,94	2,78	3,33	3,67	3,80	3,72	3,68	3,58	3,45
DGTS 36:5_A	0,02	0,12	0,21	1,44	2,21	3,03	3,51	3,66	3,70	3,91	3,79	3,71	3,47	3,29
DGTS 36:6_B	0,12	0,15	0,18	0,88	1,41	2,07	2,52	2,77	2,80	3,09	3,04	3,17	3,14	3,22
DGTS 36:7_A	0,19	0,25	0,26	1,02	3,70	4,84	4,01	3,52	3,41	3,86	3,77	3,60	3,08	2,85
DGTS 36:7_B	0,18	0,33	0,24	0,76	1,37	2,20	2,84	3,04	3,00	3,58	3,60	3,91	3,95	4,09
DGTS 36:8	0,10	0,12	-0,04	1,10	2,70	3,88	4,16	4,08	3,84	4,33	4,19	4,26	4,25	4,34
DGTS 38:5_B	0,06	0,05	-0,16	1,12	2,69	4,04	4,76	4,94	4,97	5,08	4,99	4,91	4,55	4,07
DGTS 38:6_A	0,13	0,06	0,06	1,10	2,46	3,73	4,58	4,83	4,84	5,08	5,02	4,92	4,53	4,12
DGTS 40:4	0,08	0,07	0,11	1,41	2,95	4,25	5,17	5,37	5,62	5,74	5,51	5,20	4,53	3,86
MGDG 32:4_B	0,16	0,24	0,48	1,54	2,23	3,01	3,57	3,66	3,79	3,84	3,75	3,66	3,44	3,31
MGDG 32:5	0,10	0,20	0,42	1,32	2,10	2,88	3,44	3,65	3,73	3,96	3,93	3,98	3,89	3,88
MGDG 32:6_A	0,09	0,12	0,21	1,12	1,92	2,76	3,22	3,33	3,34	3,47	3,44	3,55	3,41	3,39
MGDG 32:6_B	0,23	0,26	0,30	1,28	2,45	3,31	3,69	3,96	3,89	4,01	3,89	4,07	3,69	3,42
MGDG 32:7	0,07	0,17	0,37	1,22	1,88	2,57	3,04	3,22	3,30	3,45	3,32	3,38	3,21	3,01
MGDG 34:5_B	0,10	0,07	0,48	1,17	1,62	2,43	2,87	3,02	2,99	2,85	2,76	2,71	2,44	2,15
MGDG 34:6_A	0,06	0,08	0,28	1,18	1,55	2,20	2,39	2,50	2,53	2,51	2,44	2,51	2,43	2,35
MGDG 34:7	0,06	0,09	0,29	0,98	1,53	2,24	2,56	2,65	2,65	2,71	2,70	2,77	2,69	2,64
MGDG 34:8	0,03	0,17	0,41	1,29	1,93	2,59	2,98	3,16	3,18	3,29	3,26	3,30	3,19	3,10
MGDG 36:5	0,14	0,18	0,50	1,79	2,39	2,83	2,38	2,01	1,69	2,21	2,27	2,47	2,80	2,86
MGDG 36:7_A	-0,08	0,21	0,35	1,17	1,80	2,58	2,96	3,06	2,98	2,98	2,93	2,96	2,86	2,80
PE 34:1_A	0,00	0,00	0,23	1,43	2,44	2,74	3,55	4,13	3,89	4,45	4,41	5,00	4,98	4,86
PE 34:4_A	-0,20	-0,35	-0,48	0,51	1,17	1,41	1,96	2,47	2,88	4,07	3,87	3,46	3,91	4,37
PE 36:3	0,06	0,15	0,30	0,95	1,39	1,77	2,38	2,74	2,23	2,70	2,62	3,17	3,03	2,83
PE 36:4_A	0,10	0,17	0,44	1,12	1,43	1,65	2,25	2,76	2,31	2,85	2,71	3,35	3,34	3,06
PE 36:5	0,00	0,16	0,34	1,05	1,32	1,75	2,18	2,60	1,84	2,28	2,22	2,96	3,09	2,93
PE 36:6_B	-0,06	0,00	0,21	1,08	1,18	1,62	2,51	3,10	2,30	2,77	2,71	3,68	3,79	3,50
PE 36:7	-0,19	-0,15	-0,21	1,30	2,43	3,13	3,80	4,13	3,54	4,53	4,19	4,97	4,76	4,01
PE 38:3	0,07	0,08	0,11	0,68	1,30	1,78	2,56	3,10	2,47	3,00	2,96	3,61	3,69	3,51
PG 32:1_B	0,40	0,22	0,18	0,89	1,29	1,46	2,27	2,64	3,04	3,90	4,04	4,39	4,48	4,02
PG 34:2_B	0,22	0,01	0,26	1,38	2,01	2,72	3,73	3,94	4,10	4,10	3,89	3,83	3,57	3,07
PG 34:5_B	0,24	0,39	0,34	1,65	2,79	3,63	4,15	4,23	4,05	4,18	4,01	3,94	3,91	3,85
PG 36:6	0,02	-0,33	0,02	1,19	1,78	2,68	3,25	3,29	3,45	3,53	3,51	3,60	3,61	3,37

Supp.table 3. Continued

	0,5	1	2	4	6	8	10	11	12	13	14	16	20	24
SQDG 32:0	0,09	0,24	0,40	0,85	1,41	2,00	2,49	2,75	2,81	2,92	2,92	2,91	2,88	3,03
SQDG 32:1_A	-0,50	-1,05	-0,83	1,08	2,15	3,09	3,28	3,28	4,03	3,77	4,05	3,63	3,77	4,12
SQDG 32:1_B	0,12	0,25	0,36	0,96	1,49	2,13	2,55	2,61	2,64	2,77	2,76	2,76	2,80	2,77
SQDG 32:2_A	-0,03	0,18	0,27	0,99	1,46	2,16	2,52	2,54	2,44	2,48	2,56	2,60	2,59	2,51
SQDG 32:2_B	0,15	0,23	0,41	1,47	2,54	3,25	3,72	3,96	3,92	4,15	4,01	3,80	3,71	3,75
SQDG 32:3	0,19	0,36	0,36	0,82	1,07	1,55	2,05	2,32	2,53	2,73	2,74	2,77	3,08	3,55
SQDG 32:4	0,07	0,23	0,25	0,73	1,17	1,99	2,61	2,80	2,94	3,09	3,04	3,04	3,01	3,09
SQDG 34:1	0,10	0,21	0,31	0,61	1,24	1,94	2,80	3,23	3,44	3,56	3,45	3,35	3,16	3,05
SQDG 34:3	0,02	0,06	0,21	0,95	1,95	2,90	3,41	3,38	3,28	3,40	3,33	3,31	3,17	3,11
SQDG 36:2	0,39	0,29	0,28	0,84	1,85	2,50	2,93	3,13	3,29	3,30	3,19	3,31	3,18	3,01
SQDG 36:6_B	-0,01	0,15	0,11	0,63	0,88	1,38	1,92	2,19	2,44	2,77	2,93	3,12	3,23	3,35
TAG 48:4_B	-0,21	-0,32	0,49	0,79	0,36	0,55	1,52	2,18	2,29	2,57	2,81	2,97	2,48	2,27
TAG 50:4_A	-0,17	-0,03	0,49	1,02	0,80	1,25	2,46	3,27	3,38	3,52	3,83	3,82	3,48	3,30
TAG 50:7_B	-0,46	-0,27	0,26	1,02	1,00	1,52	2,77	3,50	3,73	4,24	4,30	4,42	4,16	3,90
TAG 58:6_A	-0,22	0,38	0,19	0,74	1,77	2,56	3,63	4,63	4,92	4,94	4,76	3,71	2,18	1,93
TAG 58:6_B	-0,03	-0,44	0,37	0,73	1,25	2,07	3,29	3,97	4,32	4,35	4,03	3,15	0,96	1,04
DAG 34:3_B	-0,39	-0,34	0,21	0,47	0,17	1,38	3,08	3,27	4,13	4,64	5,27	4,91	4,67	4,07
DGDG 34:6_A	-0,06	-0,17	-0,25	0,27	0,83	1,51	2,23	2,49	2,71	2,89	2,87	3,01	3,32	3,44
DGTS 30:2_A	0,13	0,16	0,16	0,40	0,61	1,26	2,13	2,59	2,89	3,03	3,21	3,87	3,99	4,08
DGTS 30:3_A	0,13	0,09	-0,14	-0,42	-0,08	0,52	1,38	1,86	2,11	2,34	2,44	3,09	3,33	3,55
DGTS 30:3_B	0,20	0,19	-0,04	0,02	0,52	1,15	1,31	1,36	1,40	1,43	1,39	1,76	1,99	2,18
DGTS 30:3_C	0,20	0,11	-0,20	-0,10	0,29	0,88	1,43	1,73	1,89	2,35	2,55	3,03	3,42	3,76
DGTS 30:4_B	0,13	-0,05	-0,36	-0,31	0,29	1,06	1,02	0,89	0,93	0,78	0,72	1,28	1,67	2,15
DGTS 32:1_A	0,14	0,14	0,23	0,39	0,72	1,43	2,22	2,56	2,87	3,04	3,06	3,26	3,41	3,44
DGTS 32:1_B	0,08	0,11	0,20	0,22	0,25	0,51	1,18	1,79	2,28	2,52	2,70	3,17	3,45	3,62
DGTS 32:3_A	0,11	0,06	-0,04	0,17	0,53	1,22	1,90	2,34	2,63	2,93	3,01	3,17	3,26	3,29
DGTS 32:3_C	0,10	0,12	0,15	0,39	0,82	1,45	2,31	2,78	3,13	3,40	3,37	3,64	3,63	3,83
DGTS 32:4_A	0,07	0,07	-0,03	0,09	0,57	1,39	2,32	2,82	3,13	3,33	3,33	3,47	3,58	3,66
DGTS 32:5_A	0,10	0,08	-0,15	0,01	0,68	1,56	2,14	2,24	2,22	2,90	3,10	3,58	3,94	4,41
DGTS 32:5_B	0,11	0,05	-0,05	0,26	1,14	2,02	2,40	2,33	2,26	2,77	2,98	3,56	4,00	4,50
DGTS 32:5_C	0,01	-0,22	-0,49	-0,33	0,49	1,59	2,01	2,31	2,39	2,80	3,10	3,79	4,13	4,40
DGTS 32:6_A	0,02	-0,03	-0,25	0,06	1,12	2,18	2,58	2,45	2,33	2,83	2,99	3,53	4,00	4,38
DGTS 32:6_B	0,07	0,01	-0,35	0,10	1,18	2,30	2,94	2,90	2,64	3,31	3,45	4,15	4,51	4,86
DGTS 32:7	0,00	-0,17	-0,54	-0,32	0,77	1,94	2,54	2,29	2,18	2,79	3,04	3,65	4,01	4,33
DGTS 32:8	-0,12	-0,41	-0,82	-0,61	0,97	2,27	2,84	2,71	2,97	3,50	3,82	4,39	4,63	4,87
DGTS 34:2	-0,12	-0,42	-0,54	-0,07	0,28	0,83	1,82	2,34	2,79	3,10	3,13	3,18	3,13	3,07
DGTS 34:6_D	0,09	0,11	-0,20	0,30	1,32	2,39	3,01	3,27	3,29	3,86	3,93	4,22	4,52	4,94
DGTS 34:7_A	-0,15	-0,22	-0,50	-0,08	0,85	2,15	2,30	2,19	2,41	2,82	3,01	3,07	3,43	3,78
DGTS 34:7_B	0,04	-0,14	-0,65	-0,31	0,77	2,00	2,54	2,62	2,53	3,13	3,22	3,70	4,05	4,46
DGTS 34:7_C	0,07	-0,18	-0,36	0,37	1,61	2,80	3,01	2,92	2,74	3,14	3,30	3,56	3,64	3,87
DGTS 34:8	-0,10	-0,28	-0,79	-0,26	1,24	2,44	2,73	2,68	2,48	3,01	3,11	3,58	3,81	4,07
DGTS 36:5_B	0,01	-0,07	-0,04	0,46	0,74	1,49	2,26	2,80	3,04	3,41	3,39	3,42	3,38	3,34
DGTS 36:6_A	0,27	0,30	-0,40	-0,23	1,63	2,82	2,53	1,78	0,22	0,71	1,73	1,33	1,98	1,95
DGTS 38:3	-0,10	-0,27	-0,34	0,19	0,95	2,02	3,12	3,76	4,22	4,36	4,32	4,25	3,86	3,50
DGTS 38:4_B	-0,05	-0,17	-0,16	0,39	1,11	2,18	3,33	3,95	4,31	4,66	4,66	4,72	4,28	3,88
DGTS 38:6_B	0,08	0,05	-0,08	0,01	1,00	2,23	3,31	3,92	4,37	4,84	4,79	4,78	4,37	4,09
FA 24:0	-0,15	0,23	-0,09	0,10	0,10	0,74	1,06	1,31	1,79	1,37	1,83	1,61	1,67	1,56
LysoPE 18:3	0,07	0,06	0,31	0,46	0,80	1,17	2,10	2,44	3,25	3,67	3,57	3,96	3,80	3,69
MGDG 34:0	1,45	1,21	0,27	-0,20	1,56	2,08	2,06	1,89	1,92	0,86	0,62	0,22	-0,82	1,41
MGDG 34:6_B	0,20	0,24	-0,08	0,43	1,02	2,10	2,76	2,91	2,92	3,08	3,01	3,00	2,92	2,81
MGDG 36:6_A	0,02	-0,05	-0,12	0,50	0,67	1,46	1,29	1,07	0,69	0,59	0,94	0,92	1,31	1,59
PE 34:3_A	-0,11	-0,17	-0,20	0,39	1,00	1,50	2,36	2,93	2,69	3,46	3,40	3,83	3,96	3,89
PE 36:6_A	-0,21	-0,28	-0,58	0,28	1,26	1,96	2,52	2,89	2,44	3,32	3,26	4,04	4,14	3,87
SQDG 34:4	0,03	0,15	-0,16	-0,03	0,19	0,70	1,36	1,63	1,77	2,55	2,85	3,14	3,56	3,69
SQDG 34:5	0,01	0,03	-0,24	0,00	0,18	0,73	1,34	1,52	1,62	2,35	2,59	2,87	3,23	3,39
SQDG 34:6_B	-0,09	-0,07	-0,22	-0,05	0,25	0,95	1,57	1,82	1,97	2,67	2,86	3,22	3,61	3,76
SQDG 36:5	0,06	0,07	-0,07	0,13	0,21	0,66	1,56	1,98	2,60	3,20	3,40	3,50	3,48	3,49
SQDG 36:6_A	-0,06	0,02	-0,14	0,07	0,54	1,27	1,72	2,06	2,65	3,12	3,08	3,11	3,32	3,36
TAG 46:5	0,32	0,15	-0,03	-0,71	0,46	1,96	2,96	2,66	2,53	1,77	2,08	2,17	2,47	2,75
DGDG 32:4_B	-0,47	-0,64	-0,43	-1,77	-0,30	0,49	1,70	1,64	2,11	2,28	2,67	2,45	2,84	2,95
DGTS 30:1_A	0,13	0,15	0,17	0,20	0,15	0,47	0,86	1,15	1,42	1,59	1,96	2,78	3,23	3,48
DGTS 30:1_B	0,12	0,11	-0,01	-0,26	-0,47	-0,38	-0,17	0,21	0,51	0,84	1,16	1,86	2,38	2,70
DGTS 30:2_B	0,14	0,02	-0,28	-0,33	-0,11	0,24	0,58	0,86	1,08	1,35	1,54	2,14	2,59	2,89
DGTS 30:2_C	-0,15	-0,49	-1,06	-1,64	-1,71	-1,17	-0,71	-0,19	0,35	0,52	0,75	1,30	1,54	1,62
DGTS 30:3_D	0,06	-0,21	-0,81	-1,41	-1,50	-1,08	-0,51	-0,20	0,00	0,34	0,63	1,29	1,63	1,88
DGTS 30:4_A	0,16	0,01	-0,33	-0,57	-0,19	0,44	0,84	1,15	1,25	1,70	1,95	2,54	2,95	3,38
DGTS 32:2_B	-0,10	-0,40	-0,62	-0,35	-0,16	0,36	0,97	1,32	1,78	2,06	2,26	2,47	2,67	2,74
DGTS 32:3_D	-0,02	-0,22	-0,82	-0,91	-0,75	-0,15	0,62	1,09	1,48	1,87	1,99	2,27	2,55	2,73
DGTS 34:3_B	-0,05	-0,23	-0,72	-0,61	-0,29	0,34	1,38	1,96	2,36	2,66	2,71	2,90	3,00	3,02
FA 26:0	-0,16	-0,05	-0,15	-0,26	-0,47	0,29	0,53	0,92	1,73	1,56	1,89	1,84	2,31	2,75
MGDG 32:1_A	0,42	0,36	-0,22	-0,72	-0,22	0,34	0,59	0,80	1,02	0,94	0,78	0,73	0,61	0,81
MGDG 34:1	1,51	1,30	0,08	-0,56	0,13	0,31	1,27	1,94	2,26	1,12	1,08	0,90	-0,02	1,94
MGDG 36:3_A	1,17	1,41	0,44	-3,44	-4,05	-2,90	-1,85	-2,23	0,07	0,15	1,26	0,49	1,37	2,47

Supp.table 3. Continued

	0,5	1	2	4	6	8	10	11	12	13	14	16	20	24
PE 34:4_C	0,14	0,36	0,19	-0,33	-0,40	0,46	0,65	1,37	4,29	6,12	5,56	2,86	5,22	6,44
SQDG 34:6_A	-0,10	-0,02	-0,40	-0,35	-0,20	0,36	1,00	1,26	1,53	2,26	2,42	2,79	3,11	3,27
SQDG 34:7	-0,06	-0,13	-0,58	-0,54	-0,36	0,27	0,95	1,20	1,41	2,36	2,79	3,14	3,40	3,30
TAG 42:4	-0,21	-0,19	0,13	0,02	-0,97	-0,10	0,16	0,64	1,19	0,36	1,16	1,05	-0,25	0,89
TAG 44:0	-0,77	-0,85	-0,27	-0,53	-0,65	-0,02	-0,71	0,95	1,50	0,74	1,30	0,74	0,25	0,52
TAG 44:1	-0,47	-0,11	0,15	-0,93	-0,24	-0,52	-0,64	1,80	2,29	1,55	1,34	1,39	0,09	1,50
TAG 46:0	-0,48	-0,55	-0,20	-0,30	-0,31	0,19	-0,15	1,08	1,50	1,06	1,47	1,04	0,42	1,12
TAG 46:1	-0,02	-0,02	-0,15	-0,88	-0,54	-0,46	-0,27	1,25	1,38	0,92	0,77	0,39	-0,45	0,83
TAG 46:2	-0,51	-0,44	-0,35	-0,42	-0,14	-0,36	0,11	1,34	1,67	1,77	1,99	1,91	1,02	1,17
TAG 46:3	-0,82	-1,30	-0,94	-0,93	-1,17	-1,04	0,03	0,64	0,85	1,28	1,49	1,81	1,02	0,78
TAG 48:0	-0,58	-0,76	-0,32	-0,27	-0,38	0,06	0,21	1,22	1,55	1,14	1,68	1,15	1,00	1,22
TAG 48:1	0,04	0,19	0,09	-0,52	-0,54	-0,47	0,10	1,45	1,91	1,60	1,70	1,14	1,17	1,79
TAG 48:2	-0,39	-0,23	-0,15	-0,14	-0,31	-0,30	0,42	1,33	1,67	1,98	2,40	2,20	1,82	1,75
TAG 48:3_A	-0,31	-0,54	0,08	0,37	0,38	0,36	0,98	1,82	2,23	2,28	2,56	2,29	2,11	2,07
TAG 48:3_B	-0,59	-0,84	-0,55	-0,39	-0,98	-0,72	0,50	1,31	1,72	2,06	2,49	2,59	2,41	2,12
TAG 48:4_A	-0,88	-1,40	-0,54	0,15	0,10	0,49	1,86	2,80	3,25	3,03	2,95	3,05	2,95	2,86
TAG 50:0	-0,78	-0,69	-0,19	-0,07	-0,29	0,21	0,28	1,29	1,46	1,21	1,47	1,03	0,13	1,22
TAG 50:1	0,02	-0,02	0,01	0,09	-0,26	0,28	1,36	2,77	3,08	2,44	2,98	1,78	1,23	2,20
TAG 50:2	-0,12	-0,01	0,09	0,47	0,05	0,35	1,61	2,78	2,96	3,14	3,51	3,04	2,52	2,49
TAG 50:3	-0,56	-0,52	-0,22	0,27	-0,25	0,10	1,76	2,56	2,89	3,11	3,61	3,50	3,17	2,88

Supp. table 4 Changes of lipids after rapamycin treatment
Log_2 fold changes of the cellular amount (per µg chlorophyll) of lipids for the rapamycin treated *Chlamydomonas* culture in comparison to the control. The header of this table displays the TPs in hours after rapamycin treatment. An increase after rapamycin treatment is indicated by reddish colors (yellow: between 0.5 and 1; orange: between 1 and 2; red: above 2) and a decrease is indicated by bluish colors (light blue: between -0.5 and -1; dark blue: between -1 and -2; very dark blue: below -2). Significant changes ($p < 0.05$) are indicated by bold numbers.

	0.25	0.5	1	2	4	6	8	10	11	12	13	14	16	20	24
TAG 42:4	0.11	-0.33	-0.21	-0.57	-0.62	1.93	0.70	1.09	-0.38	0.72	1.11	-0.23	0.77	2.46	0.19
TAG 44:0	-0.38	-0.43	0.19	-0.38	-0.05	1.81	1.59	1.92	0.94	0.94	1.17	0.46	0.93	1.66	0.56
TAG 44:1	-0.71	-0.24	-0.31	-0.19	1.01	2.19	2.67	2.78	1.55	0.74	1.19	0.68	1.05	1.20	0.11
TAG 46:0	-0.26	-0.42	0.12	-0.35	-0.02	1.67	1.42	1.82	0.78	1.00	1.10	0.40	0.93	1.75	0.62
TAG 46:1	-0.60	-0.71	-0.52	-0.10	1.12	1.86	2.33	2.45	1.93	1.58	1.99	1.58	1.64	1.79	0.48
TAG 46:2	-0.74	-0.87	-0.60	-0.35	0.90	1.96	2.56	2.42	1.92	1.62	1.64	1.09	1.25	1.31	0.32
TAG 46:3	-0.94	-0.85	-0.45	-0.66	0.50	1.49	1.98	1.41	1.23	1.23	1.41	0.99	0.84	0.55	-0.42
TAG 46:5	-0.02	-0.22	0.59	1.05	2.45	2.77	2.69	2.78	3.59	4.35	5.04	4.60	3.11	2.62	2.70
TAG 48:0	-0.20	-0.08	0.20	-0.33	0.40	1.68	1.52	1.65	0.56	0.99	1.26	0.63	0.93	1.53	0.66
TAG 48:1	-0.52	-0.56	-0.18	0.15	1.52	2.45	2.75	2.58	1.97	1.68	2.04	1.69	1.76	1.58	0.71
TAG 48:2	-0.61	-0.50	-0.14	0.04	1.24	2.39	2.92	2.52	2.01	1.79	1.83	1.31	1.42	1.46	0.75
TAG 48:3_A	-0.59	-0.54	-0.19	-0.30	0.77	1.85	2.59	2.32	2.13	2.05	2.21	1.91	1.89	1.49	0.67
TAG 48:3_B	-0.63	-0.33	0.10	0.01	1.18	2.40	2.86	1.99	1.60	1.57	1.69	1.39	1.22	1.01	0.49
TAG 48:4_A	-0.51	0.87	1.08	0.36	1.23	1.91	2.32	1.54	1.23	1.27	1.95	1.98	1.52	1.14	0.60
TAG 48:4_B	-0.87	-0.69	-0.14	-0.33	0.80	1.89	2.50	2.04	1.87	2.00	2.02	1.70	1.41	1.11	0.28
TAG 48:4_C	-1.39	-0.93	-0.54	-0.03	1.67	2.92	3.82	3.18	2.69	2.77	2.72	2.32	1.85	0.68	-0.07
TAG 48:5	-0.80	-0.52	-0.15	0.28	1.87	3.08	4.07	3.60	3.18	3.19	3.16	3.02	2.57	1.28	0.11
TAG 48:6	-1.42	-1.04	-0.21	-0.34	0.96	2.54	3.95	3.53	3.13	3.27	3.05	2.71	2.50	1.30	-0.73
TAG 48:7	-0.88	-0.18	0.16	0.20	1.26	2.20	3.21	2.63	2.38	2.56	2.56	2.31	2.01	1.01	0.25
TAG 50:0	-0.18	-0.18	0.35	-0.27	0.23	1.60	1.53	1.64	0.61	1.28	1.57	0.78	1.18	2.01	0.67
TAG 50:1	-0.41	0.24	0.39	0.78	2.15	2.87	3.15	2.50	1.83	1.78	2.42	2.18	2.36	2.40	1.24
TAG 50:2	-0.34	-0.06	0.24	0.64	1.93	2.99	3.26	2.49	1.99	2.01	2.22	1.73	1.76	1.76	1.07
TAG 50:3	-0.44	0.20	0.51	0.70	1.83	2.98	3.32	2.22	1.85	1.90	2.17	1.67	1.45	1.31	0.83
TAG 50:4_A	-0.43	0.29	0.59	0.54	1.60	2.60	2.98	2.41	2.12	2.33	2.59	2.21	1.86	1.49	0.84
TAG 50:4_B	-0.48	0.01	0.36	0.81	2.08	3.20	3.75	3.00	2.72	2.74	2.87	2.54	2.16	1.23	0.47
TAG 50:5_A	-0.58	0.14	0.54	0.98	2.19	3.13	3.70	3.24	2.96	3.08	3.27	3.22	3.09	2.04	0.88
TAG 50:5_B	-0.51	0.04	0.33	0.48	1.59	2.93	3.52	2.80	2.50	2.79	2.62	2.22	1.94	1.20	0.29
TAG 50:6_A	-0.49	0.11	0.37	0.47	1.45	2.62	3.31	2.90	2.66	2.85	2.78	2.48	2.19	1.45	0.55
TAG 50:6_B	-0.44	0.09	0.35	0.31	1.14	2.29	2.87	2.28	2.08	2.47	2.43	2.01	1.66	1.00	0.37
TAG 50:7_A	-0.47	0.17	0.46	0.10	0.86	1.88	2.66	2.53	2.54	2.81	2.92	2.75	2.26	1.67	0.86
TAG 50:7_B	-0.40	0.03	0.29	0.34	1.27	2.21	2.87	2.46	2.27	2.44	2.57	2.28	1.88	1.07	0.54
TAG 50:8_A	-0.66	0.20	0.44	0.03	0.85	1.72	2.45	2.23	2.07	2.30	2.50	2.33	1.84	1.51	0.63
TAG 50:8_B	-0.82	0.13	0.34	0.16	1.03	1.98	2.81	2.57	2.43	2.48	2.62	2.49	2.46	1.09	0.10
TAG 50:9_A	-0.62	0.08	0.03	0.20	1.14	1.94	2.76	2.51	2.36	2.37	2.61	2.56	2.83	1.52	0.06
TAG 50:9_B	-0.59	-0.06	0.17	-0.03	0.53	1.50	2.35	2.09	1.97	2.08	2.23	2.20	2.57	1.47	0.20
TAG 50:10_A	-0.57	0.27	1.57	-0.19	0.26	1.09	1.85	1.57	1.43	1.44	1.78	1.90	2.57	1.54	0.15
TAG 50:10_B	-0.58	-0.01	0.56	0.43	0.75	1.55	2.06	1.56	1.52	1.43	1.69	1.67	2.24	1.08	-0.02
TAG 50:11	-0.64	0.30	1.61	0.11	0.60	1.26	1.48	0.90	0.86	0.77	1.22	1.36	2.33	1.36	-0.11
TAG 52:2	-0.33	0.28	0.89	1.66	3.10	3.73	4.09	3.86	3.26	3.07	3.64	3.14	3.14	2.51	1.50
TAG 52:3	-0.15	0.10	0.66	1.21	2.42	3.37	3.71	3.21	2.70	2.58	2.89	2.62	3.02	2.27	1.44
TAG 52:4_A	-0.32	0.85	1.14	1.52	2.50	3.38	3.51	2.89	2.63	2.51	3.06	3.18	3.86	2.95	1.81
TAG 52:4_B	-0.19	0.14	0.75	1.21	2.22	3.19	3.58	2.90	2.57	2.47	2.64	2.36	2.82	2.23	1.34
TAG 52:5_A	-0.37	0.65	0.93	1.16	2.08	3.10	3.37	2.61	2.43	2.46	2.54	2.22	2.71	2.38	1.34
TAG 52:5_B	-0.22	0.02	0.50	0.85	1.92	2.99	3.49	2.69	2.42	2.38	2.22	1.83	2.28	1.86	1.01
TAG 52:6_A	-0.34	0.71	0.93	1.01	1.77	2.75	3.14	2.48	2.36	2.52	2.40	1.96	2.27	2.10	1.26
TAG 52:6_B	-0.43	0.17	0.40	0.51	1.60	2.68	3.32	2.48	2.30	2.40	2.25	1.82	2.10	1.60	0.84
TAG 52:7_A	-0.42	0.35	0.57	0.54	1.43	2.44	2.98	2.40	2.27	2.37	2.38	1.98	2.19	1.72	0.92
TAG 52:7_B	-1.12	0.20	-0.09	0.32	1.56	2.46	3.13	2.63	2.28	2.27	2.36	1.94	2.38	1.52	0.50
TAG 52:8_A	-0.56	0.58	0.78	0.59	1.27	2.20	2.65	2.14	2.01	2.18	2.31	2.07	2.64	1.90	0.76
TAG 52:8_B	-0.51	0.24	0.45	0.42	1.16	2.01	2.65	2.24	2.16	2.12	2.25	1.99	2.56	1.65	0.78
TAG 52:9_A	-0.32	0.21	0.80	0.50	0.73	1.63	2.05	1.57	1.56	1.51	1.65	1.52	2.42	1.95	0.86
TAG 52:9_B	-0.38	0.07	0.70	0.36	0.63	1.56	2.01	1.51	1.44	1.18	1.41	1.27	2.27	1.62	0.61
TAG 52:10_A	-0.35	0.15	1.49	1.22	0.82	1.53	1.62	1.05	1.19	0.70	0.77	0.80	2.29	2.05	0.76
TAG 52:10_B	-0.39	0.03	0.90	0.64	0.74	1.48	1.66	0.98	1.00	0.56	0.87	0.83	2.02	1.46	0.38
TAG 52:11	-0.39	0.00	1.48	1.11	0.68	1.31	1.24	0.55	0.76	0.29	0.48	0.65	2.07	1.72	0.42

	0.25	0.5	1	2	4	6	8	10	11	12	13	14	16	20	24
TAG 54:3	-0.12	-0.17	0.60	0.42	2.04	2.73	3.01	3.02	2.64	2.51	2.76	2.39	2.76	2.32	1.28
TAG 54:4_A	-0.18	0.59	0.61	0.95	1.79	2.58	3.06	2.91	2.74	2.78	3.02	2.95	3.21	2.51	1.44
TAG 54:4_B	0.02	-0.35	0.26	0.39	2.09	2.80	3.11	2.80	2.38	2.27	2.57	2.38	2.79	2.07	1.40
TAG 54:5_A	-0.10	0.57	0.62	0.80	2.04	2.56	2.47	2.13	2.00	1.91	2.42	2.44	2.98	2.29	1.20
TAG 54:5_B	0.04	-0.40	0.09	0.54	2.03	2.72	3.06	2.69	2.36	2.15	2.40	2.33	2.79	2.03	1.36
TAG 54:6_A	-0.17	0.42	0.60	1.04	1.80	2.77	3.16	3.04	2.87	2.15	2.13	1.45	2.51	2.52	1.59
TAG 54:6_B	-0.21	0.60	0.46	0.37	1.56	2.30	2.49	1.89	1.66	1.51	1.83	1.94	2.82	2.08	1.07
TAG 54:6_C	0.03	-0.41	-0.05	0.30	1.60	2.35	2.78	2.22	1.87	1.72	1.83	1.85	2.65	1.96	1.19
TAG 54:7_A	-0.23	0.85	0.82	0.65	1.18	1.90	2.22	1.92	1.83	1.51	1.73	1.43	2.50	2.28	1.36
TAG 54:7_B	-0.22	0.83	0.57	0.46	1.49	2.21	2.40	1.68	1.52	1.59	1.71	1.77	2.81	2.27	1.05
TAG 54:7_C	-0.05	-0.42	0.01	0.50	1.43	2.11	2.52	1.76	1.43	1.50	1.47	1.39	2.39	2.10	1.18
TAG 54:8_A	-0.13	0.11	0.42	0.47	1.12	1.72	2.03	1.52	1.36	1.31	1.38	1.14	2.11	2.11	1.09
TAG 54:8_B	-0.34	0.91	0.46	0.20	1.07	1.87	2.15	1.34	1.12	1.23	1.25	1.10	2.16	1.97	0.85
TAG 54:8_C	-0.19	-0.41	0.20	0.40	1.31	2.04	2.35	1.41	0.89	1.07	1.01	0.86	1.99	1.99	0.94
TAG 54:9_A	-0.30	1.08	1.00	0.51	0.61	1.20	1.56	1.02	0.92	1.09	1.11	0.87	1.69	1.97	1.18
TAG 54:9_B	-0.23	1.19	0.81	0.34	0.94	1.56	1.76	0.92	0.74	1.00	1.04	0.83	1.79	1.78	0.75
TAG 54:10_A	-0.14	1.90	1.17	0.23	0.13	0.69	0.98	0.33	0.28	0.60	0.76	0.59	1.27	1.71	0.87
TAG 54:10_B	-0.75	1.02	0.70	0.13	0.77	1.39	1.47	0.48	0.30	0.62	0.80	0.63	1.46	1.57	0.41
TAG 56:4	-0.20	-0.04	0.13	0.19	1.85	2.57	2.97	2.56	2.23	2.05	2.31	2.43	3.07	2.56	1.37
TAG 56:5_A	-0.44	0.96	0.79	0.93	1.95	2.47	2.81	2.51	2.28	2.18	2.47	2.50	2.87	2.51	1.22
TAG 56:5_B	0.00	-0.36	-0.13	0.16	1.69	2.44	2.91	2.51	2.22	2.10	2.35	2.55	3.16	2.49	1.48
TAG 56:6_A	-0.52	0.47	0.59	0.39	1.09	1.89	2.31	2.13	1.90	1.80	1.99	1.98	2.62	2.31	1.02
TAG 56:6_B	-0.08	-0.43	0.00	0.01	1.03	2.08	2.48	2.25	1.92	1.82	1.99	1.96	2.71	2.43	1.07
TAG 56:7_A	-0.23	0.18	0.62	0.93	1.49	2.28	2.69	2.32	2.06	1.68	1.77	1.52	2.51	2.11	1.17
TAG 56:7_B	-1.69	1.84	0.75	0.35	0.92	1.66	2.18	1.87	1.73	1.75	1.84	1.93	2.75	2.32	1.04
TAG 56:7_C	0.05	-0.62	-0.05	0.08	1.20	2.05	2.48	1.92	1.64	1.59	1.69	1.63	2.47	2.54	1.21
TAG 56:8_A	-0.54	0.28	1.17	1.03	1.06	1.83	2.07	1.44	1.47	1.09	1.20	1.18	2.43	2.10	1.17
TAG 56:8_B	-0.39	-0.37	0.81	0.08	0.74	1.46	1.94	1.37	1.28	1.38	1.43	1.65	2.52	1.88	0.47
TAG 58:5	0.19	-0.62	-0.15	-0.10	1.21	1.69	1.94	1.48	1.22	1.17	1.43	1.67	2.62	3.01	1.02
TAG 58:6_A	-0.37	-1.19	-1.28	-0.06	0.14	1.34	1.49	1.14	0.76	0.80	1.06	0.94	1.76	2.05	-0.10
TAG 58:6_B	0.43	-1.51	-1.17	-0.26	0.27	1.82	1.87	1.38	0.94	1.07	1.12	1.01	1.96	2.73	0.58
DAG 34:1	0.24	0.02	-0.01	-0.03	0.54	0.85	1.00	0.72	0.51	0.39	0.76	0.84	1.05	1.26	0.88
DAG 34:2	-0.01	-0.24	-0.03	-0.04	0.25	0.87	0.92	0.26	0.03	-0.12	0.06	-0.13	0.32	0.99	0.52
DAG 34:3_A	0.15	-1.15	-1.41	-1.45	-0.86	0.14	0.35	0.31	0.42	0.43	0.54	0.25	0.55	1.13	-0.17
DAG 34:3_B	-0.13	-0.22	0.13	-0.25	-0.33	-0.82	-1.64	-1.96	-3.44	-1.06	-0.54	-0.49	-0.20	0.60	0.73
DAG 34:5_A	1.46	1.44	1.05	0.18	2.24	2.84	0.74	0.27	-0.79	-0.40	-1.36	-0.43	1.24	0.74	-0.38
DAG 34:5_B	1.77	0.94	1.45	0.37	0.39	1.10	0.63	0.19	0.29	0.50	0.16	0.27	1.16	1.21	0.61
DAG 34:6_A	1.30	1.05	1.21	0.74	1.57	1.89	1.31	1.17	0.83	0.91	0.24	0.48	1.57	1.78	0.72
DAG 34:6_B	1.15	1.04	1.37	0.32	0.53	1.15	-0.05	-0.08	-0.12	0.09	-0.14	0.11	1.00	1.51	0.88
DAG 34:7	1.15	0.83	0.91	0.62	1.41	1.36	0.71	0.30	0.32	0.17	-0.59	-0.16	0.65	1.14	0.25
DAG 36:3	-0.16	-0.31	0.77	1.68	0.98	1.63	1.63	1.23	1.74	-0.64	-1.19	-1.06	1.65	2.37	0.54
DAG 36:5	0.06	-0.70	1.28	0.81	-0.95	0.33	-0.02	-0.15	-0.76	-1.61	-2.32	-1.85	0.63	1.88	0.06
DAG 36:6	-0.47	0.66	0.80	0.17	-1.03	-0.23	-0.22	-0.75	-1.11	-1.32	-1.46	-1.17	0.50	1.75	-0.10
DAG 36:7_A	-0.10	0.12	0.09	-0.04	-0.63	-0.30	0.20	0.03	0.23	-0.46	-0.59	-0.95	0.00	1.59	0.51
DAG 36:7_B	-0.01	0.05	0.15	-0.50	-1.18	-0.90	-0.22	-0.86	-1.80	-1.32	-1.71	-1.51	-0.14	2.08	0.04
FA 18:1	0.28	0.50	1.06	0.97	1.15	1.31	0.77	-0.04	-0.04	-0.47	-0.49	0.25	1.18	0.98	0.27
FA 18:2	0.70	0.95	1.62	1.33	1.62	2.17	1.07	0.36	0.37	0.04	-0.15	0.59	1.59	1.13	-0.03
FA 18:3	1.96	1.45	1.79	1.46	2.17	2.18	1.09	0.60	0.78	0.09	-0.17	0.44	1.29	1.39	0.05
FA 24:0	-0.22	-0.32	-0.59	-0.52	0.09	0.94	0.73	0.56	0.62	0.70	0.97	0.44	0.62	0.76	0.71
FA 26:0	0.03	-0.10	-0.20	-0.36	-0.12	1.09	1.01	1.06	0.67	0.75	0.76	0.24	0.20	0.47	0.10
LysoPE 18:3	0.65	0.40	0.49	-0.11	0.59	1.00	0.99	0.72	0.62	0.29	-0.18	0.24	0.02	0.62	0.51

List of publications and presentations

Publications

Hummel J, Segu S, Li Y, Irgang S, **Jueppner J**, Giavalisco P (2011), "*Ultra performance liquid chromatography and high resolution mass spectrometry for the analysis of plant lipids",* Frontiers in plant science, doi: 10.3389/fpls.2011.00054

Poster

Jueppner J, Irgang S, Caldana C, Willmitzer L, Giavalisco P (2012), "*TOR (Target of rapamycin) and its role in cell growth in the unicellular green alga Chlamydomonas reinhardtii*", 15th International Conference on the Cell & Molecular Biology of Chlamydomonas, Potsdam, Germany

Jueppner J, Irgang S, Brust H, Caldana C, Willmitzer L and Giavalisco P (2011), "*Inhibition of TOR by rapamycin leads to a reduction in growth rate and an accumulation of starch in Chlamydomonas reinhardtii*", FEBS workshop Plant Organellar Signaling from Algae to higher plants, Primosten, Crotia

Eidesstattliche Erklärung

Hiermit erkläre ich, dass ich die vorliegende Arbeit selbständig am Max-Planck-Institut für Molekulare Pflanzenphysiologie angefertigt habe und keine weiteren als die angegebenen Hilfsmittel und Quellen genutzt habe. Ich versichere, dass die vorliegende Doktorarbeit an keiner anderen Hochschule als der Universität Potsdam eingereicht wurde.

Potsdam, den 28. April 2015

_____

Jessica Jüppner